Self-interference Cancellation for Full-duplex MIMO Transceivers

Mohamad Abdulrahman Ahmed

Newcastle University

Newcastle upon Tyne, UK.

A thesis submitted for the degree of

Doctor of Philosophy

July 2017

TO

my beloved wife, **Duaa**

AND

my loving sons, **Abdulrahman** , **Hasan**, and my daughter **Aya**.

Declaration

NEWCASTLE UNIVERSITY

SCHOOL OF ELECTRICAL AND ELECTRONIC ENGINEERING

I, Mohamad Abdulrahman Ahmed, declare that this thesis is my own work and it has not been previously submitted, either by me or by anyone else, for a degree or diploma at any educational institute, school or university. To the best of my knowledge, this thesis does not contain any previously published work, except where another persons work used has been cited and included in the list of references.

Signature:

Student: Mohamad Abdulrahman Ahmed

Date:

SUPERVISOR'S CERTIFICATE

This is to certify that the entitled thesis "Self-interference Cancellation for Full-duplex MIMO Transceiver" has been prepared under my supervision at the school of Electrical and Electronic Engineering / Newcastle University for the degree of PhD in Electrical and Electronic Engineering.

Signature:

Supervisor: Dr. Charalampos Tsimenidis

Date:

Acknowledgements

In the beginning of my acknowledgement, I must start by thanking almighty Allah for giving me the strength and the courage throughout my life and especially in the last four years for the completion of my PhD study. Praise be to Allah for his blessings and my success in becoming what I am now.

I am pleased to have the opportunity to express my sincere gratitude to those precious people who have assisted me in completing my PhD study, and reaching this stage of my education would have been unthinkable without the support of those to whom I would like to give particular mention here.

First and foremost, I would like to express my thanks and gratitude to my supervisor, Dr. Charalampos Tsimenidis, for all his efforts, continuous support, motivation, immense knowledge and constructive criticism which have assisted me throughout my PhD research and in the writing of this thesis. I appreciate the vital role he has played as a tremendous mentor for my research, and I owe to him all of the experience I have benefited from in the field of scientific research.

I would like to express my warm appreciation of my country, Iraq, and especially my sponsor, the Ministry of Higher Education and Scientific Research (MoHESR), and the University of Mosul and to the Iraqi Cultural Attache in London for providing financial support for my PhD scholarship.

Furthermore, my honest appreciation goes to my lovely wife, Duaa, and my children Abdulrahman, Hasan and Aya for their constant support and great patience. Special occasions and great moments they had missed for the sake of my studies. All these sacrifices had been offered to me without any complain.

Additionally, I would like to express my sincere appreciation to my mother, my brothers Ahmed and Hisham and all my sisters for their support in all of the stages of my education. I am very thankful for their kindness and I owe

them my life and success. I dedicate this success to the spirit of my great father.

I would like also to thank the School of Electrical and Electronic Engineering at Newcastle University for assistance and support since my first day in the university, especially the kind Postgraduate Research Coordinator, Gillian Webber and the lovely Receptionist, Deborah Alexander.

I express my warm thanks to my fellow postgraduate students at the school of Electrical and Electronics Engineering: Ahmed, Sanker, Sabah, Ali, Zaid, Bilal, Sinan, Mohammed and Alla for their stimulating discussions, endless support, and for sharing their frank views on a number of issues related to the research topic.

My final thanks go to all my family, my friends, and to all the people who have helped me over the past years. Although I cannot mention all their names here, they all deserve my sincere gratitude.

Abstract

In recent years, there has been enormous interest in utilizing the full-duplex (FD) technique with multiple-input multiple-output (MIMO) systems to complement the evolution of fifth generation technologies. Transmission and reception using FD-MIMO occur simultaneously over the same frequency band and multiple antennas are employed in both sides. The motivation for employing FD-MIMO is the rapidly increasing demand on frequency resources, and also FD has the ability to improve spectral efficiency and channel capacity by a factor of two compared to the conventional half-duplex technique. Additionally, MIMO can enhance the diversity gain and enable FD to acquire further degrees of freedom in mitigating the self-interference (SI). The latter is one of the key challenges degrading the performance of systems operating in FD mode due to local transmission which involves larger power level than the signals of interest coming from distance sources that are significantly more attenuated due to path loss propagation phenomena. Various approaches can be used for self-interference cancellation (SIC) to tackle SI by combining passive suppression with the analogue and digital cancellation techniques. Moreover, active SIC techniques using special domain suppression based on zero-forcing and null-space projection (NSP) can be exploited for this purpose too. The main contributions of this thesis can be summarized as follows. Maximum-ratio combining with NSP are jointly exploited in order to increase the signal-to-noise ratio (SNR) of the desired path and mitigate the undesired loop path, respectively, for an equalize-and-forward (EF) relay using FD-MIMO. Additionally, an end-to-end performance analysis of the proposed system is obtained in the presence of imperfect channel state information by formulating mathematically the exact closed-form solutions for the signal-to-interference-plus-noise ratio (SINR) distribution, outage probability, and average symbol-error rate for uncoded M-ary phase-shift keying over Rayleigh fading channels and in the presence of additive white Gaus-

sian noise (AWGN). The coefficients of the EF-relay are designed to attain the minimum mean-square error (MMSE) between the transmission symbols. Comparison of the results obtained with relevant state-of-the-art techniques suggests significant improvements in the SINR figures and system capacity.

Furthermore, iterative detection and decoding (IDD) are proposed to mitigate the residual self-interference (SI) remaining after applying passive suppression along with two stages of SI cancellation (SIC) filters in the analogue and digital domains for coded FD bi-directional transceiver based multiple antennas. IDD comprises an adaptive MMSE filter with log-likelihood ratio demapping, while the soft-in soft-out decoder utilizes the maximum *a posteriori* (MAP) algorithm. The proposed system's performance is evaluated in the presence of AWGN over non-selective (flat) Rayleigh fading single-input multiple-output (SIMO) and MIMO channels. However, the results of the analyses can be applied to multi-path channels if orthogonal frequency division multiplexing is utilised with a proper length of cyclic prefix in order to tackle the channels' frequency-selectivity and delay spread. Simulation results are presented to demonstrate the bit-error rate (BER) performance as a function of the SNR, revealing a close match to the SI-free case for the proposed system. Furthermore, the results are validated by deriving a tight upper bound on the performance of rate-$1/2$ convolutional codes for FD-SIMO and FD-MIMO systems for different modulation schemes under the same conditions, which asymptotically exhibits close agreement with the simulated BER performance.

Contents

List of Figures

List of Tables

Nomenclature

Acronyms

5G	Fifth generation
ADC	Analogue-to-digital converter
AF	Amplify-and-forward
$ASER$	Average-symbol-error rate
$AWGN$	Additive while Gaussian noise
$Balun$	Balanced/unbalanced
BER	Bit-error rate
$BICM$	Bit interleaved coded modulation
$BLAST$	Bell Labs layered space time
$BPSK$	Binary phase shift keying
CDF	Cumulative distribution function
CSI	Channel state information
DF	Decode-and-forward
DoF	Degree of freedom
DAC	Digital-to-analogue conversion
dB	Decibel
$E2E$	End-to-end
EF	Equalize-and-forward

$EXIT$ EXtrinsic Information Transfer

FD Full-duplex

FDD Frequency domain duplex

FDM Frequency division multiplexing

FF Filter-and-forward

FFT Fast Fourier transform

GCQ Gauss-Chebyshev quadrature

HD Half-duplex

IDD Iterative detection and decoding

IC Interference cancellation

ICI Inter-channel interference

$IDFT$ Inverse discrete Fourier transform

$IFFT$ Fast Fourier transform

$i.i.d.$ Independent and identically distributed

ISI Inter-symbol interference

I/Q In-phase/Quadrature

LI Loop-interference

LoS Line-of-sight

LNA Low noise amplifier

LO Local oscillator

$MIMO$ Multiple-input multiple-output

$MISO$ Multiple-input single-output

$MMSE$ Minimum mean-square error

MAP Maximum *a posteriori*

MRC Maximum-ratio combining

ML Maximum-likelihood

MSE Mean square error

MGF Moment generation function

NSP Null-space projection

NSC Non-systematic convolutional encoder

$OFDM$ Orthogonal frequency division multiplexing

PDF Probability density function

PSK Phase-shift keying

PA Power amplifier

PEP Pairwise error probability

PIC Parallel interference cancellation

$QPSK$ Quadrature Phase Shift Keying

QAM Quadrature amplitude modulation

RF Radio frequency

RSC Recursive systematic convolutional encoder

SI Self-interference

SIC Self-interference cancellation

$SISO$ Single-input single-output

$SIMO$ Single-input multiple-output

STC Space-time coding

$SINR$ Signal-to-interference-plus-noise ratio

SVD Singular-value decomposition

$STBC$ Space-time block coding

SNR	Signal-to-noise ratio
$SiSo$	Soft-in soft-out
TDD	Time domain duplex
TDC	Time-domain cancellation
ZF	Zero-forcing

Notations

$\mathbf{A}$	Uppercase boldface characters for matrices
$\mathbf{a}$	Lowercase boldface characters for vectors
$\mathbf{A}^T$	Transpose of the matrix **A**
$\mathbf{A}^*$	Conjugate the matrix **A**
$\mathbf{A}^H$	Hermitian the matrix **A**
$\|\mathbf{a}\|$	The Euclidean norm of the vector **a**
$\|\mathbf{A}\|$	The Euclidean norm of the matrix **A**
$\|\mathbf{A}\|$	The determinant of the matrix **A**
$\Gamma(a)$	The complete Gamma function of the variable a
$\mathbb{E}\{\mathbf{a}\}$	The statistical expectation of the random vector **a**
$\Re[A]$	The real part of the complex number A
$\Im[A]$	The imaginary part of the complex number A
$a!$	The factorial of the integer number a
$\binom{a}{b}$	The binomial coefficient which is evaluated as $\frac{a!}{b!(a-b)!}$

Chapter 1

Introduction

1.1 Introduction

Due to the increasing demand on frequency resources for the next generations of wireless communication, research efforts have recently been initiated by industrial and academic groups around the world in order to utilize the in-band full-duplex (FD) technology for further improvements in spectral efficiency [1]. Previous generations of wireless communication were basically designed to depend on the half-duplex (HD) technique, in which different time and/or frequency bands are used to separate transmitted and received signals [2,3]. Fig. 1.1 shows how two nodes communicate with each other by using different duplex schemes, in which separation in the time domain allows the system to utilize the same frequency band for transmission, while orthogonal time slots are allocated for transmitted and received signals. This scheme is called the time domain duplex (TDD). In the frequency domain duplex (FDD), which is sometimes referred to as out-of-band FD, all the time slots can be used by the transmitter and receiver since transmission occurs in different frequency bands. The third scenario combines the above two schemes, in which two frequency bands are assigned for communication and the symbols transmitted in each node are set in orthogonal time slots. This technique is called HD-FDD. The fourth type is the subject of interest in this thesis, in which a simultaneous transmission over the same frequency band is utilised to enhance the spectral efficiency in (bit/second/Hz) by a factor of two compared to HD-FDD [4]. This is due to the fact that the conventional techniques employed for improvement in spectral efficiency, such as smart antennas, adaptive modulation and coding are approaching the limits of their potential [5].

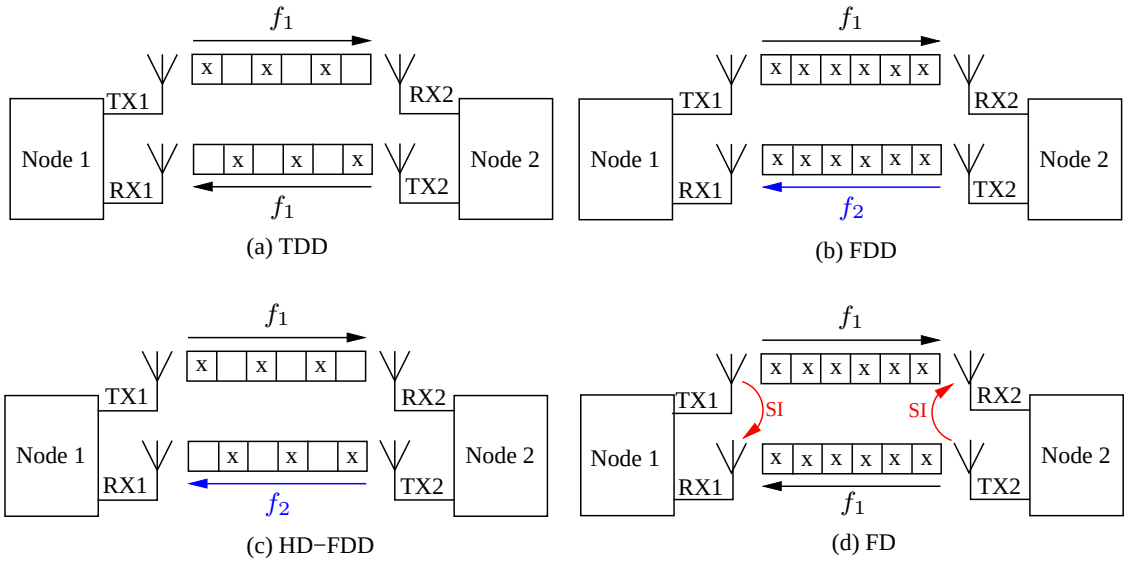

Figure 1.1: Different duplexing schemes

On the other hand, one of the key challenges in FD wireless communication is the self-interference (SI), sometimes referred to as loop-interference, which can have an undesirable effect on overall system performance. This is principally caused by the signals transmitted by the FD transceiver which exhibit greater energy than the desired incoming signals due to path loss propagation phenomena. The large power differential between the signal of interest, which arrives weakly from a distance source, and the SI signal created by the FD transceiver itself poses extreme difficulties for the receiver which needs to reconstruct and detect the desired signal.

At this point, different state-of-the-art approaches are available regarding the effect of SI on FD systems. One example of femto-cell FD cellular systems has been considered, in which the transmitted power from the base-stations and mobile handsets is set to 21 dBm, with an isolation of 15 dB is assumed between the transmit and receive signals [4]. For a noise floor at the receiver of -100 dBm, each base-station in this system has $21 - 15 - (-100) = 106$ dB of SI above the noise floor which needs to be addressed. In a second example [6], a typical WiFi radio of 80 MHz bandwidth and operating in FD mode is considered. A transmitted signal of 20 dBm and a noise floor of -90 dBm are assumed for this system, and thus the SI power above the noise floor can be determined as $20 - (-90) = 110$ dB which needs be mitigated. Without loss of generality, differences in wireless systems in terms of various cell sizes and numbers of antennas might require higher transmission power yielding stronger power of SI, and thus additional SI suppression will need consequently to be achieved. Further scenarios for different FD systems, along with various algorithms utilized to suppress SI, are outlined in Table 1 in [7] for a recently published review.

Multiple-input multiple-output (MIMO) technology can be employed with FD systems by sending a stream of data using several antennas over independent channels and receiving it by using multiple spatial antennas to increase the diversity gain and to obtain more degrees of freedom (DoF) in tackling SI [8, 9]. This is discussed later on in this thesis in more detail.

Several methods have been proposed in this field to mitigate SI that can be grouped in two categories, namely passive and active SI cancellation (SIC). Passive methods rely on separation between the transmitting and receiving antennas in order to increase the isolation loss amongst them, and hence reduce the magnitude of local interference. In contrast, active approaches are implemented either in the analogue domain, which always occur before the analogue-to-digital converter (ADC), or in the digital domain after the

ADC, in which the SI signal is subtracted from the overall incoming signal in the passband and/or baseband domains, respectively. This operation requires precise knowledge of the interfering signal and its channel, and therefore the better estimation of the SI, the more robust and effective the implementation of SIC. Furthermore, a combination of methods in different domain can be used to obtain better performance. Further details are discussed in Chapter 2 in more depth.

1.2 Background and Literature Review

In order to mitigate SI in transceivers operating in FD mode, a crucial key stage is to reduce the effects of the transmitted power of an FD transceiver on its receiving input. This is due to the fact that the arriving SI power is much stronger than the desired incoming signal, which drowns the latter in loop-interference (LI) [10]. Therefore, any signal processing in the analogue or digital domains might be susceptible to fail in recovering the signal of interest as a result of limited dynamic range and quantization resolution of the ADC circuitry, which consequently causes saturation in the input of the receiver [9–13]. In order to suppress SI in FD systems, it is first required to reduce the effects of local power coupling to avoid the drowning of the desired incoming signal in loop-interference which is significantly stronger, and to mitigate the saturation of the ADC circuitry due to limited dynamic range and quantization resolution [9–14].

In this stage, passive suppression has been proposed at the receiver front-end by using natural-isolation techniques via antenna separation to diminish and block the line-of-sight (LoS) path. This can be achieved by orienting transmit antenna elements in the opposite direction than those of the receiving antennas, which consequently maximizes LI attenuation by increasing the insertion loss. This can be further increased by utilizing orthogonal polarization schemes by designing an array of antennas for the transmitters and receivers of the FD relays in such a way that orthogonal polarization between them is achieved for this purpose [8, 9, 15–17].

At this stage in FD systems, different mechanisms have been proposed and deployed in the literature to mitigate SI passively, Table 1.1 presents the most significant proposals applied to suppress SI to a level that enables the next stages of SIC before and after the ADC in order to treat the residual SI and detect the desired signal properly.

Table 1.1: Major research into the passive suppression of SI

Year	Reference	Contribution	Assumption
2004	Anderson et al. [18]	Antennas isolation and separation approaches are proposed in which measurements and simulations of power delay profile based on wideband multipath channels are presented.	An ideal amplifier in each FD node is assumed for simulation purposes, and the leakage channel attenuation of SI is equal to time-varying antenna isolation.
2007	Bliss et al. [19]	An adaptive transmit/receive antennas array is utilized for the FD-MIMO based relay, in which a partitioning technique is exploited to select some antennas for transmitting and assigning others for receiving.	Signal processing mechanisms is used to enable the transmit/receive antennas array methods adaptively.
2009	Ju et al. [20]	FD relays based on time and antennas sharing proposed for the passive mitigation of SI. A precoder and decoder design for this purpose is required.	SI suppression is implemented via a precoding algorithm.
2010	Duarte et al. [17]	Antenna separation techniques are implemented along with active analogue and digital SIC.	For distances of 20 cm and 40 cm between the transmit and receive antennas, AS achieves SI reductions of 39 dB and 45 dB, respectively.
2010	Choi et al. [21]	Destructive interference of SI is proposed based on antennas separation by using two antennas for transmitting positioned at d and $d + \lambda/2$ away from a single receiving antenna.	Ideal positioning of antennas is required to obtain perfect SI suppression.

Continued on next page

Table 1.1 – *Continued from previous page*

Year	Reference	Contribution	Assumption
2010	Haneda et al. [11]	A compact antenna for a relay is proposed for FD communication and for the measurements of the SI channel. An isolation of about 48 dB is obtained in the presence of a multipath SI channel.	The compact size and isolation obtained might be unsuitable for other practical applications operating in FD mode.
2011	Everett et al. [22]	Directional antennas are utilized to minimize the intersection of the main lobes of the transmit and receive antennas, in order to improve the diversity gain, decrease SI and consequently empower FD operation for wireless communication.	Directional antennas are placed 20 cm away from each other, and 5 dB is used as the transmission power.
2012	Everett [23]	Polarization decoupling is used with FD, in which the transmit and receive antennas are proposed and designed with orthogonal polarization in order to minimize the coupling and enhance the passive suppression of SI.	A combination of absorptive shielding and directional isolation in addition to cross-polarization are assumed in the design of this antenna for this FD system.

Continued on next page

Table 1.1 – *Continued from previous page*

Year	Reference	Contribution	Assumption
2012	Knox [24]	Single antenna in FD communication for transmitting and receiving are connected via a circulator, in which up to 45 dB of isolation is obtained between the two channels for transmission with an insertion loss of 0.75 between the two paths.	A single microstrip antenna is used with a circulator for FD transmission in the same frequency band of $(902 - 928)$ MHZ for FD operation.
2014	Everett et al. [25]	Passive suppression is investigated by applying isolation techniques at the FD transceiver, such as using directional antennas, absorptive shielding and cross-polarization. The results reveal that more than 70 dB of passive suppression of SI can be achieved in particular circumstances.	Near-antenna reflection should be minimized to be applicable to FD. Moreover, all the suggested techniques are designed to mitigate the direct path of SI, while the indirect paths, that create frequency selective channels of SI, require active cancellation methods.
2015	Heino et al. [26]	Antenna design is presented with the passive suppression of SI for FD-MIMO systems, in which an attenuation of 40 dB is achieved, using a resonant wave-traps mechanism for a compact device. An additional 30 dB of radio frequency (RF) cancellation is achieved.	The proposed system can suppress only the linear components of SI perfectly, while the non-linear distortions of SI due to transmit/receive chains need more sophisticated algorithms.

Continued on next page

Table 1.1 – *Continued from previous page*

Year	Reference	Contribution	Assumption
2015	Laughlin et al. [27]	Hybrid junctions with electrical balance duplexer have been exploited to apply significant isolation between the transmit and receive terminals. This technique is proposed for small size devices and one antenna is used for transmission.	Dynamic adaptation is required to tackle the limited isolation bandwidth resulting from the impedance variation in the single antenna in both time/frequency domains, which causes sensitive transmit to receive isolation.
2016	Korpi et at. [28]	A novel antenna design for in-band FD relays and for different operational conditions. A high isolation of up to 70 dB between the transmit and receive antennas is achieved via wave-traps techniques for realistic multipath channels.	Transmitted power of up to 30 dB is assumed for transmission by using instantaneous bandwidths of 20 and 80 MHZ. Matching results are obtained in both a realistic environment and an anechoic chamber when the proposed antennas are examined.

After reducing the SI to an acceptable level using passive means, the conditions are suitable now to use the active suppression approaches by exploiting various means of signal processing for reduction of residual interference. This requires precise knowledge of the transmitted data along with the loop channel. In fact, perfect knowledge of the transmitted information is available at a transceiver operating in FD mode, but it is necessary to estimate the accurate SI channels. Thus, less error in SI channel estimation means better mitigation of SI [9]. One of the conventional methods which has been used in this area is based on the idea of using the known transmitted data with the estimated loop channel in order to replicate the interference signal. The latter can then be subtracted from the overall received signal which consists of the desired and SI signals. This scheme is called time-domain cancellation (TDC) [8, 9, 29]. In brief, passive SI reduction can be used in conjunction with active suppression approaches that exploit local knowledge of the transmitted data and loop channel information, in both analogue and digital domains, to remove SI. The latter needs to be accurately estimated in order to achieve successful

mitigation [9].

Cooperative communication utilizing either amplify-and-forward (AF), decode-and-forward (DF), equalize-and-forward (EF) or filter-and-forward (FF) relaying has recently gained increased attention due to its potential to enhance spectral efficiency and channel capacity, and to extend wireless coverage. The rates achievable under a limited transmit/receive dynamic range of FD-MIMO using DF relaying [13] and a bidirectional transceiver [14] have been studied in the presence of channel estimation errors, in which the maximization of the end-to-end (E2E) lower bound achievable rate based on a transmission scheme is proposed, which requires a non-convex optimization problem to be solved. The overall capacity of a FD-MIMO system based on AF relaying has been presented using an optimal transformation matrix that maximizes the mutual information under average power constraint at the relay output under the assumption of perfect channel estimation [30]. The latter work extends the results obtained by employing MIMO system instead of using a single antenna at each transmitter and receiver [3]. An alternative HD design has also been presented [31] in which an AF-relaying cooperative linear transceiver is analysed under perfect source-to-destination channel state information (CSI) aided by an applied optimization routine to maximize the mutual information in the transmission system. However, several studies in this area have used different algorithms to mitigate this problem, such as the design of an adaptive feedback canceller to try to restore the signal of interest blindly based on spectrum shaping [14] or adaptively directing the relay receiving array towards the minimum variance distortion-less response [32]. Additionally, an adaptive filter based on least mean-square has been proposed to track amplitude and phase variations in single channel transmission in order to create signal, with delay and frequency offset compensation for SI cancellation [33]. This idea might be upgraded to be suitable for multi-channel communication. Moreover, several space-time coding (STC) techniques have been proposed to tackle SI and improve the efficiency of this type of transmission operating in FD mode. One of the recent types of STC which has been proposed for FD relays is called distributed linear convolutional based STC. This has two schemes, the first of which scheme is exploited for entire SI cancellation, while the second is used for partial loop channel reduction where some of the interference signal might be exploited as self-coding [34]. Furthermore, several publications have studied and analysed numerically the performance of FD-MIMO relay systems in order to mitigate SI using various approaches in the presence and absence of perfect CSI in order to obtain the optimal signal-to-interference-plus-noise ratio (SINR) with respect to bit error

rate (BER) [13, 35, 36].

Furthermore, in order to make FD nodes more tolerant of channel impairments, FD-MIMO can be merged with orthogonal frequency division multiplexing (OFDM) in order to obtain the benefits of both techniques and consequently enhance the overall performance. OFDM is exploited in this area as one of the most important modulation and multiplexing schemes, which is extraordinarily robust against multipath fading. Thus, information with high data rates over frequency selective fading channels earn the ability to be transmitted and detected successfully by distributing and carrying the total high symbol rate over individual and orthogonal sub-carriers. Therefore, the signals will be more robust against channel impairments since this type of multiplexing scheme improves the data rate and reliability of transmission [10, 37]. At this stage, different approaches and algorithms have been proposed and implemented in the literature to tackle the SI actively in the analogue and digital domains. Major recent publications which reflect this interest are outlined briefly in Table 1.2.

Table 1.2: Major researches of active SIC

Year	**Reference**	**Contribution**	**Assumption**
2009	Riihonen et al. [38]	Spatial suppression via null-space projection (NSP) with minimum mean-square error (MMSE) filters applied as SIC for FD-MIMO based relay.	Linear receive and transmit filters for the estimated channel of loop-interference are applied to force the SI to zero at the FD-MIMO relay.
2010	Duarte et al. [17]	Experimental results show the feasibility of FD by applying an auxiliary RF transmit chain in which a cancellation signal is passed through in order to be subtracted from the overall incoming signal.	Bidirectional transceiver with two nodes is used, each of which is equipped with two antennas, one for transmitting and the other for receiving.

Continued on next page

Table 1.2 – *Continued from previous page*

Year	Reference	Contribution	Assumption
2011	Riihonen et al. [9]	TDC based on the subtraction of an SI replica from the overall incoming signal is presented. Moreover, spatial suppression is employed for SI mitigation by utilizing antenna subset selection and NSP.	MMSE filtering is utilized to maintain the quality of the signal of interest which may be affected by SIC.
2012	Riihonen et al. [10]	Analogue and digital filters are designed for SI suppression before and after the ADC, respectively. The FD-MIMO-OFDM transceiver is considered and its performance is analysed.	Non-ideal ADC with limited dynamic range is assumed. OFDM is used to overcome the frequency selectivity of the MIMO channel.
2012	Lopez-Valcarce et al. [39]	Adaptive algorithm is proposed, implemented and analysed for blindly restoring the spectrum shape of the desired signals.	FD-based AF-relay, and the carrier frequency used is an 842 MHZ with 8 MHZ OFDM signal.
2013	Bharadia et al. [6]	Active SIC is proposed in the analogue and digital domain for an FD single antenna transceiver-based circulator. The cancellation of linear and non-linear components of SI is achieved.	The overall cancellation in all domains can reach up to 110 dB.

Continued on next page

Table 1.2 – *Continued from previous page*

Year	Reference	Contribution	Assumption
2014	Korpi et al. [40]	Distortions occurring due to the non-linearity of the transmit/receive components are considered and analysed. Active SIC of up to 75 dB is achieved using RF and digital cancellation.	The dynamic range requirements for the ADC are taken into account. Transmitted power of (20-30) dBm is assumed.
2014	Duarte et al. [41]	Active analogue SIC along with passive suppression is presented for a multiple antenna wideband WiFi system. A parallel transmit chain is exploited to create a replica of the SI signal containing the non-linear effects of the transmit components.	Two transmitting antennas with one receiving antenna are utilized in each FD bidirectional node. Additionally, OFDM is used to mitigate the frequency selectivity of the channel.
2014	Bharadia et al. [42]	Novel designs of analogue and digital SIC circuits are proposed in order to attenuate the SI power to the level of the thermal noise floor of the receiver. A multi-tape analogue SIC circuit is designed in which fixed delays and variable attenuators are controlled adaptively.	Each antenna is connected to a circulator to ensure simultaneous transmit and receive. SIC achieves a reduction of 110 dB in SI power at a carrier frequency of 2.45 GHZ and 20 MHZ bandwidth.

Continued on next page

Table 1.2 – *Continued from previous page*

Year	Reference	Contribution	Assumption
2014	Li et al. [43]	Analogue SIC at the RF domain is followed by two iterative stages of digital SIC. Analytical and simulation results are demonstrated.	The distortion effects caused due to the non-ideal characteristics of the receive chain components are considered to be not a big problem after applying RF cancellation.
2015	Elsayed Ahmed el at. [44]	A novel digital SIC is proposed by passing the SI signal in the RF domain through an auxiliary receive chain to create an SI copy in the digital domain, which is then subtracted from the overall digital signal coming through the main receive chain.	The effect of the transmit/receive impairments is cancelled by using this algorithm, which achieves mitigation of SI approaching 3 dB above the noise floor of the receiver.
2015	Chen et al. [45]	A multi-stage SIC is proposed for a single antenna FD wireless transceiver, in which a circulator is employed to separate the transmitted and received signals. Two stages of passive suppression-based analogue SIC are implemented to remove the strongest paths of SI caused by antenna reflections, circulator leakages and other weaker multi-path reflections. Digital SIC is applied afterwards to mitigate the residual SI.	The overall SIC achievement over a bandwidth of 20 MHZ is 122 dB, in which 72 dB is obtained from the passive suppression and analogue SIC, while 50 dB is acquired from the digital domain SIC. The latter is exploited to remove the residual multi-path SI and the distorted SI components due to non-linearity impairments caused by the transmit/receive chains.

Continued on next page

Table 1.2 – *Continued from previous page*

Year	Reference	Contribution	Assumption
2016	Xiong et al. [46]	A channel estimation algorithm for FD-MIMO relays with large scale antenna arrays is presented in which the desired path and the SI channels are estimated simultaneously. A performance analysis of the proposed estimator is conducted for validation purposes.	The slowly-varying characteristics of the SI channel are exploited for estimation by utilizing the maximum-likelihood (ML) criteria and an expectation-maximization algorithm to minimize complexity.
2016	Antonio el al. [47]	Adaptive and blind SIC algorithms for DF and FF relay-based wideband FD-MIMO-OFDM are developed in which the spectral properties of the source signal are exploited to identify the SI channel.	The proposed algorithms can provide a level of residual SI below the noise floor of the FD-relay by using the samples (in time) for fewer OFDM symbols.

Furthermore, most of the recent state-of-the-art studies related to wireless FD communication have been reviewed elsewhere [1, 4, 5, 7], highlighting the most promising techniques for mitigating SI in different domains.

1.3 The Key Contributions of This Thesis

The key contributions of this thesis are to mitigate the residual SI remaining after applying different passive and active stages of SIC. This is due to the fact that all the techniques utilised in the literature for this purpose, as discussed earlier in this chapter, cannot thoroughly tackle the SI in the real world. Moreover, it is the first time to combine two techniques as MRC and NSP for the sake of enhancing the overall SINR of the proposed system. In this thesis, it is the first time to utilize channel coding techniques with IDD for FD-MIMO, in which the desired signals can be equalized and detected after applying further reduction of SI by exploiting an iterative approach. Additionally, it is worth men-

tioning that the techniques utilized in this thesis are in the digital domain, i.e. applied to the baseband signals, by assuming that the necessary aforementioned SIC approaches in the literature are employed in the RF and analogue/digital domains. Furthermore, the performance analyses of the proposed systems introduced in this thesis are evaluated in order to confirm the simulation results, in which the exact and tight upper bound expressions are obtained on the performance of the uncoded and coded FD systems, respectively.

1.4 Research Contributions and Thesis Organization

The aim of this research is to investigate FD capability in the context of wireless communication systems based on multiple antennas in the presence and absence of channel coding. Moreover, an extensive survey of past research work in this area is compiled, and a simulation test bench for numerical analysis and performance evaluation is implemented. Additionally, theoretical analysis and performance evaluation using the closed-form probability of error, outage probability and capacity solutions are presented. Furthermore, different methods for cancellation and detection are introduced in the presence of local generated SI.

The organization of this thesis is summarised as follows:

Chapter 2 introduces and explains the employment of the FD mode with multiple antenna transceivers. Different system models are described briefly, such as spatial multiplexing, precoding and diversity coding. Additionally, the reconstruction of transmitted symbols exploiting various equalization and detection methods is considered. Furthermore, SIC approaches are outlined and discussed, in which passive and active methods in both the analogue and digital domains are utilized to tackle the SI which accompanies with FD operation.

Chapter 3, discusses the joint utilization of NSP and MRC for an uncoded FD-MIMO relaying system in order to suppress the SI and to enhance the overall received power of the desired signal. Moreover, performance analyses of the proposed system are derived for two hops in the presence of channel estimation errors. In this chapter, the performance analysis is achieved by obtaining exact formulas for the probability density functions (PDF)s of the output SINR for each hop, followed by evaluating the outage probabilities, average-symbol-error rate (ASER) and finally the upper bound capacity of this system.

Chapter 4, gives an overview and discuses the structure of two of the most powerful linear channel coding schemes, which are the convolutional and turbo codes. Addition-

ally, the encoding representation and decoding algorithms are described in more detail. Furthermore, IDD for coded FD-SIMO is proposed and applied in the digital domain to provide an additional alleviation of the residual SI, which remains after applying different passive and active SICs. The purpose of using IDD as SIC is to achieve a level of performance that is very close to the SI-free case. Moreover, tight and union upper bounds of the proposed system are derived for the performance of rate-$1/2$ convolutional codes with quadrature phase shift keying (QPSK) modulation scheme in order to validate the simulation results.

In Chapter 5, IDD is exploited this time in the context of coded FD-MIMO to apply effective mitigation of the remaining SI in the digital domain. The aim is to achieve a level of performance very close to that of the SI-free scenario after a particular number of iterations. The proposed system is validated by deriving a tight upper bound on the performance of rate-1/2 convolutional codes with M-ary quadrature amplitude modulation (QAM). Further, an extrinsic information transfer (EXIT) chart is utilized as a semi-analytic tool to show how the IDD components are converging, when the soft information is exchanged between them. It also measures approximately the number of iterations required to satisfy this convergence.

In Chapter 6, the main conclusions of the research and the contributions of this thesis are presented, and proposed future work related to this field of study are outlined.

1.5 Publications Arising From This Research

- **Journal Papers**

1. **M. A. Ahmed**, C. C. Tsimenidis and A. F. Al Rawi, "Performance analysis of full-duplex-MRC-MIMO with self-interference cancellation using null-space-projection," in IEEE Transactions on Signal Processing, vol. 64, no. 12, pp. 3093-3105, June 2016.
2. **M. A. Ahmed** and C. C. Tsimenidis, "A tight upper bound on the performance of iterative detection and decoding for coded full-duplex SIMO systems," in IEEE Communication Letters., vol. 20, no. 3, pp. 606-609, March 2016.
3. **M. A. Ahmed** and C. C. Tsimenidis, "Tight upper bound performance of full-duplex MIMO-BICM-IDD systems in the presence of residual self-interference," submitted to IEEE Transactions on Wireless Communication, Dec. 2016.

- **Conference papers**

1. **M. A. Ahmed**, C. C. Tsimenidis and S. Y. Le Goff, "Performance analysis of full-duplex MIMO-SVD-SIC based relay in the presence of channel estimation errors," in Proc. IEEE 10th International Conference on Wireless and Mobile Computing, Networking and Communications (WiMob), Larnaca, 2014, pp. 467-472.
2. **M. A. Ahmed** and C. C. Tsimenidis, "Coded full-duplex MIMO with iterative detection and decoding," in Proc. IEEE International Conference on Communications (ICC), London, 2015, pp. 4859-4864.
3. **M. A. Ahmed**, C. T. Healy, A. F. Al Rawi, and C. C. Tsimenidis, "Bi-directional beamforming bit error ratio analysis for wireline backhaul networks," in Proc. 24th European Signal Processing Conference (EUSIPCO), Budapest, 2016.

Chapter 2

SIC Approaches for FD-MIMO Systems

2.1 Introduction

Recently, several research studies have been launched with the aim to mitigate SI in transceivers employing FD operation to complement the evolution of the next standard for wireless communications, the fifth generation (5G), and beyond. This is due to the fact that utilizing FD, where the transmitted and received signals use the same frequency band simultaneously, with perfect SIC can improve the spectral efficiency and the channel capacity by a factor of two with respect to systems using the conventional HD operation. However, implementing perfect SIC is impractical due to the large power differences between a weak desired signal coming from a distant source and the strong SI caused by the FD transceiver's transmitting antennas. This energy difference between the two signals might exceed tens of decibels (dBs), yielding difficulties in properly detecting the signal of interest. This is because the SI's power, which is roughly 100 dB above the noise floor of the receiver, causes saturation of the FD receivers' front-end components, such as the low noise amplifier (LNA), the mixer and ADC. Hence, these hardware components need to be designed in such a way that they are able to perform precise signal processing over a huge dynamic range, which consequently leads to an increase in the quantization noise of the desired signal. The suppression of SI can be implemented using different methods passively in the propagation domain and/or actively in the analogue and digital domains; that is, before and after the ADC respectively, as shown in Fig. 2.1. Additionally, utilizing the MIMO technique by using multiple antennas in both the transmitter and receiver, with any FD transceiver topologies, such as relay, bidirectional, or base-station, will provide the systems with an additional DoF in the suppression of SI via the employment of equalization methods like zero-forcing (ZF), MMSE filtering and NSP. Furthermore, employing multiple antennas for transmitting and/or receiving plays a vital role in combating fading without the need to expand the bandwidth of the transmitted signal by achieving spatial diversity. Moreover, utilizing a spatial multiplexing technique for wireless communications improves the date rate, since multiple uncorrelated spatial channels can be created to deliver the transmitted signal [48].

In this chapter, an overview of MIMO-based transmission is introduced with brief description and discussion of different systems models, such as spatial multiplexing, precoding and diversity coding. Moreover, various equalization and detection approaches are presented to recover the transmitted symbols. Furthermore, the background theory of applying FD mode to wireless communication systems is demonstrated, along with the

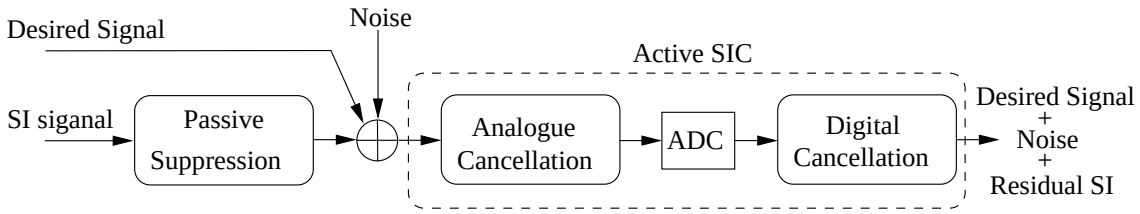

Figure 2.1: SIC stages for FD systems.

approaches exploited to mitigate the SI, which is associated with FD operation.

2.2 Multiple Antennas

The term MIMO is used to describe a communication system, in which the transmitter and receiver are equipped with N_{tx} and N_{rx} antennas, respectively, in order to create spatial uncorrelated MIMO channels to carry the transmitted information. The special case when $N_{tx} = N_{rx} = 1$ is called a single-input single-output (SISO) system and the channel created is called the SISO channel. The second special scenario is called single-input multiple-output (SIMO) when $N_{tx} = 1$ and $N_{rx} > 1$, which creates the SIMO channel, while the topology when $N_{tx} > 1$ and $N_{rx} = 1$ is called a multiple-input single-output (MISO), which creates the MISO channel.

For a MIMO system, as shown in Fig. 2.2, the impulse response of the channel between the m^{th} transmit antenna, where $m = 1, 2, ..., N_{tx}$, and the n^{th} receive antenna, in which $n = 1, 2, ..., N_{rx}$, can be denoted as $h_{n,m}(\tau; t)$ where τ and t represent the delay and time variables, respectively. Therefore, the entire MIMO channel can be denoted as a matrix of $N_{rx} \times N_{tx}$ random time-varying complex elements, i.e. $\mathbf{H}(\tau; t) \in \mathbb{C}^{N_{rx} \times N_{tx}}$,

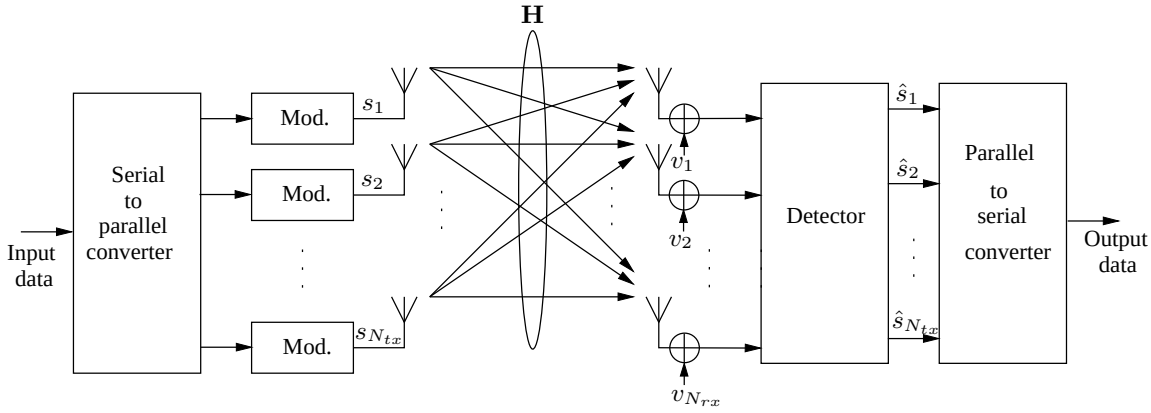

Figure 2.2: MIMO communication system with multiple transmit and receive antennas.

which can be defined as

$$\mathbf{H}(\tau;t) = \begin{bmatrix} h_{11}(\tau;t) & h_{12}(\tau;t) & ... & h_{1N_{tx}}(\tau;t) \\ h_{21}(\tau;t) & h_{22}(\tau;t) & ... & h_{2N_{tx}}(\tau;t) \\ \vdots & \vdots & & \vdots \\ h_{N_{rx}1}(\tau;t) & h_{N_{tx}2}(\tau;t) & ... & h_{N_{rx}N_{tx}}(\tau;t) \end{bmatrix}. \tag{2.1}$$

At a time instant t and for a signal transmitted from the m^{th} antenna, $s_m(t)$, and received by the n^{th} antenna, $r_n(t)$ can be expressed as

$$\begin{aligned} r_n(t) &= \sum_{m=1}^{N_{tx}} \int_{-\infty}^{\infty} h_{n,m}(\tau;t) s_m(t-\tau) d\tau + v(t), \\ &= \sum_{m=1}^{N_{tx}} h_{n,m}(\tau;t) * s_m(\tau) + v(t), \end{aligned} \tag{2.2}$$

where the mathematical process in the second equality of (2.2) represents the convolution, which is denoted by the asterisk symbol, and $v(t)$ is the AWGN with zero mean and variance σ_v^2. We can rewrite (2.2) using the matrix notation as

$$\mathbf{r}(t) = \mathbf{H}(\tau;t) * \mathbf{s}(\tau) + \mathbf{v}(t), \tag{2.3}$$

where $\mathbf{r}(t) \in \mathbb{C}^{N_{rx}\times 1}$, while $\mathbf{s}(t) \in \mathbb{C}^{N_{tx}\times 1}$ and $\mathbf{v}(t) \in \mathbb{C}^{N_{rx}\times 1}$. It is noteworthy that what has been discussed so far is for the case of a frequency-selective MIMO channel, that is when the coherent bandwidth of the channel is much smaller than the bandwidth of the transmitted signal. Thus, for a frequency-nonselective channel, sometimes referred to as a frequency-flat channel, that is when the coherent bandwidth of the MIMO channel is much larger than the bandwidth of the transmitted signal, the same equations (2.1)-(2.3) can be considered after omitting the delay index τ [48], as the signal has arrived at the receiver via one path only, and other paths are neglected due to the influence of scattering and attenuation [48, 49].

2.2.1 Maximum Ratio Combining

One of the techniques that can be exploited to satisfy a maximum available diversity gain is called maximum ratio combining (MRC) [50]. This approach can be applied to a MIMO system to obtain an optimum combining of the transmitted signals at the receiver, after passing through a MIMO channel in the presence of independent AWGN

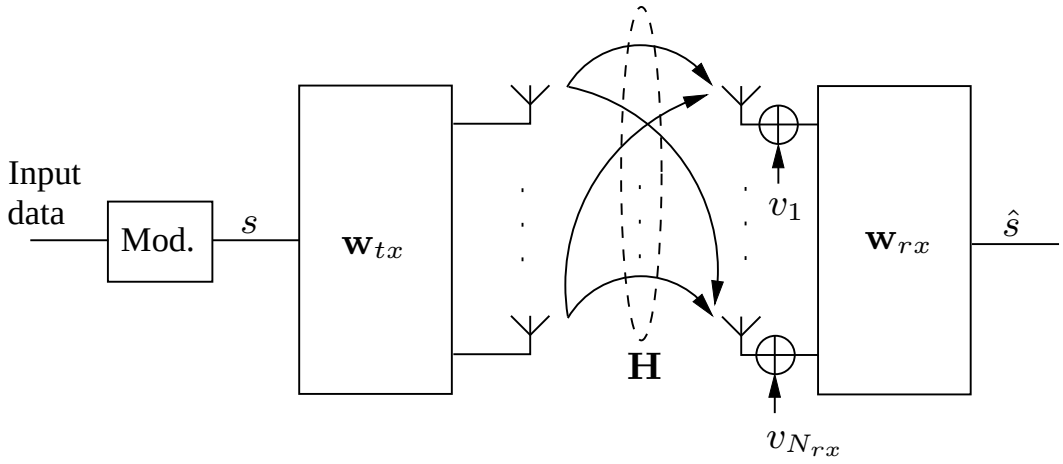

Figure 2.3: MRC-MIMO communication system.

and under circumstances of an interference environment. Moreover, perfect knowledge of the CSI is required to obtain optimum MRC performance. This can be satisfied either by applying beamforming weight vectors at the transmitter, the receiver, or both. These MRC weight vectors are chosen in such a way as to provide the reception of signals over the strongest path of the MIMO channel. In other words, this can be achieved by selecting the received signals that passed through a path of the eigenvector associated with the largest eigenvalue, λ_{max}, of the Wishart matrix of a MIMO channel $\mathbf{H}$, i.e. $\mathbf{H}^{\mathcal{H}}\mathbf{H}$ [51, 52]. For a wireless MIMO-MRC system equipped with N_{tx} transmit and N_{rx} receive antennas, as shown in Fig. 2.3, the received signal at time instant t can be expressed as

$$\mathbf{r}[t] = \mathbf{H}[t]\mathbf{w}_{tx}[t]s[t] + \mathbf{v}[t], \tag{2.4}$$

where $\mathbf{r}[t] \in \mathbb{C}^{N_{rx}\times 1}$ is the received vector, and $s[t]$ represents a complex transmitted symbol at time instant t which belongs to a single stream of transmitted data that converted to a vector when it passes through the transmit MRC beamforming weight vectors, $\mathbf{w}_{tx}[t] = \mathbf{u}_{\max}[t]$, in which $\mathbf{u}_{\max}[t]$ represents the unit norm corresponding to the largest eigenvalue $\lambda_{\max}[t]$ of the Wishart matrix $\mathbf{H}^{\mathcal{H}}[t]\mathbf{H}[t]$ as mentioned above, and for the unity Euclidean norm of $\mathbf{u}_{\max}[t]$, i.e. $\|\mathbf{u}_{\max}[t]\|^2 = 1$. Additionally, $\mathbf{v}[t] \sim \mathbb{CN}(0, \sigma_v^2\mathbf{I}_{N_{rx}})$ is the complex-valued AWGN. Furthermore, in order to reconstruct the transmitted symbol, the received MIMO signal, $\mathbf{r}[t]$, is to pass through the MRC weight vector at the receiver, which can be defined as $\mathbf{w}_{rx}[t] = \mathbf{H}[t]\mathbf{u}_{\max}[t]$. Therefore, the detected symbol can be

written as

$$\hat{s}[t] = \mathbf{w}_{rx}^{\mathcal{H}}[t]\mathbf{r}[t]. \tag{2.5}$$

2.2.2 Space-Time Block Codes

Space-time block coding (STBC) is an effective approach that can be employed to achieve transmit diversity gain, when other diversity means are not available due to various constraints such as the size limitation of the receiving device, which makes it difficult to position multiple receive antennas with sufficient separation in order to receive multiple replicas of the transmitted signal over different independent channels [49].

One of the schemes that can be utilized to obtain transmit diversity is called Alamouti STBC scheme. A MISO system of two transmit antennas and one receive antenna is required in order to implement this approach, in which two transmitted symbols from an M-ary PSK or QAM signal constellation, s_1 and s_2, can be transmitted in the first time instant from the first and second antennas, respectively. Meanwhile, in the second time slot, $-s_2^*$ is transmitted using the first antenna and s_1^* from the second one, in which the asterisk denotes here to the complex conjugate of a particular transmitted symbol. The generator code of Alamouti STBC can be expressed as

$$\mathbf{G}_{STBC} = \begin{bmatrix} s_1 & s_2 \\ -s_2^* & s_1^* \end{bmatrix}, \tag{2.6}$$

which is shown in Fig. 2.4 too. Moreover, the MISO channel for $N_{tx} = 2$ and $N_{rx} = 1$ can be defined as

$$\mathbf{H} = [h_{11} \;\; h_{12}]. \tag{2.7}$$

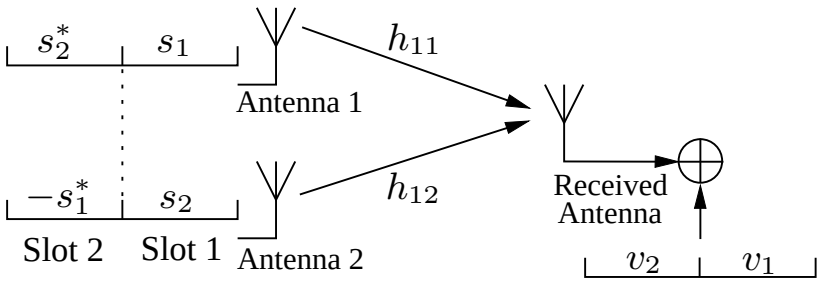

Figure 2.4: The Alamouti STBC MISO scheme.

Furthermore, by assuming that, during the two time slots the channel $\mathbf{H}$ is invariant, therefore the received signal in the successive time slots, i.e. r_1 and r_2, respectively, can be expressed as

$$r_1 = h_{11}s_1 + h_{12}s_2 + v_1, \tag{2.8a}$$

$$r_2^* = -h_{11}^*s_2 + h_{12}^*s_2 + v_2^*, \tag{2.8b}$$

where v_1 and v_2 represent an uncorrelated AWGN at the receiving antenna in the first and second time slots, respectively, with zero-mean and variance equal to σ_v^2. By assuming that the CSI is perfectly known by the receiver, the detected symbols $\hat{s}_1$ and $\hat{s}_2$ can be estimated using the optimum detector in which the probability of error is minimized as follows

$$(\hat{s}_1, \hat{s}_2) = \arg\max_{s_1,s_2}(s_1, s_2|\mathbf{r}, \mathbf{H}), \tag{2.9a}$$

$$(\hat{s}_1, \hat{s}_2) = \arg\max_{s_1,s_2}(s_1, s_2|\bar{\mathbf{H}}^{\mathcal{H}}\mathbf{r}, \mathbf{H}), \tag{2.9b}$$

where $\mathbf{r} = [r_1 \;\; r_2^*]^T$ and $\bar{\mathbf{H}}$ is defined as

$$\bar{\mathbf{H}} = \begin{bmatrix} h_{11} & h_{12} \\ h_{12}^* & -h_{11}^* \end{bmatrix}, \tag{2.10}$$

in which a one-to-one transformation is performed by multiplying the received symbols by $\bar{\mathbf{H}}^{\mathcal{H}}$ in order to equalize the effect of the MISO channel [53].

It is noteworthy that using this mechanism, where two time slots are allocated to transmit two symbols using two transmit antennas means that the overall transmission rate of Alamouti STBC scheme is one symbol, or $\log_2(M)$ bits, per channel use [48, 49].

2.3 Symbols Detection in MIMO Systems

Due to the inter-channel interference (ICI) which accompanies the utilization of spatial multiplexing for MIMO systems, the transmitted symbols from all antennas for a particular time instant overlap in time and frequency domains. Hence, in order to recover the transmitted symbols, various detection approaches can be utilized to produce a compensation for ICI. In this chapter, four of the most popular detectors are considered for MIMO systems, which are the ML, MMSE, ZF and detection by using SVD technique.

2.3.1 ML Detector

ML detection can be implemented by finding the minimum Euclidean distance between all the possible transmitted symbols over the channel $\mathbf{H}$ and the received signal as

$$\hat{\mathbf{s}}_{ML} = \arg\min_{\mathbf{s}\in\mathcal{S}} \|\mathbf{r} - \mathbf{H}\mathbf{s}\|^2, \tag{2.11}$$

where $\mathcal{S} = \{\alpha_1, \alpha_2, ..., \alpha_M\}$, $\alpha_\tau \in \mathbb{C}^{1\times M}$ represents a set of all possible symbols, $\mathbf{s}$, in the constellation of size $M = 2^m$, and m is the number of bits in each symbol. In other words, ML detection chooses the optimum symbol vector $\hat{\mathbf{s}}_{ML}$ that satisfies a minimum Euclidean distance metric, $\mu(\mathbf{s})$, as

$$\mu(\mathbf{s}) = \sum_{i=1}^{N_{rx}} \left| r_i - \sum_{j=1}^{N_{tx}} h_{ij} s_j \right|^2. \tag{2.12}$$

It is noteworthy that the ML detector performs optimum detection as the maximum *a posteriori* (MAP) detector when the transmitted symbols are equally likely [49]. On the other hand, an exponential increase in the complexity of detection occurs for any increase in the modulation order and/or the number of transmitting antennas [53].

2.3.2 MMSE Detector

The aim of MMSE detection is to minimize linearly the error between the actual transmitted signal and a combination of the received signal. This can be obtained by minimizing the mean square error (MSE) of the metric $J(\mathbf{w}_{MMSE})$ as

$$J(\mathbf{w}_{MMSE}) = \arg\min_{\mathbf{w}_{MMSE}} \mathbb{E}\{\|\mathbf{s} - \mathbf{w}_{MMSE}^{\mathcal{H}}\mathbf{r}\|^2\}. \tag{2.13}$$

The well-known optimum Wiener solution to equation (2.13) is given as [48, 49, 53]

$$\mathbf{w}_{MMSE} = [\mathbf{H}\mathbf{H}^{\mathcal{H}} + \sigma_v^2 \mathbf{I}_{N_{rx}}]^{-1}\mathbf{H}^{\mathcal{H}}, \tag{2.14}$$

where σ_v^2 is the noise variance as defined earlier in this chapter, and $\mathbf{I}_{N_{rx}}$ represents the identity matrix of dimensions $N_{rx} \times N_{rx}$. After evaluating the MMSE weight matrix for a known or estimated MIMO channel, it can be applied to the received signal in order to

obtain the estimate of the transmitted symbols as

$$\hat{\mathbf{s}} = \mathbf{w}_{MMSE}^{\mathcal{H}}\mathbf{r}. \tag{2.15}$$

2.3.3 ZF Detector

the ZF detector, also called the inverse-channel detector, is applied to satisfy a nullification of ICI by using one of the following weight matrices

$$\mathbf{w}_{ZF} = \begin{cases} \mathbf{H}^{-1} & \text{if } N_{tx} = N_{rx}, \\ (\mathbf{H}^H\mathbf{H})^{-1}\mathbf{H}^H & \text{if } N_{tx} < N_{rx}, \end{cases} \tag{2.16}$$

where, in the second case when $N_{tx} < N_{rx}$, the weight matrix is evaluated using the pseudoinverse of the MIMO channel $\mathbf{H}$. The ZF weight matrix is applied to the received signal in order to obtain the detected symbols as

$$\hat{\mathbf{s}} = \mathbf{w}_{ZF}\mathbf{r}. \tag{2.17}$$

2.3.4 Detection Using SVD Technique

All of the methods of detection discussed earlier depend on having knowledge about the CSI at the receiver. On the other hand, when the MIMO channel matrix is known to the transmitter in addition to the receiver, SVD can be utilized as a linear detection method. The SVD of a MIMO channel matrix $\mathbf{H}$ with rank R can be expressed as [48]

$$\mathbf{H} = \mathbf{U}\mathbf{\Sigma}\mathbf{V}^{\mathcal{H}}, \tag{2.18}$$

where $\mathbf{U} \in \mathbb{C}^{N_{rx}\times R}$, and $\mathbf{V} \in \mathbb{C}^{N_{tx}\times R}$ are unitary matrices, i.e. $\mathbf{U}^{\mathcal{H}}\mathbf{U} = \mathbf{I}_{N_{rx}}$ and $\mathbf{V}^{\mathcal{H}}\mathbf{V} = \mathbf{I}_{N_{tx}}$. Moreover, $\mathbf{U}$ and $\mathbf{V}$ have orthonormal column vectors. Additionally,

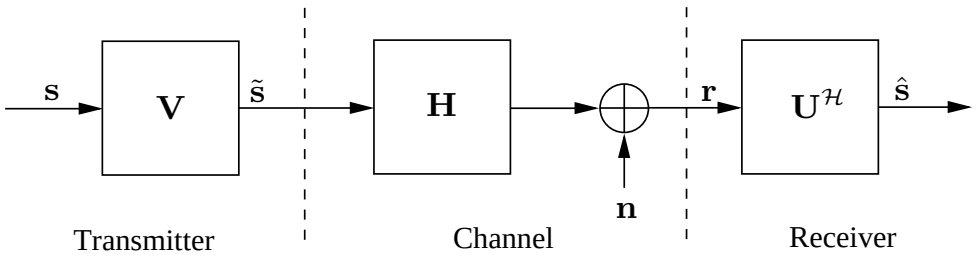

Figure 2.5: Singular-value decomposition as a linear transformation for signal detection in a MIMO system when the CSI is known to both transmitter and receiver.

the diagonal matrix $\mathbf{\Sigma} \in \mathbb{R}_{+}^{R \times R}$ contains the eigenvalues of the channel in descending order. As shown in Fig. 2.5, the linear transformation of the vector $\mathbf{s}$ is implemented at the transmitter as

$$\tilde{\mathbf{s}} = \mathbf{V}\mathbf{s}, \tag{2.19}$$

and the received signal can be expressed as

$$\mathbf{r} = \mathbf{H}\tilde{\mathbf{s}} + \mathbf{n} = \mathbf{H}\mathbf{V}\mathbf{s} + \mathbf{n}, \tag{2.20}$$

where $\mathbf{n}$ here represents the AWGN with zero-mean and variance equal to σ_n^2. The received signal is processed via passing through linear transformation, $\mathbf{U}^{\mathcal{H}}$ as

$$\hat{\mathbf{s}} = \mathbf{U}^{\mathcal{H}}\mathbf{r} = \mathbf{U}^{\mathcal{H}}\mathbf{H}\mathbf{V}\mathbf{s} + \mathbf{U}^{\mathcal{H}}\mathbf{n}, \tag{2.21a}$$

$$= \mathbf{U}^{\mathcal{H}}\mathbf{U}\mathbf{\Sigma}\mathbf{V}^{\mathcal{H}}\mathbf{V}\mathbf{s} + \mathbf{U}^{\mathcal{H}}\mathbf{n} = \mathbf{\Sigma}\mathbf{s} + \mathbf{U}^{\mathcal{H}}\mathbf{n}. \tag{2.21b}$$

It can be noticed that the detected signal, $\hat{\mathbf{s}}$, needs to be rescaled, as the transmitted signal appears, in the second equality of (2.21b), multiplied by the channel's singular values $\mathbf{\Sigma}$. Therefore, it can be compensated for by either applying the linear transformations $\mathbf{V}\mathbf{\Sigma}^{-1}$ at the transmitter or $\mathbf{\Sigma}^{-1}\mathbf{U}^{\mathcal{H}}$ at the receiver. It is worth noting that there are two main disadvantages associated with using SVD for MIMO detection. Firstly, full knowledge of CSI is required at the transmitter as well as the receiver, as mentioned earlier. The second issue is that employing SVD means that the signal diversity over the MIMO channel is not exploited in symbol detection [48].

2.4 OFDM for Frequency Selective Fading Channel

OFDM is considered to be as one of the best modulation and multiplexing techniques. It has been proposed and applied successfully to tackle the effects of frequency-selective fading channels [48]. This is due to the fact that OFDM has the ability to carry high data rates over orthogonal subcarriers. In other words, OFDM can convert the wideband signal, whose bandwidth is greater than the coherent bandwidth of the channel, to several narrowband signals each of which has a smaller bandwidth than the coherent bandwidth of the channel. This can be implemented by exploiting digital signal processing techniques such as the inverse fast Fourier transform (IFFT), which is utilized for the purpose of

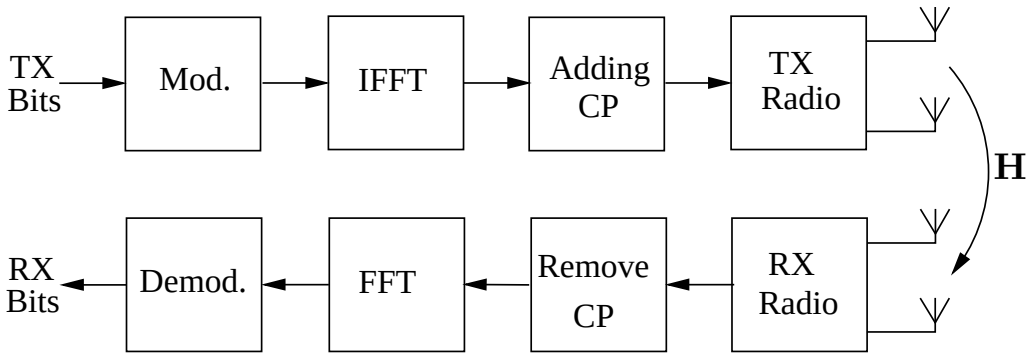

Figure 2.6: Block diagram of OFDM transmitter (up) and OFDM receiver (down) utilizing IFFT/FFT along with adding/removing the CP, respectively.

implementing the evaluation of the inverse discrete Fourier transform (IDFT) efficiently [53]. OFDM is considered to be one of the most efficient and robust mechanisms utilized to tackle the effects of the frequency selectivity of channels, significantly improving the spectrum efficiency and mitigating inter-symbol interference (ISI). This is because by using OFDM, a high data rate signal can be carried over these overlapping orthogonal subcarriers with lower data rates. Additionally, OFDM reduces the complexity and cost of the receiver circuit, as the fast Fourier transform (FFT) with a one-tap equalizer is adequate to detect a signal passed over a multipath channel. These properties mean that the OFDM can outperform other modulation techniques such as conventional frequency division multiplexing (FDM) and single carrier modulation [48]. Additionally, the cyclic prefix can be added to the OFDM frame to tackle the effect of the delay spread of the channels. Fig. 2.6 shows a block diagram of the OFDM transmitter and receiver utilizing IFFT/FFT, along with adding or removing the cyclic prefix, respectively.

On the other hand, there are some disadvantages which reduce the overall performance of the OFDM, which are outside of the scope of this thesis, such as the sensitivity to phase noise and symbol timing, or so-called carrier frequency offset. This problem leads the local oscillators in both the transmitter and receiver to lose synchronization, which consequently leads to both ISI and ICI being produced due to the corruption impacting the orthogonality between subcarriers [54]. Furthermore, the problem of the peak-to-average power ratio (PAPR) can significantly influence the efficiency of the power amplifier in the RF stage.

The mathematical description of the IFFT can be expressed as [48]

$$s_n = \frac{1}{N}\sum_{k=0}^{N-1} S_k \exp(\frac{j2\pi kn}{N}), \quad n = 0, 1, ...N-1, \tag{2.22}$$

where S_k represents the baseband signal which can be modulated by utilizing a modulation scheme as M-ary QAM, or M-ary phase-shift keying (PSK) scheme, N is the number of subcarriers for a particular OFDM frame, while n and k represent the discrete indices for time and frequency, respectively. On the other hand, FFT operation is required at the receiver in order to demodulate the OFDM signal, and this process can be expressed as [48]

$$S_k = \frac{1}{N}\sum_{k=0}^{N-1} s_n \exp(\frac{-j2\pi kn}{N}), \quad n = 0, 1, ...N-1. \tag{2.23}$$

For wideband MIMO channels which suffer from frequency selectivity, OFDM can be exploited to process each subcarrier separately using MIMO processing algorithms, since the characteristics of the channel fading for each frequency bin can be considered as a flat fading or as a narrow-band channel [50]. Furthermore, the SIC approaches applied to FD-MIMO systems with narrow-band MIMO channels, as discussed later in this chapter and the following chapters, can be employed efficiently for wideband MIMO channels as long as OFDM with an appropriate length of cyclic prefix is utilized [9].

2.5 Self-interference Cancellation Approaches

2.5.1 Passive SI Suppression

Passive suppression methods of SI rely on separation between the transmit and receive antennas in order to increase the isolation loss amongst them electromagnetically in the propagation domain and hence, reduce the magnitude of the local interference. Different approaches have been proposed and implemented for this purpose in this domain to increase the path loss and diminish and block the LoS path. This is achieved basically by orienting the transmitting antenna elements to the opposite direction from those of the receiving antennas, which consequently maximizes the loop-interference attenuation by increasing the insertion loss. The latter can be further increased by utilizing orthogonal polarization schemes [8, 9, 15, 16, 55].

Furthermore, passive suppression has been proposed at the receiver front-end by using different techniques such as natural-isolation via antenna separation and absorptive shielding, cross-polarization, directional isolation, antenna-aid cancellation and RF circulator-based passive suppression [1, 4, 7, 25]. All of these techniques are implemented primarily

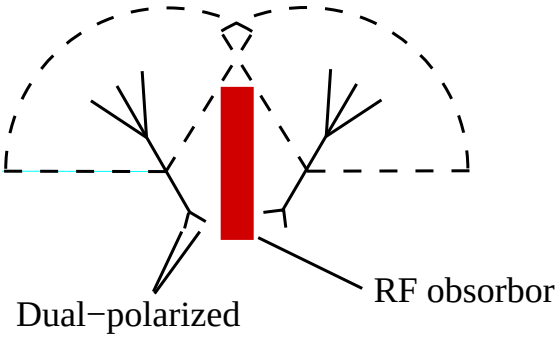

Figure 2.7: Passive suppression of SI using orthogonal polarization, directional isolation and absorptive shielding.

to avoid the impractical huge dynamic range required to process the received signals accurately in the front-end of the downstream receiver circuitry.

In practice, natural-isolation via antenna separation can be implemented by increasing the distance between the antennas of the transmitting and receiving terminals so as to attenuate the SI signal via increasing the free-space path loss, which can be expressed as [48]

$$L_P = \left(\frac{\lambda}{4\pi d}\right)^2, \tag{2.24}$$

where d represents the distance between the transmit and receive antennas, λ is the wavelength of the transmitted signal which can be calculated as $\lambda = c/f$, in which $c = 3 \times 10^8\ (m/s)$ is the speed of light, and f is the frequency of the transmitted signal. It can be noticed from (2.24) that d is inversely proportional to the path loss for a particular frequency. Additionally, natural-isolation can be performed by using absorption shielding to be placed in order to attenuate the LoS path [25, 55] as shown in Fig. 2.7.

An additional SI suppression can be implemented by utilizing a cross-polarization technique, sometimes also referred to as orthogonal polarization. This electromagnetic isolation mechanism can be performed via designing the antennas of the transmit and receive chains of the FD transceiver with orthogonal polarization so that transmit and receive using vertical and horizontal polarization, respectively, or vice versa [4, 56]. Moreover, directional isolation techniques can be employed via orienting the two sets of transmit and receive antennas of a FD node to the directions that a null zone can be produced, or at least a minimal intersection, between the main lobes of the radiation patterns [25, 57], as shown in Fig. 2.7. Furthermore, passive suppression can be achieved by utilizing antenna-aid cancellation which can be summarized as employing three antennas, two for

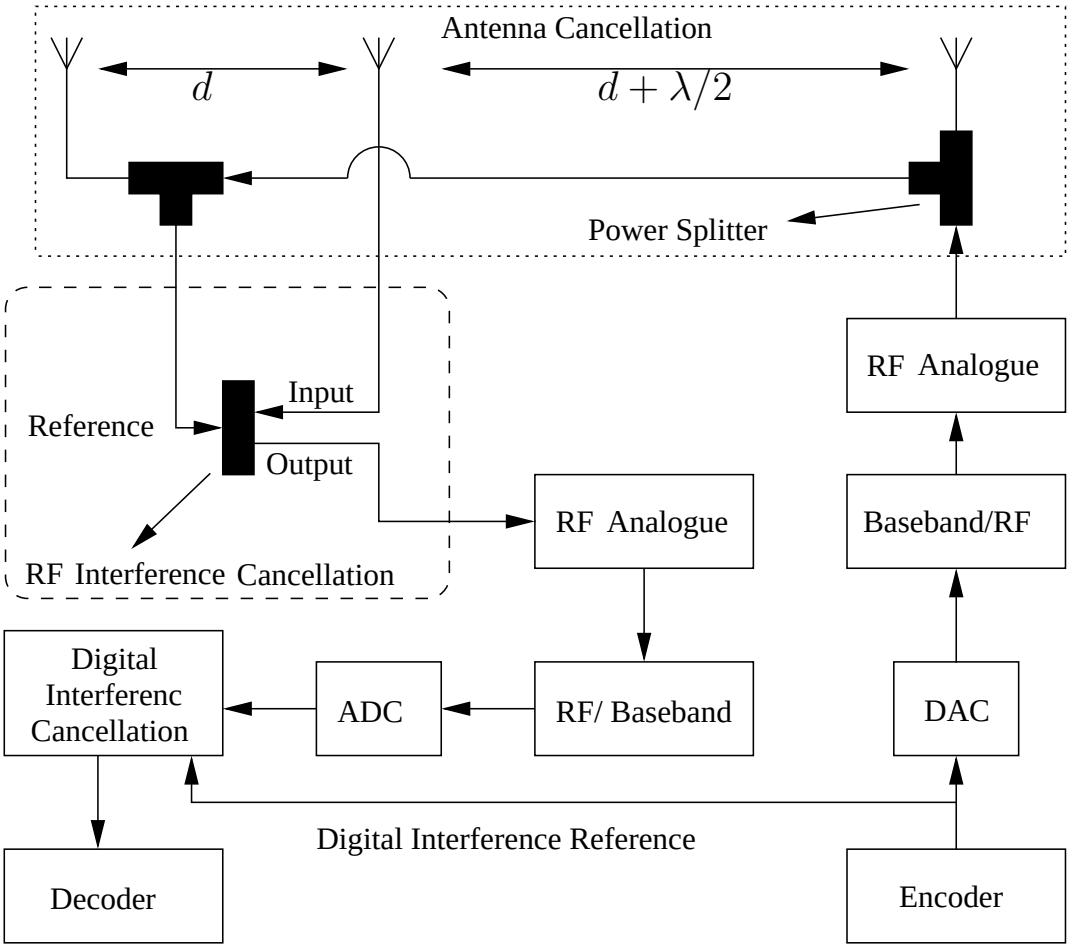

Figure 2.8: Antenna Cancellation

transmitting and one for receiving, in such a way that the two transmit antennas are positioned away from the single receive antenna by distances of d and $d + n\lambda/2$, where n is an odd number, in order to satisfy the conditions for destructive interference, as shown in Fig. 2.8. This is because these distances will result in a phase difference of π between the two transmitted signals at the received antenna; hence, they cancel each other out [7, 56]. Similarly, this out-of-phase signal can be created internally in the FD transceiver and coupled with the SI estimated channel in order to cancel the SI signal in the analogue domain [55, 56], as discussed later in this chapter. In the propagation domain, passive suppression can also be implemented via utilizing a circulator-based technique. This technique is considered to be one of the best types of passive suppressions of SI [45], particularly for FD transceivers employing shared antennas for transmitting and receiving. The circulator is an electromagnetic device which can be exploited in the RF and microwave bands. This device contains three ports 1 to 3, that allow signals to pass through successive ports only, providing limited isolation in the other direction as shown in Fig 2.9. For instance, if the transmit and receive terminals are connected to ports 1 and

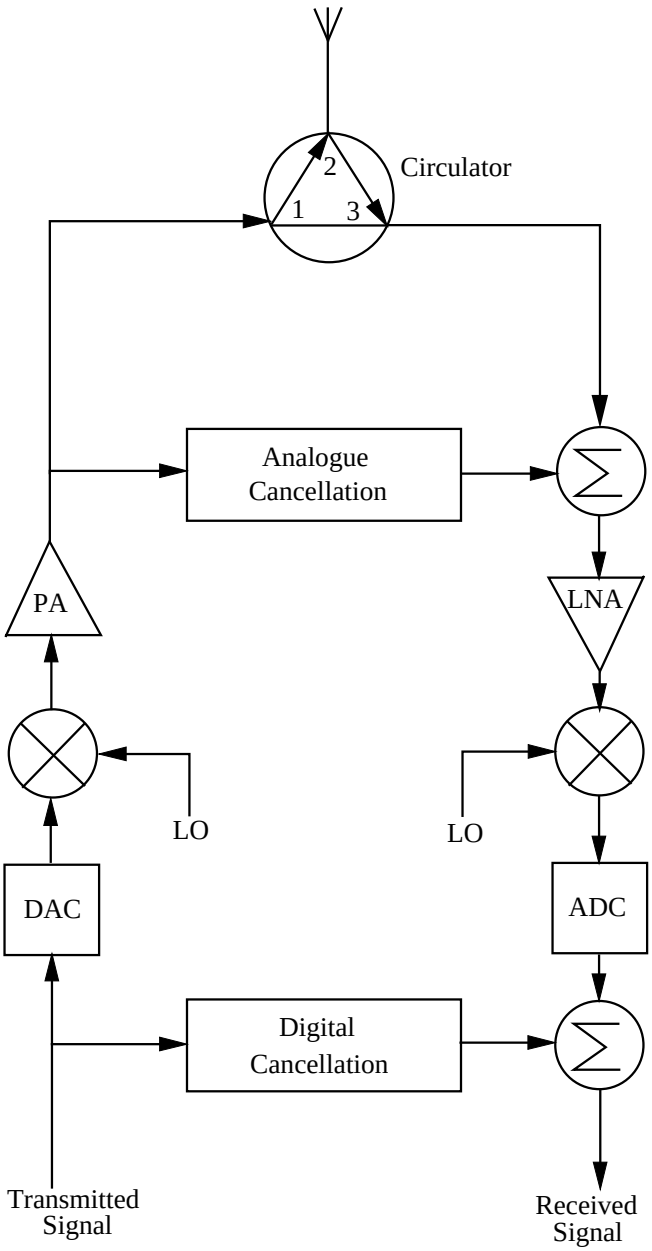

Figure 2.9: FD transceiver utilizes Circulator along with analogue and digital cancellations.

3, respectively, and the antenna is connected to port 2, then the transmitted signals are passed to the antenna through port 2 without allowing them to pass to port 3, while the signals received by the antenna are passed from port 2 to port 3 and the path towards port 1 is blocked. However, this device is unable to provide complete separation between the non-sequential ports, which means that valuable leaks of the transmitted signals might be passed to the receive circuitry, causing SI.

In fact, all the means of passive suppression discussed above are unable to combat SI in its entirety; hence, other stages of SIC are required to be performed actively in the analogue and digital domains in order to obtain efficient FD systems with lower complexity,

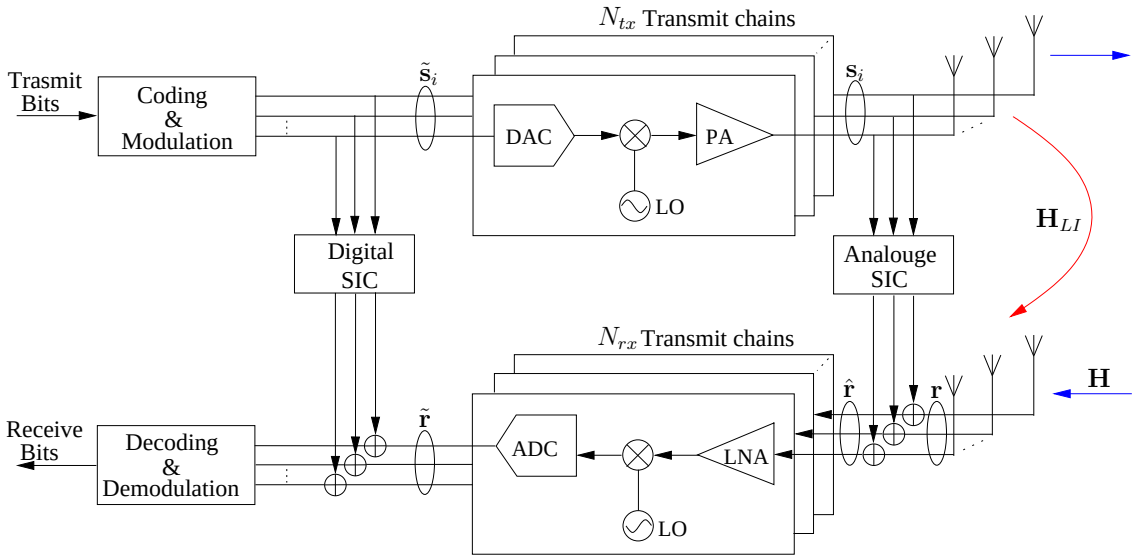

Figure 2.10: Self-interference cancellation stages for FD-MIMO system.

minimum BER, and an acceptable throughput which outperforms the conventional HD technique.

2.5.2 Active SIC

Active SIC is proposed to implement further reductions of SI power in order to be at the level of noise or below. This is due to the fact that all the methods of passive suppressions mentioned in Section 2.5.1 are in practice unable to provide a total mitigation of SI in the real-world. Hence, for the sake of further minimization of SI, other stages of SIC can be performed either within the RF stage and/or in the baseband stage, i.e. the analogue and digital domains [7]. Fig. 2.10 shows a FD-MIMO transceiver which can be a relay or bidirectional transceiver utilizing FD operation and equipped with N_{tx} and N_{rx} antennas in the transmit and receive terminals, respectively. For a continuous time instant t, the analogue received signal at the received terminal of the FD transceiver can be expressed as

$$\mathbf{r}[t] = \mathbf{H}[t]\mathbf{s}_o[t] + \mathbf{H}_{LI}[t]\mathbf{s}_i[t] + \mathbf{v}[t], \tag{2.25}$$

where $\mathbf{H}[t] \in \mathbb{C}^{N_{rx}\times N_{tx}}$, and $\mathbf{H}_{LI}[t] \in \mathbb{C}^{N_{rx}\times N_{tx}}$ represent the desired and SI channels, respectively. Moreover, $\mathbf{v}[t] \in \mathbb{C}^{N_{rx}\times 1}$ is the AWGN vector at the input of the received terminal of the FD transceiver, with zero mean and variance equal to σ_n^2. The covariance matrix of the noise is denoted as $\mathbf{R}_\mathbf{v} = \mathbb{E}\left\{\mathbf{v}[t]\mathbf{v}^{\mathcal{H}}[t]\right\}$. Additionally, $\mathbf{s}_o[t]$ represents the desired incoming signal from a distant source, while $\mathbf{s}_i[t]$ is the LI signal causing

SI. The covariance matrices of the desired and the SI signals can be denoted as $\mathbf{R}_{\mathbf{s}_o} = \mathbb{E}\left\{\mathbf{s}_o[t]\mathbf{s}_o^{\mathcal{H}}[t]\right\}$ and $\mathbf{R}_{\mathbf{s}_i} = \mathbb{E}\left\{\mathbf{s}_i[t]\mathbf{s}_i^{\mathcal{H}}[t]\right\}$, respectively.

Some information is required to be fully or partially known by the FD transceiver in order to implement active SIC. For instance, $\mathbf{s}_i[t]$ should be known by the FD transceiver itself, while $\mathbf{H}[t]$ and $\mathbf{H}_{LI}[t]$ can be particularly estimated by utilizing one of the techniques proposed for FD transceivers [58, 59]. Furthermore, channel estimation noise might be produced due to the impractical implementation of perfect channel estimation in the real-world. Therefore, the estimations of $\mathbf{H}[t]$ and $\mathbf{H}_{LI}[t]$, which are $\tilde{\mathbf{H}}[t]$ and $\tilde{\mathbf{H}}_{LI}[t]$, respectively, can be expressed as

$$\tilde{\mathbf{H}}[t] = \mathbf{H}[t] - \boldsymbol{\Delta}\tilde{\mathbf{H}}[t], \tag{2.26a}$$

$$\tilde{\mathbf{H}}_{LI}[t] = \mathbf{H}_{LI}[t] - \boldsymbol{\Delta}\tilde{\mathbf{H}}_{LI}[t], \tag{2.26b}$$

where $\boldsymbol{\Delta}\tilde{\mathbf{H}}[t] \sim \mathbb{CN}(0, \sigma^2_{\boldsymbol{\Delta}\mathbf{H}}\mathbf{I}^{N_{rx}\times N_{tx}})$ and $\boldsymbol{\Delta}\tilde{\mathbf{H}}_{LI}[t] \sim \mathbb{CN}(0, \sigma^2_{\boldsymbol{\Delta}\mathbf{H}_{LI}}\mathbf{I}^{N_{rx}\times N_{tx}})$ represent the estimation errors of $\mathbf{H}[t]$ and $\mathbf{H}_{LI}[t]$, respectively. Moreover, the variances of these estimation errors are defined as [9]

$$\sigma^2_{\boldsymbol{\Delta}\mathbf{H}} = \mathbb{E}\left\{ \left| \left\{\boldsymbol{\Delta}\tilde{\mathbf{H}}[t]\right\}_{i,j} \right|^2 \right\} = \epsilon_{\boldsymbol{\Delta}\mathbf{H}}\mathbb{E}\left\{ \left| \left\{\boldsymbol{\Delta}\mathbf{H}[t]\right\}_{i,j} \right|^2 \right\} \forall\, i,j, \tag{2.27a}$$

$$\sigma^2_{\boldsymbol{\Delta}\mathbf{H}_{LI}} = \mathbb{E}\left\{ \left| \left\{\boldsymbol{\Delta}\tilde{\mathbf{H}}_{LI}[t]\right\}_{i,j} \right|^2 \right\} = \epsilon_{\boldsymbol{\Delta}\mathbf{H}_{LI}}\mathbb{E}\left\{ \left| \left\{\boldsymbol{\Delta}\mathbf{H}_{LI}[t]\right\}_{i,j} \right|^2 \right\} \forall\, i,j, \tag{2.27b}$$

where $\epsilon_{\boldsymbol{\Delta}\mathbf{H}}$ and $\epsilon_{\boldsymbol{\Delta}\mathbf{H}_{LI}}$ are the relative estimation errors of $\mathbf{H}$ and $\mathbf{H}_{LI}$, respectively.

Despite full knowledge of the digital transmitted signal in the baseband being known by the FD transceiver, the actual analogue bandpass signal can not be precisely known. This is due to the effects of different distortions that accompany the conversion of a digital baseband signal to RF, such as the nonlinearity power amplifier (PA), the in-phase/quadrature (I/Q) imbalance of the local oscillator (LO), the imperfection of ADC and digital-to-analogue conversion (DAC), in addition to the phase noise and frequency offset associated with the carrier oscillator [9]. Therefore, after taking into account all the above imperfections, the transmitted signal can be expressed as

$$\mathbf{s}_i = \tilde{\mathbf{s}}_i + \boldsymbol{\Delta}\tilde{\mathbf{s}}_i, \tag{2.28}$$

where $\boldsymbol{\Delta}\tilde{\mathbf{s}}_i$ represents the additive transmit distortion noise with zero-mean and variance equal to the relative distortion $\epsilon_{\mathbf{s}_i}$. Moreover, the transmit noise covariance matrix can be

defined as

$$\mathbf{R}_{\mathbf{\Delta}\tilde{\mathbf{s}}_i} = \epsilon^2_{\mathbf{s}_i} \frac{\text{tr}\{\mathbf{R}_{\tilde{\mathbf{s}}_i}\}}{N_{tx}} \mathbf{I}, \tag{2.29}$$

where $\mathbf{R}_{\mathbf{\Delta}\tilde{\mathbf{s}}_i} = \mathbb{E}\{\mathbf{\Delta}\tilde{\mathbf{s}}_i \mathbf{\Delta}\tilde{\mathbf{s}}_i^{\mathcal{H}}\}$ and $\mathbf{R}_{\tilde{\mathbf{s}}_i} = \mathbb{E}\{\tilde{\mathbf{s}}_i \tilde{\mathbf{s}}_i^{\mathcal{H}}\}$ are uncorrelated, which consequently leads to $\mathbf{R}_{\mathbf{s}_i} = \mathbb{E}\{\mathbf{s}_i \mathbf{s}_i^{\mathcal{H}}\} = \mathbf{R}_{\tilde{\mathbf{s}}_i} + \mathbf{R}_{\mathbf{\Delta}\tilde{\mathbf{s}}_i}$. It is worth mentioning that the time index t has been omitted from (2.28) and beyond for the purpose of the clarity of the notation.

The main purpose of applying SIC approaches to FD transceivers is to mitigate the loop interference in order to minimize the residual SI to a level that can be considered as additional noise at the input of the FD transceiver [9]. Therefore, (2.25) can be re-written as

$$\hat{\mathbf{r}} = \mathbf{H}\mathbf{s}_o + \hat{\mathbf{v}}, \tag{2.30}$$

where $\hat{\mathbf{r}} \in \mathbb{C}^{N_{rx} \times 1}$ and $\hat{\mathbf{v}} \in \mathbb{C}^{N_{rx} \times 1}$ are the vectors of the received signal and the equivalent noise at the input of the FD receiver after applying passive and analogue SIC, as shown in Fig. 2.10. Furthermore, the MSE matrix can be extracted from (2.25) as

$$\begin{aligned} \mathbf{M} &= \mathbb{E}\{(\mathbf{H}\mathbf{s}_o + \mathbf{v} - \mathbf{r})(\mathbf{H}\mathbf{s}_o + \mathbf{v} - \mathbf{r})^{\mathcal{H}}\} \\ &= \mathbb{E}\{\mathbf{H}_{LI}\mathbf{s}_i\mathbf{s}_i^{\mathcal{H}}\mathbf{H}_{LI}^{\mathcal{H}}\} = \mathbf{H}_{LI}\mathbf{R}_{\mathbf{s}_i}\mathbf{H}_{LI}^{\mathcal{H}}. \end{aligned} \tag{2.31}$$

Moreover, the power of the SI can be determined from (2.31) by taking the trace of $\mathbf{M}$ as

$$\begin{aligned} P_{SI} = \text{tr}\{\mathbf{M}\} &= \mathbb{E}\{\text{tr}\{\mathbf{H}_{LI}\mathbf{s}_i\mathbf{s}_i^{\mathcal{H}}\mathbf{H}_{LI}^{\mathcal{H}}\}\} \\ &= \mathbb{E}\{||\mathbf{H}_{LI}\mathbf{s}_i||_2^2\} \end{aligned} \tag{2.32}$$

2.5.2.1 Analogue SIC

The cancellation at this stage is based on TDC as discussed briefly in Chapter 1. It basically depends on the assumption that the FD transceiver always has exact or approximate knowledge about its own transmitted signal. Moreover, it is required that the FD transceiver has the ability to estimate the SI channel in order to create a replica of the SI signal and then to subtract it from the received signal. The importance of implementing SIC in the analogue domain is to reduce the dynamic range of the receiving circuity to a suitable level in order to improve the feasibility of applying SIC in the digital domain.

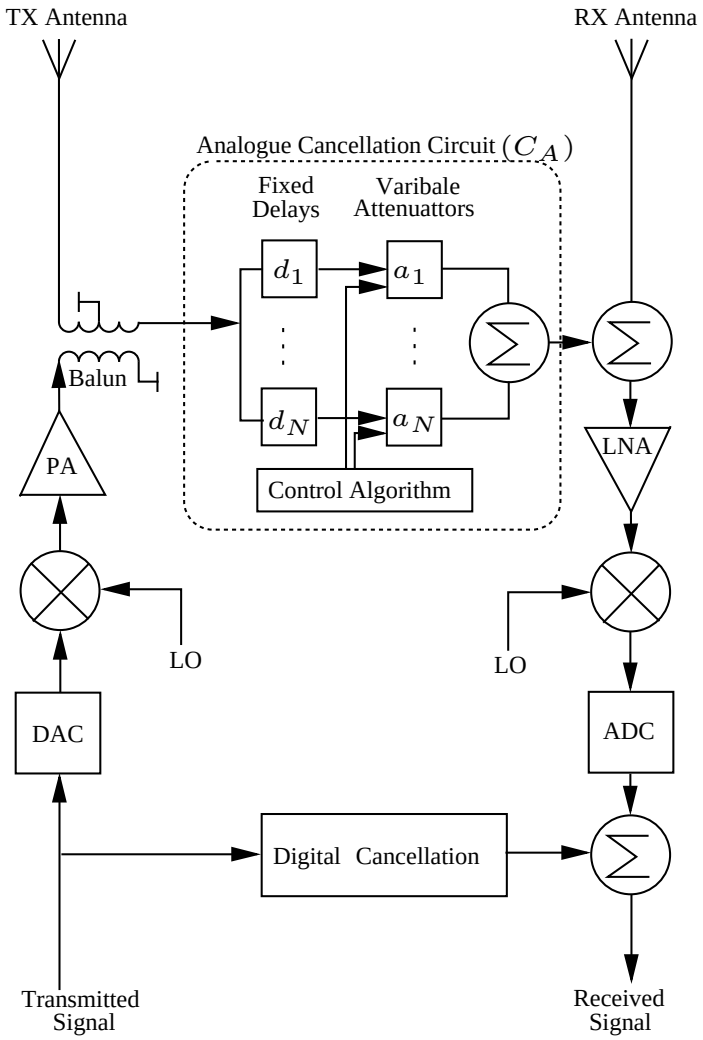

Figure 2.11: Analogue SIC circuit for FD transceiver with Balun circuit.

However, it is impractical to implement electronically an analogue circuit that can remove all the SIC components, especially in the case of multipath channels, since this requires the design of an expensive and complicated circuit to perform this task [9].

Analogue SIC can be implemented simply by passing a small replica of the transmitted signal, either by using an RF power splitter or a balanced/unbalanced (Balun) transformer. The latter is a popular RF component that can be utilized to convert forwards and backwards between the input signal and its inverse at any time instance. Fig. 2.11 shows the Balun circuit which forwards the original transmitted signal to the TX antenna, while a negative copy is sent to the analogue SIC circuit in order to reconstruct an inverse copy of the SI to be added to the entire incoming signal [7,60]. The output of the Balun circuit, which also includes the noise yielded by the transmitter chain, passes through the analogue cancellation circuit which consists of N parallel branches each of which contains a particular fixed delays connected serially to a controlled tunable attenuators. A summa-

tion is then used to merge all the N branches to create a negative copy of the transmitted signal similar to the one which arrived at the receive terminal after passing through the real multipath channel causing SI. An addition operation is required at this stage between the two signals in order to extract the signal of interest, as shown in Fig. 2.11. It is worth mentioning that the notation C_A is used to refer to the analogue SIC circuit illustrated in this figure and thereafter in this thesis.

The crucial issue in this analogue circuit is to choose precisely and adaptively the n^{th} fixed delay, d_n, in each branch, where $1 \leq n \leq N$, along with its attenuation value, a_n, that minimizes the effect of the SI to an acceptable level [6, 42, 45]. One of the approach which has been proposed is to position half of the fixed delay lines, i.e. $N/2$, with equidistant time intervals, at delays are less than the delay of the SI, d [6]. The same procedure is used for the second half of these delay lines except that they are placed at delays greater than d, as shown for example in Fig. 2.12. In practice, the value of d is not easy to determine precisely, as it is related to the characteristics of each component in the FD transceiver circuit and how these components are connected together. Therefore, it is required to estimate the range within which this delay varies, and then to position the fixed delay lines out of this range in each side, as explained earlier; that is, before and after this range.

At this point, the weights of the leading and lagging copies of the SI signal must be determined. This can be implemented by utilizing the *sinc interpolation* algorithm, in which, at each sampling time instant, sinc pulses are overlaid in order to evaluate the weights of the sinc pulses that the SI signal requires in order to be recreated. The obtained weights, which are associated with each sample of the SI signal, are combined afterwards by employing linear combination to create a replica of the SI signal.

Fig. 2.12 illustrates this algorithm, whereas in order to estimate the SI signal at time instant d, even fixed delays, $\{d_1, d_2, ..., d_N\}$, are required to be used in which $\{d_1, ..., d_{N/2}\}$ are positioned at delay instants less than d, while the delay lines $\{d_{N/2+1}, ..., d_N\}$ should be placed at delay instants greater than d. The attenuator value a_n at a delay line d_n can be determined by choosing the value of the SI sinc pulse, which is centred at the delay d, at the centre of a delay sinc pulse d_n to be the weight a_n of that fixed line delay. In the example shown in Fig. 2.12 it is assumed that the number of fixed delay lines is 6. Ideally, after evaluating and setting all the weights of these delay lines, the SI signal can be reconstructed perfectly and suppressed at this stage of the FD receiver. However, this requires a large number of delays to achieve the perfect cancellation of SI, which is im-

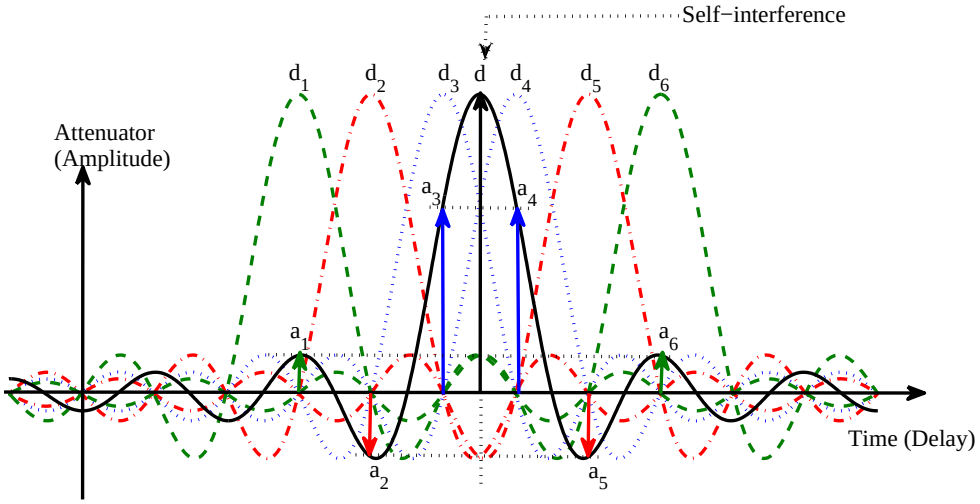

Figure 2.12: Sinc interpolation algorithm to evaluate the weights of the fixed delay lines of the analogue cancellation of SI in Fig. 2.11.

practical due to the limitations of circuit size, power consumption, complexity and the time required to retune this circuit for any change in the circumstances. This is because, during the tuning of this circuit to a particular SI signal, it is not feasible to operate the radio in the FD mode, and thus it is necessary to minimize the tuning time by minimising the delay lines to an acceptable number in order to reduce the number of variables which need to be estimated [6, 42]. This approach can be utilized to apply analogue SIC for a MIMO system in which, at each transmit chain, part of the transmitted signal is passed through an analogue SIC circuit, $\mathbf{C}_A \in \mathbb{C}^{N_{tx} \times N_{rx}}$, to create a copy of the SI signal, and then the output of the analogue SIC circuit is subtracted from the incoming signal at each receiving chain in the RF domain, as shown in Fig. 2.13. Mathematically, this process in the analogue domain can be expressed as

$$\hat{\mathbf{r}}[t] = \mathbf{r}[t] - \mathbf{C}_A \, \mathbf{s}_i[t] \tag{2.33}$$

where $\mathbf{r}[t] = \mathbf{H}[t]\mathbf{s}_o[t] + \mathbf{H}_{LI}[t]\mathbf{s}_i[t] + \mathbf{v}[t]$ represents a combination of the desired signal $\mathbf{s}_o[t]$ coming from a distant source over a MIMO channel $\mathbf{H}[t]$, the SI signal $\mathbf{s}_i[t]$ which passed through the SI channel $\mathbf{H}_{LI}[t]$, in addition to the additive thermal noise $\mathbf{v}[t]$. This means that by choosing $\mathbf{C}_A = \mathbf{H}_{LI}[t]$, SI can be removed totally if perfect knowledge of $\mathbf{H}_{LI}[t]$ is available. It is worth mentioning that the notations $[t]$ and $[n]$ in Fig. 2.13 are

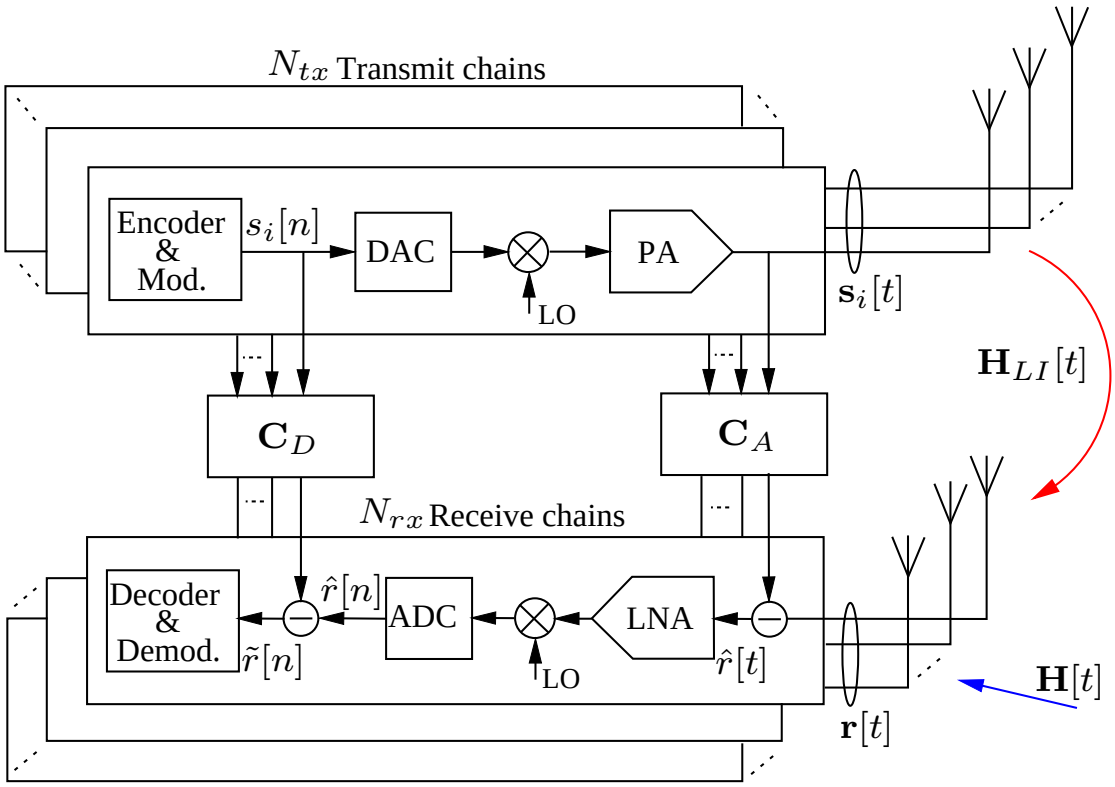

Figure 2.13: FD-MIMO transceiver with analogue cancellation filter ($\mathbf{C}_A$) along with digital SIC filter ($\mathbf{C}_D$).

used to indicate the analogue and digital versions of the variables, respectively.

Another analogue SIC approach has been proposed [17, 61] which relies on sending a cancellation signal via an additional transmit link, in which the cancellation signal is converted to RF and added to the incoming signal, where the desired and the SI signals are merged. Fig. 2.14 shows this mechanism through the two nodes a and b which communicate with each other by using the FD technique. Each node is equipped with two antennas, one for transmitting and one for receiving, along with two TX radios, each of which contains basically of PA and LO, one used for transmitting while the second is used to create a cancellation signal. Additionally, one RX radio is used for receiving and comprises of LNA and LO. In the figure, s_i, z_i, and r_i, for $i \in \{a, b\}$, are the transmitted, the cancellation and the received signals for node i, respectively. The forward channels from node a to node b and in the opposite direction are denoted as h_{ab} and h_{ba}, respectively. In contrast, h_{ii} is the SI channel at node i due to the FD operation. Additionally, g_i represents the cancellation channel, i.e. the phase and magnitude applied to the cancellation signal z_i at node i.

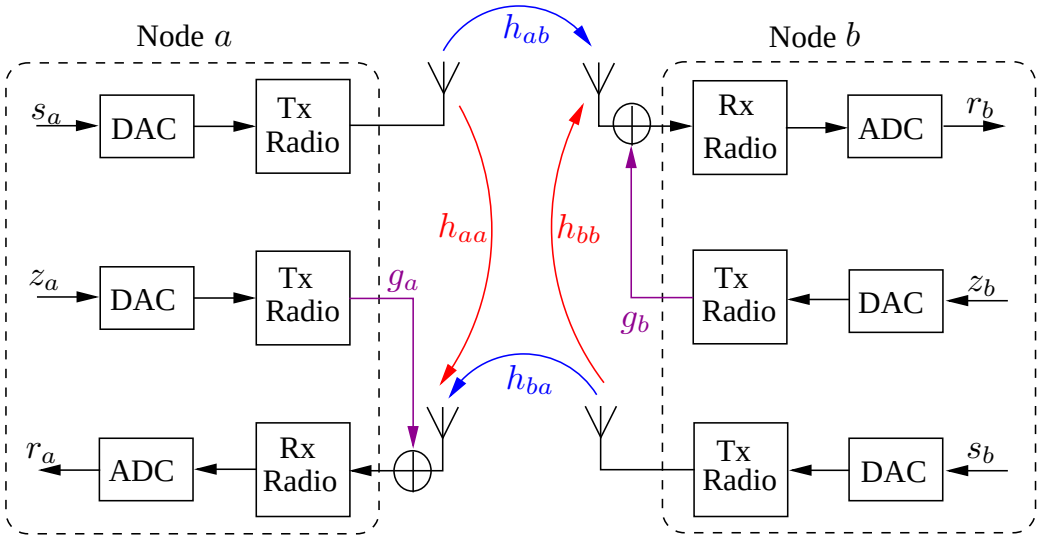

Figure 2.14: RF Cancellation of SI in the analogue domain.

The respective received signals at nodes a and b can be expressed as

$$r_a = h_{ba}s_b + h_{aa}s_a + g_a z_a + v_a, \tag{2.34a}$$

$$r_b = h_{ab}s_a + h_{bb}s_b + g_b z_b + v_b, \tag{2.34b}$$

where, v_a and v_b represent the AWGN at node a and b, respectively.

Thus, in order to cancel the SI at node i, it is necessary to set the cancellation signal intuitively as

$$z_i = -\left(\frac{h_{ii}}{g_i}\right)s_i \quad i \in \{a, b\}. \tag{2.35}$$

However, achieving perfect analogue SIC using this approach is not feasible due to distortions affecting the process of estimating the channels, such as noise and the non-linearities of the transmit and receive circuits. Therefore, the instantaneous residual SI signal remaining after this analogue cancellation can be expressed as $(h_{aa} - g_a\hat{h}_{aa}/\hat{g}_a)s_a$ and $(h_{bb} - g_b\hat{h}_{bb}/\hat{g}_b)s_b$ at nodes a and b, respectively, where $\hat{g}_i$ represents the noisy estimate of g_i. Hence, the residual powers of SI at node a and b can be written respectively as

$$P_{SI}^a = \mathbb{E}\{|(h_{aa} - g_a\hat{h}_{aa}/\hat{g}_a)s_a|^2\} \tag{2.36a}$$

$$P_{SI}^b = \mathbb{E}\{|(h_{bb} - g_b\hat{h}_{bb}/\hat{g}_b)s_b|^2\}. \tag{2.36b}$$

This analogue SIC mechanism can be applied to the FD-MIMO-OFDM system [41] as shown in Fig. 2.15. In this system, two bidirectional MIMO nodes i and j, which

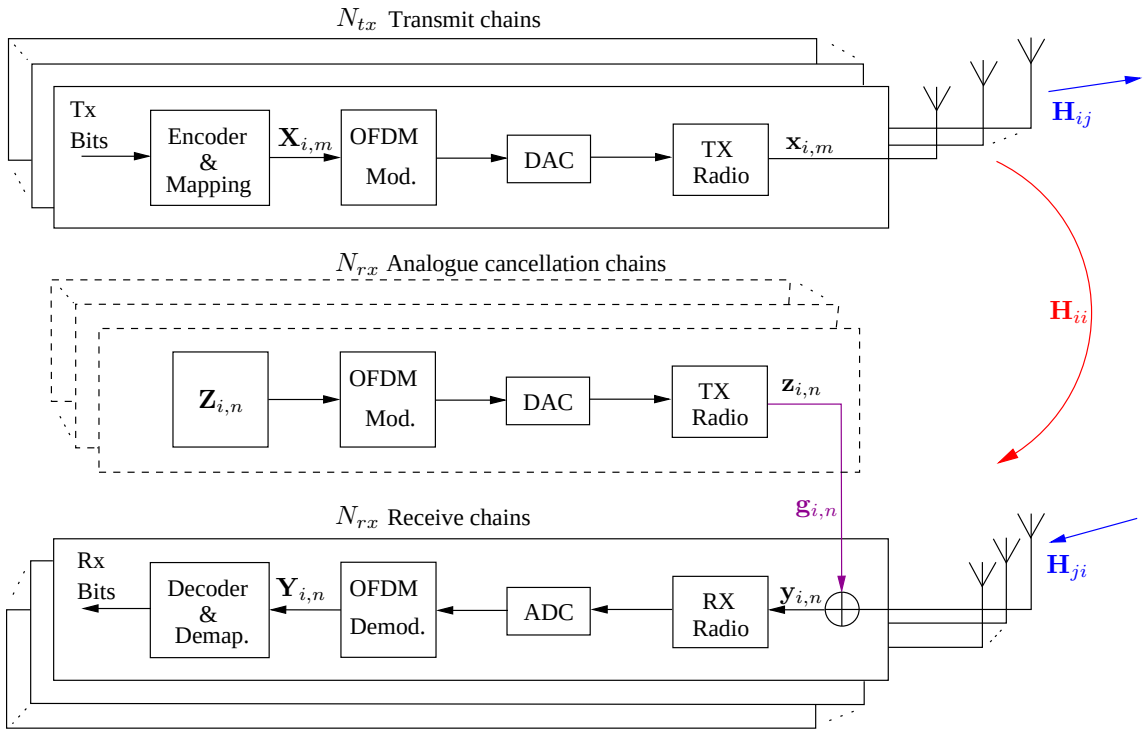

Figure 2.15: Analogue cancellation of SI for FD-MIMO-OFDM at node i

comprise N_{tx} transmit and N_{rx} receive chains, utilize FD operation with OFDM in their wireless communication. In the m^{th} transmit chain, where $m = 1, 2, ..., N_{tx}$, OFDM modulation is used via applying IFFT processing along with adding a cyclic prefix to the encoded and mapped symbols, $\mathbf{X}_{i,m}$. The OFDM signal is then converted to analogue by DAC, and passed through TX radio to produce the analogue signal at the m^{th} antenna of node i, $\mathbf{x}_{i,m}$. The channels $\mathbf{H}_{ij} \in \mathbb{C}^{N_{rx} \times N_{tx}}$, $\mathbf{H}_{ji} \in \mathbb{C}^{N_{rx} \times N_{tx}}$ and $\mathbf{H}_{ii} \in \mathbb{C}^{N_{rx} \times N_{tx}}$ represent the outgoing, incoming and the SI channels of node i, respectively. Moreover, each node contains N_{rx} chains of an analogue SIC circuit similar to the transmit chain explained above, except that the symbols in this SIC circuit need to be chosen in such a way that they lead to the optimum cancellation of SI. The output of the SIC circuit $\mathbf{z}_{i,n}$, which represents the cancellation signal, is passed through a wire to the RF adder in the n^{th} received circuit. Additionally, the magnitude and phase affecting the cancellation signal when it passed through this wire is denoted as $\mathbf{g}_{i,n}$. Hence, the output of the RF adder at the n^{th} received chain can be expressed as

$$\mathbf{y}_{i,n} = \mathbf{H}_{ji}\mathbf{x}_{j,m} + \mathbf{H}_{ii}\mathbf{x}_{i,m} + \mathbf{g}_{i,n}\mathbf{z}_{i,n} + \mathbf{v}_{i,n}, \tag{2.37}$$

where $\mathbf{x}_{j,m}$ is the desired incoming signal from node j to node i over channel $\mathbf{H}_{ji}$, and the AWGN is denoted as $\mathbf{v}_{i,n}$. It can be seen that, in order to obtain perfect SIC using this

approach, the cancellation signal should be chosen as

$$\mathbf{z}_{i,n} = -\frac{\mathbf{H}_{ii}}{\mathbf{g}_{i,n}}\mathbf{x}_{i,m} \tag{2.38}$$

However, perfect SIC is not feasible in practice due to the same reasons mentioned previously related to the effect of noise and the non-linearity of the circuit elements employed in the transmit and receive chains, which consequently lead to imperfect channel estimations of $\mathbf{H}_{ii}$ and $\mathbf{g}_{i,n}$. Therefore, the actual cancellation signal can be rewritten as $\hat{\mathbf{z}}_{i,n} = -\frac{\hat{\mathbf{H}}_{ii}}{\hat{\mathbf{g}}_{i,n}}\mathbf{x}_{i,m}$. The latter produces a residual SI power at node i, which can be expressed as

$$P_{SI}^{i} = \mathbb{E}\{\big|\big(\mathbf{H}_{ii} - \mathbf{g}_{i,n}\frac{\hat{\mathbf{H}}_{ii}}{\hat{\mathbf{g}}_{i,n}}\big)\mathbf{x}_{i,m}\big|^2\}. \tag{2.39}$$

To this end, the passive and analogue active approaches are not adequate to tackle the entire amount of SI, and therefore active SIC needs to be implemented in the digital domain in order to make the utilization of the FD mechanism feasible, as discussed in the next section.

2.5.2.2 Digital SIC

At this stage, it is assumed that all of the earlier applied SIC approaches, before the ADC, ensure a minimum required amount of cancellation to avoid ADC saturation. The aid of active digital cancellation is still required in the digital domain after the ADC as a last line of defence against SI, in order to perform further reduction of the residual SI remaining after passive and active analogue cancellation due to FD operation. Hence, advanced digital signal processing algorithms need to be applied to tackle the SI and cancel both its linear and non-linear components [62].

Linear digital SIC can be implemented by using the same conventional means utilized to mitigate normal interference caused by an undesired source. This can be done at the receiver by decoding the unwanted signal, reconstructing it and finally applying subtraction from the entire incoming signal to obtain the signal of interest. The same scenario can be performed to cancel the SI associated with FD operation by using coherent detection instead of decoding to detect the SI signal, as the FD transceiver has full knowledge about its transmitted signal, which causes SI at its receive terminal [21]. However, synchronisation issues such as delay and the phase shift between the two subtracted signals need to be

estimated precisely, which is considered to be the key challenge in applying this method. Alternatively, the *correlation peak* technique can be utilized and applied between the incoming signals and the known transmitted one, where the required delay and phase shift for implementing the subtraction can be obtained when the maximum correlation took place [21, 62].

Returning to Fig. 2.13, the transmitted signal causing SI is tapped in its discrete version $\mathbf{s}_i[n]$ before applying the DAC to the baseband processing unit of the receiver after passing through a digital filter, $\mathbf{C}_D \in \mathbb{C}^{N_{tx} \times N_{rx}}$, in order to be subtracted from the digital received signal $\hat{\mathbf{r}}[n]$, which contains the signal of interest with the residual SI remaining after applying analogue SIC [10, 63, 64]. This process can be expressed in the digital domain as

$$\tilde{\mathbf{r}}[n] = \hat{\mathbf{r}}[n] - \mathbf{C}_D \, \mathbf{s}_i[n], \tag{2.40}$$

where $\hat{\mathbf{r}}[n] = \mathbf{H}[n]\mathbf{s}_o[n] + \mathbf{H}_{LI}[n]\mathbf{s}_i[n] + \mathbf{v}[n]$. Thus, it can be noticed that SI regeneration can be implemented via choosing the digital filter as $\mathbf{C}_D = \mathbf{H}_{LI}[n]$, which can totally remove the SI if precise knowledge of $\mathbf{H}_{LI}[n]$ is available at the receiver. However, this approach does not take into account the distortions and non-idealities induced by the transmit and receive chains. This issue can be tackled by using N_{tx} auxiliary receive chains, in order to reconstruct the SI signal after passing through components and processing units identical to those which existed in the ordinary receiving chains [65], as shown in Fig. 2.16.

In this figure, it is assumed that the received signal at the digital domain, in all the N_{rx} chains and for a discrete time index n, i.e. $\hat{\mathbf{r}}[n]$, contains a combination of the desired signal and the residual SI remaining after applying passive and active analogue SICs', which can be expressed as

$$\hat{\mathbf{r}}[n] = \mathbf{H}[n]\mathbf{s}_o[n] + \mathbf{H}_{LI}[n]\mathbf{s}_i[n] + \mathbf{v}[n], \tag{2.41}$$

where $\mathbf{s}_o[n]$ is the discrete version of the desired signal coming through a MIMO channel $\mathbf{H}[n]$, while the residual SI is represented by the term $\mathbf{H}_{LI}[n]\mathbf{s}_i[n]$ and $\mathbf{v}[n]$ represents the AWGN. The regeneration of SI can be implemented via utilizing a combination of the LI channel, $\mathbf{H}_{LI}[n]$, with the SI signal, $\mathbf{s}_i[n]$. The latter is created by passing the analogue SI signal $\mathbf{s}_i[t]$ through N_{tx} auxiliary receive chains, in order to take into consideration all

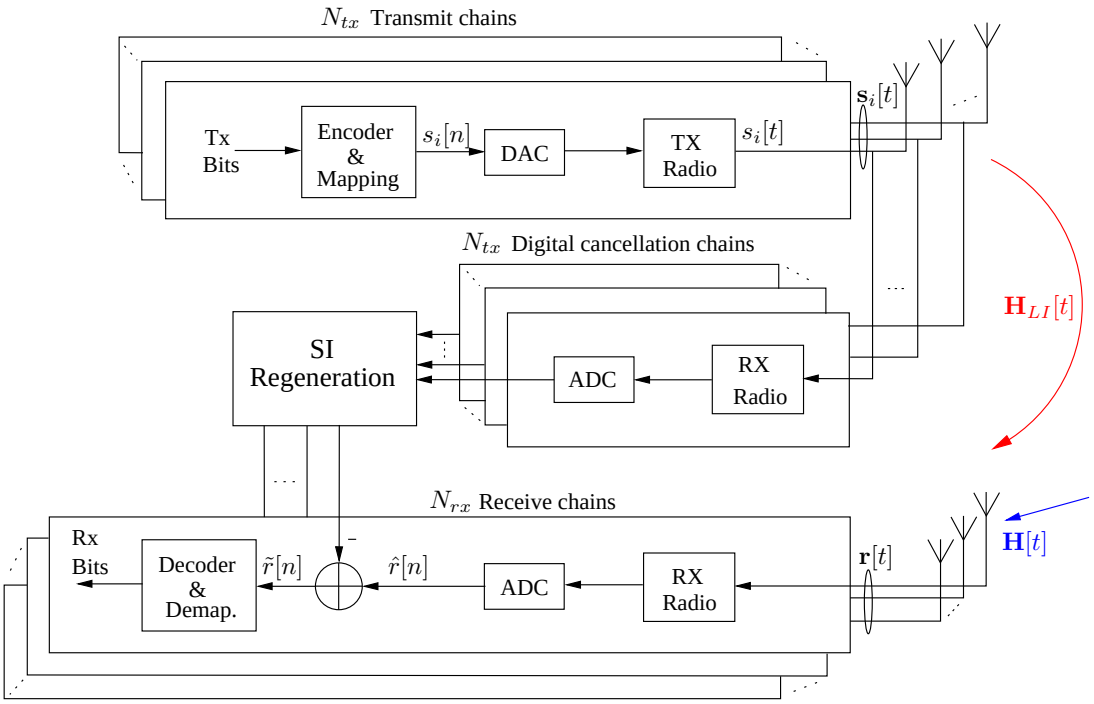

Figure 2.16: Digital cancellation of SI for FD-MIMO at node i using auxiliary receive chains along with SI regeneration.

the possible impairments and non-linearity effects which may induced in the SI signal in the ordinary receive chains. Finally, to complete this process in the digital domain, the regenerated SI signal is subtracted from $\hat{\mathbf{r}}[n]$ as

$$\tilde{\mathbf{r}}[n] = \hat{\mathbf{r}}[n] - \hat{\mathbf{H}}_{LI}[n]\hat{\mathbf{s}}_i[n], \tag{2.42}$$

where the term $\hat{\mathbf{H}}_{LI}[n]\hat{\mathbf{s}}_i[n]$ represents the estimation of the residual SI in the digital domain, since obtaining an exact estimate of SI in the real-world is impractical [10].

NSP can be adopted in order to enable the FD operation by deriving the necessary digital spatial filters (DSFs) for each transmitter, denoted as $\mathbf{F}_{\mathtt{p}} \in \mathbb{C}^{N_{tx}\times 1}$, and the receiver, denoted as $\mathbf{G}_{\mathtt{p}} \in \mathbb{C}^{1\times N_{rx}}$, in the MIMO system, where $\mathtt{p} \in \{\mathtt{a},\mathtt{b}\}$ is the port index. Each DSF is directly dependent on the eigenvectors of the SIC channel; for examples see $\mathbf{H}_{\mathtt{pp}} \in \mathbb{C}^{N_{tx}\times N_{rx}}$ in Fig. 2.17. The construction method proceeds by factorising the channel to its eigenvalues and eigenvectors by applying SVD, i.e. $\mathbf{H}_{\mathtt{pp}} = \mathbf{U}_{\mathtt{pp}}\mathbf{\Sigma}_{\mathtt{aa}}\mathbf{V}_{\mathtt{pp}}^{H}$, where $\mathbf{U}_{\mathtt{pp}} \in \mathbb{C}^{N_{rx}\times N_{rx}}$ and $\mathbf{V}_{\mathtt{pp}} \in \mathbb{C}^{N_{tx}\times N_{tx}}$ are orthonormal matrices $\because \mathbf{U}_{\mathtt{pp}}^{H}\mathbf{U}_{\mathtt{pp}} = \mathbf{U}_{\mathtt{pp}}\mathbf{U}_{\mathtt{pp}}^{H} = \mathbf{I}_{N_{rx}}$ and $\mathbf{V}_{\mathtt{pp}}^{H}\mathbf{V}_{\mathtt{pp}} = \mathbf{V}_{\mathtt{pp}}\mathbf{V}_{\mathtt{pp}}^{H} = \mathbf{I}_{N_{tx}}$. Meanwhile $\mathbf{\Sigma}_{\mathtt{pp}} \in {\mathbb{R}_{+}}^{N_{rx}\times N_{tx}}$ is a diagonal matrix which contains the eigenvalues of the channel in descending order. This technique applies strict constraints to the number of unique data streams which is bounded by the dimensions of the MIMO system, and the detailed anal-

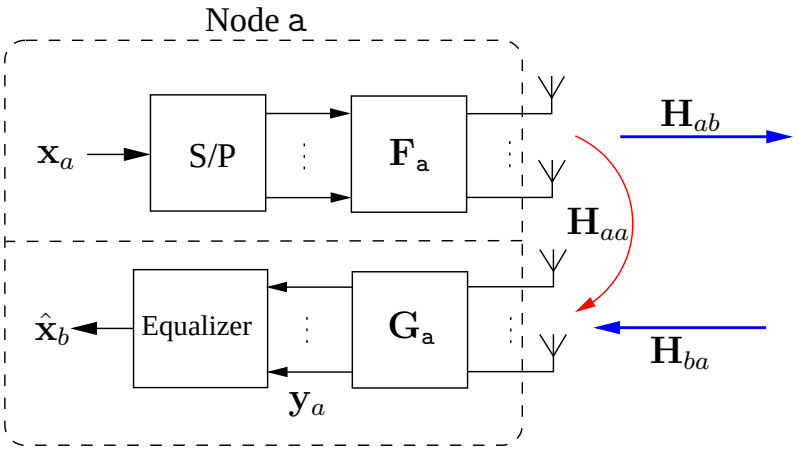

Figure 2.17: Bi-directional full-duplex MIMO system with NSP as digital SIC at node a, the same is applied to node b.

ysis is presented elsewhere [9]. The self-coupling interference model can be formulated as follows:

$$\mathbf{y}_{\mathtt{aa}} = \overbrace{\mathbf{G}_\mathtt{a} \underbrace{\mathbf{H}_{\mathtt{aa}}}_{\mathbf{U}_{\mathtt{aa}}\mathbf{\Sigma}_{\mathtt{aa}}\mathbf{V}_{\mathtt{aa}}^H} \mathbf{F}_\mathtt{a}}^{\approx 0} \mathbf{x}_\mathtt{a}, \tag{2.43}$$

and the full system model in the presence of NSP at node a becomes:

$$\mathbf{y}_\mathtt{a} = \mathbf{G}_\mathtt{a}\left(\mathbf{U}_{\mathtt{aa}}\mathbf{\Sigma}_{\mathtt{aa}}\mathbf{V}_{\mathtt{aa}}^H\mathbf{F}_\mathtt{a}\mathbf{x}_\mathtt{a} + \mathbf{H}_{\mathtt{ba}}\mathbf{F}_\mathtt{b}\mathbf{x}_\mathtt{b} + \mathbf{n}_\mathtt{a}\right), \tag{2.44}$$

where $\mathbf{x}_\mathtt{a} = [x_\mathtt{a}^1, x_\mathtt{a}^2, ..., x_\mathtt{a}^{N_{\mathtt{tx}}}]^T$ and $\mathbf{x}_\mathtt{b} = [x_\mathtt{b}^1, x_\mathtt{b}^2, ..., x_\mathtt{b}^{N_{\mathtt{tx}}}]^T$ are the complex symbols transmitted at nodes a and b, respectively. Moreover, $\mathbf{n}_\mathtt{a}$ is the AWGN at node a.

The goal in designing these filters is to obtain $\mathbf{G}_\mathtt{p}\mathbf{H}_{\mathtt{pp}}\mathbf{F}_\mathtt{p} = \mathbf{0}$, for $\mathtt{p} \in \{\mathtt{a}, \mathtt{b}\}$, which is referred to as NSP [8]. In designing $\mathbf{F}_\mathtt{p}$ and $\mathbf{G}_\mathtt{p}$, it is necessary to choose these filters such that they minimize the term $\min \|\mathbf{G}_\mathtt{p}\mathbf{H}_{\mathtt{pp}}\mathbf{F}_\mathtt{p}\|_F^2$, where $\|.\|_F$ is the Frobenius norm.

There are several approaches that can be used for this purpose as in [8, 9, 66, 67]. Here the method proposed by [66] is applied, and in order to apply spatial multiplexing to obtain orthonormal streams, the filters are constrained such that $\mathbf{F}_\mathtt{p}^H\mathbf{F}_\mathtt{p} = I$ and $\mathbf{G}_\mathtt{p}\mathbf{G}_\mathtt{p}^H = I$. As in [66], this can be achieved by choosing

$$\mathbf{F}_\mathtt{p} = \mathbf{V}_{\mathtt{pp}}\mathbf{S}_\mathtt{p} \quad \text{and} \quad \mathbf{G}_\mathtt{p} = \mathbf{T}_\mathtt{p}\mathbf{U}_\mathtt{p}^H, \tag{2.45}$$

where $\mathbf{S}_\mathtt{p}$ and $\mathbf{T}_\mathtt{p}$ represent the binary column and row selection matrices, respectively. The optimum design for these two matrices can be achieved by satisfying the following conditions: $\mathbf{S}_\mathtt{p}^H\mathbf{S}_\mathtt{p} = I$, $\mathbf{T}_\mathtt{p}\mathbf{T}_\mathtt{p}^H = I$, $\mathbf{T}_\mathtt{p}\mathbf{S}_\mathtt{p} = \mathbf{0}$, and $\mathbf{G}_\mathtt{p}\mathbf{H}_{\mathtt{pp}}\mathbf{F}_\mathtt{p} = \mathbf{T}_\mathtt{p}\mathbf{\Sigma}_{\mathtt{pp}}\mathbf{S}_\mathtt{p}$.

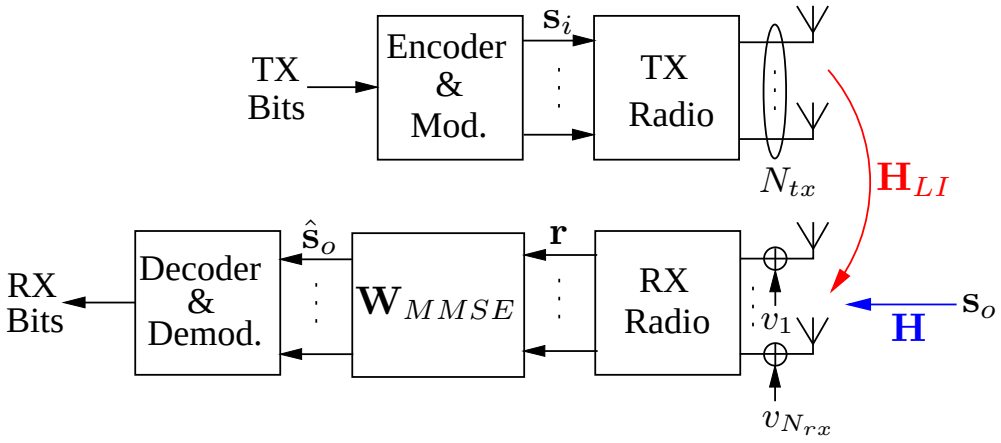

Figure 2.18: Bi-directional full-duplex MIMO transceiver with MMSE filtering.

MMSE filtering can be employed in the digital domain in order to apply further reduction in SI after applying SIC approaches in the analogue and digital domains, as shown in Fig. 2.18. The mean-square error (MSE) matrix in the input of the FD-MIMO transceiver can be defined as

$$\mathbf{M} = \mathbb{E}\Big\{ \Big[\mathbf{H}\mathbf{s}_o - \hat{\mathbf{s}}_o\Big] \Big[\mathbf{H}\mathbf{s}_o - \hat{\mathbf{s}}_o\Big]^{\mathcal{H}} \Big\}, \tag{2.46}$$

where $\hat{\mathbf{s}}_o = \mathbf{w}_{MMSE}\mathbf{r}$ and $\mathbf{r} = \mathbf{H}\mathbf{s}_o + \mathbf{H}_{LI}\mathbf{s}_i + \mathbf{v}$. By substituting $\mathbf{r}$ in $\hat{\mathbf{s}}_o$, the latter can be rewritten as

$$\hat{\mathbf{s}}_o = \mathbf{w}_{MMSE}(\mathbf{H}\mathbf{s}_o + \mathbf{H}_{LI}\mathbf{s}_i + \mathbf{v}). \tag{2.47}$$

Now, by substituting (2.47) in (2.46), we can obtain

$$\mathbf{M} = \mathbb{E}\Big\{ \Big[\mathbf{H}\mathbf{s}_o - \mathbf{w}_{MMSE}(\mathbf{H}\mathbf{s}_o + \mathbf{H}_{LI}\mathbf{s}_i + \mathbf{v})\Big] \Big[\mathbf{H}\mathbf{s}_o - \mathbf{w}_{MMSE}(\mathbf{H}\mathbf{s}_o + \mathbf{H}_{LI}\mathbf{s}_i + \mathbf{v})\Big]^{\mathcal{H}} \Big\}, \tag{2.48}$$

which can be simplified as

$$\mathbf{M} = (\mathbf{I}_{N_{rx}} - \mathbf{w}_{MMSE})\mathbf{H}\mathbf{R}_{\mathbf{s}_o}\mathbf{H}^{\mathcal{H}}(\mathbf{I} - \mathbf{w}_{MMSE})^{\mathcal{H}} + \mathbf{R}_{\hat{\mathbf{v}}}, \tag{2.49}$$

in which $\mathbf{R}_{\hat{\mathbf{v}}} = \mathbb{E}\{\hat{\mathbf{v}}\hat{\mathbf{v}}^{\mathcal{H}}\} = \mathbf{w}_{MMSE}(\mathbf{H}_{LI}\mathbf{R}_{\mathbf{s}_i}\mathbf{H}_{LI}^{\mathcal{H}} + \mathbf{R}_{\mathbf{v}})\mathbf{w}_{MMSE}^{\mathcal{H}}$ represents the covariance matrix of the residual SI plus noise after the MMSE filter, while $\mathbf{R}_{\mathbf{s}_o} = \mathbb{E}\{\mathbf{s}_o\mathbf{s}_o^{\mathcal{H}}\}$,

$\mathbf{R}_{\mathbf{s}_i} = \mathbb{E}\{\mathbf{s}_i\mathbf{s}_i^{\mathcal{H}}\}$ and $\mathbf{R}_{\mathbf{v}} = \mathbb{E}\{\mathbf{v}\mathbf{v}^{\mathcal{H}}\} = \sigma_v^2\mathbf{I}_{N_{rx}}$ are the covariance matrices of the desired transmitted signal, the SI and the noise, respectively.

The MMSE receive filter can be obtained from (2.49) by finding a derivative of the trace of $\mathbf{M}$ with respect to $\mathbf{w}_{MMSE}$ and equalize the results to zero, i.e. $\frac{\partial \mathrm{tr}\{\mathbf{M}\}}{\partial \mathbf{w}_{MMSE}} = 0$, which yields

$$\mathbf{w}_{MMSE} = \mathbf{H}\mathbf{R}_{\mathbf{s}_o}\mathbf{H}^{\mathcal{H}}(\mathbf{H}\mathbf{R}_{\mathbf{s}_o}\mathbf{H}^{\mathcal{H}} + \mathbf{H}_{LI}\mathbf{R}_{\mathbf{s}_i}\mathbf{H}_{LI}^{\mathcal{H}} + \mathbf{R}_{\mathbf{v}})^{-1}. \tag{2.50}$$

After determining the MMSE filter coefficients using (2.50), $\mathbf{w}_{MMSE}$ can be applied to the received signal $\mathbf{r}$ in order to obtain an estimate of the signal of interest $\hat{\mathbf{s}}_o$ after minimising the effect of SI as

$$\hat{\mathbf{s}}_o = \mathbf{w}_{MMSE}\mathbf{r}. \tag{2.51}$$

It is noteworthy that the knowledge of the covariance matrices along with the channels of SI and the desired signal are required to implement this MMSE filter in order to tackle SI in the digital domain. Moreover, scaling needs to be applied to (2.50) in order to satisfy $\|\mathbf{w}_{MMSE}\|_F^2 = N_{rx}$ [9].

2.6 Chapter Summary

In this chapter, the background and theory of multiple antenna transmission for wireless communication has been investigated and discussed. Different techniques in this area have been described and analysed such as spatial multiplexing, precoding and diversity coding. Furthermore, different equalization and detection techniques have been presented for the sake of recovering the desired signal after passing through MIMO channels. Moreover, the fundamentals and challenges of utilizing in-band FD transmission for wireless communication have been discussed, in which the most promising techniques exploited to mitigate the SI associated with FD operation have been outlined and discussed in more detail and for different stages of signal processing, such as the passive suppression in the RF domain and active cancellation in the analogue and digital domains, i.e. before and after the ADC, respectively.

Chapter 3

Performance Analysis of FD-MRC-MIMO with SIC Using NSP

3.1 Introduction

Due to the continually increasing demands on frequency and energy resources, FD has become an essential necessity and inevitable evolutionary step for the next generation of wireless communications, the fifth generation (5G). FD transceivers allow transmission simultaneously over the same frequency bands. This makes the need for applying SIC methods essential to tackle the SI accompanied with FD operation and obtain the optimum performance of FD.

This chapter focuses on FD-MIMO based relays, over which the source and destination nodes are communicating. In general, the relay has the ability to receive data from the source and deliver it to the destination either by using AF, DF or by EF approaches. Fig. 3.1 illustrates a FD wireless communication via a relay, in which the source (S) communicates with the destination (D) by utilizing the relay (R). Moreover, the notations $\mathbf{H}_{sr}$, $\mathbf{H}_{rd}$, and $\mathbf{H}_{sd}$ are to represent the channels of the source to relay, the relay to destination and the source to destination, respectively. While $\mathbf{H}_{rr}$ is the SI channel between the relay's output and input.

For these types of relaying, estimation and subtraction operations of SI are required to maximize the SINR, which increases the capacity, improves the overall spectral efficiency and enhances the entire performance of these systems utilizing the FD technique.

Spatial suppression schemes for FD-MIMO transceivers, such as ZF and NSP, are proposed as SIC via exploiting the spatial domain MIMO signal characteristics of the interfering channels. This can be achieved by designing spatial filters via utilizing matrix conversion approaches, as SVD of the SI channel required to suppress the SI [8, 9, 20, 29,

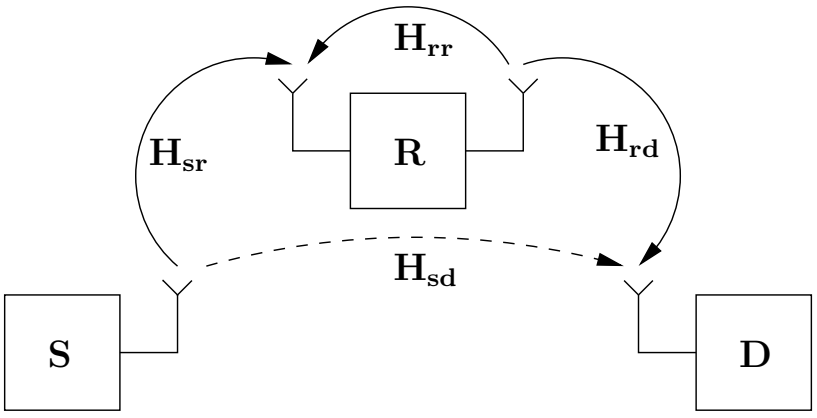

Figure 3.1: Wireless Communication using Relay

38].

In contrast, in order to increase the signal-to-noise ratio (SNR), spatial diversity can be exploited for MIMO systems to obtain the full diversity gain available, which can be achieved by utilizing MRC. This approach has been launched and deployed successfully for MIMO systems that operate in the presence of AWGN and interference environments. The MIMO-MRC system may be constructed by introducing transmit and receive beamforming weight vectors. The selection of beamforming weight vectors can be optimized to satisfy transmitting the signal over the strongest path of the channel. This implies that transmitting the signal along the direction of the eigenvector associated to the largest eigenvalue of the Wishart matrix of a channel $\mathbf{H}$, i.e. $\mathbf{H}^H\mathbf{H}$ [51, 52]. However, perfect CSI is required by the transmitter and receiver in order to obtain better performance.

In this chapter, the works in [8, 9, 20, 29, 38] are extended by combining MRC with NSP for FD-MIMO based relaying in order to maximize the SINR. Additionally, the performance analysis of the proposed system is derived for different performance metrics and in the presence of perfect and imperfect channel estimation. Furthermore, the works in [3, 13, 30, 31] are extended by utilizing EF relaying instead of DF and AF relays, and the relay transformation coefficients are derived for FD-MRC-MIMO using EF relaying in order to minimize the mean square error (MSE) between the transmitted and received symbols. Moreover, the E2E performance is demonstrated using the outage probability, ASER vs. SINR, and capacity performance metrics.

The key contributions of this chapter can be summarized as follows. Firstly, NSP and MRC are exploited jointly in order to mitigate the SI of the undesired loop path and to increase the SNR of the source-to-destination path. The motivation to use MRC-MIMO, which is selected over Full-MIMO, is due to the SNR advantage inherent in transmit and receive beamforming to achieve full diversity gain in such an interference limited environment. NSP is implemented via utilizing SVD of the CSI of the SI channel. Secondly, the E2E performance analysis of the modelled system takes into account the impact of imperfectly estimated CSI for both the desired and interference channels. Finally, the E2E upper bound mutual information of the proposed FD-MRC-MIMO is derived in the presence of SI. To the best of our knowledge, these aspects have not been thoroughly investigated in previously published research papers. The ideas, derivations and numerical results presented in this chapter are valid for flat fading channels. However, the latter condition can be always satisfied by introducing OFDM to combat ISI. As long as a cyclic prefix of sufficient length is selected to cover the delay spread of the multipath channel

the presented results will be valid.

The rest of this chapter is organized as follows. In Section 3.2, the signal and system models are introduced. In Section 3.3, the E2E performance analysis of the proposed system is demonstrated by deriving the output SINRs for the first and second hops along with their corresponding PDF. Furthermore, the outage probabilities and ASER are derived. In Section 3.5, the E2E upper bound capacity of this system is derived. Section 3.6 presents simulation results and discussion, and finally, the chapter's conclusions are drawn in Section 3.7.

3.2 Signal and System Model

In this chapter, a wireless communications system is considered in which the source communicates with destination via relay as shown in Fig. 3.2, in addition to the description and definition mentioned in Table 5.1. The EF relay operates as a FD transceiver with N_{tx} transmit and N_{rx} receive antennas. Furthermore, the source has N_s antennas used to send the signal, while, N_d antennas at the destination are used for receiving. The channels between the source and the relay, the relay-to-destination, and the relay output to its input are considered in this chapter as flat Rayleigh fading channels and they are defined as $\mathbf{H}_{sr} \sim \mathcal{CN}(\mathbf{0}, \mathbf{I}^{N_s \times N_{rx}})$, $\mathbf{H}_{rd} \sim \mathcal{CN}(\mathbf{0}, \mathbf{I}^{N_{tx} \times N_d})$, and $\mathbf{H}_{rr} \sim \mathcal{CN}(\mathbf{0}, \mathbf{I}^{N_{tx} \times N_{rx}})$, respectively. The assumption that the $\mathbf{H}_{rr}$ links are flat comes from the fact that passive suppression of SI has been implemented in the analogue domain via antenna separation and shielding to suppress the LoS path [9]. In addition, AWGN is defined generally as $\mathbf{n} \sim \mathcal{CN}(\mathbf{0}, \sigma_n^2\mathbf{I})$. In this chapter, it is assumed that there is no directly available source-to-destination path, i.e. $\mathbf{H}_{sd} = \mathbf{0}$, and all E2E communications occurs via the relay.

As highlighted in Section 3.1, the FD-MRC-MIMO system applies transmit and receive beamforming at the source terminal and relay, respectively. The weight vectors at both transmitter and receiver are designed to maximize the SNR of the desired path by exploiting the eigen-transmissions and providing full diversity gain [51, 52]. This consequently leads to improved SINR for fixed SI and noise power levels [68]. This can be obtained by using $\mathbf{w}_{tx}^{sr} = \mathbf{u}_{\max}^{sr}$ as MIMO transmit beamforming and $\mathbf{w}_{rx}^{sr} = \mathbf{H}_{sr}\mathbf{u}_{\max}^{sr}$ at the receiver as MRC reception, where $\mathbf{u}_{\max}^{sr}$ is a unit norm eigenvector corresponding to the largest eigenvalue $\lambda_{\max}^{sr}$ of the Wishart matrix $\mathbf{H}_{sr}^H\mathbf{H}_{sr}$, where unit norm implies that the Euclidean norm of $\mathbf{u}_{\max}^{sr}$ is unity, i.e. $\|\mathbf{u}_{\max}^{sr}\|^2 = 1$. This is due to the fact that maximizing SNR is subject to determining the squared-spectrum norm of the matrix $\mathbf{H}_{sr}$,

Table 3.1: Model parameters.

Notation	Description/Definition
	Source-Relay Parameters
s_o	Modulated symbol
$\mathbf{w}_{tx}^{sr}$	MRC weighting coefficients for transmitting with respect to $\mathbf{H}_{sr}$
$\mathbf{H}_{sr}$	source-relay channel coefficients
$\mathbf{\Xi}_{sr}$	The channel estimation error of $\mathbf{H}_{sr}$
	Relay Parameters
$\mathbf{r}$	Sum of the received signal from the source coupled with $\mathbf{s}_i$ over $\mathbf{H}_{rr}$
$\mathbf{G}_{rx}$	Spatial filter determined by the first unitary matrix of SVD($\mathbf{H}_{rr}$)
$\mathbf{z}$	Output of the filter $\mathbf{G}_{rx}$
$(\mathbf{w}_{rx}^{sr})^H$	MRC weighting coefficients for detection with respect to $\mathbf{H}_{sr}$
$\tilde{z}$	Weight received symbol
F	MMSE coefficient of the EF-relay
s_{ef}	Output of F
$\mathbf{w}_{tx}^{rd}$	MRC weighting coefficients for transmitting with respect to $\mathbf{H}_{rd}$
$\mathbf{G}_{tx}$	Spatial filter determined by the second unitary matrix of SVD($\mathbf{H}_{rr}$)
$\mathbf{s}_i$	Transmitted symbols from relay to destination
$\mathbf{H}_{rr}$	Self-interference Channel
$\mathbf{\Xi}_{rr}$	The channel estimation error of $\mathbf{H}_{rr}$
	Relay-Destination Parameters
$\mathbf{y}_D$	The Received signal at the destination
$(\mathbf{w}_{rx}^{rd})^H$	MRC weighting coefficients for detection with respect to $\mathbf{H}_{rd}$
$\hat{s}_o$	The received symbol at the destination after applying MRC to $\mathbf{y}_D$
$\mathbf{H}_{rd}$	Relay to destination Channel
$\mathbf{\Xi}_{rd}$	The channel estimation error of $\mathbf{H}_{rd}$

which suggests that the signal is transmitted from source-to-relay over the strongest path of $\mathbf{H}_{sr}$ [51, 52]. The same procedure can be used in the path of relay-to-destination of $\mathbf{H}_{rd}$ to obtain $\mathbf{w}_{tx}^{rd}$ and $\mathbf{w}_{rx}^{rd}$.

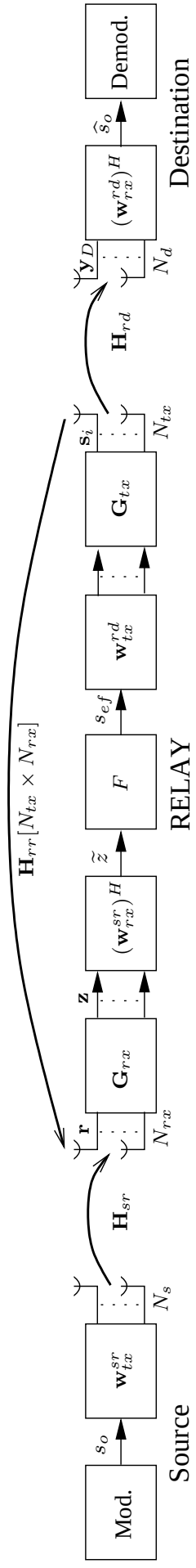

Figure 3.2: FD-MRC-MIMO system with SIC using NSP.

This research focuses on FD-MIMO based relay systems, which offer additional degrees of freedom in the spatial domain [9]. Spatial suppression schemes have been proposed and applied extensively for this issue. This is achieved by adding a receive filter, $\mathbf{G}_{rx} \in \mathbb{C}^{N_{rx} \times N_{rx}}$, at the input of the FD relay, and a transmit filter, $\mathbf{G}_{tx} \in \mathbb{C}^{N_{tx} \times N_{tx}}$, at the output of relay, as illustrated in Fig. 3.2. Both of these filters are designed based as eigen-beamformers using the SVD of the SI channel of the relay, $\mathbf{H}_{rr}$, with $\mathbf{H}_{rr} = \mathbf{U}_{rr}\mathbf{\Sigma}_{rr}\mathbf{V}_{rr}^{H}$, where $\mathbf{U}_{rr} \in \mathbb{C}^{N_{rx} \times N_{rx}}$ and $\mathbf{V}_{rr} \in \mathbb{C}^{N_{tx} \times N_{tx}}$ are unitary matrices, i.e. $\mathbf{U}_{rr}\mathbf{U}_{rr}^{H} = \mathbf{U}_{rr}^{H}\mathbf{U}_{rr} = \mathbf{I}$ and $\mathbf{V}_{rr}\mathbf{V}_{rr}^{H} = \mathbf{V}_{rr}^{H}\mathbf{V}_{rr} = \mathbf{I}$. Here, $\mathbf{U}_{rr}$ and $\mathbf{V}_{rr}$ are constructed using orthogonal column vectors of $\mathbf{H}_{rr}$. In addition, $\mathbf{\Sigma}_{rr} \in \mathbb{R}^{N_{rx} \times N_{tx}}$ is a diagonal matrix containing in descending order the singular values, $\sigma_{rr}[i] \geq 0$, for $i = 1, 2, ..., \min\{N_{rx}, N_{tx}\}$ of $\mathbf{H}_{rr}$ [8] [29].

The target in designing the filters from the SVD of the SI channel is to remove loopback interference. This can be satisfied as $\mathbf{G}_{rx}\mathbf{H}_{rr}\mathbf{G}_{tx} = \mathbf{0}$, which is referred to as NSP. This method can be used when the SI signal is not perfectly known due to linear and nonlinear distortion induced in the transmit/receive chains. However, the channel estimation error, which will be discussed in more details later in this chapter, will cause residual SI, which impacts negatively on the the overall performance of the system. In order to design $\mathbf{G}_{rx}$ and $\mathbf{G}_{tx}$, there are several approaches that can be utilized as in [2,8,9,20,29,69–71]. As the emphasis of this chapter is on the performance analysis of FD-MIMO relays in the presence of SIC, the approach outlined in [20] and [70] have been employed, which is suitable for MIMO systems with the same number of transmit and receive antennas, i.e. $N_{rx} = N_{tx}$. In this method, the two spatial filters are designed by selecting one of the two options in (3.1) in order to satisfy $\min \|\mathbf{G_{tx}}\mathbf{H_{rr}}\mathbf{G_{rx}}\|_F^2$ [9], i.e.

$$\mathbf{G}_{rx} = [\mathbf{u}_{rr}^{(0)} \quad \mathbf{u}_{rr}^{(0)}]^{\mathcal{H}}, \quad \text{if} \quad \mathbf{G}_{tx} = [\mathbf{v}_{rr}^{(1)} \quad \mathbf{v}_{rr}^{(1)}], \tag{3.1a}$$

$$\mathbf{G}_{rx} = [\mathbf{u}_{rr}^{(1)} \quad \mathbf{u}_{rr}^{(1)}]^{\mathcal{H}}, \quad \text{if} \quad \mathbf{G}_{tx} = [\mathbf{v}_{rr}^{(0)} \quad \mathbf{v}_{rr}^{(0)}], \tag{3.1b}$$

where $\mathbf{u}_{rr}^{(0)}$ and $\mathbf{v}_{rr}^{(0)}$ represent the first half columns of the matrices $\mathbf{U}_{rr}$ and $\mathbf{V}_{rr}$, respectively, while, $\mathbf{u}_{rr}^{(1)}$ and $\mathbf{v}_{rr}^{(1)}$ represent the second half columns of matrices $\mathbf{U}_{rr}$ and $\mathbf{V}_{rr}$ respectively. In addition, for non-square matrices and/or for the case of rank deficiency of $\mathbf{H}_{rr}$ when the channels are not totally independent, (3.2) can be used to design the two

filters as [69]

$$\mathbf{G}_{rx} = \mathbf{U}_{rr}^{\mathcal{H}}(:, \text{rank}(\mathbf{H}_{rr}) + 1 : N_{rx}), \tag{3.2a}$$

$$\mathbf{G}_{tx} = \mathbf{V}_{rr}(:, \text{rank}(\mathbf{H}_{rr}) + 1 : N_{tx}), \tag{3.2b}$$

where $\text{rank}(\mathbf{H}_{rr})$ represents the rank of $\mathbf{H}_{rr}$.

In Fig. 3.2, F represents the MMSE transformation coefficient of the EF-relay, which is derived in detail in Section 3.4 in order to obtain the optimum solution that minimizes the errors between the transmitted and the received symbols in the source-to-relay path in the presence of residual SI, and therefore, enhances the overall performance of the system.

3.3 E2E Performance Analysis

In this section, the E2E performance analysis is derived. The derivation is organized as follows. The deriving of the SINR, PDF of the output SINR, the outage probability, and the ASER for the first and second hops are considered in Subsections 3.3.1 and 3.3.2, respectively. The overall probability of error for the entire system can be obtained as [72]

$$P\left\{\mathbb{E}(\gamma_1, \gamma_2)\right\} = P_1\left\{\mathbb{E}(\gamma_1)\right\} + P_2\left\{\mathbb{E}(\gamma_2)\right\} - 2P_1\left\{\mathbb{E}(\gamma_1)\right\} P_2\left\{\mathbb{E}(\gamma_2)\right\}, \tag{3.3}$$

where $P\left\{\mathbb{E}(\gamma_1, \gamma_2)\right\}$ represents the E2E probability of error averaged over the two independent random variables γ_1 and γ_2, which represent the SINRs of the first and second hops, respectively, whilst, in general, $P_i\left\{\mathbb{E}(\gamma_i)\right\}, i \in \{1, 2\}$ represents the average probability of error over the independent random variable γ_i.

3.3.1 SINR of The First Hop

The focus of this chapter is on the FD relay that can send and receive data simultaneously, which in turn causes SI in the receive terminal. Thus, in this section, the SINR is derived for the first hop of the modelled system. For a given MIMO symbol and at time instant t, the received signal vector, $\mathbf{r}[t]$, at the FD-MRC-MIMO relay input can be written as

$$\mathbf{r}[t] = \sqrt{P_{sr}}\mathbf{H}_{sr}\mathbf{w}_{tx}^{sr}s_o[t] + \sqrt{P_{rr}}\mathbf{H}_{rr}\mathbf{s}_i\left(s_o[t-1]\right) + \mathbf{n}_R[t], \tag{3.4}$$

where $s_o[t] \in \exp(j(2k+1)\pi/M), \forall k = 0, \dots M-1$ represents the M-PSK symbols before applying a MIMO transmitter beamforming weight vector of the source to the relay path, $\mathbf{w}_{tx}^{sr}$. Whilst, $\mathbf{s}_i\left(s_o[t-1]\right)$ is the relay's transmitted signal as a function of the previous transmitted symbol of the source, $s_o[t-1]$, i.e. it represents the raw transmitted symbols at the relay output after applying the EF relaying operation to $s_o[t-1]$. Additionally, P_{sr} and P_{rr} are the relay's average transmit powers from the forward path, i.e. the source-to-relay path, and the backward loop path of the relay causing SI, respectively. $\mathbf{n}_R[t]$ represents the AWGN at the input of the relay. Furthermore, in the following steps, it is assumed that the processing delay in the EF relaying operation can be applied within a symbol duration.

The input for the relay EF processing stage, $\widetilde{z}[t]$, is obtained by substituting $\mathbf{s}_i[t] = \mathbf{G}_{tx}\mathbf{w}_{tx}^{rd}s_{ef}[t-1]$ in (3.4), where s_{ef} represents the equalized complex symbol after passing through the MMSE transformation filter of the EF-relay, F. Then, by performing SIC processing of $\mathbf{r}[t]$ in the first stage of the EF-relay as $\mathbf{z}[t] = \mathbf{G}_{rx}\mathbf{r}[t]$, and applying the MRC weight vector at the relay as $\widetilde{z}[t] = (\mathbf{w}_{rx}^{sr})^H\mathbf{z}[t]$, which yelids

$$\begin{aligned}\widetilde{z}[t] =& \sqrt{P_{sr}}(\mathbf{w}_{rx}^{sr})^H\mathbf{G}_{rx}\mathbf{H}_{sr}\mathbf{w}_{tx}^{sr}s_o[t] + \sqrt{P_{rr}}(\mathbf{w}_{rx}^{sr})^H\underbrace{\mathbf{G}_{rx}\mathbf{H}_{rr}\mathbf{G}_{tx}}_{\text{SIC}}\mathbf{w}_{tx}^{rd}s_{ef}[t-1] \\ &+ (\mathbf{w}_{rx}^{sr})^H\mathbf{G}_{rx}\mathbf{n}_R[t],\end{aligned} \tag{3.5}$$

where the MRC weighted vectors are defined as $\mathbf{w}_{tx}^{sr} = \mathbf{u}_{\max}^{sr}$, $\mathbf{w}_{rx}^{sr} = \mathbf{H}_{sr}\mathbf{u}_{\max}^{sr}$, and $\mathbf{w}_{tx}^{rd} = \mathbf{u}_{\max}^{rd}$ for the case of perfect CSI.

It is obvious that SIC is achieved at this stage, however, imperfect channel estimation of the undesired channel, $\mathbf{H}_{rr}$, produces residual SI. In addition, the channel estimation error for the signal of interest, $\mathbf{H}_{sr}$, will impact the performance of the system. Therefore, this issue needs to be considered by adding the effect of channel estimation error as [73]

$$\mathbf{H}_{sr} = \sqrt{1-\epsilon_{sr}^2}\widehat{\mathbf{H}}_{sr} + \epsilon_{sr}\mathbf{\Xi}_{sr}, \tag{3.6a}$$

$$\mathbf{H}_{rr} = \sqrt{1-\epsilon_{rr}^2}\widehat{\mathbf{H}}_{rr} + \epsilon_{rr}\mathbf{\Xi}_{rr}, \tag{3.6b}$$

$$\mathbf{H}_{rd} = \sqrt{1-\epsilon_{rd}^2}\widehat{\mathbf{H}}_{rd} + \epsilon_{rd}\mathbf{\Xi}_{rd}, \tag{3.6c}$$

where $\widehat{\mathbf{H}}_{sr} \sim \mathcal{CN}(0, \mathbf{I}^{N_s \times N_{rx}})$, $\widehat{\mathbf{H}}_{rr} \sim \mathcal{CN}(0, \mathbf{I}^{N_{tx} \times N_{rx}})$ and $\widehat{\mathbf{H}}_{rd} \sim \mathcal{CN}(0, \mathbf{I}^{N_{tx} \times N_d})$ represent channel estimates of $\mathbf{H}_{sr}$, $\mathbf{H}_{rr}$ and $\mathbf{H}_{rd}$, respectively. Moreover $\mathbf{\Xi}_{sr} \sim \mathcal{CN}(0, \mathbf{I}^{N_s \times N_{rx}})$, $\mathbf{\Xi}_{rr} \sim \mathcal{CN}(0, \mathbf{I}^{N_{tx} \times N_{rx}})$ and $\mathbf{\Xi}_{rd} \sim \mathcal{CN}(0, \mathbf{I}^{N_{tx} \times N_d})$ are the channel estimation errors of

$\mathbf{H}_{sr}$, $\mathbf{H}_{rr}$ and $\mathbf{H}_{rd}$, respectively, modelled as complex zero-mean Gaussian random variables with identity covariance matrices that are independent of their channels [73]. Furthermore, ϵ_{sr} and ϵ_{rr} are the channel estimation accuracies of $\widehat{\mathbf{H}}_{sr}$ and $\widehat{\mathbf{H}}_{rr}$, respectively, and in general they are defined as $\epsilon \in [0, 1]$, which implies that when $\epsilon_{sr} = \epsilon_{rr} = 0$, the channels estimation is perfect. We can use $\rho_{sr} = \sqrt{1-\epsilon_{sr}^2}$, $\rho_{rr} = \sqrt{1-\epsilon_{rr}^2}$ and $\rho_{rd} = \sqrt{1-\epsilon_{rd}^2}$ to denote the effect of channel estimation errors in $\mathbf{H}_{sr}$, $\mathbf{H}_{rr}$ and $\mathbf{H}_{rd}$, respectively. By substituting the effect of channel estimation error of (3.6) into (3.5), and applying the estimated MRC weighted vectors as $\mathbf{w}_{tx}^{sr} = \widehat{\mathbf{u}}_{\max}^{sr}$, $\mathbf{w}_{rx}^{sr} = \widehat{\mathbf{H}}_{sr}\widehat{\mathbf{u}}_{\max}^{sr}$, and $\mathbf{w}_{tx}^{rd} = \widehat{\mathbf{u}}_{\max}^{rd}$, $\widetilde{z}[t]$ can be re-written as

$$\begin{aligned}
\widetilde{z}[t] =& \sqrt{1-\epsilon_{sr}^2}\sqrt{P_{sr}}(\widehat{\mathbf{u}}_{\max}^{sr})^H\widehat{\mathbf{H}}_{sr}^H\widehat{\mathbf{G}}_{rx}\widehat{\mathbf{H}}_{sr}\widehat{\mathbf{u}}_{\max}^{sr}s_o[t] \\
&+ \epsilon_{sr}\sqrt{P_{sr}}(\widehat{\mathbf{u}}_{\max}^{sr})^H\widehat{\mathbf{H}}_{sr}^H\widehat{\mathbf{G}}_{rx}\boldsymbol{\Xi}_{sr}\widehat{\mathbf{u}}_{\max}^{sr}s_o[t] \\
&+ \sqrt{1-\epsilon_{rr}^2}\sqrt{\tilde{P}_{rr}}(\widehat{\mathbf{u}}_{\max}^{sr})^H\widehat{\mathbf{H}}_{sr}^H\widehat{\mathbf{G}}_{rx}\widehat{\mathbf{H}}_{rr}\widehat{\mathbf{G}}_{tx}\widehat{\mathbf{u}}_{\max}^{rd}s_{ef}[t-1] \\
&+ \epsilon_{rr}\sqrt{\tilde{P}_{rr}}(\widehat{\mathbf{u}}_{\max}^{sr})^H\widehat{\mathbf{H}}_{sr}^H\widehat{\mathbf{G}}_{rx}\boldsymbol{\Xi}_{rr}\widehat{\mathbf{G}}_{tx}\widehat{\mathbf{u}}_{\max}^{rd}s_{ef}[t-1] \\
&+ (\widehat{\mathbf{u}}_{\max}^{sr})^H\widehat{\mathbf{H}}_{sr}^H\,\widehat{\mathbf{G}}_{rx}\mathbf{n}_R[t],
\end{aligned} \tag{3.7}$$

where $\widehat{\mathbf{G}}_{rx}$ and $\widehat{\mathbf{G}}_{tx}$ represent the MIMO receive and transmit filters, respectively, obtained from the SVD of estimated channel of SI, $\widehat{\mathbf{H}}_{rr}$. It is important to note that $\tilde{P}_{rr}$ represents the residual power of SI after applying spatial cancellation via NSP. It can be observed that (3.7) contains the combination of the desired signal, noise, in addition to three terms of interferences, which are due to the SI channel of the FD-relay, and channel estimation errors of forward and backward loop path. Thus, the SINR of the first hop of the relay, γ_1, can be obtained from (3.7) as

$$\gamma_1 = \frac{(1-\epsilon_{sr}^2)P_{sr}\left\|(\widehat{\mathbf{u}}_{\max}^{sr})^H\widehat{\mathbf{H}}_{sr}^H\widehat{\mathbf{G}}_{rx}\widehat{\mathbf{H}}_{sr}\widehat{\mathbf{u}}_{\max}^{sr}s_o[t]\right\|^2}{C_0+C_1+C_2+C_3}, \tag{3.8}$$

with

$$C_0 = \epsilon_{sr}^2P_{sr}\left\|(\widehat{\mathbf{u}}_{\max}^{sr})^H\widehat{\mathbf{H}}_{sr}^H\widehat{\mathbf{G}}_{rx}\,\boldsymbol{\Xi}_{sr}\widehat{\mathbf{u}}_{\max}^{sr}s_o[t]\right\|^2, \tag{3.9a}$$

$$C_1 = (1-\epsilon_{rr}^2)\tilde{P}_{rr}\left\|(\widehat{\mathbf{u}}_{\max}^{sr})^H\widehat{\mathbf{H}}_{sr}^H\widehat{\mathbf{G}}_{rx}\widehat{\mathbf{H}}_{rr}\widehat{\mathbf{G}}_{tx}\widehat{\mathbf{u}}_{\max}^{rd}s_{ef}[t-1]\right\|^2, \tag{3.9b}$$

$$C_2 = \epsilon_{rr}^2\tilde{P}_{rr}\left\|(\widehat{\mathbf{u}}_{\max}^{sr})^H\widehat{\mathbf{H}}_{sr}^H\widehat{\mathbf{G}}_{rx}\,\boldsymbol{\Xi}_{rr}\widehat{\mathbf{G}}_{tx}\widehat{\mathbf{u}}_{\max}^{rd}s_{ef}[t-1]\right\|^2, \tag{3.9c}$$

$$C_3 = \left\|(\widehat{\mathbf{u}}_{\max}^{sr})^H\widehat{\mathbf{H}}_{sr}^H\widehat{\mathbf{G}}_{rx}\,\mathbf{n}_R[t]\right\|^2, \tag{3.9d}$$

where the term in the numerator of (3.8) represents the power of the desired signal. The denominator comprises four terms which are given in (3.9). The constant term C_0 represents the interference power due to channel estimation error of $\mathbf{H}_{sr}$, term C_1 represents the SI power of the channel $\mathbf{H}_{rr}$, term C_2 accounts for the power of interference caused by imperfect channel estimation of $\mathbf{H}_{rr}$, and finally, C_3 is for the noise power after passing through the MRC and SIC relay filters.

Equations (3.8) needs to be simplified in order to appreciate the contribution of the individual terms. To achieve this, firstly, we divide the numerator and denominator by $\left\|\widehat{\mathbf{G}}_{rx}\right\|^2$. Secondly, since $\widehat{\mathbf{u}}^{sr}_{\max}$ is the estimated eigenvector corresponding to the largest estimated eigenvalue $\widehat{\lambda}^{sr}_{\max}$ of the Wishart matrix $\mathbf{H}^H_{sr}\mathbf{H}_{sr}$, it is constructive to compensate for $(\widehat{\lambda}^{sr}_{\max})^2$ instead of $\left\|(\widehat{\mathbf{u}}^{sr}_{\max})^H\widehat{\mathbf{H}}^H_{sr}\widehat{\mathbf{H}}_{sr}\widehat{\mathbf{u}}^{sr}_{\max}\right\|^2$, and for $\widehat{\lambda}^{sr}_{\max}$ instead of $\left\|(\widehat{\mathbf{u}}^{sr}_{\max})^H\widehat{\mathbf{H}}^H_{sr}\right\|^2$. Moreover, from the definitions of $\mathbf{\Xi}_{sr}$ and $\mathbf{\Xi}_{rr}$ following (3.6), we have $\mathbb{E}\left\{\|\mathbf{\Xi}_{sr}\|^2\right\} = \mathbb{E}\left\{\|\mathbf{\Xi}_{rr}\|^2\right\} = 1$ due to their unity-covariance [73]. Additionally, $\|\widehat{\mathbf{u}}^{sr}_{\max}\|^2 = \left\|\widehat{\mathbf{u}}^{rd}_{\max}\right\|^2 = 1$ as they represent the unit norm eigenvectors corresponding to the largest eigenvalues $\widehat{\lambda}^{sr}_{\max}$ and $\widehat{\lambda}^{rd}_{\max}$ of the estimated channels $\widehat{\mathbf{H}}_{sr}$ and $\widehat{\mathbf{H}}_{rd}$, respectively, as defined earlier in Section 3.2. Moreover, variance of the noise is given as $E\left\{\|\mathbf{n}_R\|^2\right\} = \sigma^2_{n_R}$. By taking all these substitutions into account and after some additional straightforward mathematical manipulations, γ_1 can be rewritten as

$$\gamma_1 = \frac{(1-\epsilon^2_{sr})\Omega_{sr}\lambda^{sr}_{\max}}{\frac{(1-\epsilon^2_{rr})\Omega_{rr}}{\lambda^{sr}_{\max}}\left\|(\widehat{\mathbf{u}}^{sr}_{\max})^H\widehat{\mathbf{H}}^H_{sr}\widehat{\mathbf{H}}_{rr}\widehat{\mathbf{G}}_{tx}\widehat{\mathbf{u}}^{rd}_{\max}\right\|^2 + \epsilon^2_{sr}\Omega_{sr} + \epsilon^2_{rr}\Omega_{rr} + 1}, \tag{3.10a}$$

$$= \frac{\frac{(1-\epsilon^2_{sr})\Omega_{sr}\lambda^{sr}_{\max}}{(\epsilon^2_{sr}\Omega_{sr}+\epsilon^2_{rr}\Omega_{rr}+1)}}{\frac{(1-\epsilon^2_{rr})\Omega_{rr}}{\lambda^{sr}_{\max}(\epsilon^2_{sr}\Omega_{sr}+\epsilon^2_{rr}\Omega_{rr}+1)}\left\|(\widehat{\mathbf{u}}^{sr}_{\max})^H\widehat{\mathbf{H}}^H_{sr}\widehat{\mathbf{H}}_{rr}\widehat{\mathbf{G}}_{tx}\widehat{\mathbf{u}}^{rd}_{\max}\right\|^2 + 1}. \tag{3.10b}$$

In (3.10), $\Omega_{sr} = P_{sr}/\sigma^2_{n_R}$ represents the SNR, while $\Omega_{rr} = \tilde{P}_{rr}/\sigma^2_{n_R}$ is the interference-to-noise ratio (INR) at the input of the MMSE transformation filter of the relay, F, after passive suppression and NSP cancellation. It can be noticed that (3.10b) represents the ratio of two independent random variables and can be re-written as

$$\gamma_1 = \frac{\alpha_{sr}\widehat{\lambda}^{sr}_{\max}}{\frac{\beta}{\lambda^{sr}_{\max}}\left\|(\widehat{\mathbf{u}}^{sr}_{\max})^H\widehat{\mathbf{H}}^H_{sr}\widehat{\mathbf{H}}_{rr}\widehat{\mathbf{G}}_{tx}\widehat{\mathbf{u}}^{rd}_{\max}\right\|^2 + 1} \tag{3.11}$$

where

$$\alpha_{sr} = \frac{(1-\epsilon^2_{sr})\Omega_{sr}}{\epsilon^2_{sr}\Omega_{sr} + \epsilon^2_{rr}\Omega_{rr} + 1}, \quad \beta = \frac{(1-\epsilon^2_{rr})\Omega_{rr}}{\epsilon^2_{sr}\Omega_{sr} + \epsilon^2_{rr}\Omega_{rr} + 1}. \tag{3.12}$$

To gain insight on the relationship between SNR and SINR, we can re-write (3.12) as $\alpha_{sr} = \frac{(1-\epsilon_{sr}^2)}{\epsilon_{sr}^2+\epsilon_{rr}^2(\Omega_{rr}/\Omega_{sr})+1/\Omega_{sr}}$ and $\beta = \frac{(1-\epsilon_{rr}^2)}{\epsilon_{sr}^2(\Omega_{sr}/\Omega_{rr})+\epsilon_{rr}^2+1/\Omega_{rr}}$. The factor $\Omega_{sr}/\Omega_{rr} = P_{sr}/\tilde{P}_{rr}$ represents here the signal-to-interference ratio (SIR). Therefore, increasing the signal power for fixed levels of SI and noise power will cause α_{sr} to increase and β to decrease, which consequently results in an increase of γ_1 in (3.11).

3.3.1.1 PDF of γ_1

We return now our attention to (3.11). The SINR is considered as the ratio of two independent random variables x and y given by

$$\gamma_1 = \frac{y}{x+1}, \tag{3.13a}$$

$$x = \frac{\beta}{\widehat{\lambda}_{\max}^{sr}} \left\| (\widehat{\mathbf{u}}_{\max}^{sr})^H \widehat{\mathbf{H}}_{sr}^H \widehat{\mathbf{H}}_{rr} \widehat{\mathbf{G}}_{tx} \widehat{\mathbf{u}}_{\max}^{rd} \right\|^2, \tag{3.13b}$$

$$y = \alpha_{sr} \widehat{\lambda}_{\max}^{sr}. \tag{3.13c}$$

Following the definitions in [52] and the derivations in [74], it is worth mentioning that the term $(\widehat{\mathbf{u}}_{\max}^{sr})^H \widehat{\mathbf{H}}_{sr}^H \widehat{\mathbf{H}}_{rr} \widehat{\mathbf{G}}_{tx} \widehat{\mathbf{u}}_{\max}^{rd} / \widehat{\lambda}_{max}^{sr}$ in (3.13b) is an independent and identically distributed (i.i.d.) complex Gaussian random variable, and it is independent of $\widehat{\lambda}_{max}^{sr}$. This is due to the earlier assumption in Section 3.3.1, that the estimated SI channel, $\widehat{\mathbf{H}}_{rr}$, exhibits a circularly symmetric Gaussian distribution with zero mean and covariance matrix $\mathbf{I}^{N_{tx} \times N_{rx}}$. The mean of this term conditioned on $\widehat{\mathbf{H}}_{sr}$ is derived as

$$\mathbb{E}\left\{ (\widehat{\mathbf{u}}_{\max}^{sr})^H \widehat{\mathbf{H}}_{sr}^H \widehat{\mathbf{H}}_{rr} \widehat{\mathbf{G}}_{tx} \widehat{\mathbf{u}}_{\max}^{rd} \mid \widehat{\mathbf{H}}_{sr} \right\} = (\widehat{\mathbf{u}}_{\max}^{sr})^H \widehat{\mathbf{H}}_{sr}^H \underbrace{\mathbb{E}\left\{ \widehat{\mathbf{H}}_{rr} \right\}}_{\text{Mean=0}} \widehat{\mathbf{G}}_{tx} \widehat{\mathbf{u}}_{\max}^{rd} = 0, \tag{3.14}$$

while its variance conditioned on $\widehat{\mathbf{H}}_{sr}$ can be derived as

$$\mathbb{E}\left\{ \left\| (\widehat{\mathbf{u}}_{\max}^{sr})^H \widehat{\mathbf{H}}_{sr}^H \widehat{\mathbf{H}}_{rr} \widehat{\mathbf{G}}_{tx} \widehat{\mathbf{u}}_{\max}^{rd} \right\|^2 \mid \widehat{\mathbf{H}}_{sr} \right\} = (\widehat{\mathbf{u}}_{\max}^{sr})^H \widehat{\mathbf{H}}_{sr}^H \underbrace{\mathbb{E}\left\{ \widehat{\mathbf{H}}_{rr} \widehat{\mathbf{G}}_{tx} \widehat{\mathbf{G}}_{tx}^H \widehat{\mathbf{H}}_{rr}^H \right\}}_{\mathbf{I}^{N_{tx} \times N_{rx}}} \widehat{\mathbf{H}}_{sr} \widehat{\mathbf{u}}_{\max}^{sr}$$

$$= (\widehat{\mathbf{u}}_{\max}^{sr})^H \widehat{\mathbf{H}}_{sr}^H \widehat{\mathbf{H}}_{sr} \widehat{\mathbf{u}}_{\max}^{sr} = \left\| (\widehat{\mathbf{u}}_{\max}^{sr})^H \widehat{\mathbf{H}}_{sr}^H \right\|^2 = \widehat{\lambda}_{\max}^{sr}. \tag{3.15}$$

A closer look into (3.15) reveals that its first equality contains two independent random variables which are $\widehat{\mathbf{H}}_{rr} \widehat{\mathbf{G}}_{tx}$ and $\widehat{\mathbf{u}}_{max}^{rd}$. As defined earlier in Section 5.2, we can substitute for $\left\| \widehat{\mathbf{u}}_{\max}^{rd} \right\|^2 = \left\| \widehat{\mathbf{u}}_{\max}^{rd} (\widehat{\mathbf{u}}_{\max}^{rd})^H \right\| = 1$. Moreover, the expectation for the first random variable can be substituted by the identity matrix $\mathbf{I}^{N_{tx} \times N_{rx}}$, as the SI channel, $\widehat{\mathbf{H}}_{rr}$, is an

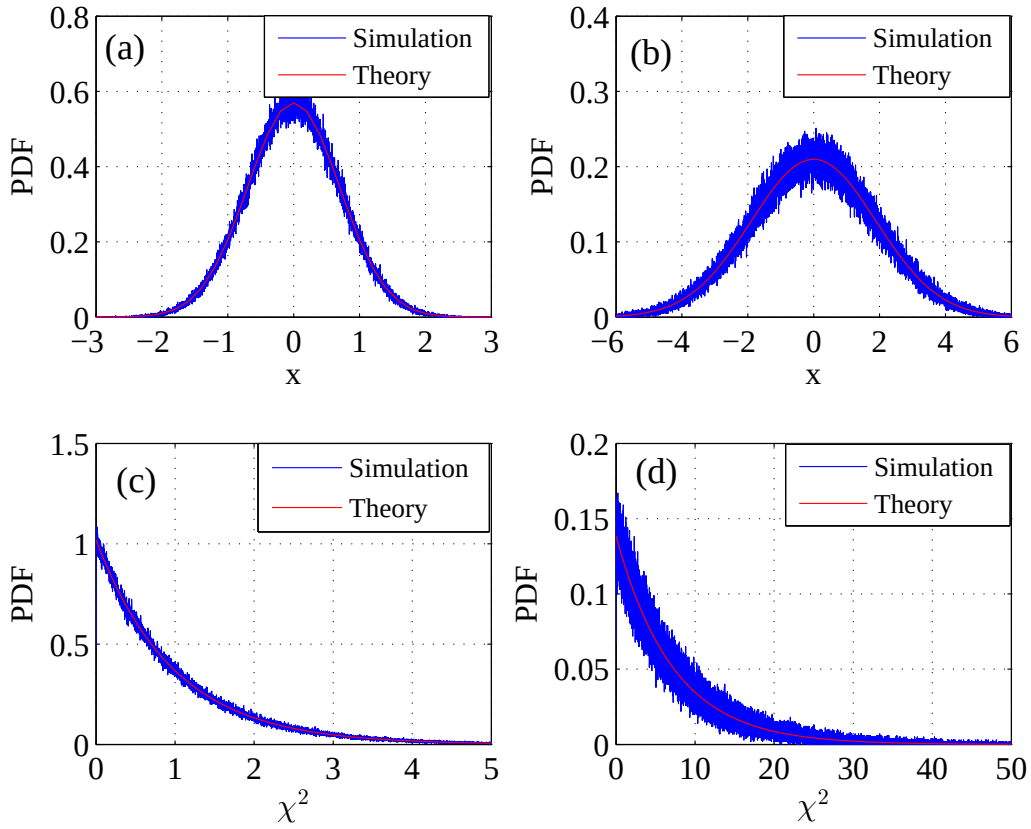

Figure 3.3: The PDF of $\Re\left\{(\widehat{\mathbf{u}}_{\max}^{sr})^H \widehat{\mathbf{H}}_{sr}^H \widehat{\mathbf{H}}_{rr} \widehat{\mathbf{G}}_{tx} \widehat{\mathbf{u}}_{\max}^{rd}\right\}$ in (a) and (b) , while the PDF of $||(\widehat{\mathbf{u}}_{\max}^{sr})^H \widehat{\mathbf{H}}_{sr}^H \widehat{\mathbf{H}}_{rr} \widehat{\mathbf{G}}_{tx} \widehat{\mathbf{u}}_{\max}^{rd}||^2$ in (c) and (d), for $\widehat{\lambda}_{max}^{sr} = 0.7$ and 1.9.

i.i.d. Rayleigh distributed random variable containing i.i.d. complex Gaussian vectors with zero-mean and covariance matrix $\mathbf{I}^{N_{tx} \times N_{rx}}$. Additionally, $\widehat{\mathbf{G}}_{tx}$ is a matrix such that $\mathbb{E}\left[\widehat{\mathbf{H}}_{rr} \widehat{\mathbf{G}}_{tx} \widehat{\mathbf{G}}_{tx}^H \widehat{\mathbf{H}}_{rr}^H\right] = \mathbf{I}^{N_{tx} \times N_{rx}}$.

In Fig. 3.3(a) and (b), the empirical (histogram) and theoretical distributions of the real part of (3.13b) are illustrated for $N_{rx} = N_{tx} = 2$, and for two different values of $\widehat{\lambda}_{max}^{sr}$, i.e. 0.7 and 1.9, respectively. It is worth noting, that due to symmetry, the distribution of the imaginary part follows a similar distribution. Since the $(\widehat{\mathbf{u}}_{\max}^{sr})^H \widehat{\mathbf{H}}_{sr}^H \widehat{\mathbf{H}}_{rr} \widehat{\mathbf{G}}_{tx} \widehat{\mathbf{u}}_{\max}^{rd}$ is a complex, zero-mean, Gaussian random variable with variance $\widehat{\lambda}_{max}^{sr}$, its norm will follow a Chi-squared distribution with N_{rx} degree of freedom [48, p. 45].

Fig. 3.3(c) and (d) demonstrate the Chi-squared distribution assumption for the variable $||(\widehat{\mathbf{u}}_{\max}^{sr})^H \widehat{\mathbf{H}}_{sr}^H \widehat{\mathbf{H}}_{rr} \widehat{\mathbf{G}}_{tx} \widehat{\mathbf{u}}_{\max}^{rd}||^2$ for the two values of $\widehat{\lambda}_{max}^{sr} = 0.7$ and 1.9, respectively.

The relationship of those two variables in (3.13b) and (3.13c) along with their scale factors in (3.12) follow the Gamma distribution [52]. Therefore, the PDF of x, $p_x(x)$, which can be denoted in general as $\mathcal{G}(x; j; \beta) = \frac{1}{\Gamma(j)} x^{j-1} \beta^{-j} e^{-x/\beta}$ [51, 75], exhibits a

shape factor $(j = 1)$ due to the fact that only one source of SI is present by assumption and the scale factor, β, which leads us to

$$p_x(x) = \frac{1}{\beta}\, e^{\frac{-x}{\beta}}. \tag{3.16}$$

In constrast, $p_y(y)$ can be given as

$$p_y(y) = \sum_{k=1}^{m} \sum_{l=n-m}^{(n+m-2k)k} c_{kl}\, \frac{1}{\Gamma(l+1)}\, y^l \left(\frac{k}{\alpha_{sr}}\right)^{l+1} e^{-\frac{k}{\alpha_{sr}}y}. \tag{3.17}$$

It is noticeable that the PDF of y follows the Gamma distribution as $\mathcal{G}(y; l+1; \alpha_{sr}/k) = \frac{1}{\Gamma(l+1)} y^l (\frac{k}{\alpha_{sr}})^{l+1} e^{-\frac{k}{\alpha_{sr}}y}$ [51, 75], with shape factor $(l+1)$ and the normalized scale factor of (α_{sr}/k). In (3.17), $m = \min\{N_s, N_{rx}\}$ and $n = \max\{N_s, N_{rx}\}$. The curve fitting coefficients, c_{kl}, of the PDF $p_y(y)$ have been determined and listed in tables for several combinations of transmit and receive antennas in [76]. Additionally, there exists a numerical method that has been proposed in [51] for the same purpose. Both approaches satisfy $\sum_{k=1}^{m} \sum_{l=n-m}^{(n+m-2k)k} c_{kl} = 1$.

After evaluating $p_x(x)$ in (3.16) and $p_y(y)$ in (3.17), the PDF of SINR of the first hop, $p_{\gamma_1}(\gamma_1)$, can be obtained by using integration as

$$p_{\gamma_1}(\gamma_1) = \int_{x=0}^{\infty} (1+x) p_y\left[(1+x)\gamma_1\right] p_x(x) dx. \tag{3.18}$$

This integration can be solved by exploiting the conversion of the term $(x+a)^n$ to a finite summation as $\sum_{k=0}^{n} \binom{n}{k} x^k a^{n-k}$ [77, Eq. (1.111)]. Subsequently, in order to obtain the final formula, it is required to compare the resulting equation with $\int_0^\infty x^{\nu-1} e^{-\mu x}\, dx = \mu^{-\nu}\Gamma(\nu)$ for positive $\mu > 0$ and $\nu > 0$ [77, Eq. (3.351.3)], i.e.

$$p_{\gamma_1}(\gamma_1) = \sum_{k=1}^{m} \sum_{l=n-m}^{(n+m-2k)k} \sum_{r=0}^{l+1} c_{kl} \frac{\Gamma(r+1)}{\Gamma_1(l+1)} \binom{l+1}{r} \left(\frac{k}{\alpha_{sr}}\right)^{l+1} \frac{1}{\beta} \left(\frac{\alpha_{sr}\beta}{\alpha_{sr} + k\beta\gamma_1}\right)^{r+1} \times \gamma_1^l e^{-\frac{k}{\alpha_{sr}}\gamma_1}. \tag{3.19}$$

3.3.1.2 Outage Probability of γ_1

To evaluate the outage probability associated with the probability that γ_1 is less than the protection ratio of the threshold SINR [78], we compute $P_{out}(\gamma_{th}) \triangleq Pr\{\gamma_1 \leq \gamma_{th}\} =$

$\int_0^{\gamma_{th}} p_{\gamma_1}(\gamma_1)\, d\gamma_1$, or equivalently

$$P_{out1}(\gamma_{th}) = \int_{\gamma_1=0}^{\gamma_{th}} \int_{x=0}^{\infty} (1+x)\, p_y\left[(1+x)\gamma_1\right]\, p_x(x)\, dx\, d\gamma_1, \tag{3.20}$$

where $p_{\gamma_1}(\gamma_1)$ is determined by (3.18).

The integration in (3.20) might be simplified by exploiting the lower incomplete Gamma function. This can be achieved by using the formula

$$\gamma(n,x) = \int_0^x r^{n-1} e^{-r} dr = \Gamma(n)\left(1 - e^{-x}\sum_{k=0}^{n-1}\left(x^k/k!\right)\right), \tag{3.21}$$

for positive integers n, which is part of (3.20) [77, Eq. (8.3521.1)]. In addition, it is required to use the binomial term $(x+a)^n$ for $a=1$, which has been previously defined in this section. The outage probability can be then expressed as

$$\begin{aligned} P_{out1}(\gamma_{th}) = \sum_{k=1}^{m} \sum_{l=n-m}^{(n+m-2k)k} c_{kl} \Bigg[1 - e^{-\frac{k\gamma_{th}}{\alpha_{sr}}} \sum_{r=o}^{l}\sum_{s=0}^{r} \frac{\Gamma(s+1)}{\Gamma(r+1)} \binom{r}{s} \left(\frac{1}{\beta}\right) \left(\frac{k\gamma_{th}}{\alpha_{sr}}\right)^r \\ \times \left(\frac{\alpha_{sr}\beta}{\alpha_{sr} + k\beta\gamma_{th}}\right)^{s+1} \Bigg]. \end{aligned} \tag{3.22}$$

3.3.1.3 ASER for M-PSK Modulation Scheme for First Hop

In order to evaluate the exact ASER, $\bar{P}_e$, for any M-PSK modulation scheme, it is constructive to define the instantaneous SER $P_e(\gamma)$ for the scheme under consideration. Subsequently, by taking the expectation of SER over the instantaneous SINR, i.e. the mean of $P_e(\gamma)$ we obtain

$$\bar{P}_e(\gamma_1) = \mathbb{E}\left\{P_e(\gamma_1)\right\} = \int_0^{\infty} P_e(\gamma_1)\, p_{\gamma_1}(\gamma_1)\, d\gamma_1, \tag{3.23}$$

where $P_e(\gamma_1)$ can be defined with respect to Q-function as $P_e(\gamma_1) = aQ(\sqrt{2g\gamma_1})$, which is a general formula valid for several modulation schemes with a and g being modulation dependent constants. For instance, $(a=1, g=1)$ for binary phase shift keying (BPSK), and $(a=2, g \approx \sin^2(\pi/M))$ as acceptable approximated SER of M-PSK [79].

Now, it can be continued to derive the ASER for several modulation schemes by recalling (3.16)-(3.18) along with (3.23) to obtain

$$\bar{P}_{e1} = \sum_{k=1}^{m} \sum_{l=n-m}^{(n+m-2k)k} \frac{a\, c_{kl}}{\beta} \int_{x=0}^{\infty} e^{\frac{-x}{\beta}} \mathcal{J}\left(2g, \frac{k\,(1+x)}{\alpha_{sr}}, l+1\right) dx, \tag{3.24}$$

where $\mathcal{J}(\,.\,,\,.\,,\,.\,)$ is defined as

$$\begin{aligned}\mathcal{J}\left(2g, \frac{k\,(1+x)}{\alpha_{sr}}, l+1\right) =& \frac{1}{\Gamma(l+1)} \left(\frac{k\,(1+x)}{\alpha_{sr}}\right)^{l+1} \int_{\gamma=0}^{\infty} Q\left(\sqrt{2g\gamma}\right) \\ & \times \exp\left(\frac{-k\,(1+x)\,\gamma}{\alpha_{sr}}\right) \gamma^{l}\, d\gamma. \end{aligned} \tag{3.25}$$

At this point, in order to complete the required integrations in (3.24) and (3.25), an alternative formulation of the Q-function known as Craig's expression needs to be utilized, which is given as, $Q\left(\sqrt{2g\gamma}\right) = \frac{1}{\pi}\int_0^{\pi/2} \exp\left(\frac{-2\,g\,\gamma}{2\,\sin^2\theta}\right) d\theta$ [79]. Additionally, by recalling again $\int_0^{\infty} \gamma^{\nu-1} e^{-\mu\gamma} d\gamma = \mu^{-\nu}\Gamma(\nu)$ and after straightforward mathematical manipulations, we can re-write (3.24), as

$$\bar{P}_{e1} = \sum_{k=1}^{m} \sum_{l=n-m}^{(n+m-2k)k} \frac{a\, c_{kl}}{\beta} \int_{x=0}^{\infty} e^{\frac{-x}{\beta}} \mathcal{I}\left(\pi/2\,,\ \frac{g\alpha_{sr}}{k\,(x+1)}\ ,\ l+1\right) dx, \tag{3.26}$$

where $\mathcal{I}(\,.\,,\,.\,,\,.\,)$ is defined in (3.27) and it has been solved in [80, Section 5.4.4] as

$$\begin{aligned}\mathcal{I}\Big(\frac{\pi}{2}, \frac{g\alpha_{sr}}{k(x+1)}, l+1\Big) &= \frac{1}{\pi}\int_0^{\pi/2} \Big(\frac{\sin^2\theta}{\sin^2\theta + \frac{g\alpha_{sr}}{k(x+1)}}\Big)^{l+1} d\theta, \\ &= \frac{1}{2} - \frac{\sqrt{g\alpha_{sr}/k}}{2} \sum_{r=0}^{l} \sum_{s=0}^{r} U_{rs}\, x^{s} \left(\frac{1}{1+(g\alpha_{sr}/k)+x}\right)^{r+\frac{1}{2}}, \end{aligned} \tag{3.27}$$

where $U_{sr} = \binom{2r}{r}\binom{r}{s}\left(\frac{1}{4}\right)^{r}$. In order to complete the integration of (3.26), we proceed by identifying the confluent hypergeometric function of the second kind embedded within (3.26). This function is defined by [77, Eq. (9.211.4)] as

$$\Psi\,(a; b; z) = \frac{1}{\Gamma\,(a)} \int_0^{\infty} e^{-zx}\ x^{a-1}\,(1+x)^{b-a-1}\, dx. \tag{3.28}$$

The ASER can be then obtained for several modulation schemes by choosing the appro-

priate digital modulation constants a and g as

$$\bar{P}_{e1} = \sum_{k=1}^{m} \sum_{l=n-m}^{(n+m-2k)k} \frac{a\, c_{kl}}{2} \Bigg[1 - \left(\frac{g\alpha_{sr}}{k}\right)^{\frac{1}{2}} \frac{1}{\beta} \sum_{r=0}^{l} \sum_{s=0}^{r} \binom{2r}{r} \binom{r}{s} \left(\frac{1}{4}\right)^{r} \Gamma(s+1) \times \left(1 + \frac{g\alpha_{sr}}{k}\right)^{(s-r+\frac{1}{2})} \Psi\left(s+1; s-r+\frac{3}{2}; \frac{1}{\beta}\left(1+\frac{g\alpha_{sr}}{k}\right)\right) \Bigg]. \tag{3.29}$$

The confluent hypergeometric function can be solved using the generalized hypergeometric function either by (3.30) [77, Eq. (9.210.2)], or (3.31) [81, Eq.(6.6.1)] for positive values of a and z, i.e.

$$\Psi(a;b;z) = \frac{\pi}{\sin(\pi b)} \left[\frac{{}_1F_1(a;b;z)}{\Gamma(a-b+1)\,\Gamma(b)} - \frac{z^{1-b}\,{}_1F_1(a-b+1;2-b;z)}{\Gamma(a)\,\Gamma(2-b)} \right], \tag{3.30}$$

$$\Psi(a;b;z) = z^{-a}\,{}_2F_0\left(a, 1+a-b; \quad ; -z^{-1}\right). \tag{3.31}$$

3.3.2 SINR of the Second Hop

The second hop of this proposed system is assumed to be a conventional MRC-MIMO system, where the relay forwards the equalized signal after applying transmit beamforming, $\mathbf{w}_{tx}^{rd} = \mathbf{u}_{\max}^{rd}$, and the spatial filter, $\mathbf{G}_{tx}$. Therefore, the received signal vector at the destination can be written as

$$\mathbf{y}_D[t] = \sqrt{P_{rd}}\mathbf{H}_{rd}\mathbf{G}_{tx}\mathbf{w}_{tx}^{rd}s_{ef}[t-1] + \mathbf{n}_D[t], \tag{3.32}$$

where P_{rd} is the relay's average transmit power to the destination. By applying the MRC weighting vector, $(\mathbf{w}_{rx}^{rd})^H$, to (3.32) we can obtain the $(t-1)^{th}$ time instant of $\hat{s}_o$ as

$$\hat{s}_o[t-1] = \sqrt{P_{rd}}(\mathbf{w}_{rx}^{rd})^H\mathbf{H}_{rd}\mathbf{G}_{tx}\mathbf{w}_{tx}^{rd}s_{ef}[t-1] \; + (\mathbf{w}_{rx}^{rd})^H\mathbf{n}_D[t], \tag{3.33}$$

where $(\mathbf{w}_{rx}^{rd})^H = (\mathbf{u}_{\max}^{rd})^H\mathbf{H}_{rd}^H$ for the case of perfect CSI $\mathbf{H}_{rd}$. By considering the impact of imperfect CSI estimation of $\mathbf{H}_{rd}$ in (3.6c) and applying the estimated MRC weighted

vectors as $(\mathbf{w}_{rx}^{rd})^H = (\widehat{\mathbf{u}}_{\max}^{rd})^H \hat{\mathbf{H}}_{rd}^H$ and $\mathbf{w}_{tx}^{rd} = \widehat{\mathbf{u}}_{\max}^{rd}$, we can re-write (3.33) as

$$\begin{aligned}\hat{s}_o[t-1] =& \sqrt{1-\epsilon_{rd}^2}\sqrt{P_{rd}}\,(\widehat{\mathbf{u}}_{\max}^{rd})^H \widehat{\mathbf{H}}_{rd}^H \widehat{\mathbf{H}}_{rd} \widehat{\mathbf{G}}_{tx} \widehat{\mathbf{u}}_{\max}^{rd} s_{ef}[t-1] \\ &+ \epsilon_{rd}\sqrt{P_{rd}} (\widehat{\mathbf{u}}_{\max}^{rd})^H \widehat{\mathbf{H}}_{rd}^H \boldsymbol{\Xi}_{rd} \widehat{\mathbf{G}}_{tx} \widehat{\mathbf{u}}_{\max}^{rd} s_{ef}[t-1] \\ &+ (\widehat{\mathbf{u}}_{\max}^{rd})^H \widehat{\mathbf{H}}_{rd}^H \mathbf{n}_D[t]. \end{aligned} \tag{3.34}$$

It can be noticed that $\hat{s}_o[t-1]$ in (3.34) contains a combination of three terms, which are the desired signal, the channel estimation error term, and the noise, respectively. Therefore, the SINR of this path, γ_2, can be extracted for the second hop of the relay as

$$\gamma_2 = \frac{(1-\epsilon_{rd}^2) P_{rd} \left\| (\widehat{\mathbf{u}}_{\max}^{rd})^H \widehat{\mathbf{H}}_{rd}^H \widehat{\mathbf{H}}_{rd} \widehat{\mathbf{G}}_{tx} \widehat{\mathbf{u}}_{\max}^{rd} s_{ef}[t-1] \right\|^2}{C_4 + C_5}, \tag{3.35}$$

where

$$C_4 = \epsilon_{rd}^2 P_{rd} \left\| (\widehat{\mathbf{u}}_{\max}^{rd})^H \widehat{\mathbf{H}}_{rd}^H \boldsymbol{\Xi}_{rd} \widehat{\mathbf{G}}_{tx}\, \widehat{\mathbf{u}}_{\max}^{rd} s_{ef}[t-1] \right\|^2, \tag{3.36a}$$

$$C_5 = \left\| (\widehat{\mathbf{u}}_{\max}^{rd})^H \widehat{\mathbf{H}}_{rd}^H \mathbf{n}_D[t] \right\|^2. \tag{3.36b}$$

It is worth mentioning that C_4 represents the interference power due to channel estimation error of $\mathbf{H}_{rd}$ and C_5 is for the noise power after passing through the MRC stage of the destination node. In order to simplify (3.35), we can apply the similar simplifications and substitutions applied previously to (3.8) in Subsection 3.3.1 in order to re-write (3.35) as

$$\gamma_2 = \alpha_{rd} \lambda_{\max}^{rd}, \tag{3.37}$$

where

$$\alpha_{rd} = \frac{(1-\epsilon_{rd}^2)\Omega_{rd}}{\epsilon_{rd}^2 \Omega_{rd} + 1}, \tag{3.38}$$

where $\Omega_{rd} = P_{rd}/\sigma_{n_D}^2$ represents the SNR of the second hop.

3.3.2.1 PDF of γ_2

Unlike (3.11), the SINR of the second hop in (3.37) depends on one random variable. Thus, compared to (3.13c), we can employ (3.17) to evaluate the PDF of the output SINR of the second hop, $p_{\gamma_2}(\gamma_2)$ as

$$p_{\gamma_2}(\gamma_2) = \sum_{k=1}^{m} \sum_{l=n-m}^{(n+m-2k)k} \frac{c_{kl}\gamma_2^l}{\Gamma(l+1)} \left(\frac{k}{\alpha_{rd}}\right)^{l+1} e^{-\frac{k}{\alpha_{rd}}\gamma_2}. \tag{3.39}$$

3.3.2.2 Outage Probability of γ_2

Similar to the derivation of the outage probability for the SINR in Subsubsection 3.3.1.2 for the first hop, we can use the definition $P_{out}(\gamma_{th}) \triangleq Pr\{\gamma_2 \leq \gamma_{th}\} = \int_0^{\gamma_{th}} p_{\gamma_2}(\gamma_2)\, d\gamma_2$, and apply the solution for this integration for positive integers n as $\gamma(n,x) = \int_0^x r^{n-1}e^{-r}dr = \Gamma(n)\left(1 - e^{-x}\sum_{k=0}^{n-1}\left(x^k/k!\right)\right)$, to obtain the outage probability as

$$P_{out2}(\gamma_{th}) = \sum_{k=1}^{m} \sum_{l=n-m}^{(n+m-2k)k} c_{kl}\left(\frac{k}{\alpha_{rd}}\right)\left[1 - e^{-\frac{k\gamma_{th}}{\alpha_{rd}}} \times \sum_{r=o}^{l} \frac{1}{\Gamma(r+1)}\left(\frac{k\gamma_{th}}{\alpha_{rd}}\right)^r\right]. \tag{3.40}$$

3.3.2.3 ASER for M-PSK Modulation Scheme for Second Hop

In order to obtain the ASER of the second hop, we can utilize directly (3.23), for γ_2, along with (3.39), and utilizing the Q-function instead of $P_e(\gamma_2)$, i.e. $P_e(\gamma_2) = aQ(\sqrt{2g\gamma_2})$, as defined previously in Subsubsection 3.3.1.3, to obtain

$$\bar{P}_{e2}(\gamma_2) = \sum_{k=1}^{m} \sum_{l=n-m}^{(n+m-2k)k} \frac{c_{kl}\, a}{\Gamma(l+1)}\left(\frac{k}{\alpha_{rd}}\right)^{l+1} \int_{\gamma_2=0}^{\infty} \gamma_2^l e^{-\frac{k}{\alpha_{rd}}\gamma_2} Q\left(\sqrt{2g\gamma_2}\right) d\gamma_2. \tag{3.41}$$

In order to complete the required integration in (3.41), an alternative formulation of the Q-function known as Craig's expression can be utilized, which is defined and solved by [79, 80] as

$$Q\left(\sqrt{2g\gamma_2}\right) = \frac{1}{\pi}\int_0^{\pi/2} \exp\left(\frac{-2\,g\,\gamma_2}{2\,\sin^2\theta}\right) d\theta. \tag{3.42}$$

Additionally, by recalling again $\int_0^\infty \gamma^{\nu-1}e^{-\mu\gamma}d\gamma = \mu^{-\nu}\Gamma(\nu)$, and after straightforward mathematical simplifications, we can re-write (3.41) as

$$\bar{P}_{e2} = \sum_{k=1}^{m} \sum_{l=n-m}^{(n+m-2k)k} \frac{a c_{kl}}{\pi} \int_0^{\frac{\pi}{2}} \left(\frac{\sin^2\theta}{\sin^2\theta + \left(\frac{g\alpha_{rd}}{k}\right)}\right)^{l+1} d\theta, \tag{3.43}$$

where the integration in (3.43) can be solved by [80, eq. 5A.21] to obtain the final expression of $\bar{P}_{e2}$ as

$$\bar{P}_{e2} = \sum_{k=1}^{m} \sum_{l=n-m}^{(n+m-2k)k} \frac{a c_{kl}}{2} \left[1 - \sqrt{\frac{R}{1+R}} \sum_{r=0}^{l} \binom{2r}{r} \frac{1}{\Big(4+4R\Big)^{r}} \right], \tag{3.44}$$

where $R = g\alpha_{rd}/k$. Now, after obtaining the outage probabilities and ASER for the first and second hops, we can evaluate the E2E performance for these two metrics by re-calling (3.3) which is given by [72] as

$$P_{out}\left(\gamma_{th}\right) = P_{out1}\left(\gamma_{th}\right) + P_{out2}\left(\gamma_{th}\right) - 2P_{out1}\left(\gamma_{th}\right) P_{out2}\left(\gamma_{th}\right) \tag{3.45}$$

$$\bar{P}_{e}(\gamma_1, \gamma_2) = \bar{P}_{e1}(\gamma_1) + \bar{P}_{e2}(\gamma_2) - 2\bar{P}_{e1}(\gamma_1)\bar{P}_{e2}(\gamma_2) \tag{3.46}$$

3.4 Linear MMSE equalizer

In this section, we will derive the coefficient F of the proposed EF relay, the results in MMSE between the transmitted symbols of the source node $s_o[t]$ and the equalized symbols in the relay $s_{ef}[t]$. From Fig. 3.2, we can express the symbol at the input of the equalization stage $\widetilde{z}[t]$ as

$$\widetilde{z}[t] = \left(\mathbf{w}_{rx}^{sr}\right)^{H} \mathbf{G}_{rx} \Big[\mathbf{H}_{sr} \mathbf{w}_{tx}^{sr} s_o[t] + \mathbf{H}_{rr} \mathbf{s}_i[t] + \mathbf{n}_R[t] \Big], \tag{3.47}$$

while the t^{th} symbol at the out of the equalization stage $s_{ef}[t]$ can be evaluated as $s_{ef} = F\,\widetilde{z}[t]$, which can be re-written using (3.47) as

$$s_{ef}[t] = F(\mathbf{w}_{rx}^{sr})^{H} \mathbf{G}_{rx} \mathbf{H}_{sr} \mathbf{w}_{tx}^{sr} s_o[t] + F\left(\mathbf{w}_{rx}^{sr}\right)^{H} \mathbf{G}_{rx} \mathbf{H}_{rr} \mathbf{s}_i[t] + F\left(\mathbf{w}_{rx}^{sr}\right)^{H} \mathbf{G}_{rx} \mathbf{n}_R[t]. \tag{3.48}$$

Now, we can define MSE, $MSE(F)$, between the transmitted symbol, $s_o[t]$, and the equalized symbol, $s_{ef}[t]$, as

$$MSE(F) \triangleq \mathbb{E}\left\{ (s_o[t] - s_{ef}[t])(s_o[t] - s_{ef}[t])^{*} \right\}. \tag{3.49}$$

From (3.48), and after some manipulation and simplification steps, (3.49) becomes

$$MSE(F) = F\left[\sigma^2_{s_o} h_o h_o^* + \sigma^2_{s_{ef}} h_I h_I^* + \overline{R}_{n_R}\right] F^* - \quad h_o^* F^* - h_I^* F^*, \tag{3.50}$$

with

$$h_o = (\mathbf{w}_{rx}^{sr})^H \mathbf{G}_{rx} \mathbf{H}_{sr} \mathbf{w}_{tx}^{sr}, \tag{3.51a}$$

$$h_I = (\mathbf{w}_{rx}^{sr})^H \mathbf{G}_{rx} \mathbf{H}_{rr} \mathbf{G}_{rx} \tag{3.51b}$$

$$\overline{R}_{n_R} = (\mathbf{w}_{rx}^{sr})^H \mathbf{G}_{rx} \mathbf{R}_{n_R} \mathbf{G}_{rx}^H \mathbf{w}_{rx}^{sr}. \tag{3.51c}$$

Following to the derivations in [82, 83], this MSE function is a convex function of F^*, therefore, the optimum value of F, which represents the MMSE between $s_o[t]$ and $s_{ef}[t]$, can be obtained by applying a differentiation to (3.50) with respect to F^* and equating the result to zero. Thus, the transformation coefficient of the EF-relay, F, can be obtained in exact form as

$$F = \left[\sigma^2_{s_o} h_o h_o^* + \sigma^2_{s_{ef}} h_I h_I^* + \overline{R}_{n_R}\right]^{-1} (h_o^* + h_I^*) \tag{3.52}$$

3.5 E2E Capacity

In this section, we derive the E2E capacity of the proposed FD-MRC-MIMO based on EF relaying in the presence of SI. This derivation aims to obtain the upper bound of the mutual information between the source and the destination by assuming perfect channel estimation. We assume that the processing delay in the EF relaying operation can be applied within a symbol duration. i.e. $\mathbf{s}_i[t] = \mathbf{G}_R\ \mathbf{r}[t-1]$, where $\mathbf{s}_i[t]$ is the transmitted signal at the relay output at time instant t and $\mathbf{G}_R = \mathbf{G}_{tx} \mathbf{w}_{tx}^{rd} F\ (\mathbf{w}_{rx}^{sr})^H\ \mathbf{G}_{rx}$ represents the combination of all stages of the EF relaying operation in Fig.3.2. Hence, we can write $\mathbf{s}_i[t]$ as a function of the received signal at the relay input, $\mathbf{r}[t-1]$, defined in (3.4) to obtain

$$\mathbf{s}_i[t] = \mathbf{G}_R\Big(\mathbf{H}_{sr} \mathbf{w}_{tx}^{sr} s_o[t-1] + \mathbf{H}_{rr}\ \mathbf{s}_i(s_o[t-2]) + \mathbf{n}_R[t-1]\Big). \tag{3.53}$$

At the destination, the received signal, $\mathbf{y}_D$ can be written as

$$\mathbf{y}_D[t] = \mathbf{H}_{rd}\ \mathbf{s}_i[t] + \mathbf{n}_D[t], \tag{3.54}$$

where $\mathbf{n}_D[t]$ represents the AWGN in the input of the destination. Moreover, MRC combining is applied to $\mathbf{y}_D[t]$ at the destination as $\hat{s}_o[t-1] = (\mathbf{w}_{rx}^{rd})^H \mathbf{y}_D[t]$. Hence, $\hat{s}_o[t-1]$ can be written as

$$\hat{s}_o[t-1] = (\mathbf{w}_{rx}^{rd})^H \mathbf{H}_{rd}\, \mathbf{s}_i[t] + (\mathbf{w}_{rx}^{rd})^H \mathbf{n}_D[t]. \tag{3.55}$$

At the moment, by substituting (3.53) in (3.55) we can obtain

$$\begin{aligned}\hat{s}_o[t-1] =& (\mathbf{w}_{rx}^{rd})^H \mathbf{H}_{rd}\mathbf{G}_R\Big(\mathbf{H}_{sr}\mathbf{w}_{tx}^{sr} s_o[t-1] + \mathbf{H}_{rr}\mathbf{s}_i[t-2] + \mathbf{n}_R[t-1]\Big) + (\mathbf{w}_{rx}^{rd})^H \mathbf{n}_D[t], \\ =& \mathbf{G}_D\mathbf{H}_{sr}\mathbf{w}_{tx}^{sr} s_o[t-1] + \mathbf{G}_D\mathbf{H}_{rr}\mathbf{s}_i[t-2] + \mathbf{G}_D\mathbf{n}_R[t-1] + (\mathbf{w}_{rx}^{rd})^H \mathbf{n}_D[t],\end{aligned} \tag{3.56}$$

where $\mathbf{G}_D = (\mathbf{w}_{rx}^{rd})^H \mathbf{H}_{rd}\mathbf{G}_R$ was introduced for simplification. From (3.56), we can find the E2E mutual information of the proposed system, which can be written as

$$\mathcal{I}(s_o; \hat{s}_o) = \log_2 \left| \mathbf{I} + \sigma_{s_o}^2 \mathbf{G}_D \mathbf{H}_{sr} \mathbf{w}_{tx}^{sr} (\mathbf{w}_{tx}^{sr})^H \mathbf{H}_{sr}^H \mathbf{G}_D^H \mathbf{R}_{nn}^{-1} \right|, \tag{3.57}$$

where $\sigma_{s_o}^2 \triangleq \mathbb{E}\{s_o s_o^*\} = \frac{P_{sr}}{N_s}$ is the variance of the transmitted signal at source node, and $\mathbf{R}_{nn}$ represents the overall covariance matrix of SI and the noises in the inputs of the relay and the destination, and it can be defined as

$$\mathbf{R}_{nn} = \mathbf{G}_D \mathbf{H}_{rr} \mathbf{R}_{s_i} \mathbf{H}_{rr}^H \mathbf{G}_D^H + \mathbf{G}_D \mathbf{R}_{n_R} \mathbf{G}_D^H + (\mathbf{w}_{rx}^{rd})^H \mathbf{R}_{n_D} \mathbf{w}_{rx}^{rd}, \tag{3.58}$$

where $\mathbf{R}_{n_R} \triangleq \mathbb{E}\{\mathbf{n}_R \mathbf{n}_R^H\} = \sigma_{n_R}^2 \mathbf{I}^{N_{rx}}$ is covariance matrix of the noise at the input of the relay, while $\mathbf{R}_{n_D} \triangleq \mathbb{E}\{\mathbf{n}_D \mathbf{n}_D^H\} = \sigma_{n_D}^2 \mathbf{I}^{N_D}$ is the covariance matrix of noise at the input of the destination node. Additionally, $\mathbf{R}_{s_i} \triangleq \mathbb{E}\{\mathbf{s}_i \mathbf{s}_i^H\} = \frac{P_i}{N_{tx}} \mathbf{I}^{N_{tx}} = \sigma_{s_{ef}}^2 \mathbf{G}_{rx} \mathbf{w}_{tx}^{rd} (\mathbf{w}_{tx}^{rd})^H \mathbf{G}_{rx}^H$, which represents the covariance matrix of the relay's transmitted signal causing SI at its receive input. Finally, $\sigma_{s_{ef}}^2 \triangleq \mathbb{E}\{s_{ef} s_{ef}^*\}$ is the variance of the equalized signal at the relay.

3.6 Simulation Results and Discussion

In this section, the E2E performance of FD-MRC-MIMO based EF relaying system after applying SIC is considered. Two configurations of the proposed system (N_s, N_{rx}, N_{tx}, N_d) are considered using, i.e. (2,2,2,2) and (4,4,4,4), respectively. The E2E performance is

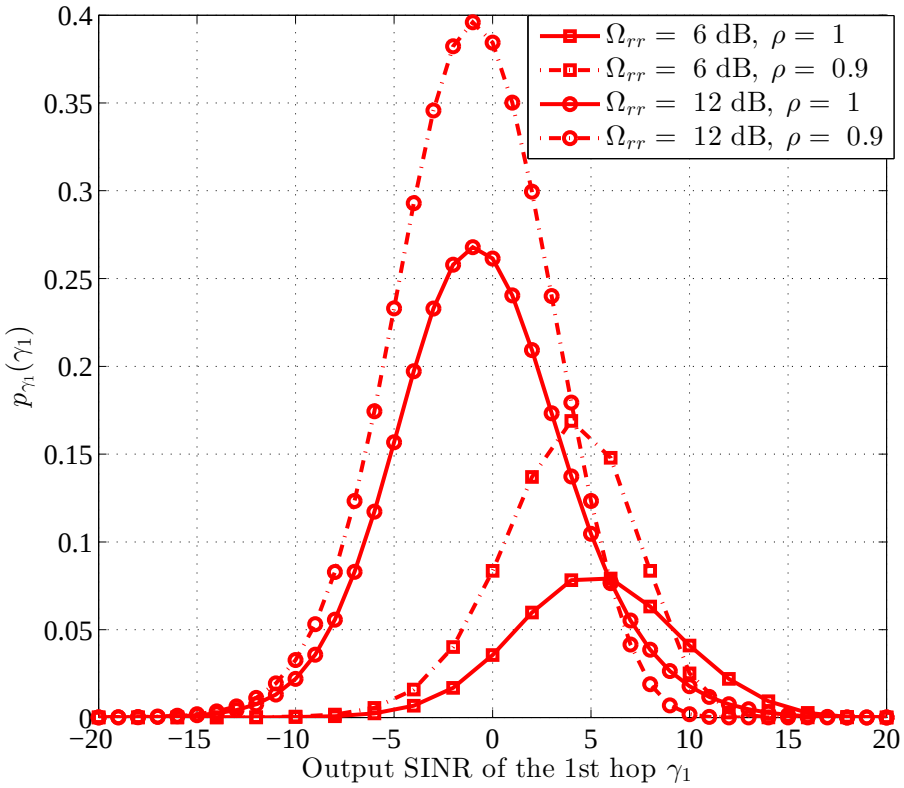

Figure 3.4: PDF of the SINR of the first hop for $(2, 2, 2, 2)$ FD-MRC-MIMO after SIC for $\Omega_{sr} = 10$ dB with perfect and imperfect channel estimation in the presence of residual SI with $\Omega_{rr} = 6$ and 12 dB.

analyzed and simulated depending on the fact that the impairment of SI impacts on the FD-relay input only due to FD operation, as assumed in this chapter, and a mitigation using SIC is applied by taking into account residual SI due to imperfect channel estimation in both desired and interference channels. In addition, the relay-to-destination path is considered a regular MIMO link. Moreover, the channels are considered to be independent flat Rayleigh fading channels. The outage probability of the output SINR, in addition to the exact ASER have been simulated and the obtained results have been analyzed. Also, we assumed that the estimation errors for all channels in this chapter are the same, i.e. $\rho = \rho_{sr} = \rho_{rr} = \rho_{rd}$.

Figs. 3.4 and 3.5 show respectively the PDFs of the SINR for the first hop, γ_1, for $(2, 2, 2, 2)$ and $(4, 4, 4, 4)$ FD-MRC-MIMO system in the case of perfect channel estimation ($\rho = 1$) and an imperfect channel estimation ($\rho = 0.9$) at $\Omega_{sr} = 10$ dB and for two values of Ω_{rr}, namely 6 and 12 dB. The illustrated PDFs demonstrate that obtaining more precise CSI via increasing the accuracy of channel estimation, results in increased output SINR.

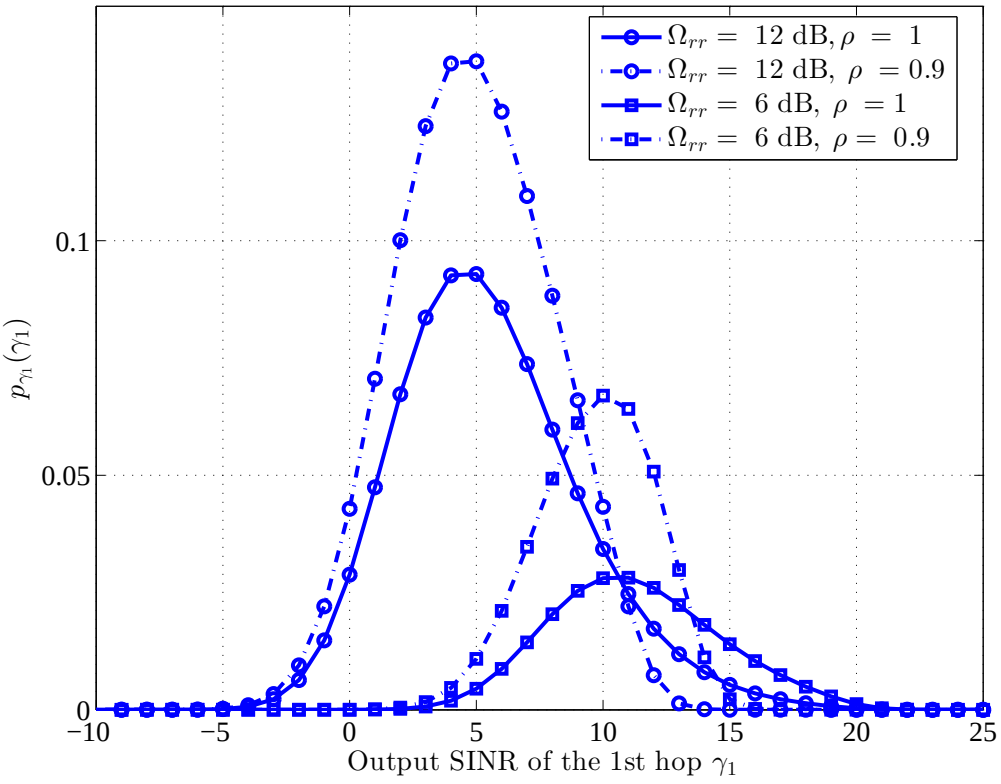

Figure 3.5: PDF of the SINR of the first hop for $(4, 4, 4, 4)$ FD-MRC-MIMO after SIC for $\Omega_{sr} = 10$ dB with perfect and imperfect channel estimation in the presence of residual SI with $\Omega_{rr} = 6$ and 12 dB.

Fig. 3.6 depicts the E2E outage probability of $(2, 2, 2, 2)$ and $(4, 4, 4, 4)$ FD-MRC-MIMO system as a function of the SINR threshold, γ_{th}, for perfect and imperfect channel estimations, i.e. $\rho = 1$ and $\rho = 0.9$, respectively, and for two cases of residual SI to noise ratios, which are $\Omega_{rr} = 6$ and 12 dB, while the SNR was fixed at $\Omega_{sr} = \Omega_{rd} = 10$ dB.

On the other hand, Fig. 3.7 shows the relationship between the overall E2E outage probability and SNR ($\Omega_{sr} = \Omega_{rd}$), for the same conditions as outlined in Fig. 3.6, except for the SINR threshold that in this case was fixed at 10 dB. It is evident from the two figures that increasing the number of antennas in FD-MRC-MIMO leads to better performance and enables the system to tolerate more residual SI caused due to channel estimation errors.

Fig. 3.8 shows the ASER for the system using QPSK modulation scheme, ($M = 4$), for the two channel estimation cases and for the two values of SI mentioned previously during this section.

Moreover, the analytical results obtained from the derived expression of ASER for QPSK modulation are compared with results obtained via Monte-Carlo simulations as

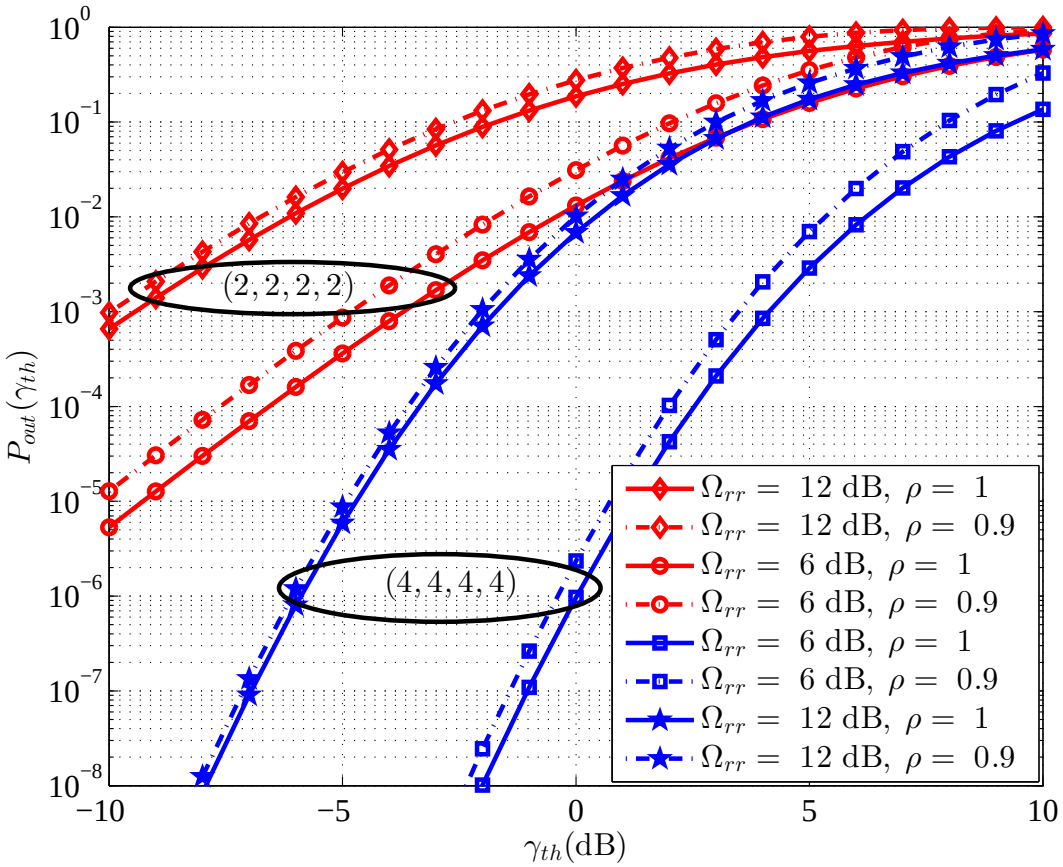

Figure 3.6: E2E outage probability of (2,2,2,2) and (4,4,4,4) FD-MRC-MIMO after SIC at $\Omega_{sr} = \Omega_{rd} = 10$ dB and residual $\Omega_{rr} = 6$ and 12 dB with perfect and imperfect channel estimation.

shown in Fig. 3.9 for a (2,2,2,2) FD-MRC-MIMO system. In this figure, it is considered higher Ω_{rr} scenarios ranging between 15 and 30 dB for four cases of channel estimation errors, i.e. $\rho = 0.9, 0.95, 0.99$ and 1. The ASER vs. SNR performance results are obtained by averaging 10^4 frames containing 2048 bits for each SNR point. A closer look at the results shows close agreement between simulation and theory. Furthermore, the impact of imperfect channel estimation under higher Ω_{rr} can be shown in this figure, where the proposed system demonstrates more tolerant and closer achievement to perfect channel estimation at 1% error in CSI. Whilst, by increasing the channels estimation error by 5% and 10%, this causes a deterioration in the performance as expected.

In addition, in Fig. 3.10, the proposed system is compared with another relevant state-of-the-art NSP technique, that is reported in [38], which utilizes SI suppression using ZF approach for a FD-MIMO relay and the results obtained in [38] are for the first hop due to the fact that the first hop is affected by the SI, whilst the second hop represents a regular MIMO link. Fig. 3.10 demonstrates the BER vs. SNR performance for (N_s, N_{rx}, N_{tx})

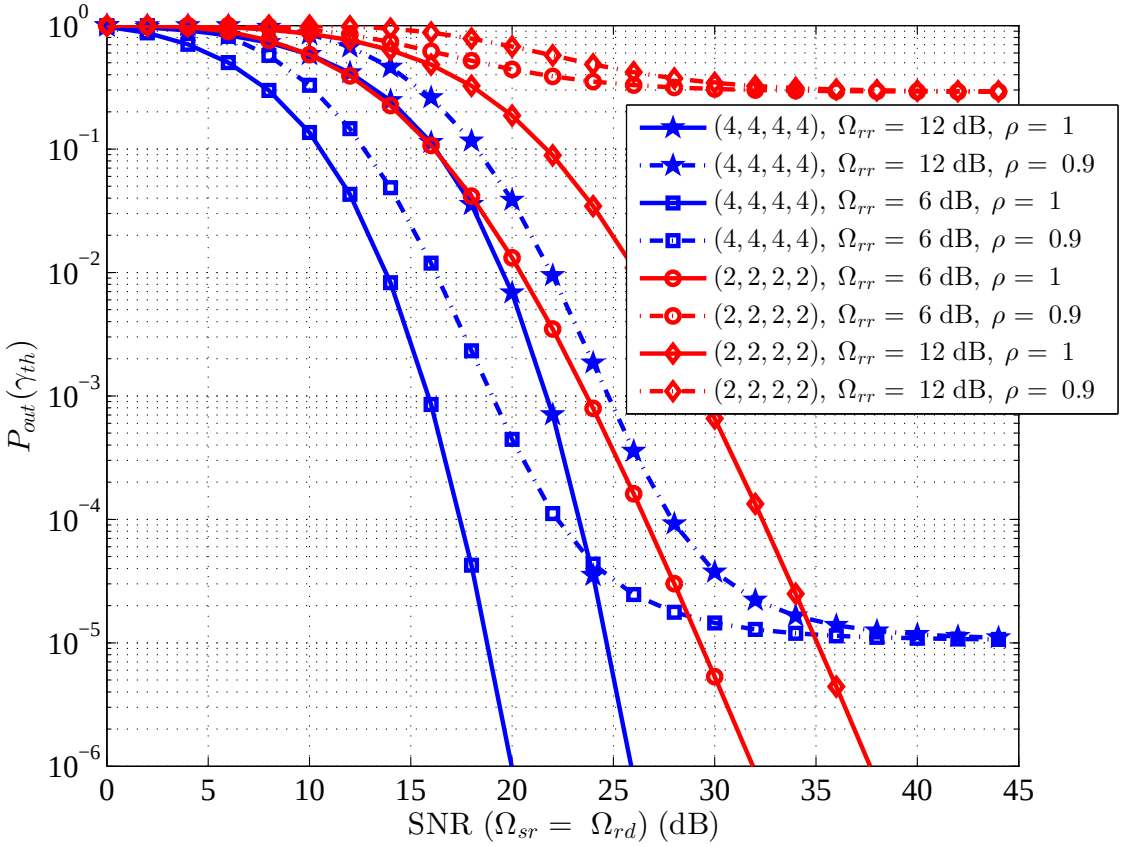

Figure 3.7: E2E Outage probability of (2,2,2,2) and (4,4,4,4) FD-MRC-MIMO after SIC at γ_{th} =10 dB in the presence of residual SI with $\Omega_{rr} = 6$ and 12 dB.

as (2,2,2) and (2,4,2) FD-MRC-MIMO after SIC using QPSK modulation. Two cases of SIR at the input of FD relay are considered, namely SIR = 10 dB and 20 dB. It can be observed that the proposed system achieves better performance at low SNR under the same conditions [38]. This is due to the exploitation the combination of MRC and SIC for increasing the SNR of the desired signal and also to reduce the INR of the SI respectively, which leads to an increase in SIR. In addition, any further mitigation of SI in the analogue domain, which consequently increases the SIR at the input of the relay, will lead the MRC-SIC system to perform better as shown in the case of SIR = 20 dB. For these simulations, the average SNR per bit and average INR per bit are defined as $\Omega_{sr}/\text{bit} = \Omega_{sr}/\log_2(M)$, $\Omega_{rr}/\text{bit} = \Omega_{rr}/\log_2(M)$, and $\Omega_{rd}/\text{bit} = \Omega_{rd}/\log_2(M)$.

Furthermore, in the context of channel capacity, Fig. 3.11 shows the results obtained from the proposed FD-MRC-MIMO system with (2,2,2,2) as a function of the source-to-relay signal-to-noise ratio, Ω_{sr}, and for two cases of the relay-to-destination signal-to-noise ratio, Ω_{rd}, which are $\Omega_{rd} = 10$ and 20 dB, respectively. A closer look at Fig. 3.11 reveals that at $\Omega_{sr} = 25$ dB and $\Omega_{rd} = 20$ dB the proposed system achieved average ca-

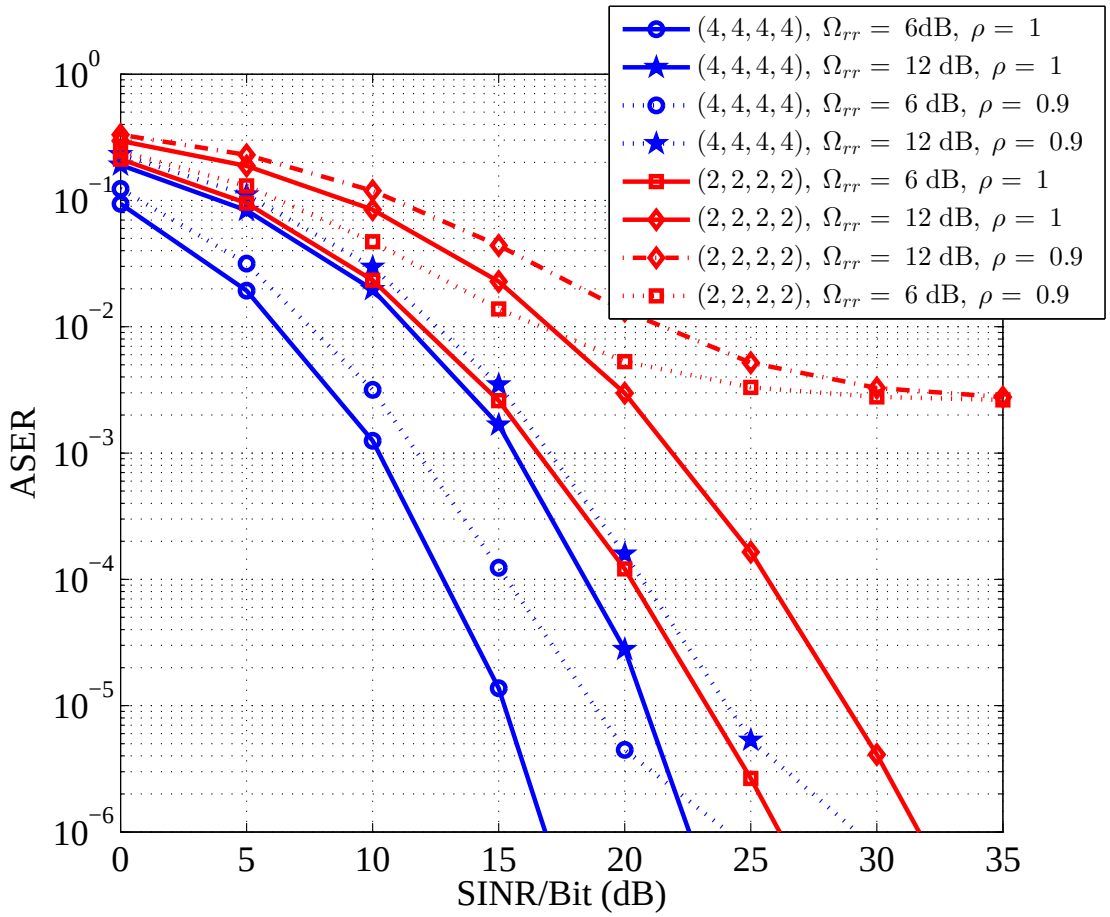

Figure 3.8: E2E exact ASER for (2,2,2,2) and (4,4,4,4) FD-MRC-MIMO after SIC for QPSK modulation scheme in the presence of residual SI with $\Omega_{rr} = 6$ and 12 dB.

pacity improvements of 9 and 14 bits/s/Hz, respectively, compared to the results obtained by [30] under the same conditions and for the two scenarios of FD-AF and HD-AF.

Additionally, the capacity performance of the proposed system for $\Omega_{rd} = 20$ dB as a function of Ω_{sr} is compared with a spatial multiplexing FD full-MIMO system with (2,2,2,2) employing MMSE equalization in the relay without NSP. The performance for two scenarios are demonstrated, that of SI-free, and for the case where no SIC is applied. At an $\Omega_{sr} = 25$ dB, a performance gain of approximately 5 and 18 bits/s/Hz is observed, respectively, between the proposed FD-MRC-MIMO and the alternative methods.

It is noteworthy that the capacity of the spatial multiplexing FD full-MIMO system with MMSE equalization outperforms the capacity of FD-AF relay at high SNR, i.e. when SNR is greater that 10 dB, due to the fact that the amplification caused by the FD-AF relay will increase the SI signal which consequently reduce overall performance. In other words, the AF relaying can be preferred on the EF-relaying operating in FD mode for applications required low SNRs for the same reason mentioned above.

Finally, Fig. 3.12 shows the cumulative distribution function (CDF) of the data rate

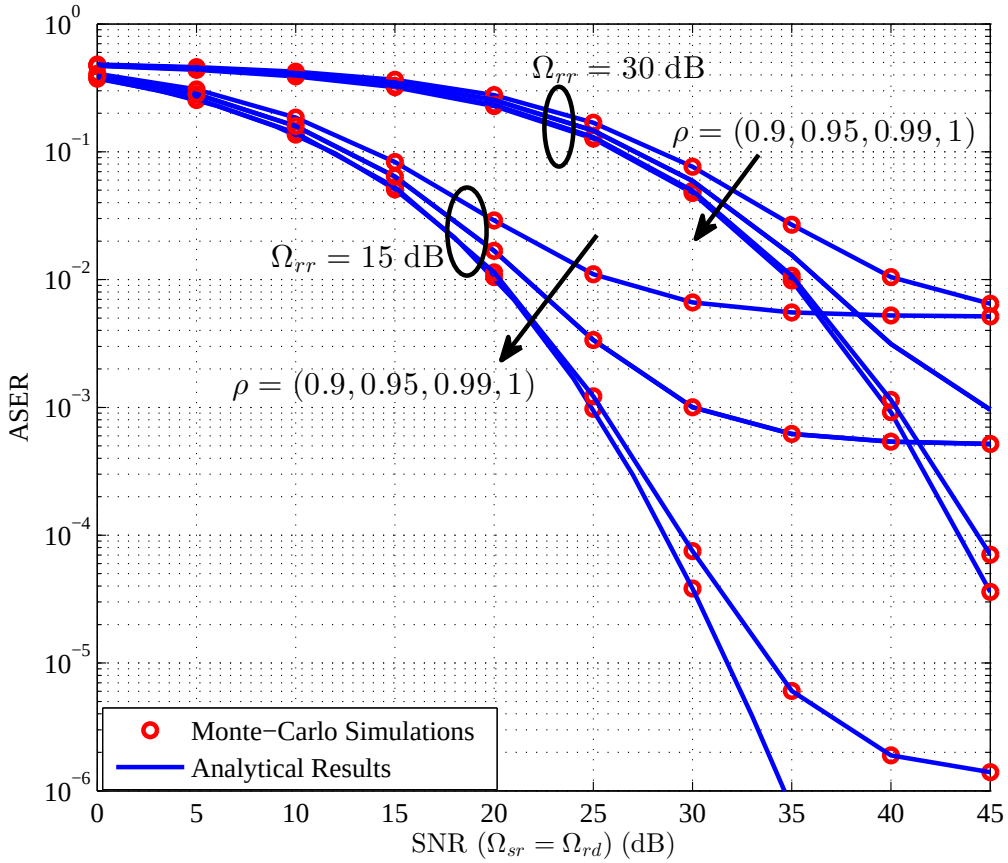

Figure 3.9: E2E analytical and Monte-Carlo results of ASER (QPSK modulation) for (2,2,2,2) FD-MRC-MIMO after SIC in the presence of residual SI with $\Omega_{rr} = 15$ and 30 dB and imperfect channel estimation errors of $\rho = (0.9, 0.95, 0.99, 1)$.

for (2,2,2,2) FD-MRC-MIMO compared to the results obtained by [30] for FD-AF and HD-AF when $\Omega_{sr} = \Omega_{rd} = 20$ dB, in addition to the two scenarios mentioned previously for the spatial multiplexing FD-MIMO system which applying MMSE equalization in the relay and the destination. It worth noting that the CDF was obtained by averaging the mutual information for multiple E2E transmission frames. Close inspection of the results, demonstrate that under the same conditions the proposed system outperforms, in terms of throughput, the approaches mentioned previously.

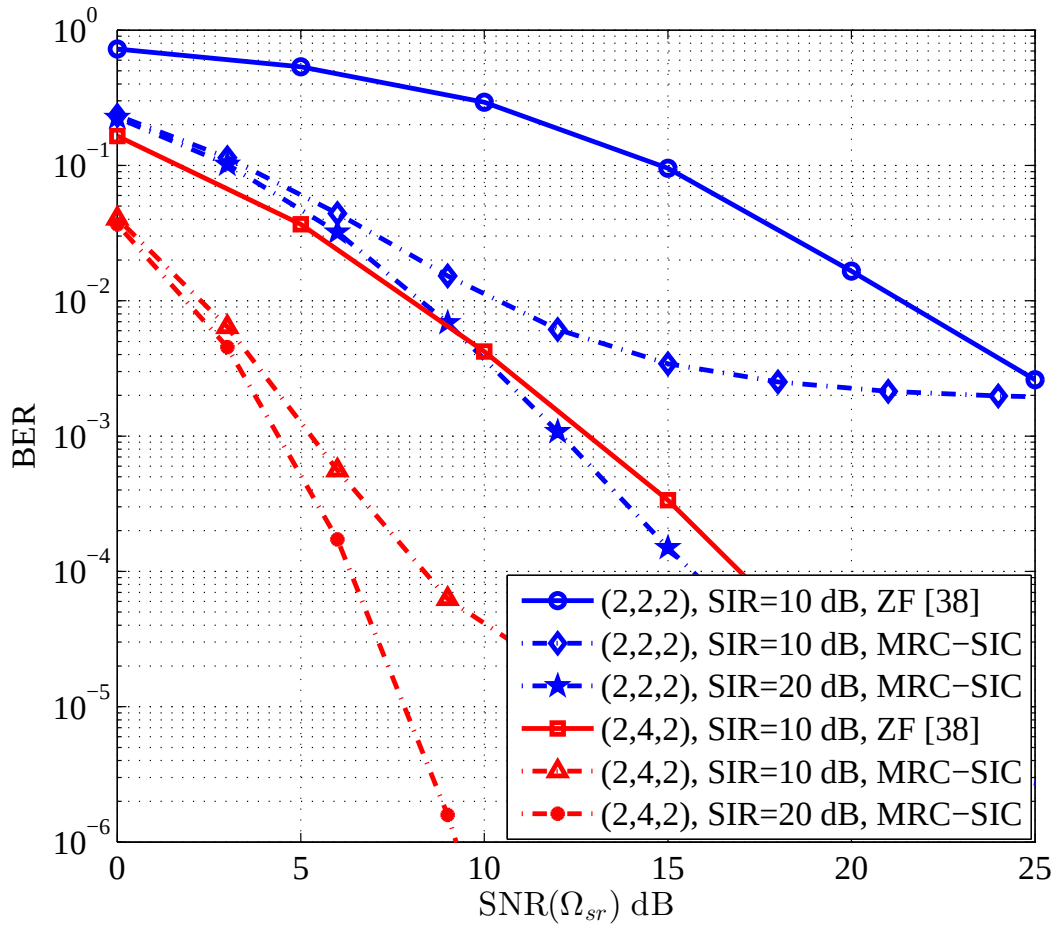

Figure 3.10: First hop SNR vs. BER performance for (2,2,2) and (2,4,2) FD-MRC-MIMO after SIC using QPSK modulation for SIR = 10 and 20 dB at the input of FD relay.

3.7 Chapter Summary

In this chapter, performance analysis for the proposed FD-MIMO-MRC relay has been presented. The proposed relay combines the MRC technique for increasing the SNR for the desired signal and additionally utilizes SIC to mitigate the SI due to the FD relay operation. The structure of the designed system was outlined using SVD, which was employed in order to cancel the SI via the NSP method. Analytical solutions for the SINR distribution and outage probability have been derived and evaluated. Moreover, the ASER for M-PSK modulation schemes has been derived and computed for QPSK. From the results presented, it is evident that obtaining precise CSI and increasing the number of antennas in FD-MIMO-MRC, especially increasing the antennas at the receiving side of the FD-MIMO relay, leads to better performance and enables the system to tolerate more residual SI caused due to CSI estimation errors. Moreover, it is obvious that increasing the SIR

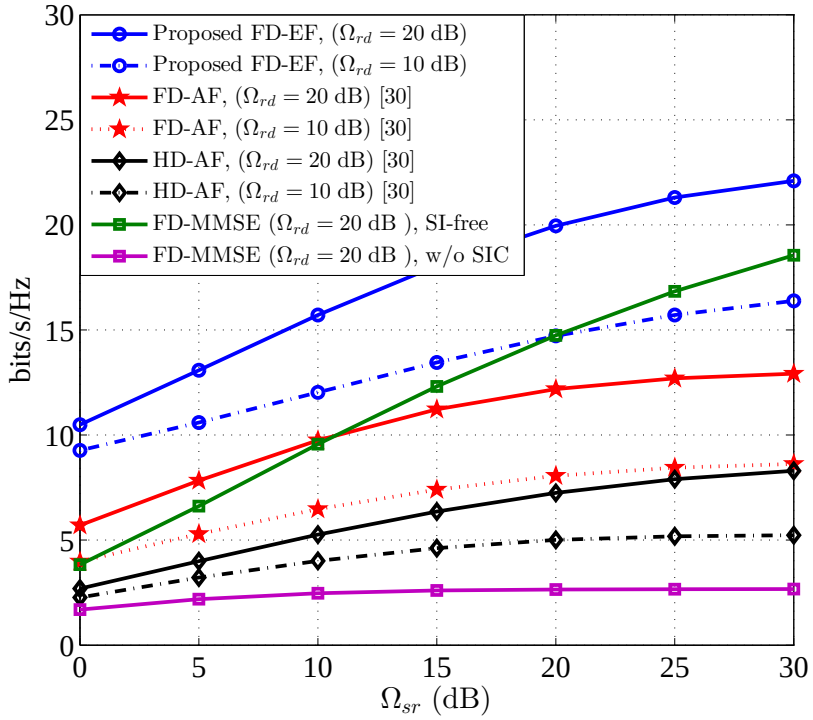

Figure 3.11: Average capacity of (2,2,2,2)-FD-MRC-MIMO based EF-relay, as a function of the mean Ω_{sr} compared to FD-AF, HD-AF and FD-MMSE relays.

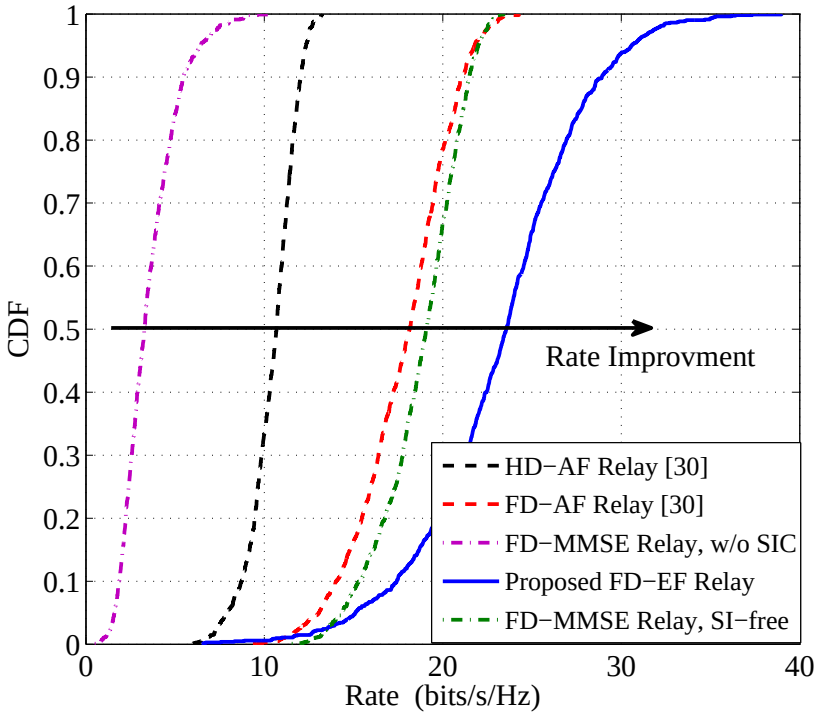

Figure 3.12: CDF of the data rate of (2,2,2,2)-FD-MRC-MIMO based EF-relay, compared to FD-AF, HD-AF and FD-MMSE relays at Ω_{sr} = Ω_{rd} = 20 dB.

at the input of a FD-MIMO transceiver by applying passive SI mitigation in the analog

domain leads to a further increase in performance of the proposed MRC-SIC system. Furthermore, the coefficients of the transformation filter of the EF-relay have been derived to minimize the MSE between the transmitted and the received symbols in the source-relay path, which consequently enhances the system performance in the ASER-SNR metric. In addition, we derive the upper bound of the E2E channel capacity of the proposed system in the presence of SI. The results showed a significant enhancement of the overall throughput. Finally, comparison of the the proposed FD-MRC-MIMO approach with another relevant state-of-the-art method was presented demonstrating a considerable performance improvement due to the combination of MRC and SIC techniques in the proposed FD-MRC-MIMO system.

Chapter 4

Iterative Detection and Decoding for FD-SIMO Systems

4.1 Introduction

FD wireless communication using multiple receive antennas has been recently the focus of intense research effort to improve the spectral efficiency [10]. Thus far, several methods have been proposed to tackle SI caused due to simultaneously transmitting and receiving signals using the same frequency band. These methods can be grouped into two broad categories: passive and active SIC. Passive methods rely on the physical separation of the transmit and receive antennas in order to increase the isolation loss between them, and hence reduce the magnitude of local interference. In contrast, active approaches are implemented either in the analogue domain, which is always operated before the ADC, or in the digital domain, i.e. after the ADC. Precise knowledge of the interfering signal and its channel can be utilized to create an SI replica in order to subtract it from the overall incoming signal. This operation can be implemented either in the passband or baseband [10, 17]. Moreover, SIC utilizing spatial domain suppression, based on ZF and NSP can be exploited for this purpose [36, 84]. In this chapter, previous studies [10, 17] which utilize passive and active cancellation without using SI spatial suppression are extended by employing IDD for the further reduction of SI in the digital domain. SI spatial suppression is omitted for the purpose of fair comparison.

IDD can be exploited for multiple-antenna transceivers in conjunction with coded FD to overcome residual SI. This is implemented by using the iterative exchange of soft information between the detector and the decoder, resulting in high throughput, better efficiency, and reliable performance in interference-limited environments [85, 86]. The work in a recent study [86] is extended in this chapter by deriving a tight upper bound on the performance of the coded FD-SIMO in the presence of residual SI after applying passive and active SIC.

The key contributions of this chapter can be summarized as follows. The fundamentals of encoding and decoding using convolutional and turbo codes are first presented. Moreover, a description and explanations of the state table, tree diagram, signal flow graph and trellis diagram are given. Furthermore, the algorithms for decoding the convolutional codes are presented, such as the MAP and ML decoding. Additionally, IDD is exploited in the context of coded FD-SIMO to mitigate more effectively the residual SI remaining after applying the multiple stages of SIC. After a number of iterations, the performance achieved is very close to that of the SI-free case. Additionally, in order to validate the simulation results, a tight upper bound is derived for the proposed FD-SIMO performance

using rate-$1/2$ convolutional codes with QPSK, which is asymptotically close to the simulated performance and can be used for the performance evaluation of such a system without the need to implement time-consuming simulations.

4.2 Channel Encoding

Since utilizing efficient and reliable data transmission over different types of channels is now urgent need, powerful channel encoding methods have become essential when implementing modern and forthcoming generations of communications systems. The highly reliable transmission of digital data in the presence of induced corruption of noise is possible as long as the transmission rate is below the channel capacity as mentioned in Shannon's law [87]. This can be achieved by encoding the transmitted digital data with an error correction code, while a decoding mechanism needs to be applied to the received message so as to recover the original digital information [88].

The characteristics of coding, in terms of detecting and correcting errors, are required to exhibit significant robustness against the corruption introduced by the transmission channel. On the other hand, the practical implementation of the designed channel codes has to be feasible with efficient performance. In this section, brief introductions and explanations of two of the most popular and powerful types of channel codes are presented, which are the convolutional and turbo codes, as they are mainly exploited in the systems proposed in this and the following chapters. The structure of this family of channel codes takes mostly and conveniently the form of trellises and graphs. Furthermore, soft decision decoding becomes possible with very close performance to channel capacity under the same conditions [48].

Moreover, low density parity check (LDPC) codes are considered to be another powerful linear error correcting block codes which can be used to achieve the reliable transmission of data that can approach the capacity bounds introduced by Shannon. However, the performance of this class of code is degraded and the complexity of the decoding algorithms is increased when low code rates of transmission and/or short lengths of frames are used for transmission [89]. In this thesis, LDPC is not considered due to the assumption that the utilized frame lengths are not too long, and also code rates of half and below are used.

4.2.1 Convolutional Codes

In a convolutional encoder, a serial stream of bits with length k passes through a linear finite-state shift register to obtain the coded bits of length n. The convolutional encoder comprises K-stage shift registers along with m-modulo-2 adders which represent linear algebraic function generators. The code rate of the convolutional codes can be expressed as $R_c = k/n$, which represents the ratio of the number of bits in the input to the number of bits at the output of the convolutional encoder. This rate represents also the ratio of the number of inputs to the number of outputs of the convolutional encoder. It is worth mentioning that the parameter K is called the constraint length, which represents the maximum number of bits at the output of the encoder affected by any change in the inputs bits [90]. Moreover, for every sequence of information of finite length at the input of the encoder, there is a codeword sequence with a finite length too. The encoding mechanism can be summarised as shifting the information bits into the shift register memories, which are in the zero-state at the first instant. During each time step, the stored bits in the memories are added via modulo-2 operation that depends on whether connections between the registers and adders are available or not as specified by the generator polynomial (G) of a particular convolutional encoder. As a result, the generated coded bits can be obtained at the output of each modulo-2 adder, and are multiplexed to create the transmitted codeword. Additionally, the stored bits at the registers are shifted to the right, where new bits are entered to the first register in order to create a new codeword in the following time step. Moreover, the convolutional codes are classified as systematic or non-systematic, which are, respectively, based on the presence or absence of the original information bits within the output coded bits. Additionally, the term recursive is applied to the convolutional encoder when a feedback loop is present from its output to the input; whereas otherwise it is non-recursive [48, 88, 90]. Fig. 4.1 shows two topologies of the convolutional encoder, which are a non-systematic convolutional encoder (NSC) in Fig. 4.1(a), and a recursive systematic convolutional encoder (RSC) in Fig. 4.1(b). Both of them have one input, two outputs, two shift register memories, each of which has D-type flip-flop as a 1-bit storage element. Moreover, the number of modulo-2 adders utilized to connect the shift registers are based on G.

In general, the notation NSC(g_1,g_2) and RSC(1,g_F/g_R) are used to refer to the two types of convolutional codes, in which, for instance in Fig. 4.1, $g_1 = g_F = [101]_2 = 5_8$, and $g_2 = g_R = [111]_2 = 7_8$. Moreover, the "1" in the RSC's notation indicates

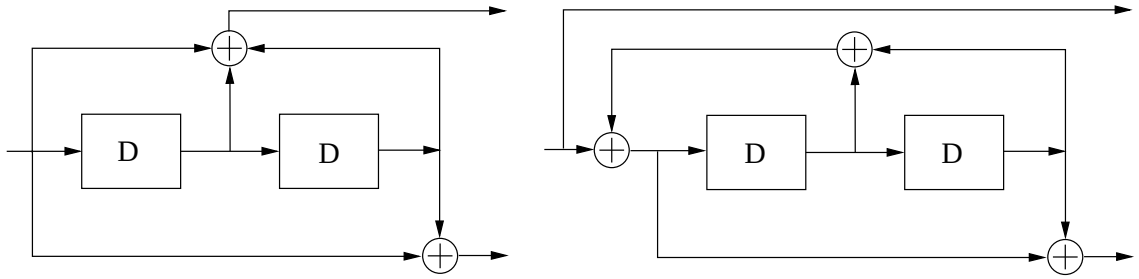

(a) NSC $(5, 7)_8$ (b) RSC $(1, 5/7)_8$

Figure 4.1: Rate-$1/2$ convolutional encoder with constraint length $K = 3$.

that the convolutional codes are systemic, which means that the input bits are included in the output codeword without any change. Additionally, the subscripts F and R in the generator polynomial of RSC respectively describe the feedback and feed-forward connections to the modulo-2 adders.

Different techniques are used to illustrate the mechanism of generating the codewords from the input bits of a convolutional encoder, such as state table, state diagram, tree diagram, signal flow graph and trellis diagram. All these approaches are to show how the next state and the output codeword of a convolutional encoder are created by the the input bits, which can be either 0 or 1, and for different current states of the shift register memories. Tables 4.1 and 4.2 show the state tables for rate-$1/2$ NSC and RSC convolutional encoders, respectively, with a constraint length $K = 3$ as shown previously in Fig. 4.1.

Table 4.1: State table for the NSC $(5, 7)_8$ shown in Fig. 4.1(a)

Input	**Current state**	**Next state**	**Output**
0	00	00	00
1	00	10	11
0	01	00	11
1	01	10	00
0	10	01	10
1	10	11	01
0	11	01	01
1	11	11	10

In the state diagram, the nodes represent the possible states of the shift register memories of a convolutional encoder, while the interconnection between any two nodes is represented by a branch showing the transition between two states in these nodes. Additionally, all branches are labelled with the corresponding output codeword obtained according to a particular input information bit. Fig. 4.2 shows the state diagrams for the

Table 4.2: State table for the RSC $(1, 5/7)_8$ shown in Fig. 4.1(b)

Input	Current state	Next state	Output
0	00	00	00
1	00	10	11
0	01	00	11
1	01	10	00
0	10	01	01
1	10	11	10
0	11	01	10
1	11	11	01

same rate-$1/2$ NSC and RSC convolutional encoders with constraint length $K = 3$ mentioned above. For both encoders, there are 4 states for the two shift register memories, which are $s \in \{(00), (01), (10), (11)\}$. Moreover, since each encoder has only one bit at its input at a time, which are either "0" or "1", therefore two branches leave each memory state to represent each possible transition to another state and the output codeword.

Fig. 4.3 shows the tree diagram for the rate-$1/2$ convolutional encoders shown in Fig. 4.1 with constraint length $K = 3$. In this figure, any branch has upper and lower sub-branches to show the two output bits for input 0 and 1 respectively. Furthermore, Figs. 4.4 and 4.5 show the trellis diagrams of the NSC and RSC encoders shown in Fig. 4.1, respectively. In those two figures, it is assumed that the trellis starts with a zero state, and the two bits on each line represent the output of a particular encoder. Moreover, the solid and dashed lines in the two trellis diagrams denote whether the input bit is 0 or 1, respectively.

It is worth mentioning that the two codes discussed above have very similar state, tree and trellis diagrams, and also they have the same minimum free distance, which

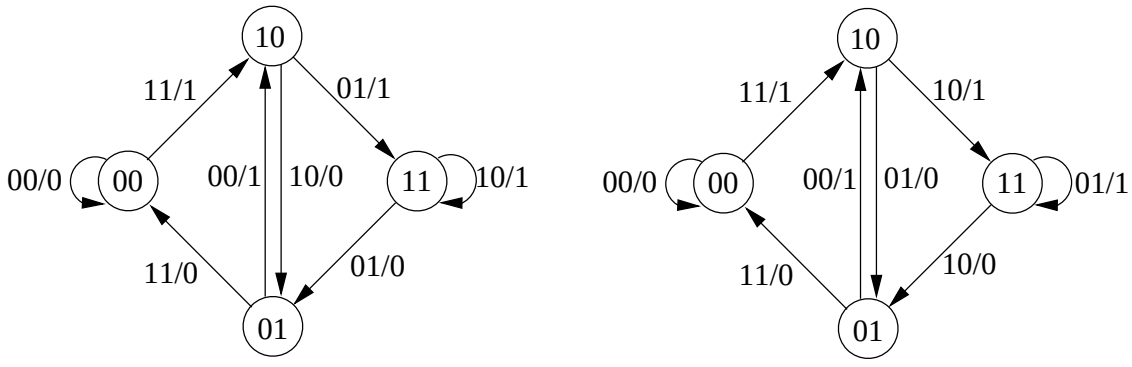

(a) NSC $(5, 7)_8$ (b) RSC $(1, 5/7)_8$

Figure 4.2: State diagram for rate-$1/2$ convolutional encoders shown in Fig. 4.1 with constraint length $K = 3$.

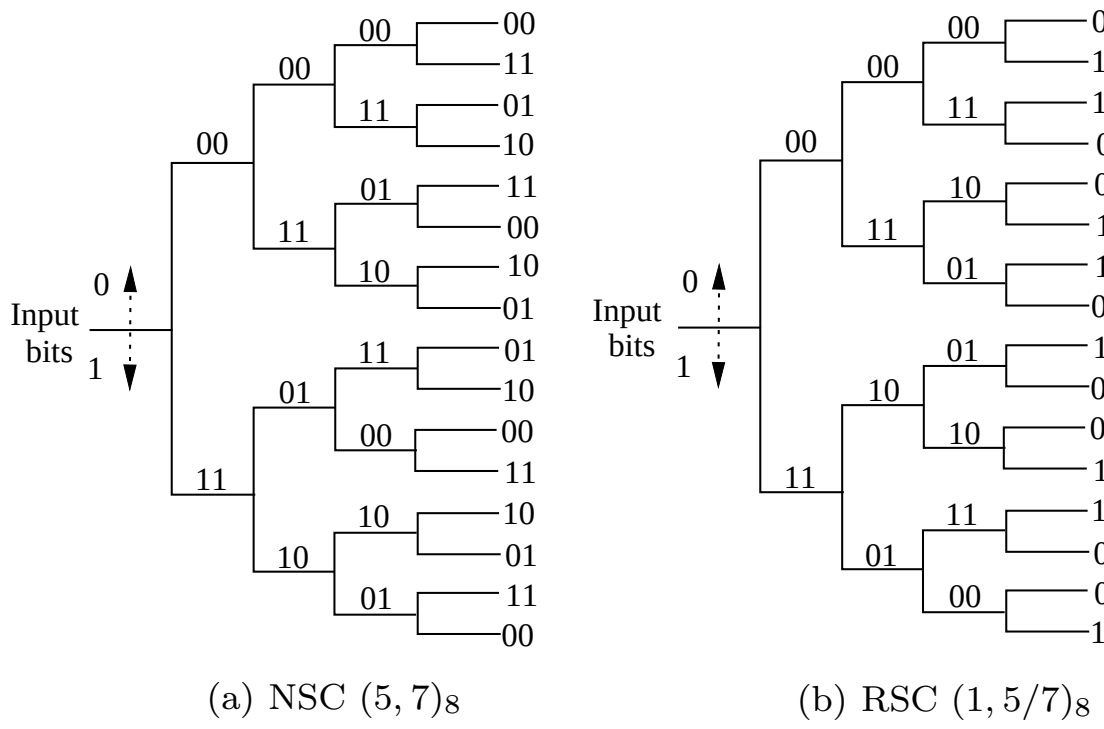

Figure 4.3: Tree diagram for rate-$1/2$ convolutional encoders shown in Fig. 4.1 with constraint length $K = 3$.

is defined as a minimum Hamming distance between two encoded sequences [48] and is denoted by d_{free}. In other words, d_{free} represents a minimum distance metric for the code diverging from the all-zero path and returning afterwards to this path [90]. Although the two codes have the same probability of first event error, however, they have different BERs performance which relies on the corresponding input-output of the encoder. Therefore, RSC outperforms the corresponding NSC as it has better BER performance at low SNR [90]. Hence, this thesis emphasises the use of RSC as it exhibits more tolerance of noise and the interference limited environments inherited in FD systems.

4.2.2 Decoding of Convolutional Codes

The need for error correction has become essential, especially for a communications system that has a random process modelled channel. This is due to the fact that these types of channels are always unable to remap the received symbols exactly to the same given transmitted symbols [88]. In order to appreciate how the decoding of convolutional codes takes place, a brief explanation of the communications system and the corresponding applied probabilistic theorems for decoding is given next.

Following the assumptions and notations given in Fig. 4.6, the input information se-

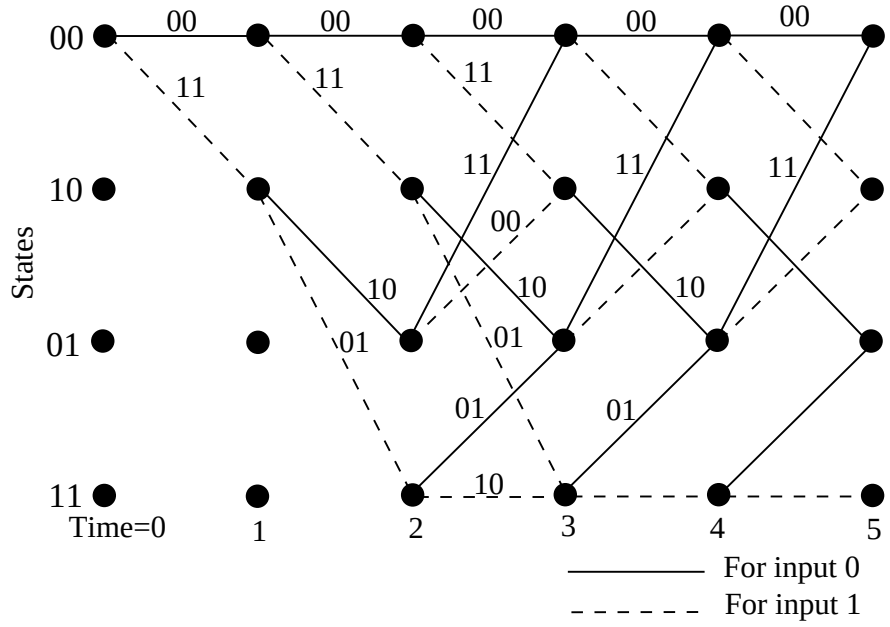

Figure 4.4: Trellis diagram for rate-$1/2$ NSC convolutional encoder with constraint length $K = 3$ and $G(5, 7)_8$.

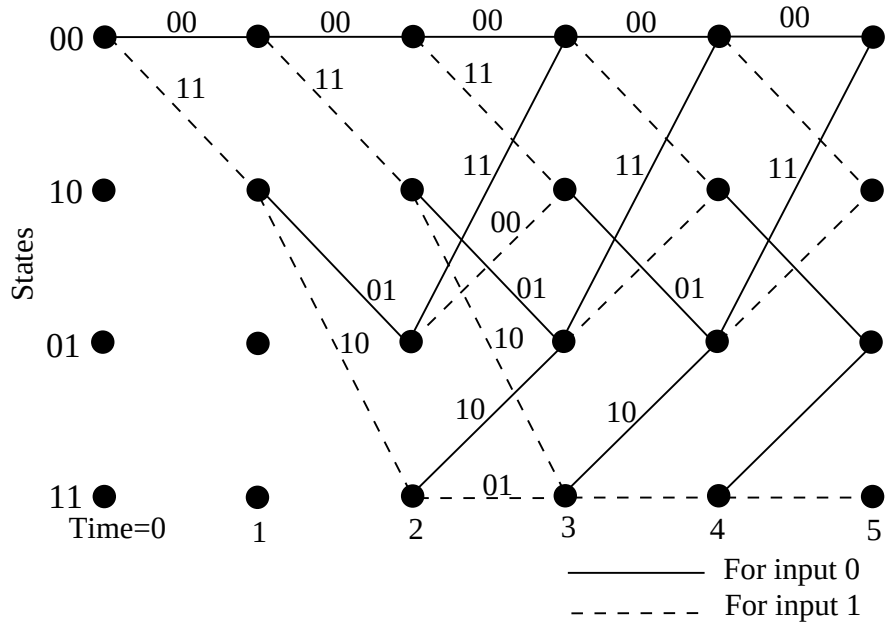

Figure 4.5: Trellis diagram for rate-$1/2$ RSC convolutional encoder with constraint length $K = 3$ and $G(1, 5/7)_8$.

quence to the convolutional encoder is denoted as $\mathbf{u} = (u_1, u_2, ..., u_t, ...)$, and the coded bits are mapped using BPSK as $\mathbf{x} = (\mathbf{x}_1, \mathbf{x}_2, ..., \mathbf{x}_t, ...)$, in which logic zero and logic one coded bits are mapped to $+1$ and -1, respectively. By using rate-$1/2$ convolutional encoders, like one of those shown in Fig. 4.1, the symbol $\mathbf{x}_t = (x_t^{(1)}, x_t^{(2)}) \in \mathbf{x}$ at time index $t > 0$ represents the modulated coded bits generated at the output of the convolutional

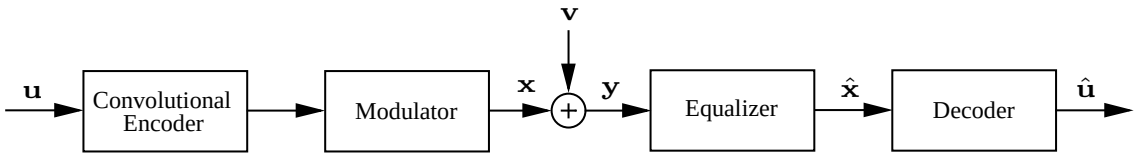

Figure 4.6: Convolutional codes' encoding and decoding.

encoder and modulator for an input bit u_t. The transmitted symbols are assumed to be passed through an AWGN channel denoted as $\mathbf{v} \sim \mathbb{CN}(0, \sigma_v^2)$ and arrive at the receiver as $\mathbf{y} = (\mathbf{y}_1, \mathbf{y}_2, ..., \mathbf{y}_t, ...)$. The latter needs to be decoded properly due to the impairments caused by this channel in order to obtain an acceptable estimation of the transmitted symbols and bits, which are denoted as $\hat{\mathbf{x}}$ and $\hat{\mathbf{u}}$, respectively.

In order to decode the received sequence $\mathbf{y}$, it is necessary to determine the conditional probability related to the transmitted symbols $\mathbf{x}$ given $\mathbf{y}$ is received, which can be expressed as $P_r(\mathbf{x}|\mathbf{y})$. This inverse probability problem can be solved using Bayes' theorem as follows [88, 90]

$$P_r(\mathbf{x}|\mathbf{y}) = \frac{P_r(\mathbf{y}|\mathbf{x})P_r(\mathbf{x})}{P_r(\mathbf{y})}, \tag{4.1}$$

where $P_r(\mathbf{x}|\mathbf{y})$ represents the *a posteriori* probability (APP) for $\mathbf{x}$, while $P_r(\mathbf{x})$ is called the *a priori* or intrinsic probability. Moreover, the conditional probability $P_r(\mathbf{y}|\mathbf{x})$ represents the likelihood of $\mathbf{x}$ and it is subject to the communication channel. The convolutional decoder aims to find an optimum estimation of the codeword sequences $\hat{\mathbf{x}}$ by maximizing the APP $P_r(\mathbf{x}|\mathbf{y})$, which is referred as MAP decoding and can be obtained from (4.1) after omitting the normalization factor $P_r(\mathbf{y})$ which is constant, when the optimal decoding decision is determined as

$$\hat{\mathbf{x}} = \arg\max_{\mathbf{x}}(P_r(\mathbf{x}|\mathbf{y})) = \arg\max_{\mathbf{x}}(P_r(\mathbf{y}|\mathbf{x})P_r(\mathbf{x})). \tag{4.2}$$

Additionally, when all the transmitted codeword symbols are equally likely, the term $P_r(\mathbf{x})$ becomes a constant and it can be neglected in (4.2) so as to perform ML decoding as discussed previously in Chapter 2. The determination of ML according to the above assumption can be expressed as

$$\hat{\mathbf{x}} = \arg\max_{\mathbf{x}}(P_r(\mathbf{x}|\mathbf{y})) = \arg\max_{\mathbf{x}}(P_r(\mathbf{y}|\mathbf{x}))). \tag{4.3}$$

The ML decoder is type of error correction that selects the most likely codeword for which the received symbols are produced. In other words, for a given received sequence $\mathbf{y}$ and transmitted codewords $\mathbf{x}$ over an AWGN channel, as shown in Fig. 4.6, the ML decoder maximizes the probability $P_r(\mathbf{y}|\mathbf{x})$ by choosing the decoded codeword $\hat{\mathbf{x}}$ according to argument in (4.3), where the probability $P_r(\mathbf{y}|\mathbf{x})$ of a memoryless channel can be defined as

$$P_r(\mathbf{y}|\mathbf{x}) = \prod_t \prod_i P_r\left(y_t^{(i)}|x_t^{(i)}\right) \tag{4.4}$$

4.2.3 Log Likelihood Ratios

For several communications systems over different types of channels, the log likelihood ratio (LLR) can be used as a convenient metric to find a single value to represent a coded bit [88]. This ratio is utilized to make a decision as to whether a particular coded bit in a received codeword might be "1" or "0" according to the sign and magnitude of the ratio, that are used to represent the hard decision and the reliability of this decision for this coded bit. The LLR or the soft value of the coded bit $u_t^{(i)}$, where $i \in \{1, 2\}$ for a rate-$1/2$ convolutional encoder, can be defined as

$$\mathcal{L}(u_t^{(i)}) = \log\left(\frac{P_r(u_t^{(i)} = 1)}{P_r(u_t^{(i)} = 0)}\right). \tag{4.5}$$

Thus, for a positive sign of $\mathcal{L}(u_t^{(i)})$, $u_t^{(i)}$ should be represented as "1", otherwise it is "0". Moreover, $|\mathcal{L}(u_t^{(i)})|$ is the reliability of this decision, which means that the greater the difference between the two probabilities in this ratio, the more certain that this decision is reliable. For a binary variable $u_t^{(i)}$ passed through binary systematic channel, $P_r(u_t^{(i)} = 1)$ can be determined from $P_r(u_t^{(i)} = 0)$ [89] as

$$P_r(u_t^{(i)} = 1) = 1 - P_r(u_t^{(i)} = 0). \tag{4.6}$$

Hence, by substituting (4.6) in (4.5), and for a known $\mathcal{L}(u_t^{(i)})$, the two probabilities can be evaluated as

$$P_r(u_t^{(i)} = 1) = \frac{\exp(\mathcal{L}(u_t^{(i)}))}{1 + \exp(\mathcal{L}(u_t^{(i)}))}, \tag{4.7a}$$

$$P_r(u_t^{(i)} = 0) = \frac{\exp(-\mathcal{L}(u_t^{(i)}))}{1 + \exp(-\mathcal{L}(u_t^{(i)}))}. \tag{4.7b}$$

The main advantage of using logarithmic representation for the likelihood ratio of the probabilities is to reduce the complexity of the implementation, especially when the multiplication of probabilities is required where the operation is replaced by adding the LLRs instead of multiplying the probabilities [88, 90].

The coded bit arriving at the receiver, after passing through an AWGN represented as $\mathbf{v} \sim \mathbb{CN}(0, \sigma_v^2)$, can be expressed as

$$y_t^{(i)} = \sqrt{E_c} x_t^{(i)} + v_t, \tag{4.8}$$

where E_c is the average energy of the transmitted coded bit. Furthermore, according to the LLR definition, the LLR of the received i^{th} coded bit at time index t, $y_t^{(i)}$, given that $x_t^{(i)}$ is transmitted, can be expressed as

$$\mathcal{L}\big(y_t^{(i)} | x_t^{(i)}\big) = \log\left(\frac{P_r(y_t^{(i)} | x_t^{(i)} = +1)}{P_r(y_t^{(i)} | x_t^{(i)} = -1)}\right). \tag{4.9}$$

The PDFs $P_r\big(y_t^{(i)} | x_t^{(i)} = +1\big)$ and $P_r\big(y_t^{(i)} | x_t^{(i)} = -1\big)$ can be statistically expressed at the output of a discrete memoryless fading channel with AWGN as

$$P_r\big(y_t^{(i)} | x_t^{(i)} = +1\big) = \frac{1}{\sqrt{2\pi\sigma_v^2}} \exp\Big(-\frac{1}{2\sigma_v^2}\big(y_t^{(i)} + \sqrt{E_c}\big)^2\Big), \tag{4.10a}$$

$$P_r\big(y_t^{(i)} | x_t^{(i)} = -1\big) = \frac{1}{\sqrt{2\pi\sigma_v^2}} \exp\Big(-\frac{1}{2\sigma_v^2}\big(y_t^{(i)} - \sqrt{E_c}\big)^2\Big). \tag{4.10b}$$

It should be noted that it is assumed that the conversion of the BPSK to the bipolar form uses the mapping of $\{0 \to +1\}$ $\{1 \to -1\}$ as shown in Fig.4.7.

Now, by substituting (4.10) in (4.9), the former can be rewritten and further simplified

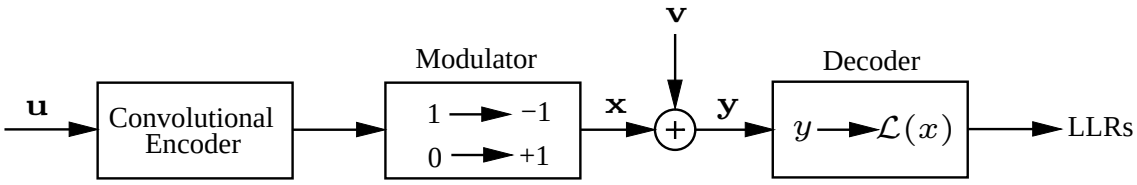

Figure 4.7: Convolutional codes decoding

as

$$\begin{aligned}\mathcal{L}\big(y_t^{(i)}|x_t^{(i)}\big) &= \log\left(\frac{\frac{1}{\sqrt{2\pi\sigma_v^2}}\exp\Big(-\frac{1}{2\sigma_v^2}\big(y_t^{(i)}+\sqrt{E_c}\big)^2\Big)}{\frac{1}{\sqrt{2\pi\sigma_v^2}}\exp\Big(-\frac{1}{2\sigma_v^2}\big(y_t^{(i)}-\sqrt{E_c}\big)^2\Big)}\right),\\ &= \log\exp\Big(-\frac{1}{2\sigma_v^2}\big(y_t^{(i)}+\sqrt{E_c}\big)^2+\frac{1}{2\sigma_v^2}\big(y_t^{(i)}-\sqrt{E_c}\big)^2\Big),\\ &= \frac{1}{2\sigma_v^2}\Big(-4\sqrt{E_c}y_t^{(i)}\Big) = \frac{-2\sqrt{E_c}}{\sigma_v^2}y_t^{(i)}, \end{aligned} \tag{4.11}$$

where the term $\dfrac{2\sqrt{E_c}}{\sigma_v^2}$ is called the channel reliability or the soft decision of the uncoded bit u_t. Additionally, the sign in the final equality of (4.11) refers to the hard decision.

4.2.4 Turbo Codes

Turbo codes were first introduced by Berrou, Glavieux and Thitimajshima in 1993. This new class of convolutional codes has been deployed as a powerful channel coding method for the achievement of reliable communication, as it exhibits BER and channel capacity performances close to the theoretical limit according to Shannon's theorem [90, 91]. A turbo encoder is constructed by exploiting two RSC convolutional codes concatenated in parallel, in which an interleaver denoted as Π is used to separate them as in the block diagram shown in Fig. 4.8. Moreover, Fig. 4.9 shows the systematic diagram of a rate-$1/3$ turbo encoder that consists of two rate-$1/2$ RSC convolutional encoders each of which has the generator polynomial $G(1, 5/7)_8$. Hence the generator polynomial of this turbo code can be denoted as $G(1, 5/7, 5/7)_8$.

Information bits of length L, i.e. $\mathbf{u} = [u_1\ u_2\ ...\ u_L]$, are passed through the first RSC encoder to create the first parity check sequence $\mathbf{p}^{(1)} = [p_1^{(1)}\ p_2^{(1)}\ ...\ p_L^{(1)}]$ along with the original uncoded bits $\mathbf{u}$. The latter is also interleaved and supplied to the second RSC encoder in order to obtain the second parity check sequence $\mathbf{p}^{(2)} = [p_1^{(2)}\ p_2^{(2)}\ ...\ p_L^{(2)}]$.

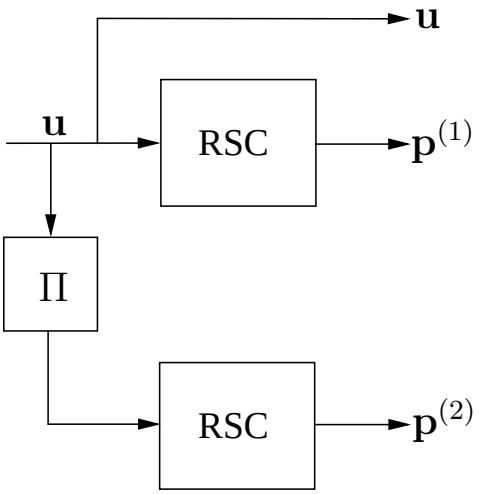

Figure 4.8: Block diagram of turbo encoder consisting of two RSC convolutional encoders separated by an interleaver

Hence the coded bits of at the output of this turbo encoder can be expressed as

$$\mathbf{c} = \left[u_1\, p_1^{(1)}\, p_1^{(2)}\, u_2\, p_2^{(1)}\, p_2^{(2)}\, \ldots\, u_L\, p_L^{(1)}\, p_L^{(2)}\right]. \tag{4.12}$$

Furthermore, the rate-$1/3$ of this turbo code can be increased to half rate by utilizing a

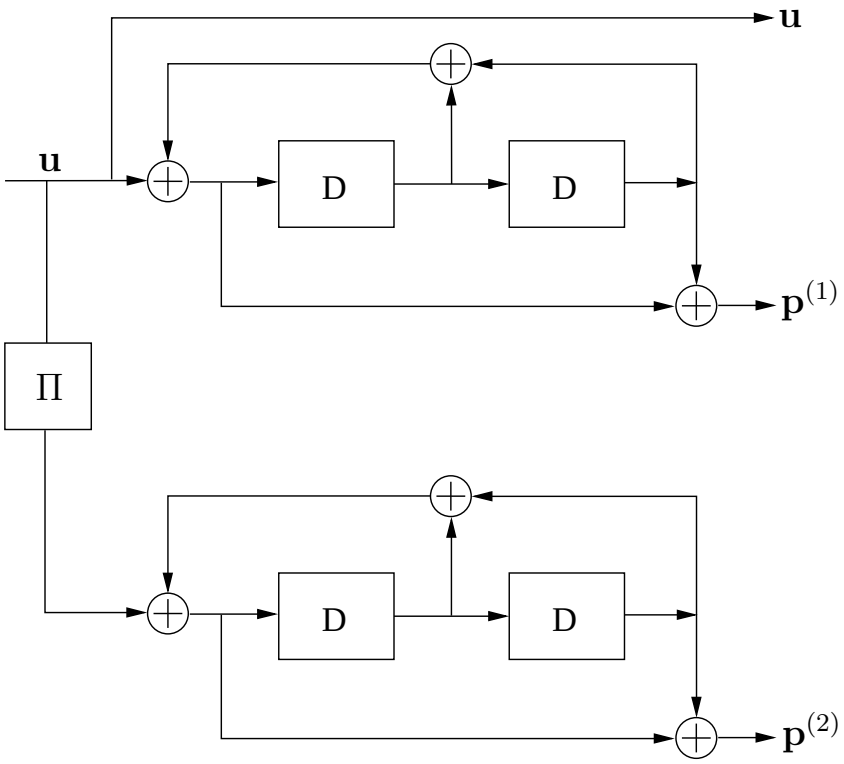

Figure 4.9: Systematic diagram of rate-$1/3$ turbo encoder that consists of two rate-$1/2$ RSC convolutional encoders each of which has the generator polynomial $G(1, 5/7)_8$.

puncturing technique, in which half of the bits in $\mathbf{p}^{(1)}$ and $\mathbf{p}^{(2)}$ are punctured, i.e. deleted, while the original information bits $\mathbf{u}$ should remain without any change [48]. Additionally, the coded bits in (4.12) are then mapped to create the codeword, which are denoted as $\mathbf{x}^{(u)}$, $\mathbf{x}^{(1)}$ and $\mathbf{x}^{(2)}$, which correspond to the coded bits $\mathbf{u}$, $\mathbf{p}^{(1)}$ and $\mathbf{p}^{(2)}$, respectively.

4.2.5 Decoding of Turbo Codes

For a given transmitted codeword created by a turbo encoder and passed through an AWGN channel, the received sequence can be divided, after perfect synchronization, into three inputs to the turbo decoder, which are denoted as $\mathbf{y}^{(u)}$, $\mathbf{y}^{(1)}$ and $\mathbf{y}^{(2)}$ corresponding to the corrupted received codeword of $\mathbf{x}^{(u)}$, $\mathbf{x}^{(1)}$ and $\mathbf{x}^{(2)}$, respectively, as shown in Fig. 4.10. The symbols Π and Π^{-1} are used to denote the operations of interleaving and deinterleaving, respectively.

In this figure, two soft-input soft-output (SiSo) decoder components are used to implement the decoding process, each of which uses the MAP algorithm to determine the *a posteriori* probabilities of the information bits. Moreover, an iterative exchange of the soft information is utilized between the two SiSo decoders to improve the system's performance. The three inputs, in the form of LLR's, provide the SiSo decoders with the required soft information, where $\mathbf{y}^{(u)}$ and $\mathbf{y}^{(1)}$ are fed to the first SiSo decoder, while $\mathbf{y}^{(2)}$ along with the interleaved version of $\mathbf{y}^{(u)}$, i.e. $\Pi(\mathbf{y}^{(u)})$, is supplied to the second SiSo de-

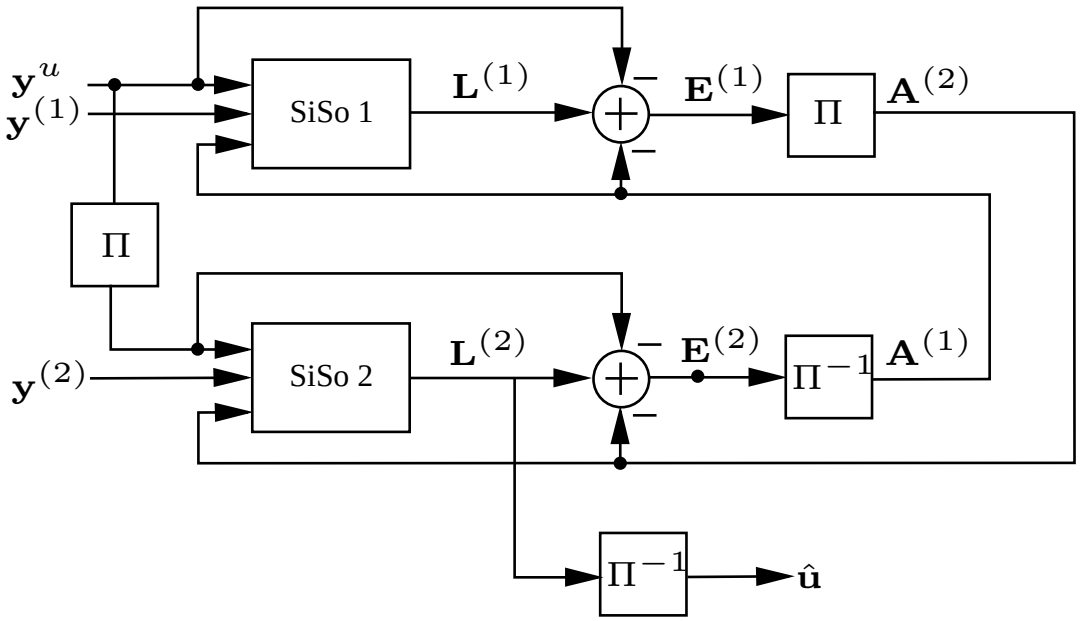

Figure 4.10: Iterative SiSo decoding for turbo codes.

coder. Additionally, each SiSo decoder shares its determined extrinsic information about the systematic and parity check bits with the other SiSo decoder. This extrinsic soft LLR information, which is also referred to as feedback information, of SiSo i is applied as an additional *a priori* input to SiSo j, where $i, j \in \{1, 2\}$ and $i \neq j$, in order to be used in the next iteration as shown in Fig. 4.10.

At each iteration, the first SiSo decoder evaluates the *a posteriori* information $\mathbf{L}^{(1)}$. The latter is used to create the *extrinsic* information $\mathbf{E}^{(1)}$ as

$$\mathbf{E}^{(1)} = \mathbf{L}^{(1)} - \mathbf{y}^{(u)} - \mathbf{A}^{(1)}, \tag{4.13}$$

where $\mathbf{y}^{(u)}$and $\mathbf{A}^{(1)}$ represent, respectively, the information about the message bits and the *a priori* information delivered by the second component decoder, which are both known from the previous iteration, i.e. before the decoding of SiSo 1 [88]. It is noteworthy that $\mathbf{y}^{(u)}$and $\mathbf{A}^{(1)}$ are subtracted from $\mathbf{L}^{(1)}$ in order to create a soft *a priori* observation that is entirely independent of all the soft observations exploited by the SiSo 2 in the previous iteration [92]. At this stage, $\mathbf{E}^{(1)}$ is interleaved in order to create the *a priori* information $\mathbf{A}^{(2)}$, which is an additional input to the second decoder along with the interleaved sequence of the received systematic bits $\Pi(\mathbf{y}^{(u)})$ and the second received parity check $\mathbf{y}^{(2)}$. The same procedures are implemented in the second SiSo decoder to evaluate the *a posteriori* information $\mathbf{L}^{(2)}$, which is used to create the *extrinsic* information $\mathbf{E}^{(2)}$ as

$$\mathbf{E}^{(2)} = \mathbf{L}^{(2)} - \Pi(\mathbf{y}^{(u)}) - \mathbf{A}^{(2)}, \tag{4.14}$$

where the term $\Pi(\mathbf{y}^{(u)}) + \mathbf{A}^{(2)}$ is removed from $\mathbf{L}^{(2)}$ for the same reasons mentioned above. The *extrinsic* information $\mathbf{E}^{(2)}$ is then deinterleaved to produce the *a priori* information $\mathbf{A}^{(1)}$ for the first component decoder. It is worth mentioning that the deinterleaver and interleaver prior to $\mathbf{A}^{(1)}$ and $\mathbf{A}^{(2)}$ keep the *a priori* information in the same order of the systematic bits at the input of SiSo 1 and SiSo 2, respectively. After a particular number of iterations, $\mathbf{L}^{(2)}$ is deinterleaved and passed to a hard decision process to obtain an estimation of the original transmitted information bits.

4.3 Iterative Detection and Decoding

Iterative detection and decoding (IDD), which is sometimes referred to as a turbo-like receiver or turbo-BLAST (Bell Labs layered space time), is employed at the receiver via several iterative exchanges of soft information between the detector and the decoder, as shown in Fig. 4.11. In this figure, the upper side shows the bit interleaved coded modulation (BICM) at the transmitter terminal, in which the information bits $\mathbf{u}$ are passed through a convolutional encoder with a code rate of R_c. The coded bits are then scrambled by an interleaver in order to tackle any probable successive bursts of errors at the input of the channel decoder. The interleaved coded bit is mapped to create the transmitted symbols. In this section, it is assumed that the BPSK is used to modulate the interleaved and coded bits in the same way as illustrated in Fig. 4.7. The symbols Π and Π^{-1} are used to denote the operations of interleaving at the transmitter and deinterleaving at the receiver, respectively.

The IDD is implemented at the receiver by utilizing an iterative exchange of the soft information between the detector and decoder, which are separated by the deinterleaver and interleaver as shown in the lower side of Fig. 4.11. The notation $\Lambda_k(x_i)$, $\lambda_k(x_i)$ and $\lambda_k(x_n)$ denotes the *a posteriori*, *extrinsic* and *a priori* LLR soft information, respectively, where each is represented in an LLR form. Additionally, the subscript $k \in \{1, 2\}$ indicates

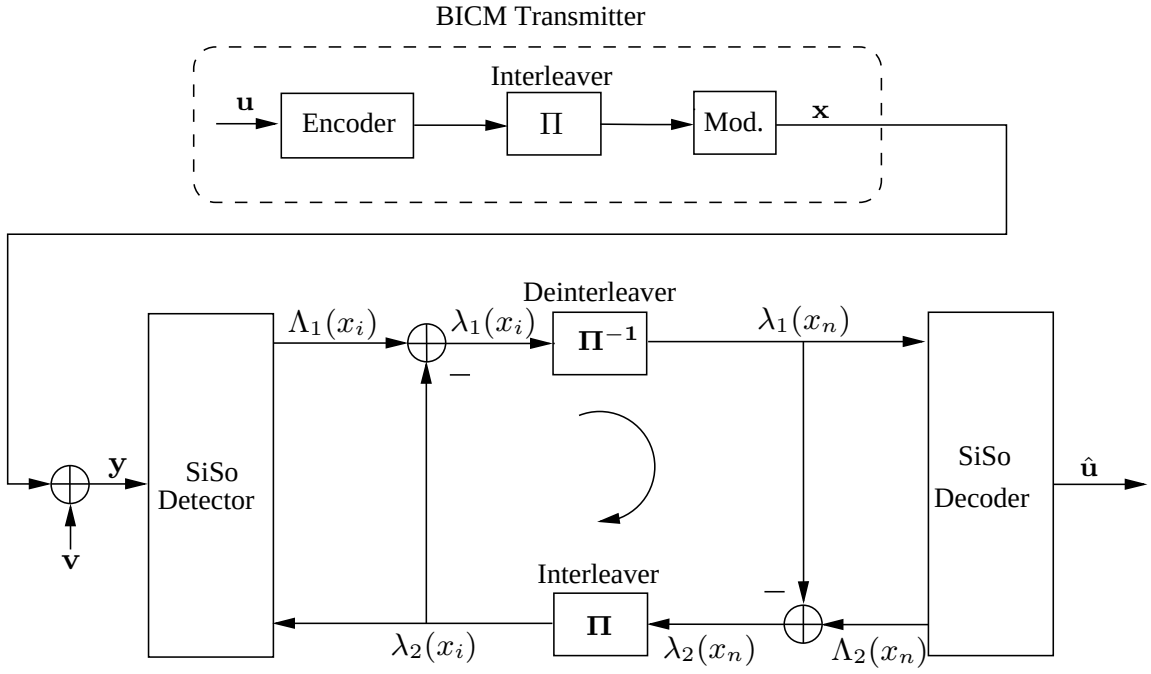

Figure 4.11: BICM transmitter (top) and turbo-BLAST (IDD) receiver (bottom).

the direction of flow of the soft information, in which 1 is used for the forward direction from the detector to decoder, while 2 refers to the backward direction from decoder to detector [85, 93, 94]. Moreover, the indices i and n show that the LLR for a particular bit has different positions in a received frame due to the operations of interleaving and deinterleaving between the SiSo detector and decoder. The SiSo detector passes the *a posteriori* LLR, $\Lambda_k(x_i)$, for every transmitted BICM symbol, that is either $+1$ or -1, to the SiSo decoder, where $\Lambda_k(x_i)$ is defined as

$$\Lambda_1(x_i) \triangleq \log\left(\frac{P_r(x_i = +1|y)}{P_r(x_i = -1|y)}\right). \tag{4.15}$$

By using Bayes' rule, (4.15) can be rewritten as

$$\begin{aligned}\Lambda_1(x_i) &= \log\left(\frac{P_r(y|x_i = +1)}{P_r(y|x_i = -1)}\right) + \log\left(\frac{P_r(x_i = +1)}{P_r(x_i = -1)}\right),\\ &= \lambda_1(x_i) + \lambda_2(x_i),\end{aligned} \tag{4.16}$$

where $\lambda_2(x_i)$ represents the *a priori* LLR of the BICM bit x_i that is determined by the SiSo decoder in the previous iteration, then interleaved and delivered to the SiSo detector. Additionally, the term $\lambda_1(x_i)$ represents the extrinsic information obtained after removing the effect of the *a priori* LLR, $\lambda_2(x_i)$, from the *a posteriori* LLR, $\Lambda_1(x_i)$. Moreover, the extrinsic information, $\lambda_1(x_i)$, is deinterleaved to restore each bit to its original position before the interleaver at the BICM transmitter, as $\lambda_1(x_n)$. The latter is then passed to the SiSo decoder in order to be employed in the next iteration as *a priori* information.

On the other side, the SiSo channel decoder determines the *a posteriori* LLR of each coded bit, $\Lambda_2(x_n)$, according to the prior information $\lambda_1(x_n)$ and the channel code's constraints, such as the trellis structure [94], where $\Lambda_1(x_n)$ is expressed as

$$\begin{aligned}\Lambda_2(x_n) &= \log\left(\frac{P_r(x_i = +1|\lambda_1(x_n); \text{decoding})}{P_r(x_i = -1|\lambda_1(x_n); \text{decoding})}\right),\\ &= \lambda_1(x_n) + \lambda_2(x_n).\end{aligned} \tag{4.17}$$

From the second equality of (4.17), it can be noticed that the SiSo decoder's output is constructed from the sum of the prior information $\lambda_1(x_n)$ and the extrinsic information $\lambda_2(x_n)$. Moreover, $\Lambda_2(x_n)$ is used in the last iteration to make a decision on the coded bits. The extrinsic information $\lambda_2(x_n)$ is interleaved again to create the prior informa-

tion of the coded bits, $\lambda_2(x_i)$, which is fed to the SiSo detector to be utilized in the next iteration. It is worth mentioning that the extrinsic information terms $\lambda_1(x_i)$ and $\lambda_2(x_i)$ are independent and uncorrelated at the first iteration; however, their correlation increases afterwards, through the iterations, as they are indirectly created from the same information, but this improvement reaches a saturation point and becomes insignificant after a particular number of iterations [94].

4.4 IDD for Coded FD-SIMO Bidirectional Transceiver

4.4.1 Signal and System Model

In this chapter, a wireless scenario is considered in which two bi-directional nodes a and b are communicating using FD-SIMO transceivers, each being equipped with a single transmitting antenna and N_{rx} receive antennas as shown in Fig. 4.12. A SIMO scenario is considered, as this is the most common case encountered in uplink cellular communication between a device with a single antenna and a base-station with multiple antennas [95]. The work can be extended to multiple transmit antennas; however, there is limited scope for this as the diversity gain is expected to be restricted due to antenna spacing limitations on the terminal. Furthermore, if the number of the utilized receive antennas is of an order similar to that of the transmit antennas, a further increase in interference is expected [48], which consequently will cause performance degradation for a system exploiting the FD technique. Furthermore, the modelling of the forward channels between the two nodes are denoted as $\mathbf{H}_{ab}$ and $\mathbf{H}_{ba}$, while $\mathbf{H}_{aa}$ and $\mathbf{H}_{bb}$ denote the SI channels. Additionally, all SIMO channels in this chapter are considered to be Rayleigh fading channels with zero mean and unit variance. Since reception at node b is considered in this chapter, $h_i(\zeta)$ may denote the magnitude of the Rayleigh fading process for the channel from node a to the ζ^{th} receiving antenna at node b, in the i^{th} signalling interval, which is i.i.d. with $\mathbb{E}\left\{h_i(\zeta)^2\right\} = 1$ and its PDF is defined as [48]

$$p_h\left(h_i(\zeta)\right) = \frac{1}{(N_{rx}-1)!} h_i(\zeta)^{(N_{rx}-1)} \exp\left(-h_i(\zeta)\right), \forall h_i(\zeta) > 0. \tag{4.18}$$

Moreover, the AWGN at the receive port of any node is defined as $\boldsymbol{\nu} \sim \mathcal{CN}(0, \sigma_v^2\mathbf{I})$.

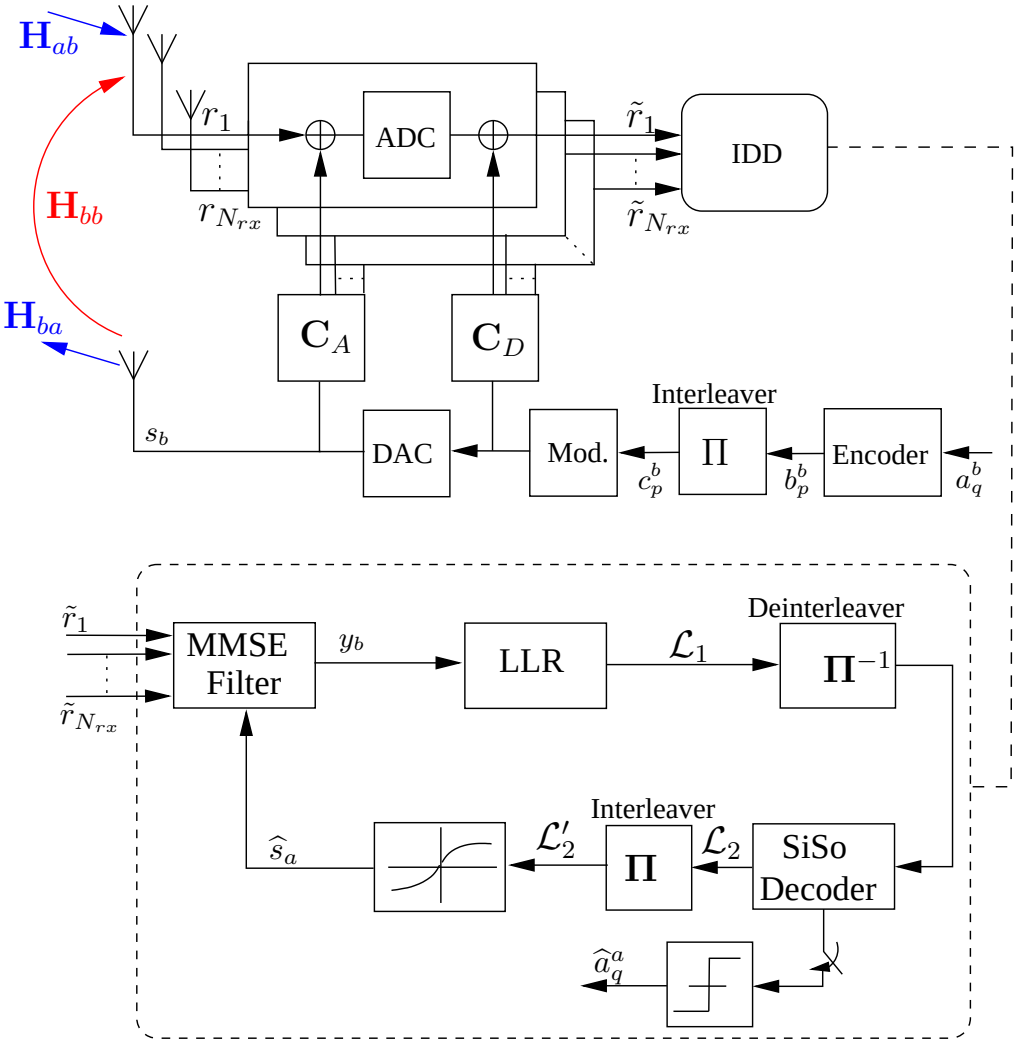

Figure 4.12: FD-SIMO transceiver architecture at node b.

4.4.2 Transmitter Structure

Without loss of generalization, this chapter focuses not only on the link from node a to node b, but also on mitigating the SI caused by the transmitter of node b to its receive port. At the transmitter, as shown in Fig. 4.12, the sequence of information bits at node b, a_q^b, of total length Q is passed through an RSC encoder, and is then interleaved to create the encoded and interleaved bit sequence, c_p^b, of total length P. The same process is applied at node a. The coded bits in each node are mapped to QPSK symbols, where the transmitted symbols from nodes a and b are defined as $s_a, s_b \in \mathcal{S} = \{\exp[j(2k+1)\pi/4] : k = 0, 1, 2, 3\}$.

4.4.3 Receiver Structure

For a given SIMO symbol interval, the received signal vector, $\boldsymbol{r}_b = [r_b^1, r_b^2, ..., r_b^{N_{rx}}]^T$, at node b can be written as

$$\mathbf{r}_b = \sqrt{p_a}\mathbf{H}_{ab}s_a + \sqrt{\widetilde{p}_b}\mathbf{H}_{bb}s_b + \mathbf{v}_b, \tag{4.19}$$

where p_a is the average received power from node a, while $\widetilde{p}_b$ represents the power from node b's transmit port to its receive port after implementing passive suppression of SI via antenna separation to diminish and block the LoS path [10, 17]. In this chapter, it is assumed that the CSI and the noise variance are perfectly known to the receiver. SIC can be implemented at the receiver in the analogue and digital domains by applying analogue and digital cancellation filters, i.e. $\mathbf{C}_A \in \mathbb{C}^{N_{rx}\times 1}$ and $\mathbf{C}_D \in \mathbb{C}^{N_{rx}\times 1}$, respectively. The known transmitted signals are filtered by $\mathbf{C}_A$ and $\mathbf{C}_D$ to generate replicas of SI to be subtracted from the received signals in both domains. Possible implementations of the two filters are $\mathbf{C}_A = -\mathbf{H}_{bb}$ and $\mathbf{C}_D = -\mathbf{A}(\mathbf{H}_{bb} + \mathbf{C}_A)$, where $\mathbf{A}$ represents a real diagonal matrix resulting from the ADC process. However, it is not possible in practice to achieve perfect cancellation [10, 40]. It is also worth mentioning that since the raw information bits of the local transmitter are directly available to the local receiver, there is no obvious additional benefit in jointly decoding the information streams.

4.4.4 SI Mitigation via IDD

This stage of SIC is required to remove the residual SI remaining after applying the previous stages of SIC. Fig. 4.12 shows the block diagram of IDD for node b. It is worth noting that an identical type of receiver is used at node a. The detector comprises adaptive MMSE filter with LLR demapper. A SiSo decoder performs soft channel decoding of the extrinsic information from the LLR demapper. During the first iteration the detector and decoder need to be initialized since the *a priori* and *a posteriori* information has not been obtained yet. For these reasons, the MMSE filter cannot achieve interference cancellation during the first iteration; therefore, it performs classical MMSE filtering and passes its outputs, y_b, to the LLR demapper. The latter first transforms the filtered symbols to LLR symbols then performs a soft demapping of these symbols to bit-wise LLRs. This

operation can be expressed mathematically as

$$\mathcal{L}_1[c_p^a] = \log \frac{Pr\left\{c_p^a = 1 \mid \tilde{\mathbf{r}}_b, \mathbf{w}_b\right\}}{Pr\left\{c_p^a = 0 \mid \tilde{\mathbf{r}}_b, \mathbf{w}_b\right\}}, \tag{4.20}$$

which represents the LLR of each coded bit with respect to the MMSE filter output, $y_b = \mathbf{w}_b^{\mathcal{H}}\, \tilde{\mathbf{r}}_b$, with $\tilde{\mathbf{r}}_b$ and $\mathbf{w}_b$ being its input and filter weights, respectively. The LLRs (or soft bits) are deinterleaved and processed by the SiSo decoder. This *a priori* information provided to the decoder is processed by exploiting the linear to logarithmic approximation of the maximum *a posteriori* algorithm (linear-log-MAP), as utilized in this chapter. This operation can be written in mathematical form as

$$\mathcal{L}_2[c_p^a] = \log \frac{Pr\left\{c_p^a = 1 \mid \mathcal{L}_1[c_p^a]\right\}}{Pr\left\{c_p^a = 0 \mid \mathcal{L}_1[c_p^a]\right\}}. \tag{4.21}$$

At this stage, a soft estimation for all symbols from the decoder output, which is defined as

$$\widehat{s}_a \triangleq \mathbb{E}\{s_a\} = \sum_{\alpha_t \in \mathcal{S}.} \alpha_t Pr\left\{s_a = \alpha_t\right\}, \tag{4.22}$$

which can be obtained as [86]

$$\widehat{s}_a = \frac{1}{\sqrt{2}}\left[\tanh\left(\frac{\mathcal{L}_2'[c_{p,1}^a]}{2}\right) + j\tanh\left(\frac{\mathcal{L}_2'[c_{p,2}^a]}{2}\right)\right], \tag{4.23}$$

where $\mathcal{L}_2'$ represents the LLR symbols after re-interleaving, i.e. $\mathcal{L}_2'[.] = \Pi\Big(\mathcal{L}_2[.]\Big)$. Additionally, $c_{p,1}^a$ and $c_{p,2}^a$ denote the successive odd and even coded bits at node a, respectively. At the end of the first iteration, and for the iterations beyond, the information required is provided to the adaptive MMSE filter in order to perform further cancellation of the residual SI. This filter is designed to achieve a minimization of the mean-square Error (MSE) between its output and the l^{th} symbol transmitted by node a, $s_a(l)$. The resulting coefficients are obtained by minimizing the mean square error of the metric $J(\mathbf{w}_b(l))$ [86] as

$$J(\mathbf{w}_b(l)) = \arg\min_{\mathbf{w}_b(l)} \left\|\mathbf{w}_b(l)^{\mathcal{H}}\, \widetilde{r}_b(l) - s_a(l)\right\|^2 \tag{4.24}$$

The solution of this problem was given in [10], [85] and [86] for different types of

interference. Similarly, in our case of SI, the solution can be given as

$$\mathbf{w}_b(l) = \Big[\Lambda_s(l)\mathbf{H}_{ab}(l)^{\mathcal{H}}\mathbf{H}_{ab}(l) + \Lambda_i(l)\mathbf{H}_{bb}(l)^{\mathcal{H}}\mathbf{H}_{bb}(l) + \sigma^2_{v_b}\mathbf{I}_{Nrx}\Big]^{-1}\mathbf{H}_{ab}(l)^{\mathcal{H}}, \quad (4.25)$$

where $\Lambda_s(l) = \mathbb{E}[\hat{s}_a\hat{s}_a^*]$ represents the variance of $\hat{s}_a$, while $\Lambda_i(l) = \mathbb{E}[s_b s_b^*]$ denotes the variance of the symbols s_b causing SI at node b. Once the computation of the adaptive MMSE filter coefficients, $\mathbf{w}_b(l)$, is complete, they are used along with the IDD input, $\widetilde{r}_b(l)$, to obtain the input of the LLR demapper as $y_b(l) = \mathbf{w}_b(l)^{\mathcal{H}}\widetilde{r}_b(l)$. All of these signal processing steps discussed so far for the first iteration are repeated for a predefined number of iterations so that the system converges to an acceptable BER with respect to the average SINR. After the last iteration is completed, a hard decision is applied to the SiSo decoder output in order to obtain node a transmitted bits as

$$\widehat{a}_q^a = \text{sign}\Big(\mathcal{L}_2\big[a_q^a\big]\Big), \quad (4.26)$$

where

$$\mathcal{L}_2[a_q^a] = \log\frac{Pr\left\{a_q^a = 1 \mid \mathcal{L}_1[c_p^a]\right\}}{Pr\left\{a_q^a = 0 \mid \mathcal{L}_1[c_p^a]\right\}}. \quad (4.27)$$

4.5 Upper Bound for QPSK over SIMO Rayleigh Fading Channels

The conventional performance upper bound (union bound) has been derived in [96] and [97] from the transfer function of the convolutional code for infinitely-long input sequences. Additionally, it doesn't take into account the impact of termination[1], therefore, this approach is not efficient for short information sequences with terminated trellises. A more accurate and tighter upper bound has been suggested in [98] and improved by [99] via defining a new generalized weight enumerator (GWE) of the terminated convolutional code by modifying the trellis diagram for a finite-length information sequence. This method has been derived for single-input single-output communication systems. In this section, we derive a tight upper bound for a rate-1/2 convolutional code with QPSK modulation scheme over the SIMO Rayleigh fading channel.

[1]Termination means that the convolutional trellis returns to zero-state by adding some padding bits to the original message [88].

4.5.1 Union Upper Bounds

In general, the union bound for the BER, $\bar{P}_b$, for rate-1/n is given by [48, 99] as

$$\bar{P}_b \leq \sum_{d=d_{free}} B_d P_d\left(\mathbf{s}, \mathbf{y}\right), \tag{4.28}$$

where P_d denoted for the pairwise error probability (PEP) between the transmitted and estimated sequences $\mathbf{s} = \{s_1, s_1, ..., s_{N_{tx}}\}$ and $\mathbf{y} = \{y_1, y_1, ..., y_{N_{tx}}\}$, respectively, when the Hamming distance between them is equal to d, B_d are the coefficients obtained by applying the derivation to the transfer function of the code, $T\left(B, D\right)$, as

$$\left.\frac{\partial T\left(B, D\right)}{\partial B}\right|_{B=1} = \sum_{d=d_{free}}^{\infty} B_d D^d, \tag{4.29}$$

where D and B represent the Hamming distance of the coded and input sequences, respectively. Additionally, d_{free} in (4.28) represents is the free distance, which can be computed for a convolutional code of rate-$1/n$ and a constraint length K as

$$d_{free} \leq \min_{l>1} \left\lfloor \frac{2^{l-1}}{2^l - 1}(K + l - 1)n \right\rfloor, \tag{4.30}$$

in which the operation $\lfloor x \rfloor$ is to choose the largest integer within x [48].

4.5.2 A Tight Upper Bound

In order to obtain a tight upper bound for a rate-1/2 convolutional code with constraint length K using L terminating information bits for QPSK, the technique used in [98, 99] is followed to derive the weight enumerator. In addition, it is required to derive the PEP of the coded QPSK system over the SIMO Rayleigh fading channel in order to obtain a closed-form expression for a tight upper bound on the BER.

4.5.2.1 Generalized Weight Enumerator

Since reception at node b is considered here, the transmitted symbol from node a, s_a, will be denoted by the simpler notation s, and the equalized symbol at node b, y_b, will be denoted simply by y. In order to evaluate the weight enumerator of rate-1/2 convolutionally coded QPSK, we assume that a message of all zeros is transmitted as $s = \frac{1}{\sqrt{2}} + j\frac{1}{\sqrt{2}}$, depending on the QPSK signal constellation defined earlier in Subsection 4.4.2 as shown

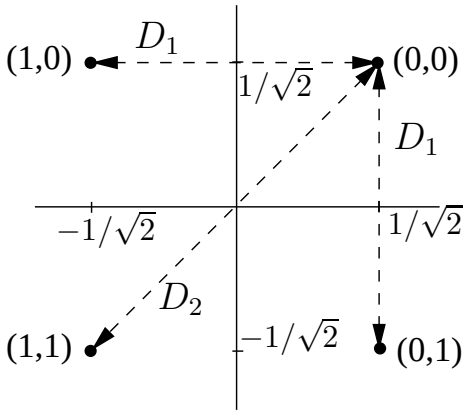

Figure 4.13: QPSK signal constellation.

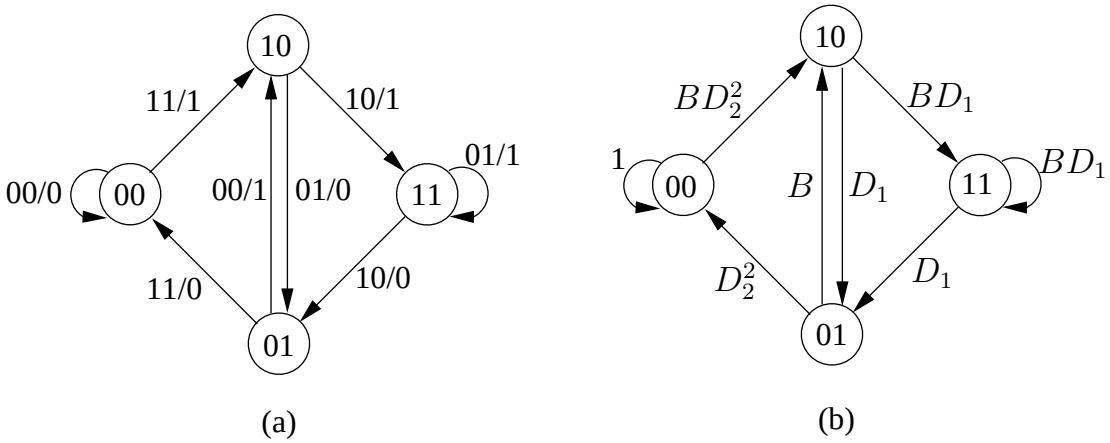

Figure 4.14: (a) State diagram for code C_1 (b) Corresponding branch labels

in Fig. 4.13.

Let the received signal, $\mathbf{y}$, differ from the transmitted signal, $\mathbf{s}$, by exactly d symbols, which are distributed as d_1 symbols of $S_1 = \pm\frac{1}{\sqrt{2}} \mp j\frac{1}{\sqrt{2}}$ with distance D_1, and d_2 symbols of $S_2 = -\frac{1}{\sqrt{2}} - j\frac{1}{\sqrt{2}}$ with Euclidean distance D_2. For instance, Fig. (4.14) (a) and (b) show, receptively, the state diagram and its corresponding branch labels for the code C_1 of constraint length $K = 3$ and generator polynomial $G = (1, 5/7)_8$.

Each branch in Fig. 4.14 (a) has a representation $(\mathrm{output}/\mathrm{input})$, where $\mathrm{output} \in \{00, 01, 10, 11\}$ and $\mathrm{input} \in \{0, 1\}$. The corresponding branch labels in Fig. 4.14 (b) are obtained from the state diagram of C_1 discussed earlier, in which the inputs 0 and 1 are labelled as 1 and B, respectively. Moreover, the $\mathrm{outputs}$ 00, 01, 10 and 11 are labelled as 1, D_1, D_1 and D_2^2, respectively.

According to the above definitions and assumptions, the GWE of QPSK is given as

[99]

$$W\left(B, D_1, D_2\right) = \sum_{\eta} \sum_{d_1} \sum_{d_2} c_{\eta,d_1,d_2} B^{\eta} D_1^{d_1} D_2^{2d_2}, \tag{4.31}$$

where c_{η,d_1,d_2} represents the number of error events comprising d_1 symbols of D_1 Euclidean distance and d_2 symbols of D_2 Euclidean distance when the input Hamming distance is η.

The weight enumerator for terminated convolutional codes is obtained in [98, 99] for BPSK and QPSK, receptively, by modifying the conventional trellis diagram for the convolutional codes in order to obtain tighter upper bounds. In the modernized trellis diagram, any branch merges into zero state at any trellis depth is redirected to a new state denoted as 2^{K-1}. This makes the weight enumerator more tolerant and resilient against multiple error events. Fig. 4.15 shows the new trellis diagram of code C_1 with QPSK and for a particular information length, $L = 5$, in which the labels of the branches between a trellis depth $t-1$ and t are drawn according to the branch metric shown in Fig. 4.14 (b).

In order to find the weight enumerator for the code C_1 with QPSK, it is required to define a set of states, $\overline{\mathbf{S}}_t = (0, \ldots, 2^{K-1}-1)$, at depth t as illustrated in Fig. 4.15. Moreover, the labels of the branched between the successive states, i.e. the state $\overline{\mathbf{S}}_{t-1}$ of depth $t-1$ and the state $\overline{\mathbf{S}}_t$ of depth t, can be denoted as $\overline{G}_{\overline{\mathbf{S}}_{t-1},\overline{\mathbf{S}}_t}(B, D_1, D_2)$. Additionally, we can denote by $\overline{F}_{\overline{\mathbf{S}}_t}(B, D_1, D_2)$ to the temporary polynomial to store the coefficient of state $\overline{\mathbf{S}}_t$ of depth t. At the beginning, it is required to initialize $\overline{F}_{\overline{\mathbf{S}}_0}(B, D_1, D_2)$ as

$$\overline{F}_{\overline{\mathbf{S}}_0}(B, D_1, D_2) = \begin{cases} 1 & \text{if } \overline{\mathbf{S}}_0 = 0 \\ 0 & \text{otherwise,} \end{cases} \tag{4.32}$$

while for the next trellis depth from $t = 1$ to $t = L + K - 1$, $\overline{F}_{\overline{\mathbf{S}}_t}(B, D_1, D_2)$ is evaluated as

$$\overline{F}_{\overline{\mathbf{S}}_t}(B, D_1, D_2) = \sum_{\overline{\mathbf{S}}_{t-1} = \Lambda_{\overline{\mathbf{S}}_t}} \overline{F}_{\overline{\mathbf{S}}_{t-1}}(B, D_1, D_2) \times \overline{G}_{\overline{\mathbf{S}}_{t-1},\overline{\mathbf{S}}_t}(B, D_1, D_2), \tag{4.33}$$

where $\Lambda_{\overline{\mathbf{S}}_t}$ represents the set of all previous states that have branches merging to $\overline{\mathbf{S}}_t$, i.e. the states at trellis depth $t-1$ lead to $\overline{\mathbf{S}}_t$. Furthermore, the desired weight enumerator at trellis depth $t = L + K - 1$ is represented by the polynomial $\overline{F}_{\overline{\mathbf{S}}_t = 2^{K-1}}(B, D_1, D_2)$ [100]. For instance, we can obtain the weight enumerator for the code C_1 according to the procedure

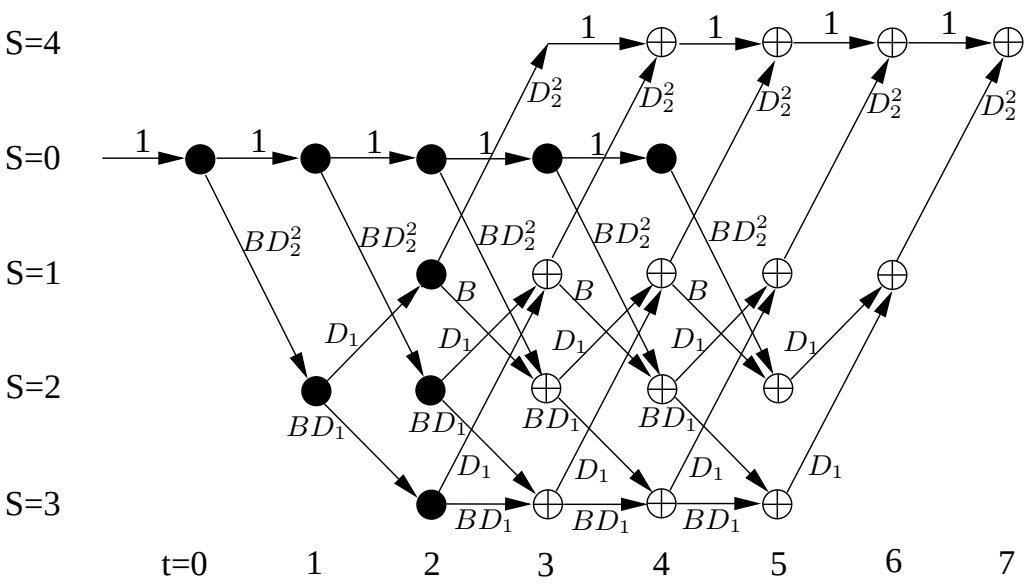

Figure 4.15: Modified Trellis Diagram

explained above and for an information length $L = 5$ as

$$W(B, D_1, D_2) = 5BD_1D_2^4 + 7B^2D_1^2D_2^4 + 8B^3D_1^3D_2^4 + 5B^4D_1^4D_2^4 + B^5D_1^5D_2^4. \tag{4.34}$$

Moreover, Table 4.3 illustrates the weight enumerators for different information lengths, L, of rate-half convolutional encoders of constrained length, $K = 3$ to $K = 9$, and for various generator polynomials, G. This table is obtained by following the procedures in [98, 99].

4.5.2.2 Pairwise Error Probability

Following the derivations in [99, 101], the conditional PEP, $P_2\big(s, y|\{h_i(\zeta)\}\big)$, of coded QPSK using rate-1/2 convolutional codes over the SIMO Rayleigh fading channel and under the impact of SI can be expressed as

$$\begin{aligned} P_2(s, y|\{h_i(\zeta)\}) =& Q\Bigg\{\Bigg(\frac{\gamma}{2}\Big[\sum_{i=1}^{d_1}\sum_{\zeta=0}^{N_{rx}-1}|h_i(\zeta)|^2|y_i - s_i|^2 \\ &+ \sum_{i=1}^{d_2}\sum_{\zeta=0}^{N_{rx}-1}|h_i(\zeta)|^2|y_i - s_i|^2\Big]\Bigg)^{1/2}\Bigg\}, \end{aligned} \tag{4.35}$$

where y_i denotes the i^{th} element in the vector y, and s_i denotes the i^{th} element in the vector s. Also, γ represents the average SINR, which can be expressed as, $\gamma = \frac{\gamma_s}{\gamma_I+1}$,

Table 4.3: Weight Enumerators for QPSK

K	G	L	Weight Enumerator
3	$(1, 5/7)_8$	≥ 12	$LBD_1D_2^2 + (2L-3)B^2D_1^2D_2^2 + (4L-12)B^3D_1^3D_2^2 +$ $(8L-36)B^4D_1^4D_2^2 + 2(16L-96)B^5D_1^5D_2^2 +$ $(32L-240)B^6D_1^6D_2^2 + (64L-576)B^7D_1^7D_2^2 + ...$
4	$(1, 15/17)_8$	≥ 9	$(L-1)B^2D_1^2D_2^2 + LBD_1D_2^3 + (2L-5)B^3D_1^3D_2^2 +$ $(L-2)B^2D_1^2D_2^3 + (4L-17)B^4D_1^4D_2^2 +$ $(3L-12)B^3D_1^3D3^2 + (8L-48)B^5D_1^5D_2^4 +$ $(L-3)B^2D_1^2D_2^4 + (8L-44)B^4D_1^4D_2^3 +$ $(16L-124)B^6D_1^6D_2^2 + ...$
5	$(1, 23/35)_8$	≥ 10	$LBD_1^3D_2^2 + (L-3)B^3D_1^3D_2^2 + (L-4)B^2D_1^2D_2^3 +$ $(L-7)B^6D_1^4D_2^2 + (L-2)B^3D_1^3D_2^3 + (L-5)B^5D_1^3D_2^3 +$ $(L-5)B^5D_1^5D_2^2 + (L-8)B^7D_1^5D_2^2 + (L-2)B^2D_1^4D_2^3 +$ $(3L-13)B^4D_1^4D_2^3 + (2L-14)B^6D_1^4D_2^3 + (2L-7)B^2D_1^6D_2^2 +$ $(4L-26)B^4D_1^6D_2^2 + (3L-25)B^6D_1^6D_2^2 + (L-9)B^8D_1^6D_2^2 + ...$
6	$(1, 53/75)_8$	≥ 9	$(L-2)B^2D_1^4D_2^2 + LBD_1^3D_2^3 + (L-2)B^3D_1^3D_2^3 +$ $(L-6)B^5D_1^3D_2^3 + (L-4)B^3D_1^5D_2^2 + (2L-13)B^5D_1^5D_2^2 +$ $(2L-16)B^7D_1^5D_2^2 + (L-4)B^4D_1^2D_2^4 + (L-1)B^2D_1^4D_2^3 +$ $(3L-14)B^4D_1^4D_2^3 + (L-7)B^6D_1^4D_2^3 + (L-8)B^8D_1^6D_2^2 + ...$
7	$(1, 133/171)_8$	≥ 11	$LBD_1^2D_2^4 + (2L-4)B^2D_1^4D_2^3 + (2L-8)B^3D_1^4D_2^3 +$ $(2L-5)B^3D_1^6D_2^2 + (2L-12)B^4D_1^6D_2^2 + (L-6)B^5D_1^6D_2^2 +$ $(L-9)B^6D_1^6D_2^2 + (L-2)B^2D_1^4D_2^4 + (L-5)B^3D_1^4D_2^4 +$ $(2L-14)B^4D_1^4D_2^4 + ...$
8	$(1, 247/371)_8$	≥ 12	$(L-1)B^2D_1^4D_2^3 + (L-3)B^3D_1^3D_2^4 + LBD_1^5D_2^3 +$ $(L-4)B^3D_1^5D_2^3 + (L-3)B^3D_1^7D_2^2 + (L-8)B^5D_1^7D_2^2 +$ $(L-7)B^7D_1^7D_2^2 + (L-2)B^2D_1^4D_2^4 + (3L-14)B^4D_1^6D_2^3 +$ $(L-11)B^6D_1^6D_2^3 + (2L-12)B^4D_1^8D_2^2 + ...$
9	$(1, 561/753)_8$	≥ 12	$LBD_1^4D_2^4 + (L-4)B^3D_1^4D_2^4 + (2L-3)B^2D_1^6D_2^3 +$ $(L-2)B^3D_1^6D_2^3 + (L-4)B^4D_1^6D_2^3 + 7(L-7)B^5D_1^6D_2^3 +$ $(3L-12)B^3D_1^8D_2^2 + (L-5)B^4D_1^8D_2^2 + (3L-22)B^4D_1^6D_2^4 +$ $(3L-20)B^5D_1^6D_2^4 + (2L-16)B^6D_1^6D_2^4 + ...$

where $\gamma_s = p_a/\sigma_v^2$ and $\gamma_I = \tilde{p}_b/\sigma_v^2$ denote the SNR and INR on node a, respectively. According to the QPSK mapping defined earlier, $|y_i - s_i|^2 = 2$ for d_1 symbols of S_1 in the first term of (4.35), while it is equal to 4 for d_2 symbols of S_2 in the second term. After substituting these values in (4.35) and using Craig's expression of the Q-function [102], which is given by

$$Q(x) = \frac{1}{\pi}\int_0^{\pi/2} \exp\left(\frac{-x^2}{2\sin^2\theta}\right) d\theta, \tag{4.36}$$

we can rewrite (4.35) as

$$P_2(s,y|\{h_i(\zeta)\}) = \frac{1}{\pi}\int_0^{\pi/2} \mathbb{E}_{h_i(\zeta)}\left\{ \exp\left(\frac{\gamma \sum_{i=1}^{d_1}\sum_{\zeta=0}^{N_{rx}-1}|h_i(\zeta)|^2}{-2\,\sin^2\theta}\right) \times \exp\left(\frac{\gamma \sum_{i=1}^{d_2}\sum_{\zeta=0}^{N_{rx}-1}|h_i(\zeta)|^2}{-\sin^2\theta}\right)\right\} d\theta. \tag{4.37}$$

In order to evaluate the unconditional PEP, we begin by noting that the random variables $H_i = \sum_{\zeta=0}^{N_{rx}-1}|h_i(\zeta)|^2$ for $i = 1, 2, \ldots, d_1+d_2$ are independent and chi-square distributed with $2N_{rx}$ degrees of freedom and they follow the PDF of the SIMO Rayleigh fading channel defined earlier in (4.18). Therefore, the expectation can be evaluated separately to obtain the final expression for $P_2(\mathbf{s},\mathbf{y})$ as

$$P_2(s,y) = \frac{1}{\pi}\int_0^{\pi/2}\prod_{i=1}^{2}\left(\frac{\sin^2\theta}{\sin^2\theta+\gamma_i}\right)^{m_i} d\theta, \tag{4.38}$$

where $\gamma_1 = \gamma/2$, $\gamma_2 = \gamma$, $m_1 = d_1(N_{rx}-1)$, and $m_2 = d_2(N_{rx}-1)$. The exact solution of (4.38) is computed in [102, eq. (5A.59)] as

$$\begin{aligned}
P_2(s,y) &= \frac{(\frac{\gamma_1}{\gamma_2})^{m_2-1}}{2(1-\frac{\gamma_1}{\gamma_2})^{m_1+m_2+1}}\left[\sum_{k=0}^{m_2-1}(\frac{\gamma_2}{\gamma_1}-1)^k B_k I_k(\gamma_2) - \frac{\gamma_1}{\gamma_2}\sum_{k=0}^{m_1-1}(1-\frac{\gamma_1}{\gamma_2})^k C_k I_k(\gamma_1)\right],\\
B_k &= \frac{A_k}{\binom{m_1+m_2-1}{k}}, \quad C_k = \sum_{n=0}^{m_2-1}\frac{\binom{k}{n}}{\binom{m_1+m_2-1}{n}}A_n,\\
A_k &= (-1)^{m_2-1+k}\frac{\binom{m_2-1}{k}}{(m_2-1)!}\prod_{n=1,n\neq k+1}^{m_2}(m_1+m_2-n),\\
I_k(\gamma) &= -1\sqrt{\frac{\gamma}{1+\gamma}}\left[1+\sum_{n=1}^{k}\frac{(2n-1)!!}{n!2^n(1+\gamma)^n}\right],\\
(2n-1)!! &= 1\times 3\times \ldots \times (2n-1), \quad \binom{k}{n} = 0\ \forall\ n>k.
\end{aligned} \tag{4.39}$$

After obtaining the exact $P_2(s,y)$, a tight upper bound can be evaluated as

$$P_b = \frac{1}{L}\sum_{d_2}\sum_{d_1}\sum_{\eta}\eta\, c_{\eta,d_1,d_2}\, P_2(s,y). \tag{4.40}$$

Alternatively, (4.35) can be solved by exploiting the Q-function inequality, $Q(x) \leq$

$\frac{1}{2}\exp(-x^2/2)$, to yield

$$\tilde{P}_2\Big(s,y|\{h_i(\zeta)\}\Big) \leq \frac{1}{2}\mathbb{E}\left\{\exp\left(-\gamma/2\sum_{i=1}^{d_1}\sum_{\zeta=0}^{N_{rx}-1}|h_i(\zeta)|^2\right)\exp\left(-\gamma\sum_{i=1}^{d_2}\sum_{\zeta=0}^{N_{rx}-1}|h_i(\zeta)|^2\right)\right\}. \tag{4.41}$$

Furthermore, as we have two chi-squared distributed random variables in (4.41), which can be expressed in general form as

$$\Psi_{d_l} = \sum_{q=1}^{d_l}\sum_{p=0}^{N_{rx}-1}|h_q(p)|^2,\ \forall l \in \{1,2\}, \tag{4.42}$$

the expectation of conditional expression in (4.41) can be solved easily using the formula [97]

$$\mathbb{E}\left\{\exp(\xi\Psi_{d_l})\right\} = \frac{1}{(1-\xi)^{d_l(N_{rx}-1)}}. \tag{4.43}$$

Therefore, the unconditional PEP, $\tilde{P}_2(s,y)$, which is expressed as

$$\tilde{P}_2(s,y) = \mathbb{E}_h\left\{\tilde{P}_2\big(s,y|\{h_i(\zeta)\}\big)\right\}, \tag{4.44}$$

can be solved approximately as

$$\tilde{P}_2(s,y) \leq \frac{1}{2}\prod_{i=1}^{2}\left(\frac{1}{1+\gamma_i}\right)^{d_i(N_{rx}-1)}. \tag{4.45}$$

It is worth mentioning that $\tilde{P}_2$ in (4.45) can be used instead of $\bar{P}_b$ in (4.28) to obtain the union bound.

4.6 Simulation Results and Discussion

In this section, the performance of a coded FD-SIMO based bi-directional transceiver is investigated in the presence of SI. It is assumed that 45 dB of passive suppression of SI by antenna separation followed by two stages of analogue and digital filtering achieving 35 dB of additional SI attenuation [17]. An RSC convolutional encoder is used with code rate $R_c = Q/P = 1/2$, constraint length $K = 5$ and generator polynomials $(1, 23/35)_8$. Encoding is followed by interleaving and QPSK modulation. The overall system performance is evaluated using flat Rayleigh fading channels in the presence of AWGN.

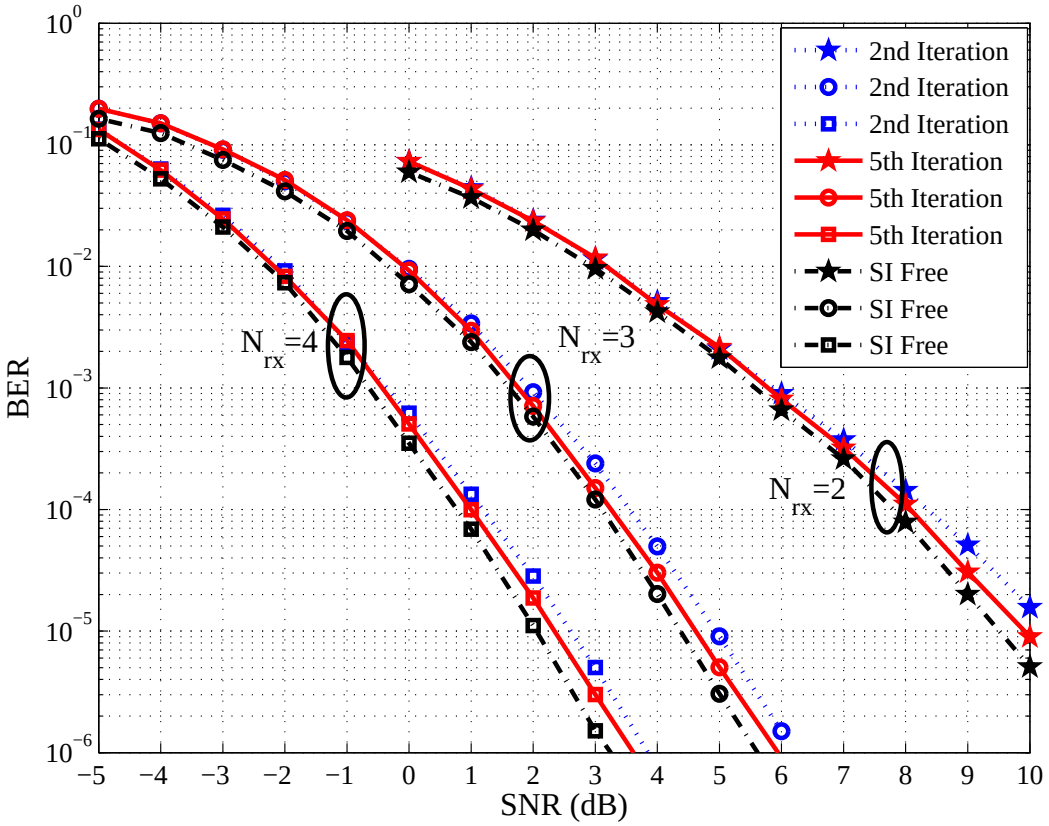

Figure 4.16: BER vs. SNR performance of iterative coded FD-SIMO in the presence of 10 dB residual INR.

Fig. 4.16 shows the system's BER-SNR performance for the 2nd and 5th iterations and for different scenarios of SIMO system, i.e. N_{rx}, as $N_{rx} = 2, 3,$ and 4. Moreover, a comparison is presented between the system performance under a residual INR of 10 dB against the interference-free case. From this figure, it is clear that the performance under SI after five iterations is very close to the SI free performance, which demonstrates that the proposed SIC has a near-optimal performance, especially with higher number of antennas at the receiving port, N_{rx}^{b}. It is worth noting that in the three investigated scenarios the performance improves whenever the number of iterations is increased.

Fig. 4.17 demonstrates a comparison between the union and the tight upper bounds on the performance of the proposed system derived in this chapter, along with the simulation of the BER-SNR performance under the same conditions mentioned above.

Fig. 4.18 shows the system's performance in BER vs. E_b/N_0 (in dB) metric for the 2nd and 5th iterations and for different receive antenna configurations, i.e. $N_{rx} = 2, 3,$ and 4, in which E_b and N_0 represent the the energy per bit and the variance of the noise, respectively. Moreover, two SI scenarios are considered, i.e. residual INR of 10 dB and

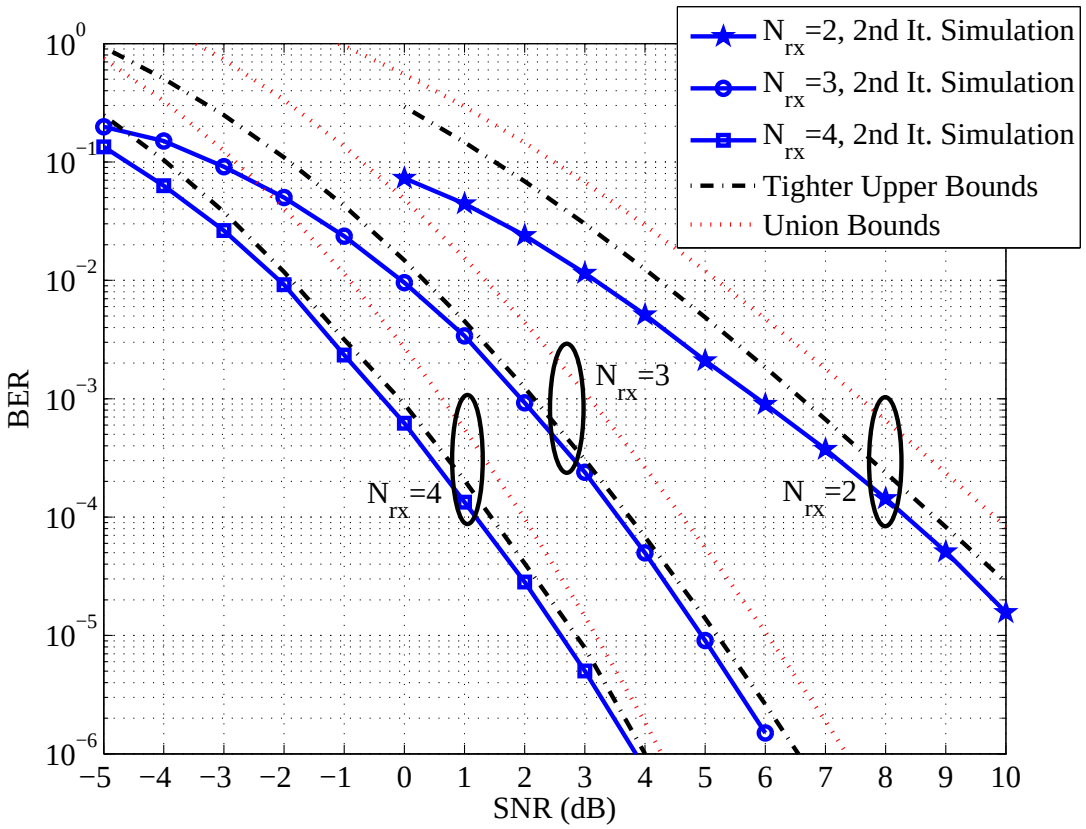

Figure 4.17: Union and tight upper bounds on the performance of coded FD-SIMO along with simulations in the presence of 10 dB residual INR.

the SI-free case. From this figure, it is clear that the performance under SI after five iterations is very close to the SI free performance, which demonstrates that the proposed SIC has a near-optimal performance, especially with higher number of receiving antennas. For $N_{rx} = 2$, the uncoded performance for the two SI scenarios is also included for reference. A closer look at the results reveals that, at a BER of 10^{-4}, the proposed coded FD-SIMO-IDD system with residual INR of 10 dB can achieve about 16 dB and 8 dB improvement comparing to the uncoded FD-SIMO in the presence and absence of SI, respectively. Furthermore, it is demonstrated in this figure the derived tight upper bound on the performance under the same conditions described above. It is worth mentioning that the weight enumerator terms d_1, d_2, c_{η,d_1,d_2}, and η, which are used to evaluate the tight upper bound on the performance of the considered convolutional codes, are illustrated in Table.4.3 for different constraint lengths, K, and generator polynomials, G. For instance, an RSC convolutional encoder of code rate $R_c = Q/P = 1/2$, constraint length $K = 5$, generator polynomials $(1, 23/35)_8$, and a length of information of $L = 15$, the weight enumerator terms are obtained from Table 4.3 as $d_1 =$

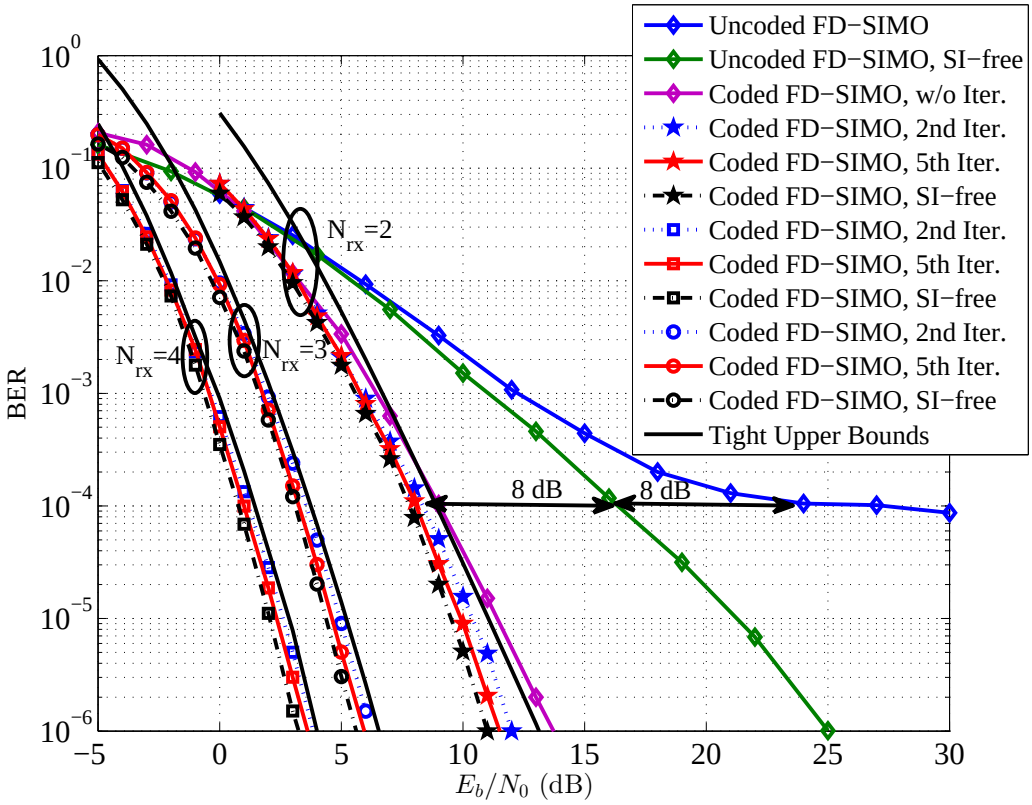

Figure 4.18: BER vs. E_b/N_0 performance of iterative coded FD-SIMO in the presence of 10 dB residual INR.

$[3,3,2,4,3,3,5,5,6,6,6,6,6,6,6]$, $d_2 = [2,2,3,2,3,3,2,2,3,3,3,2,2,2,2]$, $c_{\eta,d_1,d_2} = [15,12,11,8,13,10,10,7,13,32,16,23,34,30,6]$ and $\eta = [1,3,2,6,3,5,5,7,2,4,6,2,4,6,8]$. These terms are substituted in (4.39) and (4.40) in order to obtain the tight upper bound on the performance of the proposed coded FD-SIMO. The results reveal that the tight upper bound performances match closely at high SNR the results obtained from simulations of the proposed system after the 2nd iteration. Therefore, the derived tight upper bounds can be utilized by modem designers to accurately describe the performance of coded FD-SIMO systems without the need to run time-consuming simulations.

Fig. 4.19 illustrates the BER performance as a function of SNR for three cases of FD-SIMO, i.e. $(1,2,1)$, $(1,3,1)$, and $(1,4,1)$, after replacing the convolutional codes with turbo codes. In all simulation results presented in this chapter, the number of local (intra-turbo) iterations of the turbo decoder and global (inter-turbo) iterations of the IDD were set to 10 and 5, respectively. A closer look at the figure reveals that the system with turbo codes achieves as expected better performance comparing to convolutional codes under the same power of interference, i.e. INR$=10$ dB, which implies increased robust against SI. Moreover, it can be noticed that by increasing the receive antenna elements of

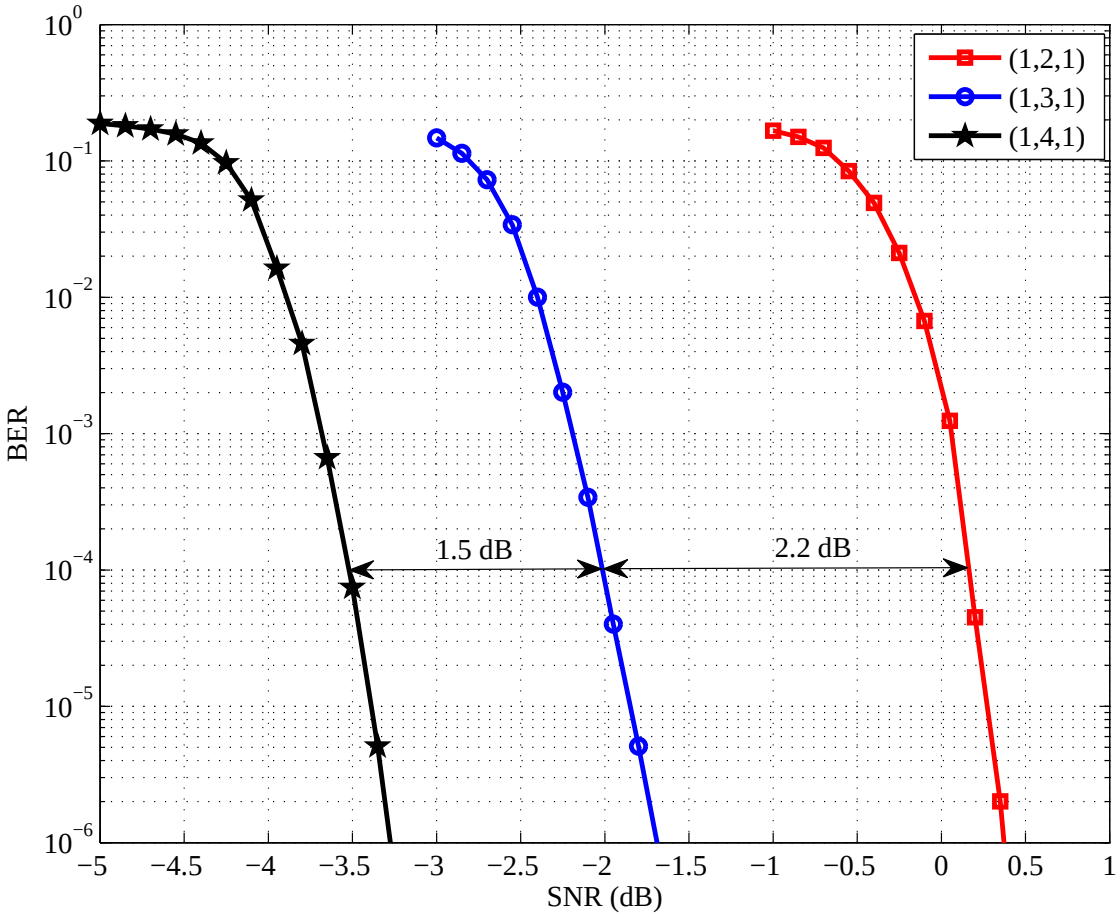

Figure 4.19: BER vs. SNR performance of iterative turbo codes FD-SIMO in the presence of 10 dB residual INR, in which the number of local and global iterations were set to 5 and 10, receptively.

the FD-SIMO transceiver, i.e. N_{rx}, additional gain can be obtained. A closer look at the figure Fig. 4.19 reveals that at a BER level of 10^{-4} the proposed system achieves a gain in SNR of 2.2 and 1.5 dB, when the receive antennas are increased from 2 to 3 then from 3 to 4, respectively.

4.7 Chapter Summary

In this chapter, an IDD receiver for a bi-directional coded FD-SIMO system has been proposed to overcome the residual SI that remains after passive, analogue and digital SIC processing. The performance of the proposed technique has been evaluated using simulations, in addition to the derivation of a tight upper bound under the same conditions to confirm our results. IDD has been implemented by exchanging the soft information of the desired signal and the SI between the equalizer and the SiSo decoder. The equalizer

performs MMSE filtering to remove residual SI, LLR demapping and MAP SiSo channel decoding. Simulations results were presented for different number of receiving antennas in the presence of AWGN and for independent SIMO flat Rayleigh fading channels. The simulation results show that increasing the number of iterations and/or the number of receive antennas improves resilience against residual SI by reconstructing more precisely the desired signal and interference.

Chapter 5

IDD for Coded FD-MIMO in the Presence of Residual SI

5.1 Introduction

Iterative soft parallel interference cancellation (soft-PIC) using soft-in soft-out (SiSo) along with IDD technique can be exploited with the coded FD-MIMO transceiver for SIC purpose[1] . This approach can be implemented by employing channel encoding using convolutional or turbo codes followed by an interleaver to combat burst errors. The BICM process is achieved by mapping the coded and interleaved bits into symbols according to the modulation scheme utilized [104]. Additionally, OFDM can be employed in conjunction with MIMO-BICM to enhance spectral efficiency and combat the effect of frequency-selective fading channels [105–108]. Although OFDM is out of the research scope of this chapter due to the flat Rayleigh fading channel assumption, the results presented here are valid for OFDM as long as the cyclic prefix used has sufficient length to cover the delay spread of the multipath channel.

Iterative detection and decoding (IDD) techniques, which are commonly referred to as turbo-like receivers or turbo-BLAST (BLAST stands for Bell Labs layered space time), are implemented in the MIMO receiver using several iterative exchanges of soft information between the detector and the decoder [85, 93, 103, 109]. IDD offers high throughput, efficiency, and reliable performance in the case of noise and interference impaired environments in wireless communications [103, 104, 110, 111]. Soft information may take the forms of MAP, ML, or an LLR [103, 106]. However, the algorithms used to evaluate this soft information require highly complex computations, which increase exponentially with the size of the constellation mapping and/or the number of antennas in MIMO systems [103, 105, 108]. Therefore, it is preferable to utilize methods that have the ability to reduce this complexity and maintain performance at an acceptable near-capacity threshold [106, 110, 111]. Such systems have been proposed and successfully employed for the mitigation of various types of wireless interference, such as ISI, co-channel interference (CCI), co-antenna interference (CAI), multiple-access (multi-antenna) interference (MAI), and multi-user interference (MUI) [85], [112–114]. In [109], a tight upper bound on the performance of the coded FD-SIMO was derived by assuming the presence of residual SI after applying passive and active SIC.

Theoretical and experimental studies of the exploitation of BLAST using the turbo principles for MIMO in [85] has shown that this combination gives higher data rates, better performance and more efficient computation compared to conventional BLAST

[1] Part of this Chapter is published in [103]

schemes with an ML detector under the same conditions and in Rayleigh-fading scenarios [93].

An improved IDD architecture with anti-gray mapping has been proposed to overcome the slow convergence rate when employing gray mapping with the traditional turbo-BLAST in a MIMO wireless communication system [110]. This improved scheme was achieved by applying the *posteriori* LLR information from the outer SiSo decoder to the detector, rather than the *extrinsic* information, which is always used in conventional IDD, in order to produce faster convergence. A similar idea has been used with OFDM in [107] for a comparison between the linear and non-linear MMSE detectors. The first detector produces a *priori* LLR information as a result of processing and equalizing the received symbols and the extrinsic soft information as the traditional turbo-BLAST, while the non-linear MMSE detector replaces the extrinsic information with *posteriori* LLR information, which is fed directly back from the SiSo decoder.

In another study [111], the authors dealt with the reduction of the high computational complexity of IDD based on soft interference cancellation (soft-IC) by simplifying the instantaneous matrix inversions at the cost of a slight reduction in performance. A modified turbo-BLAST with OFDM has been considered in [105] based on soft-PIC and MMSE filtering for the MIMO frequency selective fading channel and in the presence of imperfect channel estimation. The researchers then proposed hard-decision based equalization using bit-level interference cancellation as a form of low complexity IDD at the cost of a slight degradation in the overall system performance [106].

The systems presented in [113], [114] exploited IDD using soft-IC that can be achieved by firstly creating a soft copy of interfering symbols using the LLR information supplied by the outer SiSo decoder to the soft-IC/MMSE detector. These estimated symbols can then be combined with the interfering channel, which may be known or need to be estimated. Finally, a subtraction from the received signal is implemented in order to obtain the desired signal, however, a linear adaptive filter is required to cancel the residual interference.

The key contributions of this chapter is to extend the works in [103, 109] by exploiting IDD, in the context of coded FD-MIMO, to mitigate more effectively the residual SI remaining after applying multiple stages of SIC. After a number of iterations, the performance achieved is shown to be very close to the SI-free case. Additionally, in order to validate the simulation results, a tight upper bound on the performance of the proposed FD-MIMO for rate-1/2 convolutional codes with M-QAM is derived, which is asymp-

totically close to the simulated performance and can be used for performance evaluation of such a system without the need to implement time-consuming simulations. Moreover, EXIT chart analysis is employed as a semi-analytic method to visualize the convergence behavior between the proposed detector and decoder, and to evaluate the number of iterations required for this convergence.

The rest of the chapter is organized as follows. In Section 5.2, the signal and system models are introduced. Firstly, a description of the overall coded FD-MIMO bi-directional transceiver is presented by defining the channel and noise characteristics. Moreover, the equations for the transmitted and received signals are given. Section 5.3 presents different stages of SIC in the passive and active domains in addition to our proposed IDD system to combat the residual SI by utilizing iterative soft-PIC with adaptive MMSE filtering for coded FD-MIMO. In Section 5.5, a tight upper bound on the performance of the proposed IDD system in the presence of residual SI is derived. Moreover, in Section 5.7, EXIT chart analysis [115] is employed as a semi-analytic technique to analyse and visualize the convergence behavior of the proposed iterative system. Section 5.8 presents simulation results and discussion, and finally, the chapter's conclusions are drawn in Section 5.9.

5.2 Signal and System Model

In this chapter, a wireless scenario is considered in which two bi-directional point-to-point nodes a and b are communicating using FD-MIMO transceivers [14, 103, 109]. It is assumed that each node is equipped with N_{tx} transmit antennas and N_{rx} receive antennas, where $N_{tx} \leq N_{rx}$ as shown in Fig. 5.1. The four wireless links illustrated in this figure are denoted as $\mathbf{H}_{ab}$ and $\mathbf{H}_{ba}$ indicating the forward channels, while $\mathbf{H}_{aa}$ and $\mathbf{H}_{bb}$ denote the self interference channels. All channels in this chapter are considered to be frequency non-selective Rayleigh fading channels, i.e. flat fading channels, which can be defined generally as $\mathbf{H} \sim \mathcal{CN}(0, \mathbf{I}_{N_{tx}N_{rx}})$. Moreover, the AWGN samples at the receive port of any node are i.i.d. with zero mean and variance $\sigma^2_{v_i}$, and can be defined as $\mathbf{v}_i \sim \mathcal{CN}(0, \sigma^2_{v_i}\mathbf{I}_{N_{rx}})$, and $\sigma^2_{v_i} = \mathbb{E}\{\mathbf{v}_i\mathbf{v}_i^{\mathcal{H}}\}$, where $i \in \{a, b\}$.

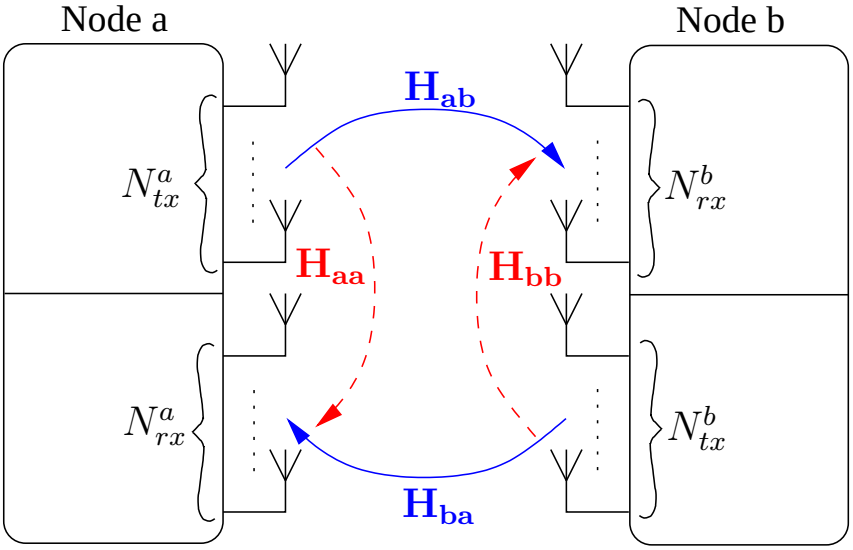

Figure 5.1: Bi-directional FD-MIMO Transceiver

5.2.1 Transmitter Structure

Without loss of generalization, this chapter focuses not only on the link from node a to node b, but also on mitigating SI caused by node b's transmitter to its receive port. At the transmitter of node b, as shown in Fig. 5.2, the q^{th} bit, a_q^b, in a sequence of information bits with total length of Q, is passed through a recursive systematic convolutional (RSC), then interleaved to create the encoded and interleaved bit sequence, c_p^b, of total length P. The code rate is defined as $R_c \in [0,1] = Q/P$.

Subsequently, the coded bits are interleaved using a random interleaver, $\Pi(\,.)$ and the interleaved bits are divided using a serial-to-parallel multiplexer into N_{tx} sub-streams. In each branch, the conversion of bits to symbols, i.e. mapping, is achieved according to the modulation scheme used. Each vector in the n^{th} antenna, $\mathbf{c}_n \triangleq [c_{n,1}, ..., c_{n,m}] \in \{0,1\}^m$, where $n = 1, 2, ..., N_{tx}$, and m represents the number of bits per each symbol, is mapped according to the function

$$\begin{aligned} \psi(\mathbf{c}_n) : \{0,1\}^m &\rightarrow \mathcal{S}, \\ s_n = \psi(\mathbf{c}_n) &\in \mathcal{S}, \end{aligned} \tag{5.1}$$

where $\mathcal{S} = \{\alpha_1, \alpha_2, ..., \alpha_M\}$, α_τ represents a set of all possible complex symbols, $\mathbf{s}$, in the constellation vector of size $M = 2^m$. In this chapter, the modulation scheme employed is Gray-labelled M-ary QAM for the transmitted symbols from the nodes a and b. These complex symbols of a particular transmitter node are defined as $\mathbf{s}_\kappa = [s_\kappa^1, s_\kappa^2, ..., s_\kappa^{N_{tx}}]^T \in$

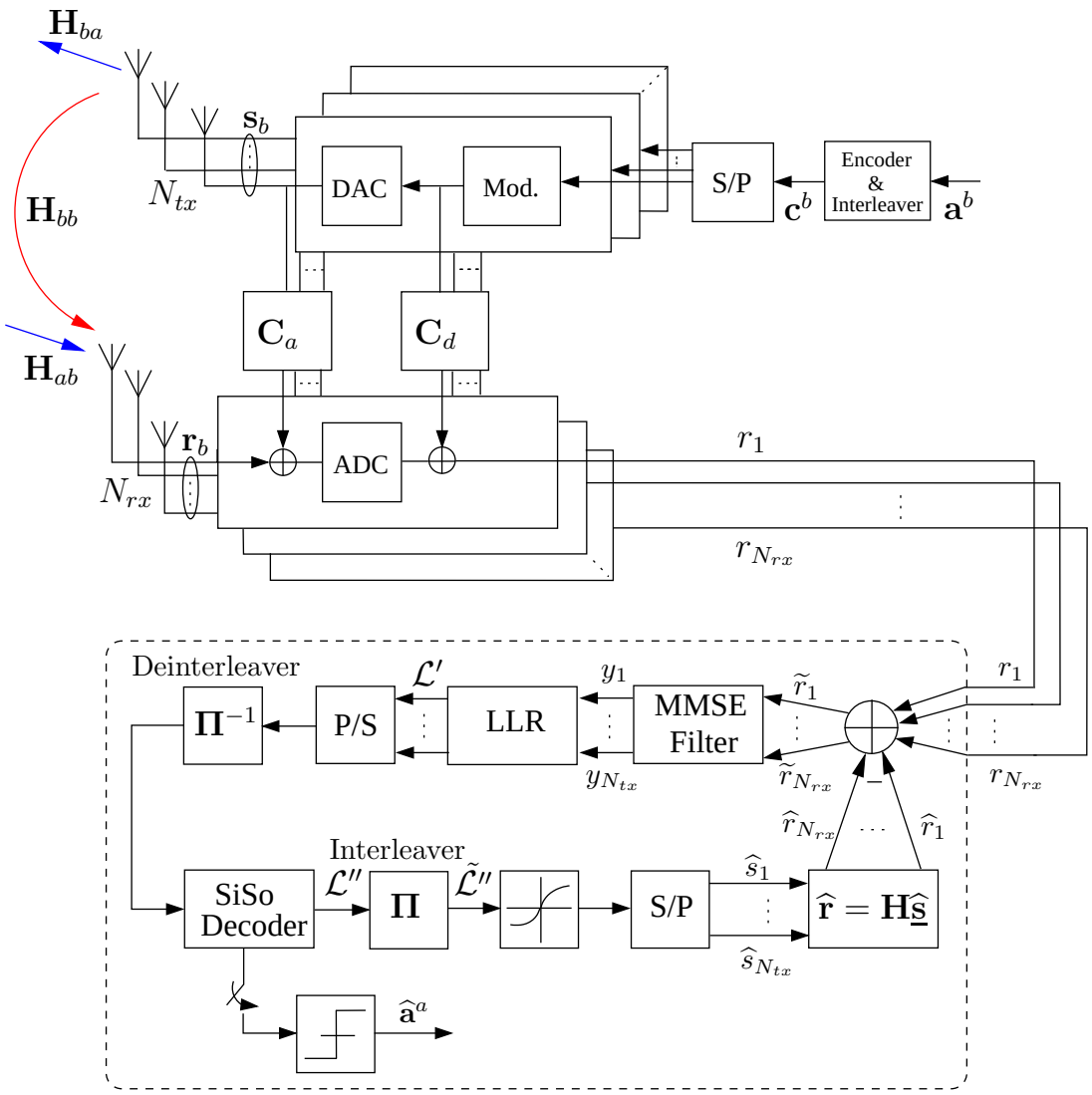

Figure 5.2: Bi-directional FD-MIMO Transceiver at node b

$\mathbb{C}^{N_{tx}\times 1}$, where $\kappa \in \{a, b\}$, in which $\mathbb{E}\{|\mathbf{s}_\kappa|^2\} = E_s/N_{tx}$ and $\mathbb{E}\{\mathbf{s}_\kappa \mathbf{s}_\kappa^{\mathcal{H}}\} = E_s/N_{tx}\mathbf{I}_{N_{tx}}$, where E_s represents the energy of the transmitted symbol. It is worth mentioning that all processing steps applied to the information bits thus far are referred to as BICM .

5.2.2 Receiver Structure

At the receiver front end of node b, before the ADC in each receive antenna branch, the received signal vector, $\boldsymbol{r}_b = [r_b^1, r_b^2, ..., r_b^{N_{rx}}]^T \in \mathbb{C}^{N_{rx}\times 1}$, can be given as

$$\mathbf{r}_b = \sqrt{\rho_a}\mathbf{H}_{ab}\mathbf{s}_a + \sqrt{\widetilde{\rho}_b}\mathbf{H}_{bb}\mathbf{s}_b + \mathbf{v}_b, \tag{5.2}$$

where ρ_a is the average received power from node a, while $\widetilde{\rho}_b$ represents the power

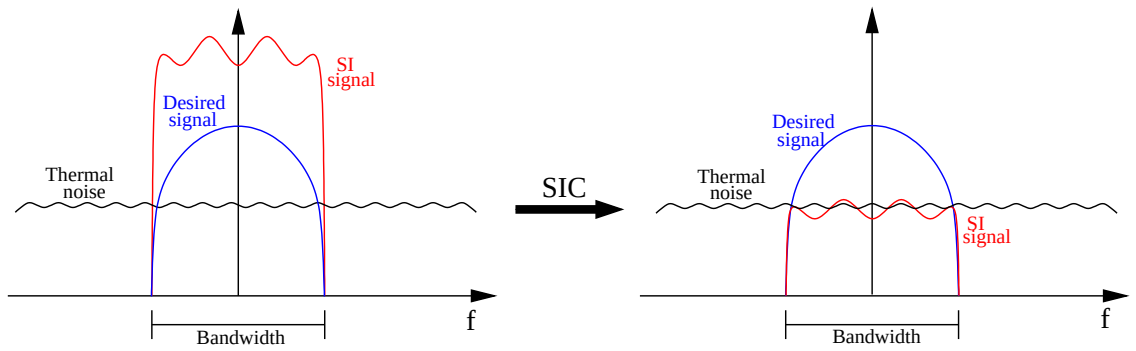

Figure 5.3: Spectrum of desired signal and SI with respect to thermal noise before and after applying SIC

from node b's transmitter port to its receiver port after implementing the passive suppression of SI as will be discussed later on in Subsection 5.3.1. In this chapter, it is assumed that the variances of the noise and the CSI are perfectly known to the receiver.

5.3 Self-interference Cancellation Stages

As mentioned briefly in Section 5.1, SI can be combated by utilizing different stages of passive and/or active SIC. This is because SI power may reach or exceed by 100 dB the power of the desired received signal [40, 116]. Thus, our aim is to attenuate the power of SI to be approximately at the level of noise floor, which is approximately -90 dBm [117] as shown in Fig. 5.3.

To the best of our knowledge, SI attenuations of about 80 to 120 dB have been reported in the literature [17,40,42,116] using different stages of SIC. However, in practice, residual SI may still be significant after SIC due to oversimplified assumptions made in FD systems. Therefore, IDD is proposed in this chapter to further reduce the residual SI that remains after applying passive and active SIC approaches.

5.3.1 Passive suppression via Antenna separation

In order to suppress SI in FD systems, it is initially required to reduce the effects of local power coupling to avoid drowning of the desired incoming signal in loop-interference, which is significantly stronger. Additionally, it is required to mitigate saturation of ADC circuitry due to its limited dynamic range and quantization resolution [9,13,14,35]. Thus, passive suppression, as discussed earlier in this thesis, has been proposed at the receiver front-end by using natural-isolation techniques, via antenna separation to diminish and

block the LoS path. This is achieved by orienting transmit antenna elements to an opposite direction than those of the receiving antennas, which consequently maximizes loop-interference attenuation by increasing the insertion loss that can be further increased by utilizing orthogonal polarization schemes [9, 17, 35].

5.3.2 Analogue Domain Cancellation

In this stage, it is required to design the analogue cancellation filter, $\mathbf{C}_A \in \mathbb{C}^{N_{tx} \times N_{rx}}$, and combine it with the analogue transmitted signal which is undoubtedly known to the transceiver. This is in order to create an analogue replica of SI and apply a subtraction before ADC. In theory, SI can be entirely removed by choosing $\mathbf{C}_A = -\mathbf{H}_{bb}$. However, it is not possible in practice to achieve perfect cancellation [10], [17]. In other words, a precise implementation of this filter is not easily within reach in the analogue domain, as it is required to be abruptly adaptive to any change in the wireless channels. Moreover, the practical design may require no more than a matrix with dimensions (N_{tx}, N_{rx}) for implementing amplifiers and phase shifters for compensation [10], which is not adequate to cancel SI totally in our case in this chapter for MIMO system. This stage is still significant as it produces, along with *AS*, an SI mitigation which is required firstly to avoid the saturation at the received port front end and secondly to overcome the quantization noise in the ADC caused by large magnitude of SI compared to the signal of interest [17].

5.3.3 Digital Domain Cancellation

Digital cancellation is utilized to suppress the residual SI passed through ADC to the digital domain. The digital filter, $\mathbf{C}_D \in \mathbb{C}^{N_{tx} \times N_{rx}}$, is designed to perform this task by taking into account the interfering channel, the analogue filter, and the ADC processing. This filter can implemented to remove the residual SI as $\mathbf{C}_D = -\mathbf{A}(\mathbf{H}_{bb} + \mathbf{C}_A)$, where $\mathbf{A}$ represents a real diagonal matrix resulting from the ADC process [10]. However, this stage of SI cancellation does not have the ability to remove all parts of residual SI coming from the analogue domain, in addition to the clipping-plus-quantization noise terms caused by ADC proceeding. Therefore, an additional signal processing stage is required to reduce the effect of residual SI. In this chapter, IDD is suggested for coded FD-MIMO for this purpose as will be discussed in the next subsection.

5.3.4 Iterative Detection and Decoding

Fig. 5.2 shows the block diagram of IDD with soft-PIC for node b. It is worth noting that an identical type of receiver is used at node a. The detector comprises an adaptive MMSE filter, which is discussed later in this subsection, and an LLR demapper. A SiSo decoder performs soft channel decoding for the extrinsic information from the LLR demapper. During the first iteration the detector and decoder need to be initialized since the *a priori* and *a posteriori* information has not been obtained yet. Therefore, at that instant, the soft estimations of the residual SI symbols are not available, and thus, they cannot be subtracted from the received signal [103]. This means that the received MIMO signal, $\mathbf{r}_b$, for this iteration, could be considered as the input for the MMSE filter, rather than the reduced interference signal, $\widetilde{\mathbf{r}}_b$, obtained in the next iterations. For the same reasons mentioned above and due to the lack of the required parameters, the MMSE filter is not ready to achieve interference cancellation during the first iteration; therefore, it performs classical MMSE filtering and passes its outputs, $\mathbf{y}$, to the LLR demapper [103]. The latter first transforms the filtered symbols to LLR symbols and performs a soft demapping of these symbols to bit-wise LLRs. This operation can be expressed mathematically as

$$\mathcal{L}'[c_n] = \ln \frac{Pr\left\{c_n = 1 \mid \mathbf{y}_b\right\}}{Pr\left\{c_n = 0 \mid \mathbf{y}_b\right\}}, \tag{5.3a}$$

$$= \ln \frac{Pr\left\{c_n = 1 \mid \widetilde{\mathbf{r}}_b, \mathbf{w}_b\right\}}{Pr\left\{c_n = 0 \mid \widetilde{\mathbf{r}}_b, \mathbf{w}_b\right\}}, \tag{5.3b}$$

where (5.3b) represents the LLR of each coded bit with respect to the MMSE filter output $\mathbf{y}_b = \mathbf{w}_b^{\mathcal{H}}\, \widetilde{\mathbf{r}}_b$, with $\widetilde{\mathbf{r}}_b$ and $\mathbf{w}_b$ being its input and filter weights, respectively. The soft LLR bits with a size of $(N_{tx} \times mN_{symbol})$, where N_{symbol} denotes the number of symbols per frame, are converted from a parallel to a serial stream, deinterleaved and processed by the SiSo decoder. This *a priori* information provided to the decoder is processed by exploiting the linear to logarithmic approximation of the maximum *a posteriori* algorithm (linear-log-MAP), as utilized in this chapter. This operation can be written in mathematical form as

$$\mathcal{L}''[c_n] = \ln \frac{Pr\left\{c_n = 1 \mid \mathcal{L}'[c_n]\right\}}{Pr\left\{c_n = 0 \mid \mathcal{L}'[c_n]\right\}}. \tag{5.4}$$

At this stage, a soft estimation for all the desired symbols from the decoder output can be obtained as [109]

$$\widehat{\mathbf{s}}_a \triangleq \mathbb{E}(\mathbf{s}_a) = \sum_{\alpha_t \in \mathcal{S}} \alpha_t Pr\left\{s_a = \alpha_t\right\}, \tag{5.5}$$

in which for $M = 4$, i.e. 4-QAM, the soft remapping of the symbols can be expressed as

$$\widehat{\mathbf{s}}_a = \frac{1}{\sqrt{2}}\left[\tanh\left(\frac{\tilde{\mathcal{L}}''[c_{n,1}]}{2}\right) + j\tanh\left(\frac{\tilde{\mathcal{L}}''[c_{n,2}]}{2}\right)\right], \tag{5.6}$$

where $\tilde{\mathcal{L}}''$ represents the LLR symbols after re-interleaving, i.e. $\tilde{\mathcal{L}}''[.] = \Pi\Big(\mathcal{L}''[.]\Big)$. Additionally, $c_{n,1}$ and $c_{n,2}$ denote the successive odd and even re-interleaved coded bits, respectively.

On the other hand, the soft remapping of 16-QAM can be expressed as [118, 119]

$$\begin{aligned}\widehat{\mathbf{s}}_a = \frac{1}{\sqrt{2.5}}\Big[&\big(1 - 2Pr\{c_{n,1} = 0\}\big)\big(1 + 2Pr\{c_{n,1} = 0\}\big) \\ &+ j\big(1 - 2Pr\{c_{n,3} = 0\}\big)\big(1 + 2Pr\{c_{n,4} = 0\}\big)\Big],\end{aligned} \tag{5.7}$$

where $Pr\{c_{n,m} = 0\}$ is the probability of the m^{th} coded bit belonging to a 16-QAM symbol of the n^{th} antenna. Moreover, $Pr\{c_{n,m} = 0\}$ can be determined as [118]

$$Pr\{c_{n,m} = 0\} = \frac{1}{2}\left(1 + \frac{1}{2}\tanh\left(\tilde{\mathcal{L}}''[c_{n,m}]\right)\right). \tag{5.8}$$

The estimated symbols, $\widehat{\mathbf{s}}_{a,n}$, are used along with CSI to create a soft replica of the received signal along with its interference. It is assumed that perfect CSI is available, since channel estimation is beyond the scope of this chapter. The estimated symbols are then reshaped into a parallel vector in order to make each symbol correspond to its original antenna element, and subsequently the estimated symbols associated with the transmitted n^{th} antenna element are forced to zero, as this is required to cancel its induced interference [103], i.e.

$$\underline{\widehat{\mathbf{s}}}_{a,n} \triangleq \left\{\widehat{s}_{a,1}, ..., \widehat{s}_{a,n-1}, 0, \widehat{s}_{a,n+1}, ..., \widehat{s}_{a,N_{tx}}\right\}. \tag{5.9}$$

In other words, $\underline{\widehat{\mathbf{s}}}_{a,n}$ represents a vector of the soft estimated symbols of the transmitted antennas after nullifying the symbol of the n^{th} antenna, which is the subject of interest

and it is at this instant subject to the soft-PIC processing [103]. The soft symbols in (5.9) are used to create an estimate of the transmitted signal with the interference after combining them with the channel, i.e. $\widehat{\mathbf{r}}_b = \mathbf{H}_{ab}\widehat{\underline{\mathbf{s}}}_{a,n}$. Subsequently, soft-PIC is performed by subtracting $\widehat{\mathbf{r}}_b$ from the received signal as

$$\widetilde{\mathbf{r}}_b = \mathbf{r}_b - \widehat{\mathbf{r}}_b = \mathbf{H}_{ab}\mathbf{s}_{a,n} + \mathbf{H}_{bb}\mathbf{s}_{b,n} + \mathbf{v}_b - \mathbf{H}_{ab}\widehat{\underline{\mathbf{s}}}_{a,n} \tag{5.10a}$$

$$= \mathbf{H}_{ab}\widetilde{\mathbf{s}}_{a,n} + \mathbf{H}_{bb}\mathbf{s}_{b,n} + \mathbf{v}_b. \tag{5.10b}$$

where $\widetilde{\mathbf{s}}_{a,n}$ is defined as

$$\widetilde{\mathbf{s}}_{a,n} \triangleq \left\{\widetilde{e}_{a,1}, ..., \widetilde{e}_{a,n-1}, s_{a,n}, \widetilde{e}_{a,n+1}, ..., \widetilde{e}_{a,N_{tx}}\right\}, \tag{5.11}$$

and $\widetilde{\boldsymbol{e}}_{a,n} = \boldsymbol{s}_{a,n} - \widehat{\underline{\boldsymbol{s}}}_{a,n}$ represents the error which arises due to the imperfect cancellation of interference on node b. This error might theoretically approach to zero when the number of iterations approaches infinity.

At the end of the first iteration, and for the iterations beyond, the information required is provided to the adaptive MMSE filter in order to perform further cancellation of the residual SI. This filter is designed to achieve a minimization of the mean squared error (MSE) between its output, $s^a_{n,l}$, with respect to the l^{th} symbol of the n^{th} transmitted antenna of node a, i.e.

$$\mathbf{J}_{n,l} = \mathbb{E}\left\|\mathbf{w}^{\mathcal{H}}_{n,l}\widetilde{\mathbf{r}}^b_{n,l} - \mathbf{s}^a_{n,l}\right\|^2. \tag{5.12}$$

The coefficient w that minimizes $\mathbf{J}_{n,l}$ can be obtained by solving $\frac{\partial \mathbf{J}_{n,l}}{\partial \mathbf{w}^b_{n,l}} = \mathbf{0}$, and was derived in [94] and also given in [103], [85] and [113] for different types of interference. Following the derivation in [94], the solution in the case of SI can be given as

$$\mathbf{w}^b_{n,l} = [\mathbf{\Lambda}_s(l)\mathbf{H}_{ab}(l)^{\mathcal{H}}\mathbf{H}_{ab}(l) + \mathbf{\Lambda}_i(l)\mathbf{H}_{bb}(l)^{\mathcal{H}}\mathbf{H}_{bb}(l) + \sigma^2_{v_b}\mathbf{I}_{Nrx}]^{-1}\mathbf{h}_{ab}(n,l)^{\mathcal{T}}, \tag{5.13}$$

where $\mathbf{h}_{ab}(n,l)$ represents the n^{th} column of $\mathbf{H}_{ab}(l)$. Furthermore, $\mathbf{\Lambda}_i(l)$ denotes the covariance matrix of the SI symbols, $\mathbf{s}_{b,n}$, which can be expressed as $\mathbf{\Lambda}_i(l) = \mathbb{E}\{\mathbf{s}_{b,n}\mathbf{s}^{\mathcal{H}}_{b,n}\}$,

while $\mathbf{\Lambda}_s(l) = \mathbb{E}\{\widetilde{\mathbf{s}}_{a,n}\widetilde{\mathbf{s}}_{a,n}^{\mathcal{H}}\}$ represents the covariance matrix of $\widetilde{\mathbf{s}}_{a,n}$ defined as

$$\mathbf{\Lambda}_s(l) \triangleq \text{diag}\Big[\mathbb{E}\{|\widetilde{e}_{a,1}|^2\}, ..., \mathbb{E}\{|\widetilde{e}_{a,n-1}|^2\}, \sigma_{s_a}^2, \mathbb{E}\{|\widetilde{e}_{a,n+1}|^2\}, ..., \mathbb{E}\{|\widetilde{e}_{a,N_{tx}}|^2\}\Big]. \quad (5.14)$$

Using the orthogonality principle, i.e. $\mathbb{E}\{(\mathbf{w}_{n,l}^{\mathcal{H}}\widetilde{\mathbf{r}}_{n,l}^b - \mathbf{s}_{n,l}^a)(\widetilde{\mathbf{r}}_{n,l}^b)^{\mathcal{H}}\} = 0$, between the input of the MMSE filter, $\widetilde{\mathbf{r}}_{n,l}^b$ and the MSE, it can be shown that the MMSE, $\mathbf{J}_{n,l}^{\min}$, achieved by using the coefficients in (4.25) can be simplified as

$$\begin{aligned}\mathbf{J}_{n,l}^{\min} &= \mathbb{E}\{\left\|\mathbf{w}_{n,l}^{\mathcal{H}}\,\widetilde{\mathbf{r}}_{n,l}^b - \mathbf{s}_{n,l}^a\right\|^2\},\\ &= \mathbb{E}\{(\mathbf{w}_{n,l}^{\mathcal{H}}\,\widetilde{\mathbf{r}}_{n,l}^b - \mathbf{s}_{n,l}^a)(\mathbf{w}_{n,l}^{\mathcal{H}}\,\widetilde{\mathbf{r}}_{n,l}^b - \mathbf{s}_{n,l}^a)^{\mathcal{H}}\},\\ &= \mathbb{E}\{(\mathbf{w}_{n,l}^{\mathcal{H}}\,\widetilde{\mathbf{r}}_{n,l}^b - \mathbf{s}_{n,l}^a)(\mathbf{s}_{n,l}^a)^{\mathcal{H}}\}, \end{aligned} \quad (5.15)$$

to obtain the final expression of $\mathbf{J}_{n,l}^{\min}$ as

$$\mathbf{J}_{n,l}^{\min} = \mathbf{\Lambda}_s(l) - \mathbf{R}_{rs}\mathbf{R}_r^{-1}\mathbf{R}_{sr}, \quad (5.16)$$

where $\mathbf{R}_{rs} = \mathbb{E}\{\widetilde{\mathbf{r}}_{n,l}^b(\mathbf{s}_{n,l}^a)^{\mathcal{H}}\}$, $\mathbf{R}_r = \mathbb{E}\{\widetilde{\mathbf{r}}_{n,l}^b(\widetilde{\mathbf{r}}_{n,l}^b)^{\mathcal{H}}\}$, and $\mathbf{R}_{sr} = \mathbb{E}\{\mathbf{s}_{n,l}^a(\widetilde{\mathbf{r}}_{n,l}^b)^{\mathcal{H}}\}$.

Since the MAP-SiSo decoder is used in this chapter, $\mathbb{E}\{|\widetilde{e}_{a,n}|^2\}$ can be computed as

$$\mathbb{E}\{|\widetilde{e}_{a,n}|^2\} = \sum_{\alpha_t \in \mathcal{S}} \left|\boldsymbol{s}_{a,n} - \widehat{\underline{\boldsymbol{s}}}_{a,n}\right|^2 Pr\left\{s_{a,n} = \alpha_t\right\}, \quad (5.17)$$

where $\sigma_{s_a}^2 = \mathbb{E}\{|\mathbf{s_{a,n}}|^2\} = 1$ represents the variance of the symbols $\mathbf{s_{a,n}}$ as defined earlier in Subsection 5.2.1.

Once the computation of the adaptive MMSE filter coefficients, $\mathbf{w}_{n,l}^b$, is complete, they are used along with output of the soft-PIC, $\widetilde{\mathbf{r}}_{n,l}^b$, to obtain the input of the LLR demapper as

$$\mathbf{y}_{n,l}^b = (\mathbf{w}_{n,l}^b)^{\mathcal{H}}\,\widetilde{\mathbf{r}}_{n,l}^b \quad (5.18a)$$

$$= \beta_{n,l}\, s_{n,l}^a + \zeta_{n,l}, \quad (5.18b)$$

where $\beta_{n,l} = (\mathbf{w}_{n,l}^b)^{\mathcal{H}}\mathbf{h}_{ab}(n,l)$, while $\zeta_{n,l}$ represents the interference-plus-noise term, which is defined as $\zeta_{n,l} = (\mathbf{w}_{n,l}^b)^{\mathcal{H}}\mathbf{h}_{bb}(n,l)\; s_{n,l}^b + (\mathbf{w}_{n,l}^b)^{\mathcal{H}}\mathbf{v}_b$, and it exhibits a Gaussian distribution with zero-mean and variance $\sigma_{\zeta_{n,l}}^2 = (\beta_{n,l} - \beta_{n,l}^2)$ [94]. At the output of the

MMSE filter, the SINR for the l^{th} spatial symbol can be calculated as

$$\gamma_l = \frac{\beta_l}{(1-\beta_l)}, \tag{5.19}$$

where the distribution of γ_l is derived in Section 5.4 by employing the moment generation function (MGF).

All of these signal processing steps discussed so far for the first iteration are repeated for a predefined number of iterations so that the system converges to an acceptable BER with respect to average SINR [103]. After the last iteration is completed, a hard decision is applied to the SiSo decoder output in order to obtain the transmitted bits as

$$\widehat{a}_q^a = \text{sign}\Big(\mathcal{L}''\big[a_q^a\big]\Big), \tag{5.20}$$

where

$$\mathcal{L}''[a_q^a] = \ln \frac{Pr\left\{a_q^a = 1 \mid \mathcal{L}'[c_p^a]\right\}}{Pr\left\{a_q^a = 0 \mid \mathcal{L}'[c_p^a]\right\}}. \tag{5.21}$$

5.4 Moment Generating Function of SINR

In this section, in order to evaluate the moment generation function (MGF), it is required to start finding an expression for the CDF of SINR, γ_l, in (5.19), which is defined in [48, 120] as

$$F(\gamma_l) = 1 - e^{-\psi\gamma_l} \sum_{n=1}^{N_{rx}} \frac{A_n(\gamma_l)}{\Gamma(n)} (\psi\gamma_l)^{n-1}, \tag{5.22}$$

where $\psi = 1/\sigma_{v_b}^2$ for node b, $\Gamma(n) = (n-1)!$ represents the Gamma function, while $A_n(\gamma_l)$ represents an auxiliary function which is defined as

$$A_n(\gamma_l) = \begin{cases} 1, & \text{for } n \leq N_{div}, \\ \frac{1}{(\gamma_l+1)^{N_{tx}-1}} \sum_{i=0}^{N_{rx}-n} C_i \gamma^i, & \text{for } n > N_{div}, \end{cases} \tag{5.23}$$

where $N_{div} = (N_{rx} - N_{tx} + 1)$ represents the diversity order of the MIMO system, and C_i represents the coefficients of x^i in the term $(1+x)^{N_{tx}-1}$ for $i \geq 0$. For instance, if

$N_{tx} = 2$ this term will appear as $(1 + x)$, which means that $C_0 = 1$ and $C_1 = 1$. The MGF of γ_l as a function of the receive and transmit antennas, N_{rx} and N_{tx}, respectively, can be defined as

$$\mathcal{M}_{N_{tx},N_{rx}}(t) \triangleq \int_0^\infty e^{-t\gamma_l} dF(\gamma_l) = t \int_0^\infty e^{-t\gamma_l} F(\gamma_l) d\gamma_l, \tag{5.24}$$

which can be solved using the techniques presented in [121, 122] resulting in

$$\mathcal{M}_{N_{tx},N_{rx}}(t) = \left[\frac{\psi}{\psi + t}\right]^{N_{div}} - te^{(t+\psi)} \sum_{n=N_{div}+1}^{N_{rx}} \sum_{i=1}^{N_{rx}-n} \sum_{k=0}^{n+i-1} \frac{\psi^{n-1} C_i D_k}{\Gamma(n)} E_{N_{tx}-k-1}(\psi + t), \tag{5.25}$$

where D_k represents the coefficients of x^k in the term $(x-1)^{n+i-1}$, which can be computed as $D_k = (-1)^k \binom{n}{k}$, for $k = 0, 1, 2, ..., n$. Additionally, $E_n(\alpha) \triangleq \int_1^\infty \frac{e^{-\alpha t}}{t^n} dt, \forall \alpha > 0$ is the generalized exponential integral function.

5.5 Tight Upper Bound Performance Analysis

In this section, a tight upper bound on the performance of the proposed coded FD-MIMO system is derived in the presence of residual SI that remains after applying the passive and active SIC methods mentioned previously in this chapter. In general, the BICM bound of the BER, $\bar{P}_b$, for a rate-1/n convolutional code is given by [48, p. 515] and [123] as

$$\bar{P}_b \leq \sum_{d=d_{free}} B_d P_d(\mathbf{s}, \mathbf{y}), \tag{5.26}$$

where $P_d(\mathbf{s}, \mathbf{y})$ represents the PEP between the transmitted and estimated sequences $\mathbf{s} = \{s_1, s_2, ..., s_{N_{tx}}\}$ and $\mathbf{y} = \{y_1, y_2, ..., y_{N_{tx}}\}$, respectively, when the Hamming distance between them is equal to d. Additionally, d_{free} is the convolutional code's free distance, B_d represents the total input weight of error events at Hamming distance d. These coefficients, which are presented in [123] for different R_c in tables, can be obtained by applying the derivation to the transfer function of the code, $T(B, D)$, as

$$\left.\frac{\partial T(B, D)}{\partial B}\right|_{B=1} = \sum_{d=d_{free}}^{\infty} B_d D^d, \tag{5.27}$$

where D and B represent the Hamming distances of the coded and input sequences, respectively.

According to (5.18b), (5.3) can be rewritten for the i^{th} ($i \in \{1, 2, ..., \log_2 M\}$) coded bit, in the l^{th} symbol belonging to the n^{th} transmit antenna element of $s^a_{n,l}$ with respect to $y^a_{n,l}$ as

$$\begin{aligned}\mathcal{L}'(n,l,i) &= \ln \frac{\sum\limits_{\tilde{s}\in\mathcal{S}^1_{n,l,i}} Pr(y^b_{n,l}|\tilde{s},\beta_{n,l},\zeta_{n,l})}{\sum\limits_{\tilde{s}\in\mathcal{S}^0_{n,l,i}} Pr(y^b_{n,l}|\tilde{s},\beta_{n,l},\zeta_{n,l})}, \\ &= \ln\left(\frac{\sum\limits_{\tilde{s}\in\mathcal{S}^1_{n,l,i}} \exp\left(-\frac{|\beta_{n,l}(s^a_{n,l}-\tilde{s})+\zeta_{n,l}|^2}{\sigma^2_{\zeta_{n,l}}}\right)}{\sum\limits_{\tilde{s}\in\mathcal{S}^0_{n,l,i}} \exp\left(-\frac{|\beta_{n,l}(s^a_{n,l}-\tilde{s})+\zeta_{n,l}|^2}{\sigma^2_{\zeta_{n,l}}}\right)}\right), \\ &= \ln(\Xi_{n,l}), \end{aligned} \tag{5.28}$$

where $\mathcal{S}^1_{n,l,i}$ and $\mathcal{S}^0_{n,l,i}$ represent the signal subsets in the constellation when the i^{th} bit in the l^{th} symbol and for the n^{th} transmit antenna is equal to 1 and 0, respectively. It is assumed that a message of all zeros is transmitted, then the PEP is expressed as

$$P_d(\mathbf{s},\mathbf{y}) = Pr\Big(\sum_{k=1}^{d}\mathcal{L}'_k\Big), \tag{5.29}$$

where $\mathcal{L}'_k$ is the input to the SiSo decoder after applying parallel-to-serial conversion and deinterleaving to $\mathcal{L}'(n,l,i)$. Since it is not straightforward to evaluate the distribution of $\mathcal{L}'_k$ in an exact expression, the MGF approach, denoted as $\mathcal{M}$, can be exploited to evaluate the probability in (5.29) as [48]

$$P_d(\mathbf{s},\mathbf{y}) = \int_{\delta-j\infty}^{\delta+j\infty} \mathcal{M}_{\sum_1^d \mathcal{L}'_k}(t)\frac{dt}{t} \tag{5.30a}$$

$$= \int_{\delta-j\infty}^{\delta+j\infty} [\mathcal{M}_{\mathcal{L}'}(t)]^d \ \frac{dt}{t}, \tag{5.30b}$$

where (5.30b) is obtained from the assumption of random interleaving. Moreover, the subscript k is omitted on $\mathcal{L}'$ in (5.30b) since the statistics of LLR are calculated at a single instant in time. Additionally, δ is a constant that can be obtained by minimizing the value of $\mathcal{M}_{\mathcal{L}'}(t)$. The procedure to obtain the optimum value of δ is described later on in this

chapter. Furthermore, $\mathcal{M}_{\mathcal{L}'}(t)$ can be evaluated similar to [121] and [122] as

$$\begin{aligned}\mathcal{M}_{\mathcal{L}'}(t) &= \mathbb{E}_{s^a_{n,l},\beta_{n,l},\zeta_{n,l}}\Big\{\exp(t\mathcal{L}')\Big\} \\ &= \frac{1}{M\,m}\sum_{t=1}^{m}\sum_{s^a_{n,l}\in\mathcal{S}}\mathcal{J}_{s^a_{n,l}}(t),\end{aligned} \tag{5.31}$$

where $m = \log_2(M)$ and $\mathcal{S}$ represents a set of all possible complex symbols of the M-QAM constellation. Additionally, $\mathcal{J}_{s^a_{n,l}}(t)$ is expressed as

$$\mathcal{J}_{s^a_{n,l}}(t) = \mathbb{E}_{\beta_{n,l},\zeta_{n,l}}\Big\{\exp\Big(t\ln(\Xi_{n,l})\Big)\Big\}, \tag{5.32}$$

which can be simplified as

$$\mathcal{J}_{s^a_{n,l}}(t) = \mathbb{E}_{\beta_{n,l},\zeta_{n,l}}\Big\{(\Xi_{n,l})^t\Big\}. \tag{5.33}$$

A closer look to the ratio in (5.33) reveals that it is dominated by a single term representing the minimum distance in the numerator and denominator, conditioned to high SINR [121]. According to the assumption of transmitting an all-zero message and by utilizing the theorem of dominated convergence [124], (5.33) can be approximated as

$$\mathcal{J}_{s^a_{n,l}}(t) \simeq \mathbb{E}_{\beta_{n,l},\zeta_{n,l}}\left\{\exp\left(\frac{t|\zeta_{n,l}|^2 - t|\beta_{n,l}(s^a_{n,l}-\tilde{s})+\zeta_{n,l}|^2}{\sigma^2_{\zeta_{n,l}}}\right)\right\}, \tag{5.34}$$

where $\tilde{s} \in \mathcal{S}^1_{n,l,i}$ represents the closest symbol to $s^a_{n,l}$ in the M-QAM constellation.

At this stage, the derivation is resumed by simplifying (5.34) and evaluate its average over $\zeta_{n,l}$ to obtain

$$\begin{aligned}\mathcal{J}_{s^a_{n,l}}(t) &\simeq \mathbb{E}_{\beta_{n,l}}\left\{\exp\left(-\frac{t(1-t)N_{tx}}{E_s}\gamma_l\big|s^a_{n,l}-\tilde{s}\big|^2\right)\right\} \\ &\simeq \mathcal{M}_{N_{rx},N_{tx}}\left\{\exp\left(\frac{t(1-t)N_{tx}}{E_s}\big|s^a_{n,l}-\tilde{s}\big|^2\right)\right\},\end{aligned} \tag{5.35}$$

where $\mathcal{M}_{N_{rx},N_{tx}}$ represents the MGF of the SINR, γ_l, which is derived in Section 5.4. Now, by substituting (5.35) in (5.31) and using the simplifications described in [121], (5.31) can be rewritten as

$$\mathcal{M}_{\mathcal{L}'}(t) = \sum_k \Delta_{M,k}\mathcal{M}_{N_{tx},N_{rx}}\Big(\frac{t(1-t)N_{tx}}{E_s}\Upsilon_{M,k}\Big), \tag{5.36}$$

where $\Upsilon_{M,k}$ and $\Delta_{M,k}$ are the squared Euclidean distances and the frequency of the occurrence for each distance presented in Table 5.1 [121], respectively.

Table 5.1: Rate-$1/2$ RSC channel encoders parameters used in (5.36)

	$\Delta_{M,k}$	$\Upsilon_{M,k}$
4-QAM	$\{1\}$	$\{2.0\}$
16-QAM	$\{3/4, 1/4\}$	$\{0.4,1.6\}$

Now, (5.36) can be substituted in (5.30b) and apply the Gauss-Chebyshev quadrature (GCQ) rule in order to obtain the PEP of the proposed system as

$$P_d\left(\mathbf{s},\mathbf{y}\right) = E_\varphi + \frac{1}{\varphi}\sum_{k=1}^{\varphi/2}\left(\Re\left[\mathcal{M}_{\mathcal{L}'}(\epsilon)^d\right] + \tau_k \Im\left[\mathcal{M}_{\mathcal{L}'}(\epsilon)^d\right]\right), \tag{5.37}$$

where $\epsilon = \delta + j\delta\tau_k$, $\tau_k = \tan\left(\frac{(2k-1)\pi}{2\varphi}\right)$, φ represents the number of nodes utilized in applying the GCQ to (5.36), and E_φ is an integration constant approaching zero when φ approaches infinity.

As previously mentioned, δ is a constant chosen to minimize the value of $\mathcal{M}_{\mathcal{L}'}(t)$. Thus, from (5.35) and the definition of MGF in (5.24) in Section 5.4, and by setting the result of the derivative with respect to the variable $-t(1-t)$ to zero, i.e. $\frac{d[-t(1-t)]}{dt} = 0$, it can be shown that the minimum value of $\mathcal{M}_{\mathcal{L}'}(t)$ is obtained at $t = 0.5$. Additionally, since $\mathcal{M}_{N_{tx},N_{rx}}$ is a monotonic increasing function, $\mathcal{M}_{\mathcal{L}'}(t)$ exhibits a minimum value at $t = 0.5$. It is noteworthy that $\mathcal{M}_{\mathcal{L}'}(\delta + j\delta\tau_k)$ is real-valued when $\Re[\epsilon] = \delta = 0.5$. Therefore, the approximate formula of the PEP in (5.37) can be written as

$$P_d\left(\mathbf{s},\mathbf{y}\right) \simeq \frac{1}{\varphi}\sum_{k=1}^{\varphi/2}\left[\sum_i \Delta_{M,i}\mathcal{M}_{N_{tx},N_{rx}}\left(\frac{(1+\tau_k^2)N_{tx}}{4E_s}\Upsilon_{M,i}\right)\right]^d. \tag{5.38}$$

5.6 The Complexity of The Proposed FD-MIMO-IDD

The complexity computation of the proposed FD-MIMO-IDD depends on the utilized equalizer and the decoding algorithm. Different approaches can be used to measure the complexity. This thesis deals with interference-limited environments, i.e. the SI accompanied to FD operation, therefore, the required real and complex operations to evaluate the filter coefficients are used to calculate the system complexity. The basic operations that used for this purposes are the addition (ADD), subtraction (SUB), multiplication (MUL), division (DIV), the square operation (SQRT), finding the maximum value (MAX) and

look-up-table operation (LUT). A comparison between the complexity of MAP and Log-MAP algorithms is illustrated in Table 5.2. It is shown that using log-MAP algorithm reduced the complexity significantly. This is due to the fact the logarithmic operation covert each multiplication to an addition which is considered less complexity [125].

Table 5.2: MAP and Log-MAP complexity

Operation	MAP	Log-MAP
MAX	$2\bar{N}_s - 1$	$4\bar{N}_s - 4$
ADD/SUB	$4\bar{N}_s$	$14\bar{N}_s - 4$
MUL	$10\bar{N}_s$	0
LUT	0	$4\bar{N}_s - 2$

where $\bar{N}_s = 2^K$ is the total number of states, and K is the number of shift registers, i.e. memories, used in a particular encoder. Moreover, the complexity of the MMSE equalization per iteration can be found from (5.13), in which the calculation of the filter coefficients, $\mathbf{w}_{n,l}^b$, has three matrix multiplication, three matrix addition and one matrix inversion, which can be expressed as $\mathcal{O}(N^3 + N^2)$, where N here is for the number of symbols received at the input of the MMSE filter [126].

5.7 EXIT Chart Analysis

EXIT chart is a semi-analytical technique that can be exploited to visualize the convergence behavior of IDD systems. It was proposed in [115] as a powerful tool to analyze and characterize the flow of the mutual information (MI), which is exchanged between the constituent detector and decoder in an iterative system. In this section, the MI terms at the input and output of the SiSo decoder are denoted as I_D^i and I_D^o, respectively, while I_E^i and I_E^o represent the MI terms at the input and output of the equalizer, respectively. These MI terms are evaluated as [127]

$$I_D = \frac{1}{2} \sum_{c \in \{\mp 1\}} \int_{-\infty}^{\infty} p_D(\xi|c) \log_2 \frac{2p_D(\xi|c)}{p_D(\xi|+1) + p_D(\xi|-1)} d\xi, \tag{5.39}$$

and

$$I_E = \frac{1}{2} \sum_{c \in \{\mp 1\}} \int_{-\infty}^{\infty} p_E(\xi|c) \log_2 \frac{2p_E(\xi|c)}{p_E(\xi|+1) + p_E(\xi|-1)} d\xi, \tag{5.40}$$

where $p_D(\xi|c)$ and $p_E(\xi|c)$ are the conditional PDFs of the SiSo decoder and equalizer, respectively, associated with their *a priori* LLR and the information bits c.

Similar to [115] and [128], it can be modelled the *a priori* LLR's of the SiSo decoder, D, and the equalizer, E as independent Gaussian random variables, n_D and n_E with zero mean and variance σ_D^2 and σ_E^2, respectively. Thus, their *a priori* LLRs can be expressed after joining the information bits, c, as $L_D = \mu_D\, c + n_D$ and $L_E = \mu_E\, c + n_E$, where $\mu_D = \sigma_D^2/2$ and $\mu_E = \sigma_E^2/2$. By assuming a sufficiently long interleaver, the general expression for these conditioned PDFs can be given as

$$p_D(\xi|c) = \frac{1}{\sqrt{2\pi}\sigma_D} \exp\left(- \frac{\left(\xi - \frac{\sigma_D^2}{2} c\right)^2}{2\sigma_D^2} \right), \tag{5.41}$$

$$p_E(\xi|c) = \frac{1}{\sqrt{2\pi}\sigma_E} \exp\left(- \frac{\left(\xi - \frac{\sigma_E^2}{2} c\right)^2}{2\sigma_E^2} \right). \tag{5.42}$$

It is worth mentioning that the information bits are assumed to be equiprobable, i.e. $Pr\{c = +1\} = Pr\{c = -1\} = 0.5$.

Now, by substituting (5.41) in (5.39) and (5.42) in (5.40), I_D and I_E can be re-written as

$$I_D(\sigma_D) = 1 - \frac{1}{\sqrt{2\pi}\sigma_D} \int_{\infty}^{\infty} e^{-\frac{\left(\xi - \frac{\sigma_D^2}{2}\right)^2}{2\sigma_D^2}} \log_2\left(1 + e^{-\xi}\right) d\xi, \tag{5.43}$$

and

$$I_E(\sigma_E) = 1 - \frac{1}{\sqrt{2\pi}\sigma_E} \int_{\infty}^{\infty} e^{-\frac{\left(\xi - \frac{\sigma_E^2}{2}\right)^2}{2\sigma_E^2}} \log_2\left(1 + e^{-\xi}\right) d\xi. \tag{5.44}$$

Alternatively, I_D and I_E can be evaluated by averaging the LLRs as [48, p. 555]

$$\begin{aligned} I_D &= 1 - \mathbb{E}_{c=+1}\Big[\log_2(1+e^{-L_D})\Big], \\ &\simeq 1 - \frac{1}{N}\sum_{n=1}^{N}\log_2(1+e^{-L_D}), \end{aligned} \tag{5.45}$$

$$\begin{aligned} I_E &= 1 - \mathbb{E}_{c=+1}\Big[\log_2(1+e^{-L_E})\Big], \\ &\simeq 1 - \frac{1}{N}\sum_{n=1}^{N}\log_2(1+e^{-L_E}), \end{aligned} \tag{5.46}$$

where N here represents the total number of LLRs.

5.8 Simulation Results and Discussion

In this section, the performance of an FD-MIMO based bi-directional transceiver of a two-node system, a and b, is considered. Performance is impaired by SI and mitigated using IDD, which firstly performs soft-PIC to mitigate the SI and then adaptive MMSE filtering to remove the residual interference. Moreover, in all the presented simulations, BICM is utilized with $1/2$-rate convolutional codes with different constraint lengths and the overall system performance is evaluated in the presence of AWGN over frequency non-selective Rayleigh fading channels. Furthermore, the modulation scheme used in the simulations is 4-QAM and 16-QAM in conjunction with spatial multiplexing MIMO. We assume 40 dB of passive suppression by antenna separation followed by two stages of analogue and digital filtering achieving 70 dB of additional SI attenuation [42].

Fig. 5.4 reveals a close agreement of the simulated BER performance as a function of SNR for the 2nd iteration with the tight upper bounds performance for the three cases of $1/2$-rate RSC channel encoders, whose parameters are illustrated in Table 5.3, and for the case of $N_{tx}^{a} = 2, N_{rx}^{b} = 4, N_{tx}^{b} = 2$ in the presence of a residual INR of 10 dB. The modulation scheme used in this figure is 4-QAM. Additionally, it is worth mentioning that in order to achieve an acceptable precision, the number of nodes, φ, chosen for the GCQ rule in (5.38) is 25.

Table 5.3: Rate-$1/2$ RSC channel encoders parameters

K	G	d_f	$\{B_d(d_{free}), B_d(d_{free}+1), ..., B_d(d_{free}+20)\}$
3	$(1, 5/7)_8$	5	{1, 4, 12, 32, 80, 192, 448, 1024, 2304, 5120, 11264, 14576, 53248, 114688, 245760, 524288, 1114112, 2359296, 4980736, 10485760}
5	$(1, 23/35)_8$	7	{4, 12, 20, 72, 255, 500, 1324, 3680, 8967, 22270, 57403, 142234, 348830, 867106, 2134239, 5205290, 12724352, 31022962, 75250693, 182320864}
7	$(1, 133/171)_8$	10	{36, 0, 211, 0, 1404, 0, 11633, 0, 77433, 0, 502690, 0, 3322763, 0, 21292910, 0, 134365911, 0, 84342587, 0}

Fig. 5.5 and 5.6 show the performance of the proposed system by utilizing two different M-QAM modulation schemes which are 4-QAM and 16-QAM, respectively. The Monte-Carlo simulations using the BER vs. SNR performance metric are considered for the 2nd and 5th iterations in the case of convolutional BICM utilizing the RSC channel encoder with constraint length $K = 5$. The SiSo decoder employed in this chapter, as mentioned previously, is a MAP decoder. In addition, different combinations of $\left(N_{tx}^a, N_{rx}^b, N_{tx}^b\right)$ are used, i.e. $(2, 4, 2)$, $(2, 6, 2)$, and $(2, 8, 2)$, where $\left(N_{tx}^a, N_{rx}^b\right)$ denotes the number of antennas being used between the transmitting port of node a and the receiving port of node b, respectively. This represents the path of the desired signal. Furthermore, N_{tx}^b denotes the number of antennas at the transmitting port of node b causing SI due the FD operation. Moreover, a comparison is presented between the system performance under a residual INR of 10 dB against the interference-free case.

From these figures, it is clear that the performance under this INR after five iterations is very close to the SI free performance, which demonstrates that the proposed SIC has a near-optimal achievement, especially with higher number of antennas at the receiving port, N_{rx}^b, and for a fixed number of transmitting antennas, N_{tx}^a. It is worth noting that in the three investigated scenarios the performance improves as the number of iterations is increased. Furthermore, these two figures demonstrate the derived tight upper bound on the performance of the proposed system under the same conditions described above, which reveals that at high SNR the tight upper bound performances match closely the results obtained from simulations of the proposed system after the 2nd iteration.

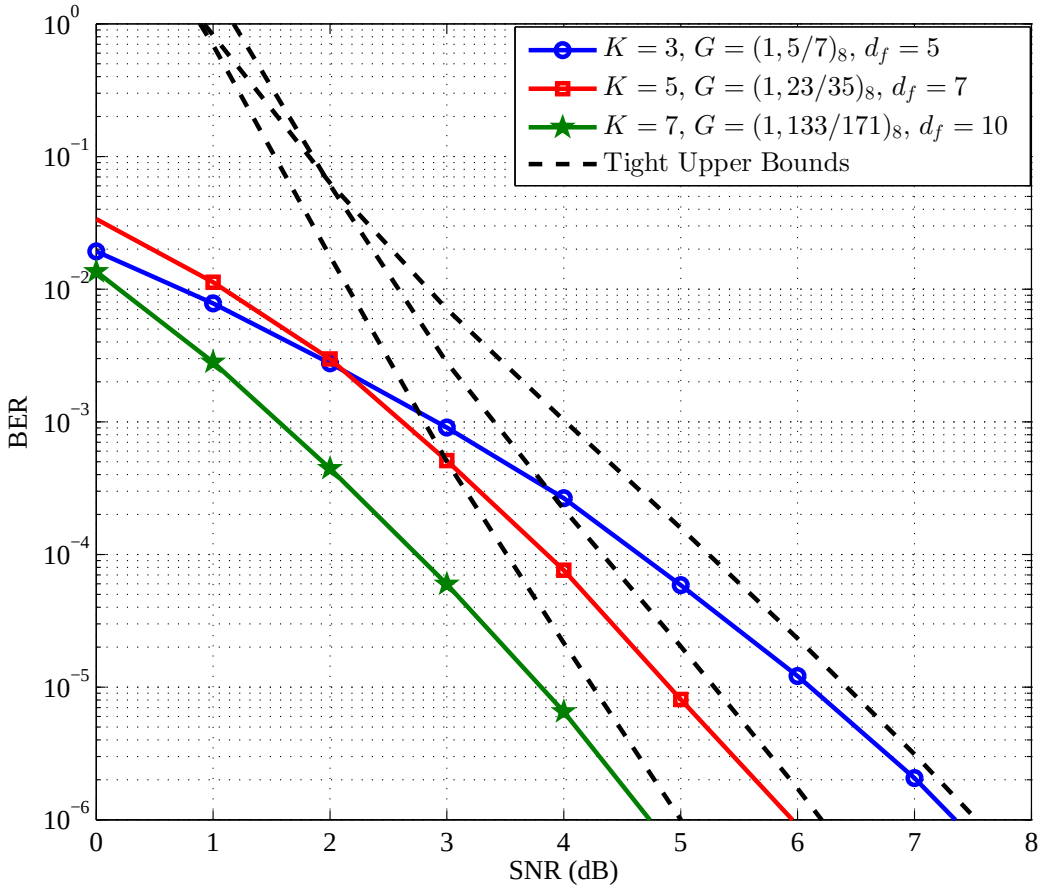

Figure 5.4: BER vs. SNR performance after the 2nd iteration along with the tight upper bounds for different $1/2$-rate convolutional codes of (2,4,2)-FD-MIMO-BICM-IDD utilizing 4-QAM in the presence of 10 dB residual INR.

Fig. 5.7 shows the PDF distributions of the LLRs related to the coded bits, which represent the output of the SiSo decoder, for the 1st to 5th iterations of the $(2, 4, 2)$-MIMO system for the RSC convolutional code with $K = 5$ under residual INR=5 dB and at an SNR=5 dB. The PDF distribution of the LLRs during the first iteration is completely different from the expected bi-modal Gaussian PDF. As explained previously in Section 5.3.4, this iteration performs the initialization of the IDD in order to start the second iteration with the required soft information. Note that as the number of iterations increases, the PDF converges to a bi-modal Gaussian PDF representing the logic $(0, 1)$ bits.

Fig. 5.8 illustrates the BER performance as a function of SNR for three cases of FD-SIMO, i.e. $(2, 4, 2)$, $(2, 5, 2)$, and $(2, 6, 2)$, after replacing the convolutional codes with turbo codes. In all simulation results presented in this chapter, the number of inner and outer iterations was set to 10 and 5 respectively. A closer look at the figure reveals that the system with turbo codes achieves as expected better performance comparing to con-

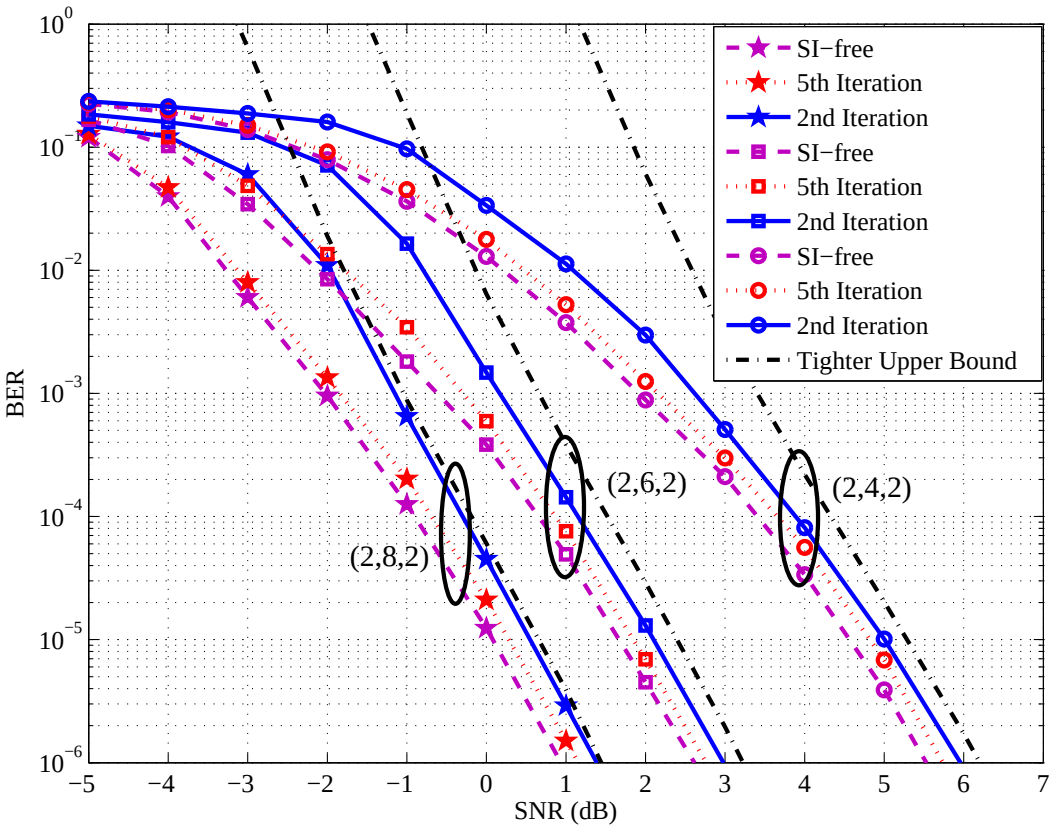

Figure 5.5: BER vs. SNR performance of FD-MIMO-BICM-IDD utilizing 4-QAM with $1/2$-rate $(1, 23/35)_8$ RSC convolutional codes for the 2nd and 5th iterations for different combinations of $\left(N_{tx}^{a}, N_{rx}^{b}, N_{tx}^{b}\right)$ and residual INR=10 dB compared to their corresponding SI-free cases.

volutional codes in the presence of residual INR of 10 dB, which implies increased robust against SI. Moreover, it can be noticed that by increasing the receive antenna elements of the FD-MIMO transceiver, i.e. N_{rx}, additional gain can be obtained. A closer look at Fig. 5.8 reveals that at a BER level of 10^{-4} the proposed system achieves a gain in SNR of 1.3 and 1 dB, when the receive antennas are increased from 4 to 5 then from 5 to 6, respectively.

Fig. 5.9 shows the EXIT chart for the proposed IDD system of $(2, N_{rx}, 2)$-FD-MIMO for different N_{rx}, i.e. $N_{rx} = 2, 4, 6$, at SNR=-5 dB and residual INR=10 dB. Since the MI at the output of the equalizer I_E^o becomes the MI to the input of the decoder I_D^i and the MI at output of the decoder, I_D^o becomes the MI to the input of the equalizer I_E^i, therefore, the EXIT chart is drawn with two axes, which are $(I_E^o = I_D^i, I_E^i = I_D^o)$. A closer look to Fig. 5.9 reveals that higher number of receiving antennas, N_{rx}, leads to faster convergence between the SiSo decoder and the proposed equalizer and additionally

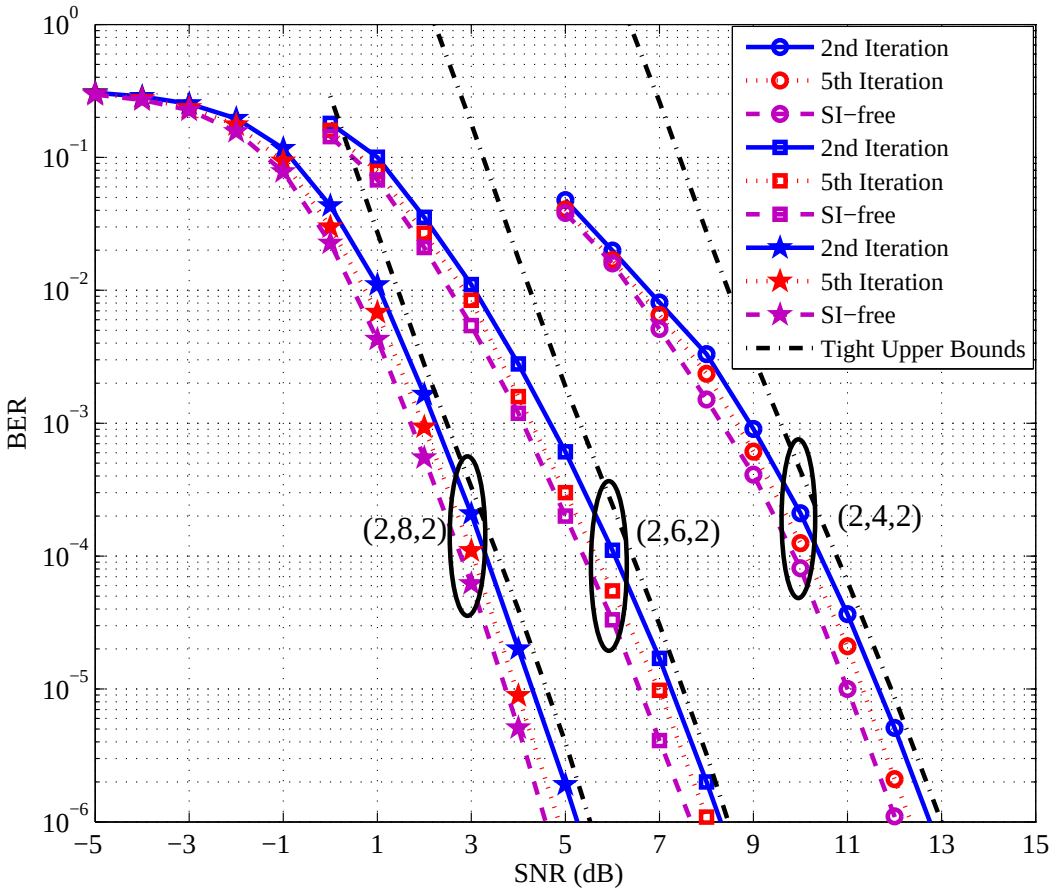

Figure 5.6: BER vs. SNR performance of FD-MIMO-BICM-IDD utilizing 16-QAM with rate-$1/2$ RSC $(1, 23/35)_8$ convolutional codes for the 2nd and 5th iterations and for different combinations of $\left(N_{tx}^a, N_{rx}^b, N_{tx}^b\right)$ and residual INR=10 dB compared to their corresponding SI-free cases.

reduces the number of iterations required to obtain this convergence. In this figure, the trajectory shows that the number of iterations required for the proposed system for $N_{rx} = 2$ is 4, while, two iterations are adequate when $N_{rx} = 6$. This demonstrates that the number of the received antennas is inversely proportional to the number of iterations required to achieve converge.

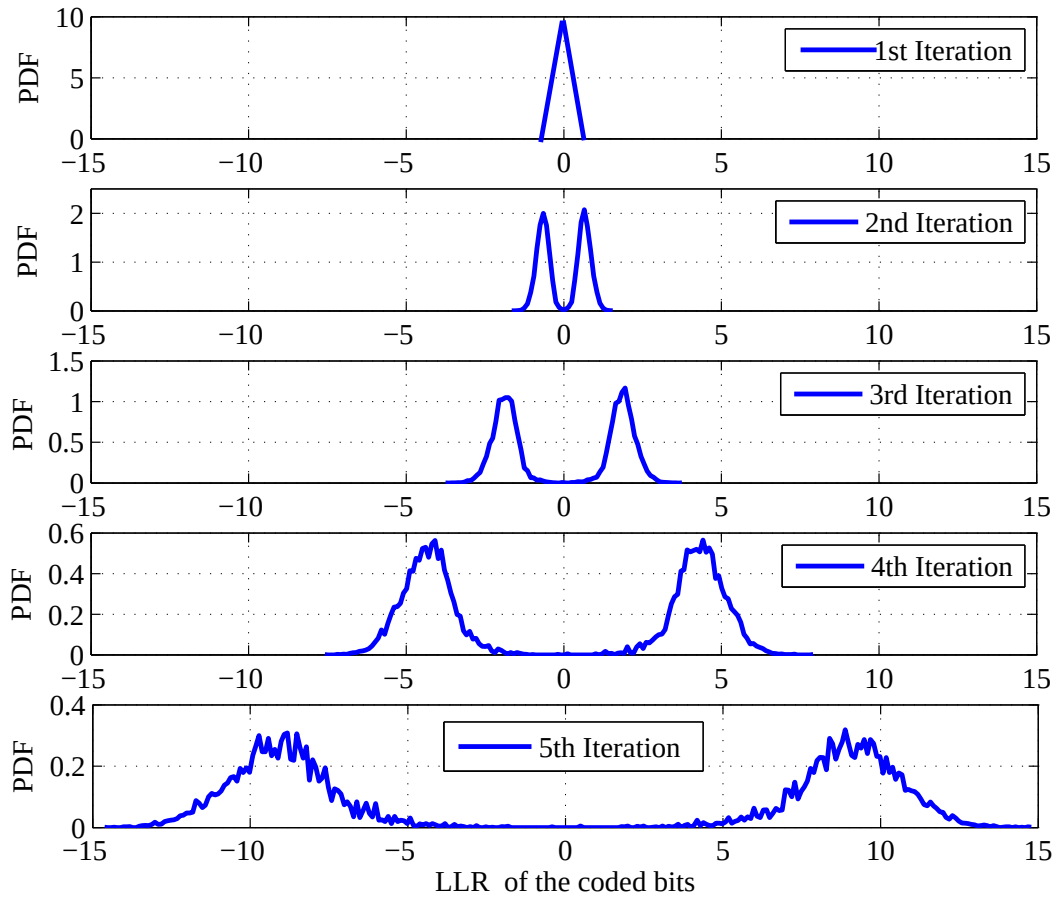

Figure 5.7: PDF distributions vs. iterations for a $(2, 4, 2)$-FD-MIMO system at SNR=5 dB and residual INR of 5 dB.

5.9 Chapter Summary

In this chapter, an active SIC for a bi-directional coded FD-MIMO transceiver has been proposed and its performance has been evaluated. The proposed receiver utilizes IDD, which comprises soft-PIC and adaptive MMSE filtering. This SIC approach has been implemented by exchanging the soft information of the signal of interest and the SI signal between the equalizer and the SiSo decoder. The equalizer performs both adaptive MMSE filtering to remove residual interference and LLR demapping. Furthermore, the SiSo channel decoding of the BICM has been used by employing a MAP decoder. The system performance was evaluated using numerical simulations obtained for several combinations of transmitting and receiving MIMO antennas in the presence of AWGN and over independent MIMO flat fading channels. Additionally, a tight upper bound on the performance of the proposed receiver is derived under the same conditions to validate

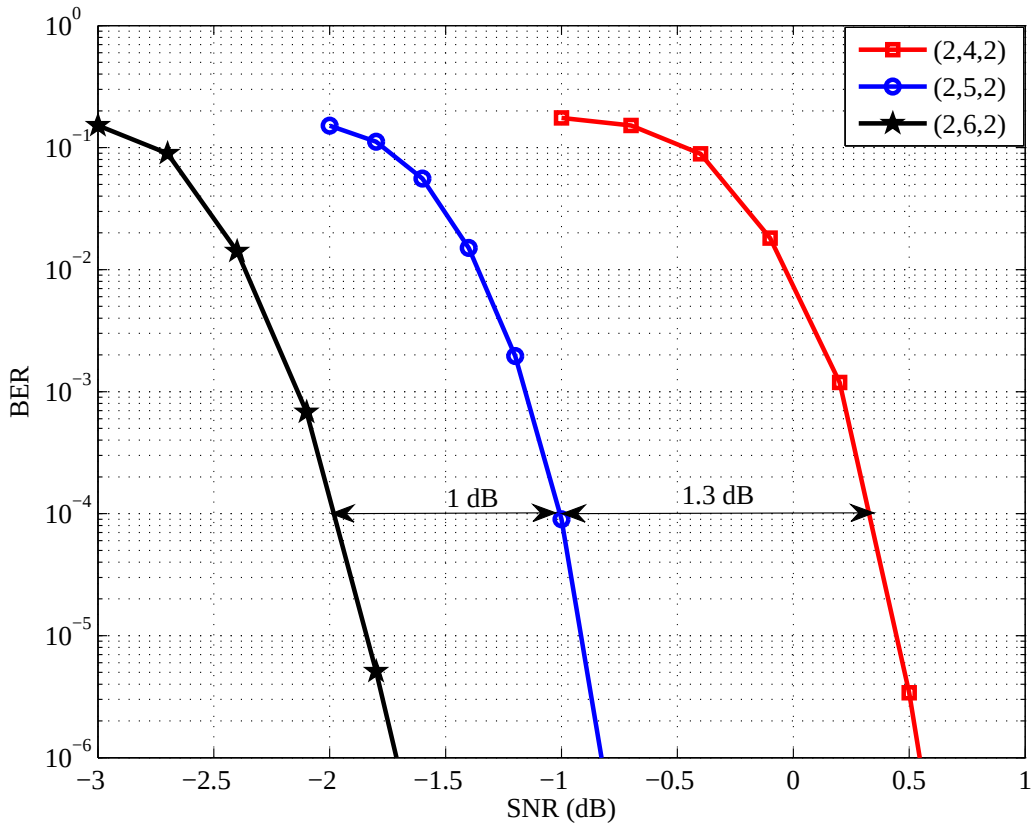

Figure 5.8: BER vs. SNR performance of iterative turbo codes FD-MIMO in the presence of 10 dB residual INR, in which the number of local and global iterations were set to 5 and 10, receptively.

the simulation results. The modulation scheme used in this chapter was M-QAM. The obtained results demonstrate that with increasing number of iterations the FD-MIMO receiver can reconstruct the desired signal and the interference more precisely. Furthermore, for a given number of SI antennas, increasing the number of receive antennas enhances the tolerance to residual interference. The proposed coded FD-MIMO transceiver with IDD offers increased resilience to interference power, which in turn enhances the overall system performance. Furthermore, the EXIT chart based results demonstrating the convergence of the proposed iterative system reveal that the number of iterations required for the SiSo decoder and the equalizer to converge is inversely proportional to the number of the received antennas.

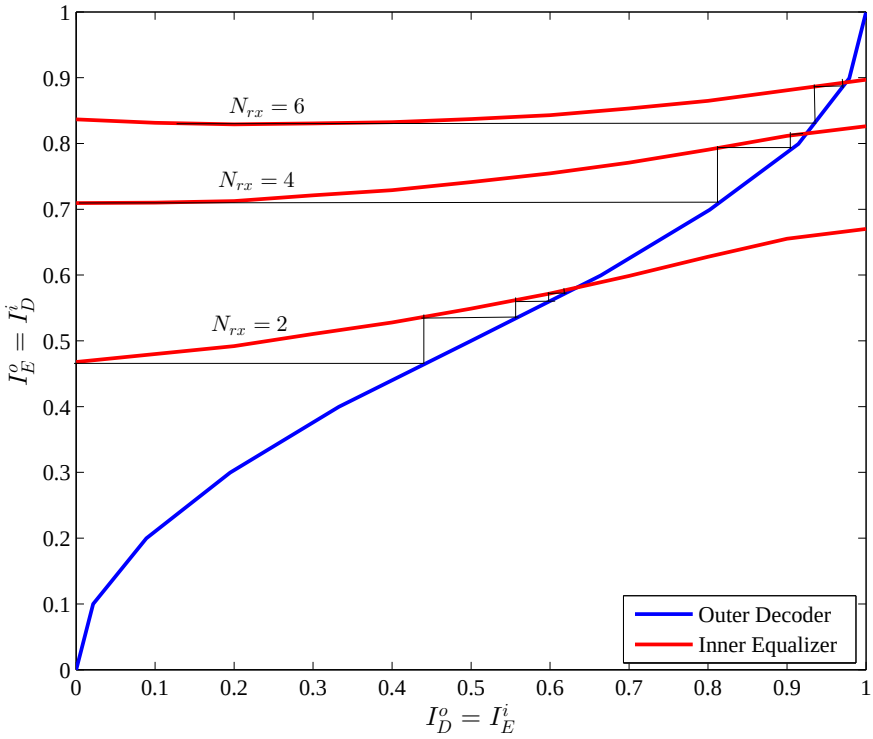

Figure 5.9: EXIT chart for a $(2, N_{rx}, 2)$-FD-MIMO system at SNR=-5 dB and residual INR of 10 dB. (The black solid lines represent the trajectory).

Chapter 6

Conclusions and Future Work

6.1 Conclusions

Conventional wireless communication exploits HD or out-of-band FD transmissions, in which TDD or FDD mechanisms are employed to share the spectrum assigned between the transmitted and received signals in such a way that provides reliable transmission with the minimum amount of interference. However, the increased demand on frequency resources and the need to reinforce spectral efficiency have led to more concentration on utilising the in-band FD technique. The key challenge which significantly affects the performance of FD transceivers is the inherent SI due to simultaneous transmitting and receiving using the same frequency band. Hence, different approaches have been proposed and applied to tackle SI and recover the desired signal in different stages of signal processing at the receiver. Passive suppression in the RF domain is considered to be the key stage and the first defensive line against SI, since it is required to attenuate the arriving SI power to a level that makes the signal processing in the following stages feasible. This can be achieved using different means of natural isolation such as antenna separation, absorptive shielding, cross-polarization, directional isolation, antenna-aid cancellation and an RF circulator. A vital role can be played by designing the transmit and receive antennas to have orthogonal polarization or orthogonal beamforming or both. Nevertheless, further mitigation of SI is required in the analogue and digital domains, i.e. before and after the ADC, to suppress the SI power to the level of thermal noise. In the analogue domain, it is necessary to obtain a precise estimation for the loop-back interference channel, in which the latter is utilized with the known signal transmitted from the transceiver itself, i.e. the SI signal, in order to create a replica of the SI, that represents a cancellation signal. The latter is subtracted from the overall incoming signal for the sake of obtaining the desired signal. Additionally, an auxiliary transmit chain, identical to the main transmit chain, can be used to create an identical copy of the SI that carries all the impairments and non-linear distortions caused by the transmitter components, in order to be subtracted from the incoming signal. In the digital domain, the same procedure can be utilized by passing the SI signal in the RF domain through an auxiliary receive chain which is identical to the main receive chain, and then to subtract it from the arriving signal in the baseband in order to remove the residual SI along with all the distortions induced by the transmitter and receiver components. Moreover, NSP can be employed for an FD-MIMO transceiver by designing digital spatial filters at the transmitter and receiver using the SVD of the loop-back SI channel. These filters have the ability to nullify the SI signal if precise knowledge

of the SI channel is available at the transmit and receive terminals of the FD transceiver. It is noteworthy that utilizing MIMO techniques can enhance the performance of systems employing FD operation, as further diversity gain is obtained and an additional DoF is acquired for SI mitigation in the spatial domain.

The main contributions of this thesis, which have fulfilled the aims of the research mentioned in Chapter 1, are summarised as follows:

- NSP and MRC have been jointly employed for an uncoded FD-MIMO based EF relaying system to suppress the SI and to enhance the overall received power of the desired signal, respectively. Moreover, the performance analyses of the proposed system have been conducted for two hops in the presence of channel estimation errors. Furthermore, MMSE filtering has been proposed and applied in the EF relay to achieve an optimum recovery of the desired signals. Additionally, a performance analysis has been achieved by obtaining for each hop the exact formulas for the PDF of the output SINR, followed by an evaluation of the outage probabilities, ASER and finally the upper bound capacity of the proposed system. The system performance results in terms of SINR figures and system capacity demonstrate significant improvements compared to the results obtained with relevant state-of-the-art techniques.

- IDD for coded FD-SIMO has been proposed and applied in the digital domain to provide an additional alleviation of the residual SI which remains after applying different passive and active SICs. Moreover, tight and union upper bounds of the proposed system have been derived on the performance of rate-$1/2$ convolutional codes with a QPSK modulation scheme, over the non-selective Rayleigh fading channel and in the presence of AWGN, in order to validate the simulation results. The results in terms of the SNR-BER metric have showed performance very close to those of the SI-free scenario after a particular number of iterations. Furthermore, the derived bounds have exhibited close match with the simulated results obtained under the same conditions.

- IDD in the context of coded FD-MIMO has been exploited and applied effectively to mitigate the remaining SI in the digital domain. Moreover, the proposed system has been validated by deriving the tight upper bound performance of rate-$1/2$ convolutional codes with M-QAM modulation schemes, over the non-selective

Rayleigh fading channel and in the presence of AWGN. Furthermore, the EXIT chart has been employed as a semi-analytic tool to observe the convergence behaviour between the iterative MMSE detector and the MAP decoder. The required target was to achieve performance very close to the SI-free scenario after a particular number of iterations, which has been achieved successfully.

6.2 Future work

The promising results obtained from this research project raise the possibility of replacing the conventional HD and out-of-the-band FD with the proposed in-band FD for the next generations of wireless communication, in order to improve spectral efficiency and reduce the bandwidth consumption. However, some aspects and challenges have not been thoroughly investigated and addressed. Therefore, some of the main points are outlined below with proposals for appropriate further research.

- An implementation of a practical hardware design for the proposed systems and a comparison of the results obtained with the simulation and the performance analysis.
- Taking into account in the simulations and performance analyses the effect of non-linearities in the hardware components in the transmit and receive chains which add further SI distortion and need to be further investigated to provide mitigation.
- Applying all of the techniques investigated in this thesis related to FD operation to other wireless communication topologies, such as cellular network, cognitive radio networks, muti-user systems and massive MIMO applications.
- To evaluate the tight bounds on the performance of FD-MIMO-IDD for different code rates of convolutional and turbo codes.
- Use of LDPC for high code rates and long frame lengths and find the bounds on the performance with FD-MIMO.
- Hybrid FD/HD mechanisms can be considered in more depth by designing a transceiver that has the ability to change the mode of transmission depending on the energy levels of the desired signal and interference, i.e. the SINR level.

- EXIT chart can be considered in more depth to evaluate the convergence of different IDD scenarios. Moreover, it can be utilized to find the performance of the iterative coded system in the BER-SNR metric.

References

[1] Z. Zhang, X. Chai, K. Long, A. V. Vasilakos, and L. Hanzo, "Full duplex techniques for 5g networks: self-interference cancellation, protocol design, and relay selection," *IEEE Commun. Mag.*, vol. 53, no. 5, pp. 128–137, 2015.

[2] T. Riihonen, S. Werner, and R. Wichman, "Hybrid full-duplex/half-duplex relaying with transmit power adaptation," *IEEE Trans. Wireless Commun.*, vol. 10, no. 9, pp. 3074–3085, Sep. 2011.

[3] ——, "Comparison of full-duplex and half-duplex modes with a fixed amplify-and-forward relay," in *Proc. IEEE Wireless Commun. and Networking Conf. (WCNC)*, Apr. 2009, pp. 1–5.

[4] A. Sabharwal, P. Schniter, D. Guo, D. W. Bliss, S. Rangarajan, and R. Wichman, "In-band full-duplex wireless: Challenges and opportunities," *IEEE J. Selected Areas in Commun.*, vol. 32, no. 9, pp. 1637–1652, 2014.

[5] T. Kaiser and N. Zarifeh, "General principles and basic algorithms for full-duplex transmission," *Signal Processing for 5G: Algorithms and Implementations*, pp. 372–401, 2016.

[6] D. Bharadia, E. McMilin, and S. Katti, "Full duplex radios," *ACM SIGCOMM Computer Communication Review*, vol. 43, no. 4, pp. 375–386, 2013.

[7] Z. Zhang, K. Long, A. V. Vasilakos, and L. Hanzo, "Full-duplex wireless communications: challenges, solutions and future research directions," *Proc. of the IEEE*, pp. 1–45, 2015.

[8] T. Riihonen, A. Balakrishnan, K. Haneda, S. Wyne, S. Werner, and R. Wichman, "Optimal eigenbeamforming for suppressing self-interference in full-duplex MIMO relays," in *Proc. 45th Ann. Conf. Inform. Sciences and Syst. (CISS)*, March 2011, pp. 1–6.

[9] T. Riihonen, S. Werner, and R. Wichman, "Mitigation of loopback self-interference in full-duplex MIMO relays," *IEEE Trans. Signal Process.*, vol. 59, no. 12, pp. 5983–5993, Dec. 2011.

[10] T. Riihonen and R. Wichman, "Analog and digital self-interference cancellation in full-duplex MIMO-OFDM transceivers with limited resolution in A/D conversion," in *Proc. 46th Asilomar Conf. Signals. Syst.*, Nov. 2012, pp. 45–49.

[11] K. Haneda, E. Kahra, S. Wyne, C. Icheln, and P. Vainikainen, "Measurement of loop-back interference channels for outdoor-to-indoor full-duplex radio relays," in *Proc. 4th European Conf. Antennas and Propagation (EuCAP)*, Apr. 2010, pp. 1–5.

[12] M. Khojastepour and S. Rangarajan, "Wideband digital cancellation for full-duplex communications," in *Proc. 46th Asilomar Conf. Signals, Syst. and Comput.*, Nov. 2012, pp. 1300–1304.

[13] B. Day, A. Margetts, D. Bliss, and P. Schniter, "Full-duplex MIMO relaying: Achievable rates under limited dynamic range," *IEEE J. Select. Areas in Commun.*, vol. 30, no. 8, pp. 1541–1553, Sep. 2012.

[14] B. Day, D. Bliss, A. Margetts, and P. Schniter, "Full-duplex bidirectional MIMO: Achievable rates under limited dynamic range," in *Proc. 45th Asilomar Conf Signals, Syst. and Comput.*, Nov. 2011, pp. 1386–1390.

[15] T. Riihonen, S. Werner, and R. Wichman, "Transmit power optimization for multiantenna decode-and-forward relays with loopback self-interference from full-duplex operation," in *Proc. 45th Asilomar Conf. Signals, Syst. and Comput.*, Nov. 2011, pp. 1408–1412.

[16] A. Sahai, G. Patel, C. Dick, and A. Sabharwal, "Understanding the impact of phase noise on active cancellation in wireless full-duplex," in *Proc. 46th Asilomar Conf. Signals, Syst. and Comput.*, Nov. 2012, pp. 29–33.

[17] M. Duarte and A. Sabharwal, "Full-duplex wireless communications using off-the-shelf radios: Feasibility and first results," in *Proc. 44th Asilomar Conf. Signals. Syst.*, Nov. 2010, pp. 1558–1562.

[18] C. R. Anderson, S. Krishnamoorthy, C. G. Ranson, T. J. Lemon, W. G. Newhall, T. Kummetz, and J. H. Reed, "Antenna isolation, wideband multipath propagation

measurements, and interference mitigation for on-frequency repeaters," in *Proc. IEEE Southeast Con.*, March 2004, pp. 110–114.

[19] D. W. Bliss, P. A. Parker, and A. R. Margetts, "Simultaneous transmission and reception for improved wireless network performance," in *2007 IEEE/SP 14th Workshop on Statistical Signal Processing*, Aug 2007, pp. 478–482.

[20] H. Ju, E. Oh, and D. Hong, "Improving efficiency of resource usage in two-hop full duplex relay systems based on resource sharing and interference cancellation," *IEEE Tran. Wireless Commun.*, vol. 8, no. 8, pp. 3933–3938, Aug. 2009.

[21] J. I. Choi, M. Jain, K. Srinivasan, P. Levis, and S. Katti, "Achieving single channel, full duplex wireless communication," in *Proc. 16th annu. int. conf. Mobile comput. and networking*. ACM, 2010, pp. 1–12.

[22] E. Everett, M. Duarte, C. Dick, and A. Sabharwal, "Empowering full-duplex wireless communication by exploiting directional diversity," in *Proc. 45th Asilomar Conf. Signals, Systems and Computers (ASILOMAR)*. IEEE, 2011, pp. 2002–2006.

[23] E. Everett, "Full-duplex infrastructure nodes: Achieving long range with half-duplex mobiles," Ph.D. dissertation, Rice University, 2012.

[24] M. E. Knox, "Single antenna full duplex communications using a common carrier," in *Proc. IEEE Wireless Microwave Technol. Conf. (WAMICON)*, April 2012, pp. 1–6.

[25] E. Everett, A. Sahai, and A. Sabharwal, "Passive self-interference suppression for full-duplex infrastructure nodes," *IEEE Trans. Wireless Commun.*, vol. 13, no. 2, pp. 680–694, 2014.

[26] M. Heino, D. Korpi, T. Huusari, E. Antonio-Rodriguez, S. Venkatasubramanian, T. Riihonen, L. Anttila, C. Icheln, K. Haneda, R. Wichman, and M. Valkama, "Recent advances in antenna design and interference cancellation algorithms for in-band full duplex relays," *IEEE Commun. Mag.*, vol. 53, no. 5, pp. 91–101, May 2015.

[27] L. Laughlin, M. A. Beach, K. A. Morris, and J. L. Haine, "Electrical balance duplexing for small form factor realization of in-band full duplex," *IEEE Commun. Mag.*, vol. 53, no. 5, pp. 102–110, 2015.

[28] D. Korpi, M. Heino, C. Icheln, K. Haneda, and M. Valkama, "Compact inband full-duplex relays with beyond 100 db self-interference suppression: Enabling techniques and field measurements," *IEEE Trans. Antennas and Propag.*, vol. PP, no. 99, pp. 1–1, 2016.

[29] T. Riihonen, S. Werner, and R. Wichman, "Residual self-interference in full-duplex MIMO relays after null-space projection and cancellation," in *Proc. 44th Asilomar Conf. Signals, Syst. and Comput.*, Nov. 2010, pp. 653–657.

[30] Y. Y. Kang and J. H. Cho, "Capacity of MIMO wireless channel with full-duplex amplify-and-forward relay," in *Proc. IEEE 20th Int. Symp. Personal, Indoor and Mobile Radio Commun.*, Sep. 2009, pp. 117–121.

[31] O. Munoz-Medina, J. Vidal, and A. Agustin, "Linear transceiver design in non-regenerative relays with channel state information," *IEEE Trans. Signal Process.*, vol. 55, no. 6, pp. 2593–2604, June 2007.

[32] E. Antonio-Rodriguez and R. Lopez-Valcarce, "Adaptive self-interference suppression for full-duplex relays with multiple receive antennas," in *Proc. IEEE 13th Int. Workshop on Signal Process. Advances in Wireless Commun. (SPAWC)*, June 2012, pp. 454–458.

[33] N. Li, W. Zhu, and H. Han, "Digital interference cancellation in single channel, full duplex wireless communication," in *Proc. 8th Int. Conf. Wireless Commun., Networking and Mobile Computing (WiCOM)*, Sep. 2012, pp. 1–4.

[34] Y. Liu, X.-G. Xia, and H. Zhang, "Distributed space-time coding for full-duplex asynchronous cooperative communications," *IEEE Trans. Wireless Commun.*, vol. 11, no. 7, pp. 2680–2688, 2012.

[35] M. Ahmed, C. Tsimenidis, and A. A. Rawi, "Performance analysis of Full-Duplex-MRC-MIMO with self-interference cancellation using null-space-projection," *IEEE Trans. Signal Process.*, vol. 64, no. 12, pp. 3093–3105, June 2016.

[36] H. Suraweera, I. Krikidis, G. Zheng, C. Yuen, and P. Smith, "Low-complexity end-to-end performance optimization in MIMO full-duplex relay systems," *IEEE Trans. Wireless Commun.*, vol. 13, no. 2, pp. 913–927, Feb. 2014.

[37] J. S. Lemos, F. A. Monteiro, I. Sousa, and A. Rodrigues, "Full-duplex relaying in MIMO-OFDM frequency-selective channels with optimal adaptive filtering," in *Proc. IEEE Global Conf. Signal and Inf. Process. (GlobalSIP)*, Dec. 2015, pp. 1081–1085.

[38] T. Riihonen, S. Werner, and R. Wichman, "Spatial loop interference suppression in full-duplex MIMO relays," in *Proc. 43rd Asilomar Conf. Signals, Syst. and Comput.*, Nov. 2009, pp. 1508–1512.

[39] R. Lopez-Valcarce, E. Antonio-Rodriguez, C. Mosquera, and F. Perez-Gonzalez, "An adaptive feedback canceller for full-duplex relays based on spectrum shaping," *IEEE J. Selected Areas Commun.*, vol. 30, no. 8, pp. 1566–1577, September 2012.

[40] D. Korpi, T. Riihonen, V. Syrjala, L. Anttila, M. Valkama, and R. Wichman, "Full-duplex transceiver system calculations: Analysis of ADC and linearity challenges," *IEEE Trans. Wireless Commun.*, vol. 13, no. 7, pp. 3821–3836, 2014.

[41] M. Duarte, A. Sabharwal, V. Aggarwal, R. Jana, K. K. Ramakrishnan, C. W. Rice, and N. K. Shankaranarayanan, "Design and characterization of a full-duplex multiantenna system for wifi networks," *IEEE Trans. Veh. Technol.*, vol. 63, no. 3, pp. 1160–1177, Mar. 2014.

[42] D. Bharadia and S. Katti, "Full duplex MIMO radios," in *Proc. 11th USENIX Symp. Networked Systems Design and Implementation (NSDI)*, 2014, pp. 359–372.

[43] S. Li and R. D. Murch, "An investigation into baseband techniques for single-channel full-duplex wireless communication systems," *IEEE Trans. Wireless Commun.*, vol. 13, no. 9, pp. 4794–4806, Sep. 2014.

[44] E. Ahmed and A. M. Eltawil, "All-digital self-interference cancellation technique for full-duplex systems," *IEEE Trans. Wireless Commun.*, vol. 14, no. 7, pp. 3519–3532, July 2015.

[45] T. Chen and S. Liu, "A multi-stage self-interference canceller for full-duplex wireless communications," in *Proc. IEEE Global Commun. Conf. (GLOBECOM)*, Dec. 2015, pp. 1–6.

[46] X. Xiong, X. Wang, T. Riihonen, and X. You, "Channel estimation for full-duplex relay systems with large-scale antenna arrays," *IEEE Trans. Wireless Commun.*, vol. 15, no. 10, pp. 6925–6938, Oct. 2016.

[47] E. Antonio-Rodríguez, S. Werner, R. López-Valcarce, T. Riihonen, and R. Wichman, "Wideband full-duplex MIMO relays with blind adaptive self-interference cancellation," *Signal Processing*, vol. 130, pp. 74–85, 2017.

[48] J. Proakis and M. Salehi, *Digital Communications*. McGraw-Hill, 2008.

[49] M. D. Tolga and A. Ghrayeb, "Coding for MIMO communication systems," 2007.

[50] A. B. Gershman and N. D. Sidiropoulos, *Space-time processing for MIMO communications*. Wiley Online Library, 2005.

[51] A. Maaref and S. Aissa, "Closed-form expressions for the outage and ergodic shannon capacity of MIMO MRC systems," *IEEE Trans. Commun.*, vol. 53, no. 7, pp. 1092–1095, July 2005.

[52] M. Kang and M.-S. Alouini, "A comparative study on the performance of MIMO MRC systems with and without cochannel interference," *IEEE Trans. Commun.*, vol. 52, no. 8, pp. 1417–1425, Aug. 2004.

[53] Y. S. Cho, J. Kim, W. Y. Yang, and C. G. Kang, *MIMO-OFDM wireless communications with MATLAB*. John Wiley & Sons, 2010.

[54] X. N. Zeng and A. Ghrayeb, "A blind carrier frequency offset estimation scheme for ofdm systems with constant modulus signaling," *IEEE Trans. Commun.*, vol. 56, no. 7, pp. 1032–1037, 2008.

[55] M. Duarte and A. Sabharwal, "Full-duplex wireless communications using off-the-shelf radios: Feasibility and first results," in *Proc. 44th Asilomar Conf. Signals, Syst. and Comput.*, Nov. 2010, pp. 1558–1562.

[56] E. Aryafar, M. A. Khojastepour, K. Sundaresan, S. Rangarajan, and M. Chiang, "Midu: enabling mimo full duplex," in *Proc. 18th annual intern. conf. Mobile comput. and networking*. ACM, 2012, pp. 257–268.

[57] E. Everett, M. Duarte, C. Dick, and A. Sabharwal, "Empowering full-duplex wireless communication by exploiting directional diversity," in *Proc. 45th Asilomar Conf. Signals, Syst. and Comput.* IEEE, 2011, pp. 2002–2006.

[58] K. M. Nasr, J. P. Cosmas, M. Bard, and J. Gledhill, "Performance of an echo canceller and channel estimator for on-channel repeaters in DVB-T/H networks," *IEEE Trans. Broadcasting*, vol. 53, no. 3, pp. 609–618, Sep. 2007.

[59] J. Ma, G. Y. Li, J. Zhang, T. Kuze, and H. Iura, "A new coupling channel estimator for cross-talk cancellation at wireless relay stations," in *Proc. IEEE Global Commun. Conf.*, Nov. 2009, pp. 1–6.

[60] M. Jain, J. I. Choi, T. Kim, D. Bharadia, S. Seth, K. Srinivasan, P. Levis, S. Katti, and P. Sinha, "Practical, real-time, full duplex wireless," in *Proc. 17th Annu. int. conf. Mobile comput. and networking*. ACM, 2011, pp. 301–312.

[61] M. Duarte, C. Dick, and A. Sabharwal, "Experiment-driven characterization of full-duplex wireless systems," *IEEE Trans. Wireless Commun.*, vol. 11, no. 12, pp. 4296–4307, Dec. 2012.

[62] F.-L. Luo and C. Zhang, *General Principles and Basic Algorithms for Full-duplex Transmission*. Wiley-IEEE Press, 2016, pp. 616–.

[63] D. Korpi, L. Anttila, V. Syrjl, and M. Valkama, "Widely linear digital self-interference cancellation in direct-conversion full-duplex transceiver," *IEEE J. Selected Areas in Commun.*, vol. 32, no. 9, pp. 1674–1687, Sep. 2014.

[64] D. Korpi, S. Venkatasubramanian, T. Riihonen, L. Anttila, S. Otewa, C. Icheln, K. Haneda, S. Tretyakov, M. Valkama, and R. Wichman, "Advanced self-interference cancellation and multiantenna techniques for full-duplex radios," in *Proc. Asilomar Conf. Signals, Syst. and Comput.*, Nov. 2013, pp. 3–8.

[65] D. Korpi, L. Anttila, and M. Valkama, "Reference receiver based digital self-interference cancellation in MIMO full-duplex transceivers," in *Proc. IEEE Globecom Workshops (GC Wkshps)*, Dec. 2014, pp. 1001–1007.

[66] T. Riihonen, M. Vehkapera, and R. Wichman, "Large-system analysis of rate regions in bidirectional full-duplex MIMO link: Suppression versus cancellation," in *Proc. 47th Annu. Conf. Infor. Sci. and Syst. (CISS)*, March 2013, pp. 1–6.

[67] P. Lioliou, M. Viberg, M. Coldrey, and F. Athley, "Self-interference suppression in full-duplex mimo relays," in *Proc. 44th Asilomar Conf. Signals. Syst.*, Nov. 2010, pp. 658–662.

[68] A. Paulraj, R. Nabar, and D. Gore, *Introduction to space-time wireless communications*. Cambridge university press, 2003.

[69] P. Lioliou, M. Viberg, M. Coldrey, and F. Athley, "Self-interference suppression in full-duplex MIMO relays," in *Proc. 44th Asilomar Conf. Signals, Syst. and Comput.*, Nov. 2010, pp. 658–662.

[70] D. Kim, H. Ju, S. Park, and D. Hong, "Effects of channel estimation error on full-duplex two-way networks," *IEEE Trans. Veh. Technol.*, vol. 62, no. 9, pp. 4666–4672, Nov. 2013.

[71] H. Ju, S. Lee, K. Kwak, E. Oh, and D. Hong, "A new duplex without loss of data rate and utilizing selection diversity," in *Proc. IEEE Veh. Technology Conf. VTC Spring*, May 2008, pp. 1519–1523.

[72] M. Hasna and M.-S. Alouini, "End-to-end performance of transmission systems with relays over Rayleigh-fading channels," *IEEE Trans.Wireless Commun.*, vol. 2, no. 6, pp. 1126–1131, 2003.

[73] R. Annavajjala, P. Cosman, and L. Milstein, "Performance analysis of linear modulation schemes with generalized diversity combining on Rayleigh fading channels with noisy channel estimates," *IEEE Trans. Inform. Theory*, vol. 53, no. 12, pp. 4701–4727, 2007.

[74] L. Yang and J. Qin, "Outage performance of MIMO MRC systems with unequal-power co-channel interference," *IEEE Commun. Lett.*, vol. 10, no. 4, pp. 245–247, Apr. 2006.

[75] S. Ikki and S. Aissa, "Impact of imperfect channel estimation and co-channel interference on regenerative cooperative networks," *IEEE Wireless Commun. Lett.*, vol. 1, no. 5, pp. 436–439, 2012.

[76] P. Dighe, R. Mallik, and S. Jamuar, "Analysis of transmit-receive diversity in Rayleigh fading," in *Proc. IEEE Global Telecommun. Conf. GLOBECOM*, vol. 2, 2001, pp. 1132–1136.

[77] A. Jeffrey and D. Zwillinger, *Table of Integrals, Series, and Products*, ser. Table of Integrals, Series, and Products Series. Elsevier Science, 2007.

[78] Y. Tokgoz and B. Rao, "The effect of imperfect channel estimation on the performance of maximum ratio combining in the presence of cochannel interference," *IEEE Trans. Veh. Technol.*, vol. 55, no. 5, pp. 1527–1534, Sep. 2006.

[79] A. Goldsmith, *Wireless Communications*. New York, NY, USA: Cambridge University Press, 2005.

[80] M. Simon and M. Alouini, *Digital communication over fading channels: a unified approach to performance analysis*, ser. Wiley series in telecommunications and signal processing. John Wiley & Sons, 2000.

[81] H. Bateman and A. Erdelyi, "Higher transcendental functions, vol. 1," 1953.

[82] S. Barbarossa, *Multiantenna Wireless Communications Systems*, ser. Artech House mobile communications library. Artech House, 2005.

[83] D. Palomar, J. Cioffi, and M. A. Lagunas, "Joint Tx-Rx beamforming design for multicarrier MIMO channels: a unified framework for convex optimization," *IEEE Trans. Signal Process.*, vol. 51, no. 9, pp. 2381–2401, 2003.

[84] H. Q. Ngo, H. Suraweera, M. Matthaiou, and E. Larsson, "Multipair full-duplex relaying with massive arrays and linear processing," *IEEE J. Select. Areas in Commun.*, vol. 32, no. 9, pp. 1721–1737, Sep. 2014.

[85] M. Sellathurai and S. Haykin, "Turbo-BLAST for wireless communications: theory and experiments," *IEEE Trans. Signal Process.*, vol. 50, no. 10, pp. 2538–2546, Oct. 2002.

[86] M. A. Ahmed and C. C. Tsimenidis, "Coded full-duplex MIMO with iterative detection and decoding," in *Proc. IEEE Int. Conf. Commun. ICC*, June 2015, pp. 4859–4864.

[87] C. Shannon, "A mathematical theory of communication," *Bell System Technical Journal*, vol. 27, pp. 379–423, 623–656, 1948.

[88] S. J. Johnson, *Iterative error correction: turbo, low-density parity-check and repeat-accumulate codes*. Cambridge University Press, 2009.

[89] R. A. Carrasco and M. Johnston, *Non-binary error control coding for wireless communication and data storage*. John Wiley & Sons, 2008.

[90] K. D. Rao, *Channel Coding Techniques for Wireless Communications*. Springer, 2015.

[91] C. Berrou, A. Glavieux, and P. Thitimajshima, "Near shannon limit error-correcting coding and decoding: Turbo-codes," in *Proc. IEEE Int. Conf. Commun. (ICC'93)*, May 1993, pp. 1064–1070, vol.2.

[92] L. Hanzo, T. H. Liew, and B. L. Yeap, *Turbo coding, turbo equalisation and space-time coding*. John Wiley & Sons, 2002.

[93] M. Sellathurai and S. Haykin, "Turbo-BLAST: performance evaluation in correlated Rayleigh-fading environment," *IEEE J. Selected Areas Commun.*, vol. 21, no. 3, pp. 340–349, Apr. 2003.

[94] X. Wang and H. Poor, "Iterative (turbo) soft interference cancellation and decoding for coded CDMA," *IEEE Trans. Commun.*, vol. 47, no. 7, pp. 1046–1061, Jul. 1999.

[95] C. Steger and A. Sabharwal, "Single-input two-way SIMO channel: diversity-multiplexing tradeoff with two-way training," *IEEE Trans. Wireless Commun.*, vol. 7, no. 12, pp. 4877–4885, Dec. 2008.

[96] A. Viterbi, "Convolutional codes and their performance in communication systems," *IEEE Trans. Commun. Technol.*, vol. 19, no. 5, pp. 751–772, Oct. 1971.

[97] Y.-L. Chen and C.-H. Wei, "Performance bounds of rate-1/2 convolutional codes with QPSK on Rayleigh fading channel," *Electron. Lett.*, vol. 22, no. 17, pp. 915–917, Aug. 1986.

[98] H. Moon and D. Cox, "Improved performance upper bounds for terminated convolutional codes," *IEEE Commun. Lett.*, vol. 11, no. 6, pp. 519–521, June 2007.

[99] P. Wijesinghe, U. Gunawardana, and R. Liyanapathirana, "Tighter performance upper bounds for terminated convolutional codes in Rayleigh fading channels," in *Proc. 6th ECTI-CON Int. Conf. Elect. Eng./Electron., Comput., Telecommun. and Inform. Technol.*, vol. 02, May 2009, pp. 800–803.

[100] ——, "Improved performance upper bounds for terminated convolutional codes in rayleigh fading channels," *ECTI trans. elect. eng., electron. and commun.*, vol. 8, no. 1, pp. 99–105, 2010.

[101] J. Luo, J. Zeidler, and J. Proakis, "Coded error performance of MIMO systems in frequency selective Nakagami fading channels," in *Proc. IEEE Int. Conf. Commun. ICC*, vol. 3, 2002, pp. 1959–1963.

[102] M. K. Simon and M. Alouini, *Digital Communication over Fading Channels*. John Wiley & Sons, 2005.

[103] M. A. Ahmed and C. C. Tsimenidis, "Coded full-duplex MIMO with iterative detection and decoding," in *Proc. IEEE Int. Conf. Commun. ICC*, June 2015, pp. 4859–4864.

[104] A. Tonello, "Space-time bit-interleaved coded modulation with an iterative decoding strategy," in *Proc. IEEE Veh. Technol. Conf.*, vol. 1, Sep. 2000, pp. 473–478 vol.1.

[105] S. Sadough and M.-A. Khalighi, "Optimal Turbo-BLAST detection of MIMO-OFDM systems with imperfect channel estimation," in *Proc. IEEE 18th Int. Symp. Personal, Indoor and Mobile Radio Commun. (PIMRC)*, Sep. 2007, pp. 1–6.

[106] N. Du and D. Xu, "Low complexity iterative receiver for MIMO-OFDM systems," in *Intelligent Signal Processing and Communication Systems, 2007. ISPACS 2007. International Symposium on*, Nov. 2007, pp. 622–625.

[107] J. Y. Hwang, D.-K. Cho, K. S. Kim, and K.-C. Whang, "A Turbo-BLAST method with non-linear MMSE detector for MIMO-OFDM systems," in *Circuits and Systems, 2006. APCCAS 2006. IEEE Asia Pacific Conference on*, Dec 2006, pp. 295–297.

[108] H. Lee, B. Lee, and I. Lee, "Iterative detection and decoding with an improved V-BLAST for MIMO-OFDM systems," in *Communications, 2006. ICC '06. IEEE International Conference on*, vol. 12, June 2006, pp. 5377–5382.

[109] M. A. Ahmed and C. C. Tsimenidis, "A tight upper bound on the performance of iterative detection and decoding for coded full-duplex SIMO systems," *IEEE Commun. Lett.*, vol. 20, no. 3, pp. 606–609, Mar. 2016.

[110] D. Na, G. Pin-biao, and C. Ning, "An improved iterative receiver scheme for Turbo-BLAST system with anti-gray mapping," in *Proc. 3rd Int. symp. Inform. Process. (ISIP)*, Oct. 2010, pp. 411–414.

[111] ——, "A low-complexity iterative receiver scheme for Turbo-BLAST system," in *Signal Processing (ICSP), 2010 IEEE 10th International Conference on*, Oct 2010, pp. 1548–1551.

[112] T. Ait-Idir, S. Saoudi, and N. Naja, "Space time turbo equalization with successive interference cancellation for frequency-selective mimo channels," *IEEE Trans. Veh. Technol.*, vol. 57, no. 5, pp. 2766–2778, Sept 2008.

[113] T. Abe and T. Matsumoto, "Space-time turbo equalization in frequency-selective MIMO channels," *IEEE Trans. Veh. Technol.*, vol. 52, no. 3, pp. 469–475, May 2003.

[114] T. Abe, S. Tomisato, and T. Matsumoto, "A MIMO turbo equalizer for frequency-selective channels with unknown interference," *IEEE Trans. Veh. Technol.*, vol. 52, no. 3, pp. 476–482, May 2003.

[115] S. Ten Brink, "Convergence behavior of iteratively decoded parallel concatenated codes," *IEEE Trans. Commun.*, vol. 49, no. 10, pp. 1727–1737, Oct. 2001.

[116] T. Chen and S. Liu, "A multi-stage self-interference canceller for full-duplex wireless communications," in *Proc. IEEE Global Commun. Conf. (GLOBECOM)*, Dec. 2015, pp. 1–6.

[117] M. Duarte, C. Dick, and A. Sabharwal, "Experiment-driven characterization of full-duplex wireless systems," *IEEE Trans. Wireless Commun.*, vol. 11, no. 12, pp. 4296–4307, 2012.

[118] L. Fang, Q. Guo, D. Huang, and S. Nordholm, "A low cost soft mapper for turbo equalization with high order modulation," in *Proc. Int. SoC Design Conf. (ISOCC)*, Nov 2012, pp. 305–308.

[119] A. Tomasoni, M. Ferrari, D. Gatti, F. Osnato, and S. Bellini, "A low complexity turbo MMSE receiver for W-LAN MIMO systems," in *Proc. IEEE Int. Conf. Commun.*, vol. 9, June 2006, pp. 4119–4124.

[120] A. Hedayat and A. Nosratinia, "Outage and diversity of linear receivers in flat-fading MIMO channels," *IEEE Trans. Signal Process.*, vol. 55, no. 12, pp. 5868–5873, Dec. 2007.

[121] M. McKay and I. Collings, "Error performance of MIMO-BICM with zero-forcing receivers in spatially-correlated rayleigh channels," *IEEE Trans. Wireless Commun.*, vol. 6, no. 3, pp. 787–792, Mar. 2007.

[122] N. Kim and H. Park, "Bit error performance of convolutional coded MIMO system with linear MMSE receiver," *IEEE Trans. Wireless Commun.*, vol. 8, no. 7, pp. 3420–3424, July 2009.

[123] P. Frenger, P. Orten, and T. Ottosson, "Convolutional codes with optimum distance spectrum," *IEEE Commun. Lett.*, vol. 3, no. 11, pp. 317–319, Nov 1999.

[124] R. Durrett, *Probability: Theory and Examples*. Cambridge University Press, 2010.

[125] H. R. Sadjadpour, "Maximum a posteriori decoding algorithms for turbo codes," in *AeroSense 2000*. International Society for Optics and Photonics, 2000, pp. 73–83.

[126] G. Shuxia, S. Yang, G. Ying, and H. Qianjin, "Low complexity minimum mean square error channel estimation for adaptive coding and modulation systems," *China Commun.*, vol. 11, no. 1, pp. 126–137, 2014.

[127] M. El-Hajjar and L. Hanzo, "EXIT charts for system design and analysis," *IEEE Commun. Surveys & Tutorials*, vol. 16, no. 1, pp. 127–153, 2014.

[128] S. Ten Brink, "Designing iterative decoding schemes with the extrinsic information transfer chart," *AEU Int. J. Electron. Commun*, vol. 54, no. 6, pp. 389–398, 2000.